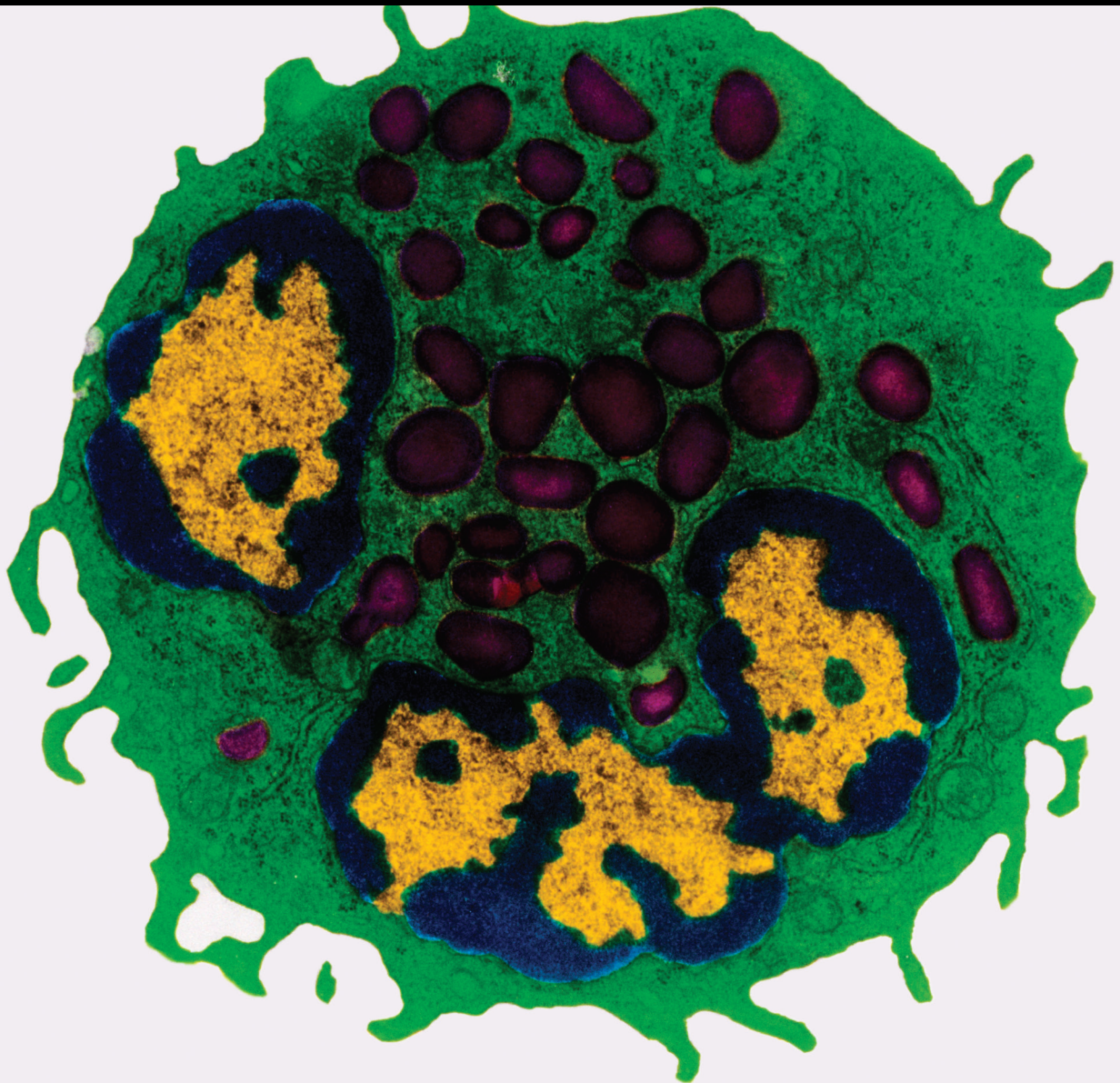


# The Role of Inflammation in the Pathophysiology of Cardiovascular Diseases 2022

Lead Guest Editor: Azizah Ugusman

Guest Editors: Simon Kennedy, Amilia Aminuddin, and Dominik Skiba



---

**The Role of Inflammation in the  
Pathophysiology of Cardiovascular Diseases  
2022**

Mediators of Inflammation

---

**The Role of Inflammation in the  
Pathophysiology of Cardiovascular  
Diseases 2022**

Lead Guest Editor: Azizah Ugusman

Guest Editors: Simon Kennedy, Amilia Aminuddin,  
and Dominik Skiba




---





Copyright © 2023 Hindawi Limited. All rights reserved.

This is a special issue published in "Mediators of Inflammation." All articles are open access articles distributed under the Creative Commons Attribution License, which permits unrestricted use, distribution, and reproduction in any medium, provided the original work is properly cited.

# Chief Editor






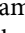
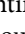
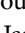
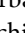
Anshu Agrawal , USA

## Associate Editors

Carlo Cervellati , Italy  
Elaine Hatanaka , Brazil  
Vladimir A. Kostyuk , Belarus  
Carla Pagliari , Brazil



## Academic Editors

Amedeo Amedei , Italy  
Emiliano Antiga , Italy  
Tomasz Brzozowski , Poland  
Daniela Caccamo , Italy  
Luca Cantarini , Italy  
Raffaele Capasso , Italy  
Calogero Caruso , Italy  
Robson Coutinho-Silva , Brazil  
Jose Crispin , Mexico  
Fulvio D'Acquisto , United Kingdom  
Eduardo Dalmarco , Brazil  
Agnieszka Dobrzyn, Poland  
Ulrich Eisel , The Netherlands  
Mirvat El-Sibai , Lebanon  
Giacomo Emmi , Italy  
Claudia Fabiani , Italy  
Fabíola B Filippin Monteiro , Brazil  
Antonella Fioravanti , Italy  
Tânia Silvia Fröde , Brazil  
Julio Galvez , Spain  
Mirella Giovarelli , Italy  
Denis Girard, Canada  
Markus H. Gräler , Germany  
Oreste Gualillo , Spain  
Qingdong Guan , Canada  
Tommaso Iannitti , United Kingdom  
Byeong-Churl Jang, Republic of Korea  
Yasumasa Kato , Japan  
Cheorl-Ho Kim , Republic of Korea  
Alex Kleinjan , The Netherlands  
Martha Lappas , Australia  
Ariadne Malamitsi-Puchner , Greece  
Palash Mandal, India  
Joilson O. Martins , Brazil  
Donna-Marie McCafferty, Canada  
Barbro N. Melgert , The Netherlands



Paola Migliorini , Italy  
Vinod K. Mishra , USA  
Eeva Moilanen , Finland  
Elena Niccolai , Italy  
Nadra Nilsen , Norway  
Sandra Helena Penha Oliveira , Brazil  
Michal A. Rahat , Israel  
Zoltan Rakonczay Jr. , Hungary  
Marcella Reale , Italy  
Emanuela Roscetto, Italy  
Domenico Sergi , Italy  
Mohammad Shadab , USA  
Elena Silvestri, Italy  
Carla Sipert , Brazil  
Helen C. Steel , South Africa  
Saravanan Subramanian, USA  
Veendamali S. Subramanian , USA  
Taina Tervahartiala, Finland  
Alessandro Trentini , Italy  
Kathy Triantafilou, United Kingdom  
Fumio Tsuji , Japan  
Maria Letizia Urban, Italy  
Giuseppe Valacchi , Italy  
Kerstin Wolk , Germany  
Soh Yamazaki , Japan  
Young-Su Yi , Republic of Korea  
Shin-ichi Yokota , Japan  
Francesca Zimetti , Italy

## Contents






### **Serum Levels of Proinflammatory Biomarkers in Military Recruits with and without Metabolic Syndrome**

Abdulrahman K. Al Asmari , Hamoud A. Al Shehri, Haseeb A. Khan , Saud Al Omani, Saeed G. Kadasah, Ghaleb B. Horaib, Ahmed Al Buraidi, Abdullah A. Al Sharif, Faye S. Mohammed, Rajamohamed Abbasmanthiri, and Nasreddien M. Osman  
Research Article (6 pages), Article ID 4613842, Volume 2023 (2023)




### **Visfatin Amplifies Cardiac Inflammation and Aggravates Cardiac Injury via the NF- $\kappa$ B p65 Signaling Pathway in LPS-Treated Mice**

Yewen Hu, Nan Wu, Weiping Du, Shuangshuang Wang, Jian Wang, Chaoxia Zhang, Xiaomin Chen , and Caijie Shen   
Research Article (9 pages), Article ID 3306559, Volume 2022 (2022)



### **Exercise Preconditioning Ameliorates Cognitive Impairment in Mice with Ischemic Stroke by Alleviating Inflammation and Modulating Gut Microbiota**

Heng Lv , Shasha Wang , Meihui Tian, Liya Wang, Jie Gao , Qitao Zhao, Zhaoyu Li, Xianjie Jia , and Ying Yu   
Research Article (15 pages), Article ID 2124230, Volume 2022 (2022)



### **LncRNA MDRL Mitigates Atherosclerosis through miR-361/SQSTM1/NLRP3 Signaling**

Ling You, Yanjie Zheng, Jing Yang , Qian Hou, Lianxia Wang, Yan Zhang, Chunxia Zhao , and Ruiqin Xie   
Research Article (13 pages), Article ID 5463505, Volume 2022 (2022)

### **GJD Modulates Cardiac/Vascular Inflammation and Decreases Blood Pressure in Hypertensive Rats**

Shadi A. D. Mohammed , Hanxing Liu, Salem Baldi, Pingping Chen, Fang Lu, and Shumin Liu   
Research Article (19 pages), Article ID 7345116, Volume 2022 (2022)


### **Anti-Inflammatory Activity of *Ferula assafoetida* Oleo-Gum-Resin (Asafoetida) against TNF- $\alpha$ -Stimulated Human Umbilical Vein Endothelial Cells (HUVECs)**

Leila Mobasheri, Mohsen Khorashadizadeh, Hossein Safarpour, Maryam Mohammadi, Gholamreza Anani Sarab , and Vahid Reza Askari   
Research Article (15 pages), Article ID 5171525, Volume 2022 (2022)

### **Vaspin Alleviates Sepsis-Induced Cardiac Injury and Cardiac Inflammation by Inhibiting Kallikrein 7 in Mice**

Na Yin, Fuze Pan, Lingyue Qiu, Zicong Yang, Rixin Xiong, Lei Shi, Ying Shi, Ning Wu, Kui Wu, Qingkuan Li, Daojun Wen, Qili Huang, Yuyan Zhang, Yuhong Mi , and Qingwei Ji   
Research Article (12 pages), Article ID 1149582, Volume 2022 (2022)

### **Heat Shock Protein 27 Levels Predict Myocardial Inhomogeneities in Hemodialysis Patients**

Andrzej Jaroszyński , Todd T. Schlegel, Jerzy Mosiewicz, Renata Stępień, and Wojciech Dąbrowski  
Research Article (6 pages), Article ID 5618867, Volume 2022 (2022)

## Research Article

# Serum Levels of Proinflammatory Biomarkers in Military Recruits with and without Metabolic Syndrome

**Abdulrahman K. Al Asmari** <sup>1</sup>, **Hamoud A. Al Shehri**,<sup>2</sup> **Haseeb A. Khan** <sup>3</sup>, **Saud Al Omani**,<sup>4</sup> **Saeed G. Kadasah**,<sup>5</sup> **Ghaleb B. Horaib**,<sup>6</sup> **Ahmed Al Buraidi**,<sup>7</sup> **Abdullah A. Al Sharif**,<sup>8</sup> **Fayez S. Mohammed**,<sup>9</sup> **Rajamohamed Abbasmanthiri**,<sup>1</sup> and **Nasreddien M. Osman**<sup>1</sup>

<sup>1</sup>Scientific Research Center, Medical Service Department (MSD), Ministry of Defence, Riyadh, Saudi Arabia

<sup>2</sup>Adult Cardiology, Prince Sultan Cardiac Center, Medical Service Department (MSD), Ministry of Defence, Riyadh, Saudi Arabia

<sup>3</sup>Department of Biochemistry, College of Science, King Saud University, Riyadh 11451, Saudi Arabia

<sup>4</sup>Department of Surgery, Prince Sultan Military Medical City, Medical Service Department (MSD), Ministry of Defence, Riyadh, Saudi Arabia

<sup>5</sup>Department of Psychiatry, Prince Sultan Military Medical City, Medical Service Department (MSD), Ministry of Defence, Riyadh, Saudi Arabia

<sup>6</sup>Dermatology Department, Medical Service Department (MSD), Ministry of Defence, Riyadh, Saudi Arabia

<sup>7</sup>Department of ENT, Prince Sultan Military Medical City, Medical Service Department (MSD), Ministry of Defence, Riyadh, Saudi Arabia

<sup>8</sup>Department of Dentistry, Prince Sultan Military Medical City, Medical Service Department (MSD), Ministry of Defence, Riyadh, Saudi Arabia

<sup>9</sup>Prince Sultan Military College of Health Science, Dhahran, Saudi Arabia

Correspondence should be addressed to Abdulrahman K. Al Asmari; [abdulrahman.alasmari@gmail.com](mailto:abdulrahman.alasmari@gmail.com)

Received 7 September 2022; Revised 10 December 2022; Accepted 6 April 2023; Published 30 April 2023

Academic Editor: Amilia Aminuddin

Copyright © 2023 Abdulrahman K. Al Asmari et al. This is an open access article distributed under the Creative Commons Attribution License, which permits unrestricted use, distribution, and reproduction in any medium, provided the original work is properly cited.

**Objectives.** Inflammatory mediators are associated with many chronic diseases; however, their role in metabolic syndrome (Met-S) is not well documented. We therefore aimed to compare the serum markers of inflammation including C-reactive protein (CRP), myeloperoxidase (MPO), interleukin-6 (IL-6), tumour necrosis factor alpha (TNF- $\alpha$ ), and TNF- $\beta$  in young military recruits with and without Met-S. We hypothesized that any significant change in inflammatory markers between the two groups would indicate the role of inflammation in Met-S that would help in future directions for screening and treatment of Met-S. **Design and Methods.** A total of 2010 adult men, aged 18-30 years, were divided into two groups: with Met-S ( $N = 488$ ) and without Met-S ( $N = 1522$ ), according to the International Diabetes Federation definition. We compared the serum levels of inflammatory biomarkers between the two groups. We also studied the correlations between the inflammatory markers and the components of Met-S to explore the biomarker potential of inflammatory markers for screening of Met-S. Logistic regression analysis was performed to test the association between inflammatory markers and Met-S. **Results.** A large number of subjects in the Met-S group were suffering from obesity. Out of the 2010 total subjects, only 731 (36.4%) had normal fasting blood sugar (FBS), while the prevalence of prediabetes and diabetes was significantly higher in subjects with Met-S. We observed significant increases in serum levels of CRP, MPO, IL-6, and TNF- $\beta$  but not TNF- $\alpha$  in subjects with Met-S as compared to subjects without Met-S. All the markers of inflammation showed significant correlations with Met-S, triglycerides (TG), blood pressure, body mass index (BMI), and age; however, none of these markers were correlated with HDL. Logistic regression analysis showed a significant association between Met-S and inflammatory markers. **Conclusions.** Serum levels of CRP, MPO, IL-6, and TNF- $\beta$  are significantly increased in young adults with Met-S. This is probably the first study reporting TNF- $\beta$  levels in Met-S. Since a proinflammatory cascade precedes many years before the onset of cardiovascular disease, these inflammatory biomarkers could help in the monitoring of high-risk individuals with Met-S who will be requiring therapeutic intervention.

## 1. Introduction

Metabolic syndrome (Met-S) and associated diseases are a global health problem. Met-S is a cluster of metabolic abnormalities characterized by hypertension, high fasting blood glucose, increased waist circumference, hypertriglyceridemia, and low high-density lipoprotein (HDL) cholesterol levels [1]. In recent years, Met-S is becoming highly prevalent even in young adults [2]. Many of the risk factors associated with Met-S including hypertension, hyperglycaemia, central obesity, and dyslipidemia are preventable and can be controlled by modifications in dietary habits and physical activity, particularly at their early stage [3]. Moreover, uncontrolled hyperglycaemia has also been directly associated with dyslipidemia [4]. Early detection of metabolic modifications that could lead to Met-S would help in the timely consideration of preventive measures such as dietary changes and lifestyle modifications [5].

Modern lifestyle, including sedentary behaviour and high intake of caloric and sugar-rich foods, contributes to metabolic ailments with preceding pathophysiological changes such as hyperglycaemia, obesity, hypertension, dyslipidaemia, and a proinflammatory state associated with accumulation of adipose tissue [6]. Adipose tissue is not just a passive storage of fat but also has roles in immune modulation and inflammatory responses including the secretion of cytokines [7]. Met-S has been independently linked with an inflammatory burden as well as increased oxidative stress [8]. Previous studies have also shown increased secretion of apolipoprotein B, uric acid, fibrinogen, plasminogen activator inhibitor 1, C-reactive protein (CRP), and proinflammatory cytokines in Met-S [7, 9, 10]. Currently, the inflammatory markers are not included in the National Cholesterol Education Program Adult Treatment Panel III (NCEP ATP III) or World Health Organization (WHO) diagnostic criteria for Met-S, but it is most probable that a proinflammatory state is one of the hallmarks of this syndrome.

In this study, we compared serum markers of inflammation including CRP, myeloperoxidase (MPO), interleukin-6 (IL-6), tumour necrosis factor alpha (TNF- $\alpha$ ), and TNF- $\beta$  in young military recruits with and without Met-S. We also studied the correlations between the inflammatory markers and the components of Met-S to explore the biomarker potential of inflammatory markers for the screening of Met-S. We hypothesized that a clear understanding of the role of inflammatory mediators in Met-S would not only help in selecting potential biomarkers for screening high-risk individuals but also pave the way for exploring therapeutic modalities such as anti-inflammatory drugs for the treatment of Met-S.

## 2. Materials and Methods

**2.1. Study Population and Medical Observations.** A total of 2010 young Saudi men, aged 18-30 years, who applied for recruitment to the Saudi armed forces were included in this study. The study was carried out at the health facility of the selection centers, and all the selected participants individu-

ally completed the consent forms. Standardized medical observations including physical examination as well as measurements related to Met-S including blood pressure, waist circumference, height, body weight, and blood biochemistry were performed by trained researchers. Blood pressure was measured using a standard sphygmomanometer one time on each arm in subjects who had been resting for 10 min, and the mean of the two measurements was taken. The complete information of each participant was filled in a specially designed questionnaire based on the guidelines of WHO [11]. The study protocol was approved by the Institutional Research and Ethics Committee.

**2.2. Inclusion and Exclusion Criteria of Participants.** The inclusion criteria were male, Saudi, and young adults in the age range of 18-30 years. The exclusion criteria were the presence of any apparent illness or disability. According to the International Diabetes Federation (IDF) definition (<http://www.idf.org>) [12], the subjects were considered to have Met-S if they had central obesity (defined as waist circumference >94 cm), plus two of the following four factors: raised fasting plasma glucose >100 mg/dL (5.6 mmol/L) or previously diagnosed type 2 diabetes; systolic BP >130 or diastolic BP >85 mm Hg or treatment of previously diagnosed hypertension; HDL-C <40 mg/dL (1.0 mmol/L) or specific treatment for this lipid abnormality; TG level >150 mg/dL (1.7 mmol/L) or specific treatment for this lipid abnormality.

**2.3. Biochemical Analysis.** Blood samples from each recruitment center were transported to Prince Sultan Military Medical City for biochemical analysis. Blood samples were centrifuged at  $1500 \times g$  for 15 min at 4°C; sera were separated and stored at -20°C until analysed. Fasting blood sugar (FBS), total cholesterol, high-density lipoprotein cholesterol (HDL), and triglycerides (TG) were analysed using a Hitachi 902 autoanalyzer. Serum levels of CRP, MPO, IL-6, TNF- $\alpha$ , and TNF- $\beta$  were measured using commercially available Quantikine enzyme-linked immunosorbent assay (ELISA) kits (R&D Systems, Bio-Techne Ltd, Abingdon, UK), according to the manufacturer's instructions.

**2.4. Statistical Analysis.** The data were analysed by using the SPSS statistical package version 14 (SPSS Chicago, IL). The chi-square test and Student's *t*-test were used for comparison between the Met-S and without Met-S groups depending on the data type, categorical or continuous, respectively. Pearson and Spearman's tests were used for correlation analysis between various biomarkers and Met-S. Logistic regression analysis was conducted to test the association between inflammatory biomarkers and Met-S. *P* values < 0.05 were considered statistically significant.

## 3. Results

The age of subjects without Met-S was  $19.85 \pm 2.70$  y while those with Met-S were aged  $21.14 \pm 3.38$  y, and this difference was statistically significant (Table 1). Most of the subjects were single (96.2%); however, among married subjects, the majority belonged to the Met-S group. The body weight and BMI were significantly higher in subjects with



TABLE 1: Characteristics of subjects with and without Met-S.

Parameter	No met-S (N = 1522)	Met-S (N = 488)	Total (N = 2010)	P value
Age (years)	19.85 ± 2.70	21.14 ± 3.38	20.16 ± 2.94	<0.001
Age (categorized), N (%)				
Age (≤21 y)	1165 (76.5)	283 (58.0)	1448 (72.0)	
Age (22-26 y)	331 (21.7)	182 (37.3)	513 (25.5)	<0.001
Age (>26 y)	26 (1.7)	23 (4.7)	49 (2.4)	
Marital status, N (%)				
Single	1476 (97.0)	457 (93.6)	1933 (96.2)	
Married	46 (3.0)	31 (6.35)	77 (3.8)	<0.01
Height (cm)	168.84 ± 6.79	171.04 ± 6.92	169.38 ± 6.89	<0.001
Weight (kg)	69.14 ± 23.07	94.35 ± 14.79	75.26 ± 23.94	<0.001
BMI (kg/m <sup>2</sup> )	24.14 ± 7.36	32.23 ± 3.60	26.10 ± 7.49	<0.001
BMI status (categorized), N (%)				
Normal (≤24.9)	855 (56.2)	0 (0.0)	855 (42.5)	
Overweight (25.0-29.9)	135 (8.9)	91 (18.6)	226 (11.2)	<0.001
Obesity (≥30.0)	532 (35.0)	397 (81.4)	929 (46.2)	
Systolic blood pressure, N (%)				
≤129.0 (normal)	674 (44.3)	40 (8.2)	714 (35.5)	
>129.0 (high)	848 (55.7)	448 (91.8)	1296 (64.5)	<0.001
Fasting blood sugar (categorized), N (%)				
<100.0 (normal)	674 (44.3)	57 (11.7)	731 (36.4)	
100.0-125.9 (prediabetes)	751 (49.3)	359 (73.6)	1110 (55.2)	<0.001
≥126.0 (diabetes)	97 (6.4)	72 (14.8)	169 (8.4)	

Values are presented as number (%) or means ± standard deviation. The chi-square test was used for categorical variables, and an independent *t*-test was used for continuous variables.

Met-S as compared to the normal group (Table 1). A large number of subjects in the Met-S group were affected by obesity. Hypertension was prevalent in both groups; however, the frequency of subjects with hypertension was significantly higher in Met-S as compared to subjects without Met-S (Table 1). Out of the 2010 total subjects, only 731 (36.4%) had normal fasting blood sugar (FBS) levels, while the prevalence of prediabetes and diabetes was significantly higher in subjects with Met-S (Table 1).

Serum levels of CRP were significantly higher in subjects with Met-S ( $42.88 \pm 1.13$  ng/mL) as compared to subjects without Met-S ( $31.99 \pm 0.69$  ng/mL) (Figure 1). The levels of MPO in sera of control subjects were  $13.46 \pm 0.12$  ng/mL, whereas the individuals with Met-S showed significantly higher levels of serum MPO ( $17.26 \pm 0.18$  ng/mL) (Figure 2). There was no significant difference in serum levels of TNF- $\alpha$  between the two groups. Whereas, serum IL-6 ( $11.25 \pm 0.22$  versus  $2.73 \pm 0.04$  pg/mL) and TNF- $\beta$  ( $52.13 \pm 1.21$  versus  $27.65 \pm 0.23$  pg/mL) levels were found to be significantly higher in subjects with Met-S as compared to subjects without Met-S (Figure 3). All the markers of inflammation including serum CRP, MPO, IL-6, TNF- $\alpha$ , and TNF- $\beta$  showed significant correlations with Met-S, TG, blood pressure, BMI, and age; however, none of these markers were correlated with HDL (Table 2). The results of logistic regression analysis showed a significant association between Met-S and inflammatory markers (Table 3). Compared to other

markers of inflammation, IL-6 showed higher odd ratios and therefore more significant association with Met-S as well as other independent variables including BMI, blood pressure, and fasting blood sugar (Table 3).

#### 4. Discussion

We observed a high prevalence of obesity and hyperglycemia in subjects with Met-S as compared to subjects without Met-S. Our results also showed a significant increase in inflammatory biomarkers including CRP, MPO, and proinflammatory cytokines in the sera of subjects with Met-S. These markers also showed significant correlations with all the components of Met-S except HDL. A significant association between Met-S and inflammation was also confirmed by logistic regression analysis. The mechanism of a direct relationship between Met-S and inflammation is not fully understood. This can partly be attributed to the stimulation of hepatic CRP production from cytokines, which originate from the adipose tissue; alternatively, insulin resistance can be responsible for the increased production of cytokines [13]. CRP is a sensitive but nonspecific marker of inflammation. High levels of CRP can be predictive markers for Met-S [14, 15] and cardiovascular disease [16, 17]. [18] have suggested that CRP could be used to identify those with risk in developing Met-S.

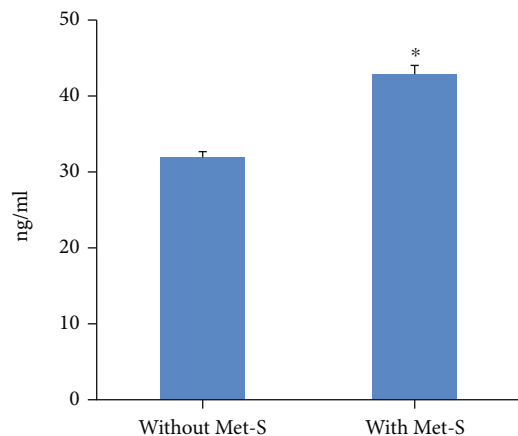


FIGURE 1: Serum levels of C-reactive protein (CRP) in subjects without Met-S ( $N = 1522$ ) and with Met-S ( $N = 488$ ). \* $P < 0.001$  using  $t$ -test.

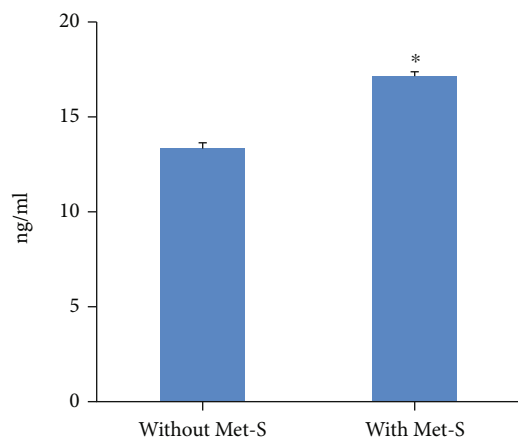


FIGURE 2: Serum levels of myeloperoxidase (MPO) in subjects without Met-S ( $N = 1522$ ) and with Met-S ( $N = 488$ ). \* $P < 0.001$  using  $t$ -test.

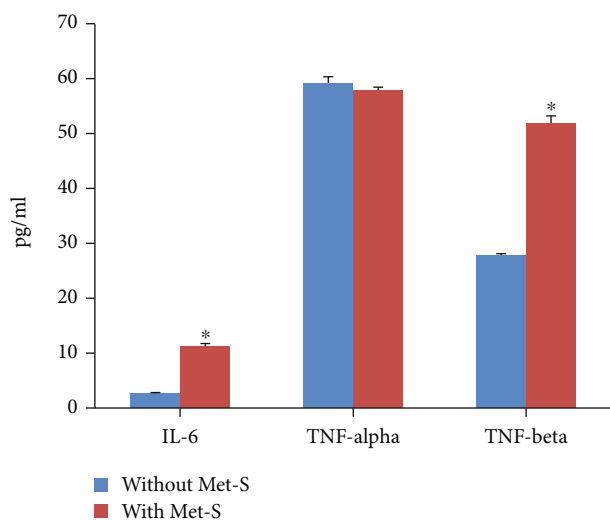


FIGURE 3: Serum levels of proinflammatory cytokines in subjects without Met-S ( $N = 1522$ ) and with Met-S ( $N = 488$ ). \* $P < 0.001$  using  $t$ -test.

TABLE 2: Correlations between serum biomarkers and components of metabolic syndrome.

	CRP	MPO	IL-6	TNF- $\alpha$	TNF- $\beta$
HDL	$R = 0.009$ $P = 0.673$	$R = -0.022$ $P = 0.316$	$R = 0.019$ $P = 0.395$	$R = 0.015$ $P = 0.502$	$R = 0.027$ $P = 0.223$
TG	$R = 0.077$ $P < 0.01$	$R = 0.116$ $P < 0.001$	$R = 0.222$ $P < 0.001$	$R = -0.159$ $P < 0.001$	$R = 0.181$ $P < 0.001$
FBG	$R = 0.024$ $P = 0.291$	$R = 0.109$ $P < 0.001$	$R = 0.171$ $P < 0.001$	$R = -0.076$ $P < 0.01$	$R = 0.125$ $P < 0.001$
Met-S	$R = 0.186$ $P < 0.01$	$R = 0.356$ $P < 0.001$	$R = 0.704$ $P < 0.001$	$R = -0.346$ $P < 0.001$	$R = 0.507$ $P < 0.001$
BP	$R = 0.077$ $P < 0.01$	$R = 0.169$ $P < 0.001$	$R = 0.333$ $P < 0.001$	$R = -0.163$ $P < 0.001$	$R = 0.263$ $P < 0.001$
BMI	$R = 0.088$ $P < 0.01$	$R = 0.153$ $P < 0.001$	$R = 0.371$ $P < 0.001$	$R = -0.167$ $P < 0.001$	$R = 0.251$ $P < 0.001$
Age	$R = 0.067$ $P < 0.01$	$R = 0.093$ $P < 0.01$	$R = 0.140$ $P < 0.001$	$R = -0.078$ $P < 0.01$	$R = 0.130$ $P < 0.001$

$R$  = correlation coefficient.

TABLE 3: Logistic regression analysis for the association between serum inflammatory markers and metabolic syndrome and other variables.

Biomarkers	Odd ratio (OR)	95% CI	$P$ value
Metabolic syndrome			
CRP	1.017	1.013-1.021	<0.01
MPO	1.207	1.176-1.239	<0.001
IL-6	3.967	3.258-4.831	<0.001
TNF- $\alpha$	0.865	0.848-0.882	<0.01
TNF- $\beta$	1.098	1.087-1.109	<0.01
Body mass index			
CRP	1.006	1.002-1.009	<0.01
MPO	1.064	1.044-1.085	<0.01
IL-6	1.355	1.300-1.412	<0.001
TNF- $\alpha$	0.949	0.935-0.962	<0.01
TNF- $\beta$	1.044	1.035-1.052	<0.01
Blood pressure			
CRP	1.006	1.002-1.010	<0.01
MPO	1.057	1.036-1.078	<0.01
IL-6	1.174	1.139-1.211	<0.001
TNF- $\alpha$	0.963	0.949-0.977	<0.01
TNF- $\beta$	1.028	1.020-1.035	<0.01
Fasting blood sugar			
CRP	1.004	1.00-1.008	<0.05
MPO	1.061	1.040-1.082	<0.01
IL-6	1.138	1.108-1.169	<0.001
TNF- $\alpha$	0.956	0.942-0.970	<0.01
TNF- $\beta$	1.025	1.018-1.032	<0.01

Myeloperoxidase (MPO) is a marker of neutrophil activation and systemic inflammation. Because MPO can diminish nitric oxide bioavailability that results in endothelial dysfunction [19, 20], it may be an active mediator of atherogenesis [21]. MPO levels have been reported to be higher in patients with coronary artery disease (CAD) and can predict future cardiovascular events, even after correction for traditional risk factors and CRP [22, 23]. Patients with CAD have reflected a strong correlation between increased risk of subsequent cardiovascular events and serum MPO levels [22, 24]. [25] have suggested that inflammatory activation precedes the onset of overt CAD by many years, and elevated MPO levels can predict the future risk of CAD in apparently healthy individuals.

The proinflammatory cytokines, IL-6, TNF- $\alpha$ , and TNF- $\beta$ , are secreted during an inflammatory response [7, 26, 27]. The procoagulant cytokine IL-6 is produced by several cell types, and it is a major source of plasma IL-6 [26, 28]. IL-6 plays several roles including acute phase inflammatory reaction, haematopoiesis, immunoglobulins secretion, and T and B cell cooperation function and regulation [26, 29, 30]. Higher levels of IL-6 have been reported in obesity, diabetes, and insulin resistance [26, 31–34]. [18] observed that IL-6 was one of the best markers of CAD risk prediction compared to other inflammatory biomarkers.

In our study, although the serum levels of TNF- $\beta$  were significantly higher in subjects with Met-S compared to subjects without Met-S, there was no difference in TNF- $\alpha$  levels between the two groups. The differences in the biological activity between TNF- $\alpha$  and TNF- $\beta$  are due to their different abilities for binding to the target cells [35]. The role of TNF- $\alpha$  in the development of obesity-related insulin resistance is still controversial. Metabolically triggered inflammation plays an important role in the pathogenesis of obesity-induced insulin resistance and type 2 diabetes mellitus [36, 37]. Previous studies have shown the detrimental effects of TNF- $\alpha$  on glucose and lipid metabolism as well as its involvement in  $\beta$ -cell apoptosis and endothelial dysfunction in diabetes [38–40]. On contrary, TNF- $\alpha$  neutralization in type 2 diabetes patients failed to affect insulin sensitivity [41, 42]. [43] noticed that despite improvements in inflammatory status, chronic TNF- $\alpha$  blockage did not improve insulin resistance or endothelial function in volunteers with obesity, insulin resistance, and Met-S.

In conclusion, serum levels of CRP, MPO, IL-6, and TNF- $\beta$  are significantly increased in young adults with Met-S, whereas no significant alteration was observed in TNF- $\alpha$ . This is probably the first study reporting TNF- $\beta$  levels in Met-S. We also observed a significantly high prevalence of obesity and hyperglycaemia in subjects with Met-S. An increase in fat tissue in subjects with obesity and/or insulin resistance in subjects with hyperglycaemia would result in low-grade systemic inflammation that could easily be monitored by inflammatory biomarkers well before the onset of cardiovascular disease.

## Data Availability

Data are available from the corresponding author upon reasonable request.

## Conflicts of Interest

The authors declare no conflicts of interest.

## Acknowledgments

The authors would like to thank all the medical and paramedical staff associated with this project for their excellent services. The statistical data analysis by Ms. Nasira Asghar of the Scientific Research Center, Medical Services Department, is gratefully acknowledged. This project was financially supported by the Advanced and Strategic Technologies Program of King Abdulaziz City for Science and Technology (KACST), Saudi Arabia (Grant No. 14-MED59-63).



## References

- [1] NCEP, “Third report of the National Cholesterol Education Program (NCEP) expert panel on detection, evaluation, and treatment of high blood cholesterol in adults (adult treatment panel III). Final report,” *Circulation*, vol. 106, no. 25, pp. 3143–3421, 2002.
- [2] H. A. Al-Shehri, A. K. Al-Asmari, H. A. Khan et al., “Recent trends of metabolic syndrome and its components in military recruits from Saudi Arabia,” *Medicine*, vol. 8, no. 11, p. 65, 2021.
- [3] H. A. Al-Shehri, A. K. Al-Asmari, H. A. Khan et al., “Association between preventable risk factors and metabolic syndrome,” *Open Medicine*, vol. 17, no. 1, pp. 341–352, 2022.
- [4] H. A. Khan, “Clinical significance of HbA1c as a marker of circulating lipids in male and female type 2 diabetic patients,” *Acta Diabetologica*, vol. 44, no. 4, pp. 193–200, 2007.
- [5] A. Sostaric, B. Jenko, N. R. Kozjek et al., “Detection of metabolic syndrome burden in healthy young adults may enable timely introduction of disease prevention,” *Archives of Medical Science*, vol. 15, no. 5, pp. 1184–1194, 2019.
- [6] A. M. James, Y. Collins, A. Logan, and M. P. Murphy, “Mitochondrial oxidative stress and the metabolic syndrome,” *Trends in Endocrinology & Metabolism*, vol. 23, no. 9, pp. 429–434, 2012.
- [7] Y. H. Lee and R. E. Pratley, “The evolving role of inflammation in obesity and the metabolic syndrome,” *Current Diabetes Reports*, vol. 5, no. 1, pp. 70–75, 2005.
- [8] G. P. Van Guilder, G. L. Hoetzer, J. J. Greiner, B. L. Stauffer, and C. A. DeSouza, “Influence of metabolic syndrome on biomarkers of oxidative stress and inflammation in obese adults,” *Obesity*, vol. 14, no. 12, pp. 2127–2131, 2006.
- [9] R. H. Eckel, S. M. Grundy, and P. Z. Zimmet, “The metabolic syndrome,” *The Lancet*, vol. 365, no. 9468, pp. 1415–1428, 2005.
- [10] B. Gustafson, A. Hammarstedt, C. X. Anderson, and U. Smith, “Inflamed adipose tissue,” *Arteriosclerosis, Thrombosis, and Vascular Biology*, vol. 27, no. 11, pp. 2276–2283, 2007.
- [11] WHO, *A Global Brief on Hypertension Silent Killer: Global Public Health Crisis*, World Health Organization, Geneva, Switzerland, 2013, [http://www.who.int/cardiovascular\\_diseases/publications/global\\_brief\\_hypertension/en](http://www.who.int/cardiovascular_diseases/publications/global_brief_hypertension/en).
- [12] International Diabetes Federation, “The IDF consensus worldwide definition of the metabolic syndrome,” [http://www.idf.org/metabolic\\_syndrome](http://www.idf.org/metabolic_syndrome).

- [13] J. Sutherland, B. McKinnley, and R. H. Eckel, "The metabolic syndrome and inflammation," *Metabolic Syndrome and Related Disorders*, vol. 2, no. 2, pp. 82–104, 2004.
- [14] M. Hassinen, T. Lakka, P. Komulainen, H. Gylling, A. Nissinen, and R. Rauramaa, "C-reactive protein and metabolic syndrome in elderly women," *Diabetes Care*, vol. 29, no. 4, pp. 931–932, 2006.
- [15] G. Sur, E. Floca, L. Kudor-Szabadi, M. L. Sur, D. Sur, and G. Samasca, "The relevance of inflammatory markers in metabolic syndrome," *Maedica*, vol. 9, no. 1, pp. 15–18, 2014.
- [16] H. A. Khan, A. S. Alhomida, S. H. Sobki, and M. A. Al, "Significant increases in monocyte counts and serum creatine kinase in acute myocardial infarction versus general infections," *Indian Journal of Pathology and Microbiology*, vol. 55, no. 4, pp. 474–477, 2012.
- [17] H. A. Khan, A. S. Alhomida, and S. H. Sobki, "Lipid profile of patients with acute myocardial infarction and its correlation with systemic inflammation," *Biomarker Insight*, vol. 8, 2013.
- [18] V. S. Rao, R. K. Nagaraj, S. Hebbagodi, N. B. Kadarinarasimhiah, and V. V. Kakkar, "Association of inflammatory and oxidative stress markers with metabolic syndrome in Asian Indians in India," *Cardiology Research and Practice*, vol. 2011, Article ID 295976, 8 pages, 2010.
- [19] H. M. Abu-Soud and S. L. Hazen, "Nitric oxide is a physiological substrate for mammalian peroxidases," *The Journal of Biological Chemistry*, vol. 275, no. 48, pp. 37524–37532, 2000.
- [20] J. A. Vita, M. L. Brennan, N. Gokce et al., "Serum myeloperoxidase levels independently predict endothelial dysfunction in humans," *Circulation*, vol. 110, no. 9, pp. 1134–1139, 2004.
- [21] S. J. Nicholls and S. L. Hazen, "Myeloperoxidase and cardiovascular disease," *Arteriosclerosis, Thrombosis, and Vascular Biology*, vol. 25, no. 6, pp. 1102–1111, 2005.
- [22] S. Baldus, C. Heeschen, T. Meinertz et al., "Myeloperoxidase serum levels predict risk in patients with acute coronary syndromes," *Circulation*, vol. 108, no. 12, pp. 1440–1445, 2003.
- [23] R. Zhang, M. L. Brennan, X. Fu et al., "Association between myeloperoxidase levels and risk of coronary artery disease," *JAMA*, vol. 286, no. 17, pp. 2136–2142, 2001.
- [24] A. Gómez García, M. Rivera Rodríguez, C. Gómez Alonso, D. Y. Rodríguez Ochoa, and A. C. Alvarez, "Myeloperoxidase is associated with insulin resistance and inflammation in overweight subjects with first-degree relatives with type 2 diabetes mellitus," *Diabetes and Metabolism Journal*, vol. 39, no. 1, pp. 59–65, 2015.
- [25] M. C. Meuwese, E. S. G. Stroes, S. L. Hazen et al., "Serum myeloperoxidase levels are associated with the future risk of coronary artery disease in apparently healthy individuals: the EPIC-Norfolk prospective population study," *Journal of the American College of Cardiology*, vol. 50, no. 2, pp. 159–165, 2007.
- [26] S. Kir, K. Ekiz, H. Alacam, R. Turkel, E. Koroglu, and B. L. Altintop, "The association between pro and anti-inflammatory markers with the components of metabolic syndrome," *Acta Endocrinologica (Bucharest)*, vol. 15, no. 4, pp. 430–435, 2019.
- [27] P. Trayhurn, "Endocrine and signalling role of adipose tissue: new perspectives on fat," *Acta Physiologica Scandinavica*, vol. 184, no. 4, pp. 285–293, 2005.
- [28] S. K. Fried, D. A. Bunkin, and A. S. Greenberg, "Omental and subcutaneous adipose tissues of obese subjects release interleukin-6: depot difference and regulation by glucocorticoid," *The Journal of Clinical Endocrinology and Metabolism*, vol. 83, no. 3, pp. 847–850, 1998.
- [29] P. M. Ridker and J. T. Willerson, "Inflammation as a cardiovascular risk factor," *Circulation*, vol. 109, pp. 2–10, 2004.
- [30] M. Santos-Rosa, J. Bienvenu, and J. Whicher, "Cytokines," in *Tietz Textbook of Clinical Chemistry*, C. A. Burtis and E. R. Ashwood, Eds., pp. 541–617, WB Saunders Company, Philadelphia, PA, USA, 3rd edition, 1999.
- [31] E. E. Kershaw and J. S. Flier, "Adipose tissue as an endocrine organ," *The Journal of Clinical Endocrinology and Metabolism*, vol. 89, no. 6, pp. 2548–2556, 2004.
- [32] O. P. Kristiansen and T. Mandrup-Poulsen, "Interleukin-6 and diabetes," *Diabetes*, vol. 54, Supplement 2, pp. S114–S124, 2005.
- [33] M. W. Rajala and P. E. Scherer, "Minireview: the adipocyte- at the crossroads of energy homeostasis, inflammation and atherosclerosis," *Endocrinology*, vol. 144, no. 9, pp. 3765–3773, 2003.
- [34] B. Vozarova, C. Weyer, K. Hanson, P. A. Tataranni, C. Bogardus, and R. E. Pratley, "Circulating interleukin-6 in relation to adiposity, insulin action, and insulin secretion," *Obesity Research*, vol. 9, no. 7, pp. 414–417, 2001.
- [35] R. Kircheis, J. Milleck, V. G. Korobko, L. N. Shingarova, and H. E. Schmidt, "Differences in the biological activity of TNF alpha and TNF beta correlate with their different abilities for binding to the target cells," *European Cytokine Network*, vol. 3, no. 4, pp. 381–390, 1992.
- [36] H. E. Bays, J. M. González-Campoy, G. A. Bray et al., "Pathogenic potential of adipose tissue and metabolic consequences of adipocyte hypertrophy and increased visceral adiposity," *Expert Review of Cardiovascular Therapy*, vol. 6, no. 3, pp. 343–368, 2008.
- [37] A. Pradhan, "Obesity, metabolic syndrome, and type 2 diabetes: inflammatory basis of glucose metabolic disorders," *Nutrition Reviews*, vol. 65, 12, Part 2, pp. S152–S156, 2007.
- [38] P. Dandona, R. Weinstock, K. Thusu, E. Abdel-Rahman, A. Aljada, and T. Wadden, "Tumor necrosis factor alpha in sera of obese patients: fall with weight loss," *The Journal of Clinical Endocrinology and Metabolism*, vol. 83, no. 8, pp. 2907–2910, 1998.
- [39] G. S. Hotamisligil, "The role of TNF $\alpha$  and TNF receptors in obesity and insulin resistance," *Journal of Internal Medicine*, vol. 245, no. 6, pp. 621–625, 1999.
- [40] S. Zhang and K. H. Kim, "TNF-alpha inhibits glucose-induced insulin secretion in a pancreatic beta-cell line (INS-1)," *FEBS Letters*, vol. 377, no. 2, pp. 237–239, 1995.
- [41] H. Dominguez, H. Storgaard, C. Rask-Madsen et al., "Metabolic and vascular effects of tumor necrosis factor-alpha blockade with etanercept in obese patients with type 2 diabetes," *Journal of Vascular Research*, vol. 42, no. 6, pp. 517–525, 2005.
- [42] N. Paquot, M. J. Castillo, P. J. Lefèbvre, and A. J. Scheen, "No increased insulin sensitivity after a single intravenous administration of a recombinant human tumor necrosis factor receptor: Fc fusion protein in obese insulin-resistant patients," *The Journal of Clinical Endocrinology and Metabolism*, vol. 85, no. 3, pp. 1316–1319, 2000.
- [43] T. C. Wascher, J. H. N. Lindeman, H. Sourij, T. Kooistra, G. Pacini, and M. Roden, "Chronic TNF- $\alpha$  neutralization does not improve insulin resistance or endothelial function in "healthy" men with metabolic syndrome," *Molecular Medicine*, vol. 17, no. 3-4, pp. 189–193, 2011.

## Research Article

# Visfatin Amplifies Cardiac Inflammation and Aggravates Cardiac Injury via the NF- $\kappa$ B p65 Signaling Pathway in LPS-Treated Mice

Yewen Hu,<sup>1,2</sup> Nan Wu,<sup>1,2</sup> Weiping Du,<sup>1,2</sup> Shuangshuang Wang,<sup>3</sup> Jian Wang,<sup>1,2</sup>  
Chaoxia Zhang,<sup>1,2</sup> Xiaomin Chen ,<sup>1,2</sup> and Caijie Shen <sup>1,2</sup>

<sup>1</sup>Department of Cardiology, Ningbo First Hospital, Ningbo, 315000 Zhejiang Province, China

<sup>2</sup>Key Laboratory of Precision Medicine for Atherosclerotic Diseases of Zhejiang Province, Ningbo, 315000 Zhejiang Province, China

<sup>3</sup>Department of Cardiology, Wenling First People's Hospital, The Affiliated Wenling Hospital of Wenzhou Medical University, Wenling, 317500 Zhejiang Province, China

Correspondence should be addressed to Xiaomin Chen; [chxmin@hotmail.com](mailto:chxmin@hotmail.com) and Caijie Shen; [shenzihai1101@126.com](mailto:shenzihai1101@126.com)

Received 19 July 2022; Revised 9 August 2022; Accepted 8 September 2022; Published 10 October 2022

Academic Editor: Simon Kennedy

Copyright © 2022 Yewen Hu et al. This is an open access article distributed under the Creative Commons Attribution License, which permits unrestricted use, distribution, and reproduction in any medium, provided the original work is properly cited.

**Background.** Visfatin is an adipocytokine that has been demonstrated to be involved in cardiovascular diseases. This study aims at determining the role of visfatin in sepsis-induced cardiac injury and identify its possible mechanisms. **Methods.** Dynamic changes in visfatin expression in mice with lipopolysaccharide- (LPS-) induced septicemia were measured. Additionally, mice were pretreated with visfatin and further administered LPS to observe the effects of visfatin on cardiac injury. Finally, septic mice were also pretreated with JSH-23 to investigate whether visfatin regulates cardiac injury via the NF- $\kappa$ B p65 pathway. **Results.** Visfatin expression levels in both the heart and serum were increased in LPS-treated mice and peaked at 6 hours, and visfatin was derived from cardiac macrophages. In septic mice, pretreatment with visfatin reduced the survival rate, worsened cardiac dysfunction, and increased the expression of cardiac injury markers, including creatine kinase myocardial bound (CK-MB) and lactate dehydrogenase (LDH). Treatment with visfatin also increased the infiltration of CD3+ cells and F4/80+ cells, amplified the cardiac inflammatory response, and elevated myocardial cell apoptosis. Treatment with JSH-23 reversed the effects of visfatin in septic mice. **Conclusions.** This study showed that visfatin amplifies the cardiac inflammatory response and aggravates cardiac injury through the p65 signaling pathway. Visfatin may be a clinical target for preventing cardiac injury in sepsis.

## 1. Introduction

Sepsis is a systemic inflammatory syndrome caused by infection, and patients who do not receive timely treatment can progress to multiple organ failure [1, 2]. Among the complications observed in septic patients, cardiac injury and subsequent cardiac dysfunction are the most serious, and the mortality is extremely high and may reach 90% [3]. Therefore, it is beneficial to find new intervention methods to improve cardiac injury and cardiac dysfunction in the treatment of patients with sepsis.

Visfatin, which is considered a secreted adipokine and was first discovered and subsequently isolated in 2005, can be expressed in tissues and organs of many mammals [4]. Visfatin is mainly released by adipocytes, macrophages,

and skeletal muscle cells through the endoplasmic reticulum or microvesicles [4, 5]. A variety of pathological conditions, including aging, oxidative stress, a high-fat diet and inflammatory responses, can promote the release of visfatin, and macrophages are the main source of visfatin in inflammatory environments [6–9].

Previous studies also showed that visfatin is closely related to cardiovascular diseases. Downregulation of visfatin expression can significantly improve endothelial dysfunction and inhibit the inflammatory response, thus reducing the aortic plaque area in ApoE<sup>-/-</sup> mice, while treatment with exogenous visfatin aggravated the inflammatory response and promoted the progression of atherosclerosis [10–12]. Circulating levels of visfatin were increased in patients with acute myocardial infarction, and elevated

TABLE 1: Primers used in this study.

Genes	Forward primer (5' → 3')	Reverse primer (5' → 3')
Visfatin	AATGTCTCCTTCGGTCTGG	CCGCTGGTGCCTATGTA AAA
MCP-1	CTTCTGTGCTGCTGCTCAT	CGGAGTTTGGGTTTGCTTGTC
TNF- $\alpha$	CCCAGGGACCTCTCTAATC	ATGGGCTACAGGCTTGCTCACT
IFN- $\gamma$	ACTGGCAAAAGGATGGTGAC	TGAGCTCATTGAATGCTTGG
IL-1 $\beta$	GGGCCTCAAAGGAAAGAATC	TACCAGTTGGGGA AACTCTGC
IL-6	AGTTGCCTTCTTGGGACTGA	TCCACGATTTCCCAGAGAAC
IL-12	AGTTTGGCCAGGGTCATTCC	TCTCTGGCCGTCTTACCAT
IL-17	TCCAGAAGGCCCTCAGACTA	AGCATCTTCTCGACCCTGAA
IL-18	ATGCTTTCTGGACTCCTGCC	GTCTGGTCTGGGGTTC ACTG
GAPDH	AAC TTTGGCATTGTGGAAGG	CACATTGGGGGTAGGAACAC

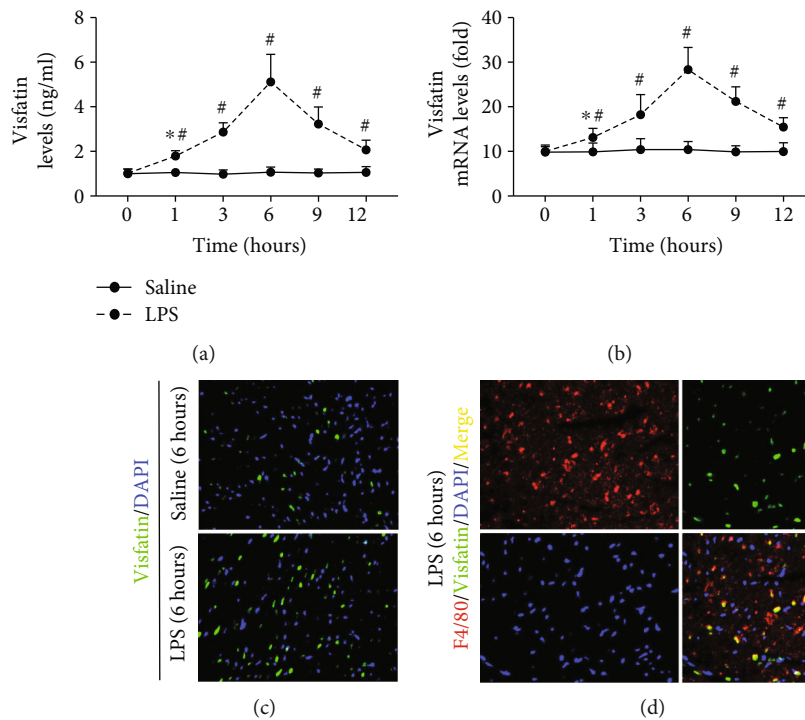


FIGURE 1: Expression of visfatin in septic mice. (a and b) Dynamic changes in visfatin levels in the serum and heart were detected in mice with LPS-induced septicemia. (c) Cardiac visfatin expression was detected in saline- and LPS-treated mice (200 $\times$ ). (d) Visfatin expression in cardiac macrophages was detected (200 $\times$ ).  $N = 5$  in each group. \* $p < 0.05$  vs. the saline group. # $p < 0.05$  vs. the previous group.

visfatin expression suggested a higher incidence of major adverse cardiovascular events [13]. In addition, visfatin is highly expressed in patients with refractory hypertension, and its expression level is positively correlated with the severity of left ventricular hypertrophy [14]. Nevertheless, the role of visfatin in sepsis-induced cardiac injury remains unknown. In this study, the role of visfatin in cardiac injury and the possible mechanisms were investigated in septic mice.

## 2. Methods and Materials

**2.1. Mice and Mouse Septicemia Models.** Wild-type male C57BL/6J mice (WT, GemPharmatech, China) aged 9-10

weeks were used in this study. First, WT mice were intraperitoneally (IP) injected with lipopolysaccharide (LPS, 10 mg/kg, Sigma) or saline, and visfatin expression at different time points and in samples was measured. Second, WT mice were pretreated with PBS or visfatin (100  $\mu$ g/kg, Adipo Bioscience) for 30 minutes [15] and then IP injected with LPS or saline for 6 hours; the effects of cardiac injury were detected in each group. Some of the mice above were observed for 8 days, and the mortality rates were recorded. Finally, they were pretreated with PBS + JSH-23 (3 mg/kg) [16], visfatin+JSH-23, DMSO+PBS, or DMSO+visfatin for 30 minutes, and then all mice received LPS for 6 hours. Some mice were followed up for 8 days to observe the survival rate.

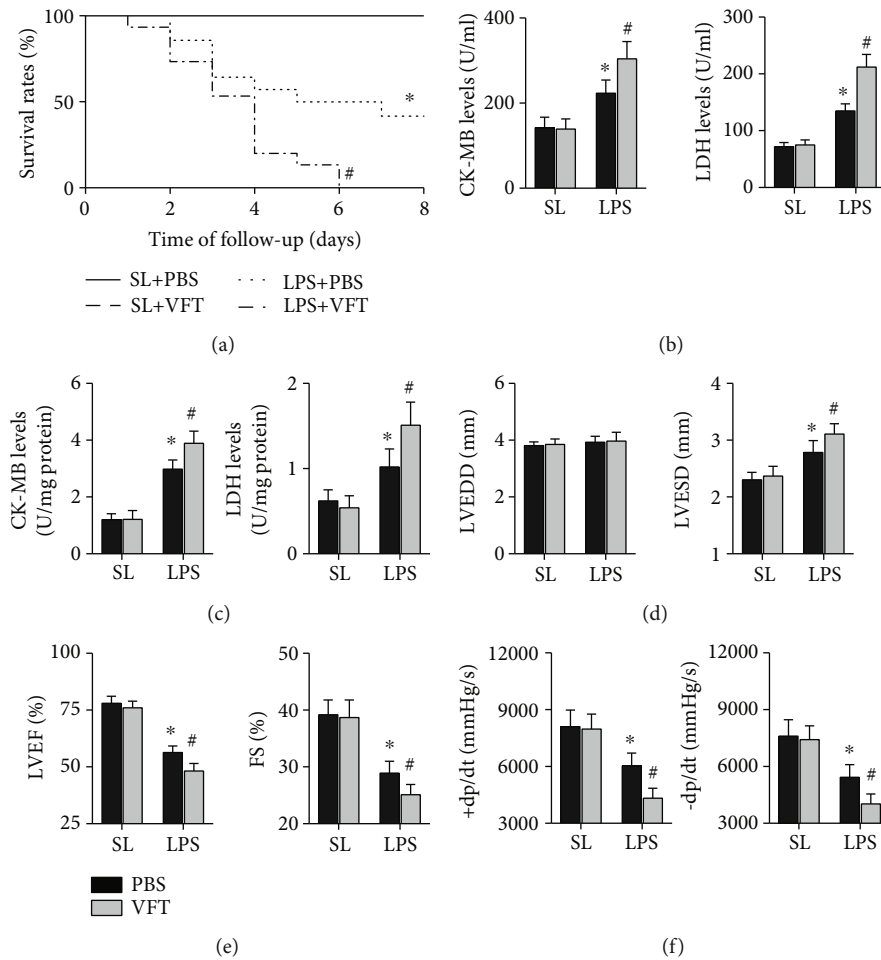


FIGURE 2: Effects of visfatin on LPS-induced cardiac injury in mice. (a) The survival rates in the four groups were analyzed during follow up;  $N = 10 - 15$  in each group. (b and c) The expression levels of CK-MB and LDH in both the serum and heart were examined. (d-f) LVEDD, LVESD, LVEF, FS, +dp/dt max, and -dp/dt max in each group were detected.  $N = 5 - 10$  in each group. \* $p < 0.05$  vs. the saline + PBS group. # $p < 0.05$  vs. the LPS + PBS group. SL means saline; VFT means visfatin.

The mice were euthanized at the end of the treatment, and then the blood and heart were collected separately. The supernatant was obtained after the blood samples were centrifuged at  $3000 \times g$  for 15 minutes and stored in liquid nitrogen. The heart samples were divided into two parts and stored in 4% paraformaldehyde on liquid nitrogen. This study was approved by the Institutional Animal Care and Use Committee of our hospital (approval NO. cardiac 20200123a).

**2.2. Detection of Cardiac Function.** Both echocardiography and hemodynamics were used to evaluate the cardiac function of each mouse. After the mice were IP injected with LPS or saline for 6 hours, they were anesthetized with 1.5% isoflurane and then placed flat on the operating table. Echocardiography with a 10-MHz linear array ultrasound transducer that included a MyLab 30CV ultrasound system (Esaote SpA, Italy) was used to obtain information on the left ventricle end-diastolic diameter (LVEDD), left ventricle end-systolic diameter (LVESD), left ventricle ejection fraction (LVEF), and fractional shortening (FS). Then, a microtip catheter transducer (Millar, Inc., USA) was inserted into the left ventricle via the right carotid artery, and the maximal

slope values of the systolic pressure increment (+dp/dt) and diastolic pressure decrement (-dp/dt) were recorded using a Millar PressureVolume system (Millar, Inc.).

**2.3. Detection of mRNA Expression Levels.** The left ventricular tissue was removed from liquid nitrogen, ground into a powder, and then extracted with TRIzol Reagent (Roche). After the total RNA was collected, the concentration was determined, and  $2 \mu\text{g}$  of total RNA was used to synthesize cDNA using a reverse transcription kit (Roche) according to the manufacturer's instructions. Then, the cDNA was used to perform PCR amplification with LightCycler 480 SYBR Green Master Mix (Roche) to detect the expression levels of target mRNAs, including visfatin, monocyte chemoattractant protein-1 (MCP-1), tumor necrosis factor- $\alpha$  (TNF- $\alpha$ ), interferon- $\gamma$  (IFN- $\gamma$ ), IL-1 $\beta$ , IL-6, IL-12, IL-17, and IL-18, in each group; the expression levels of target mRNAs were measured and normalized to GAPDH mRNA levels. The primers used are listed in Table 1.

**2.4. Analysis of NF- $\kappa$ B p65 Pathway Phosphorylation.** Left ventricular tissue was lysed using radioimmunoprecipitation

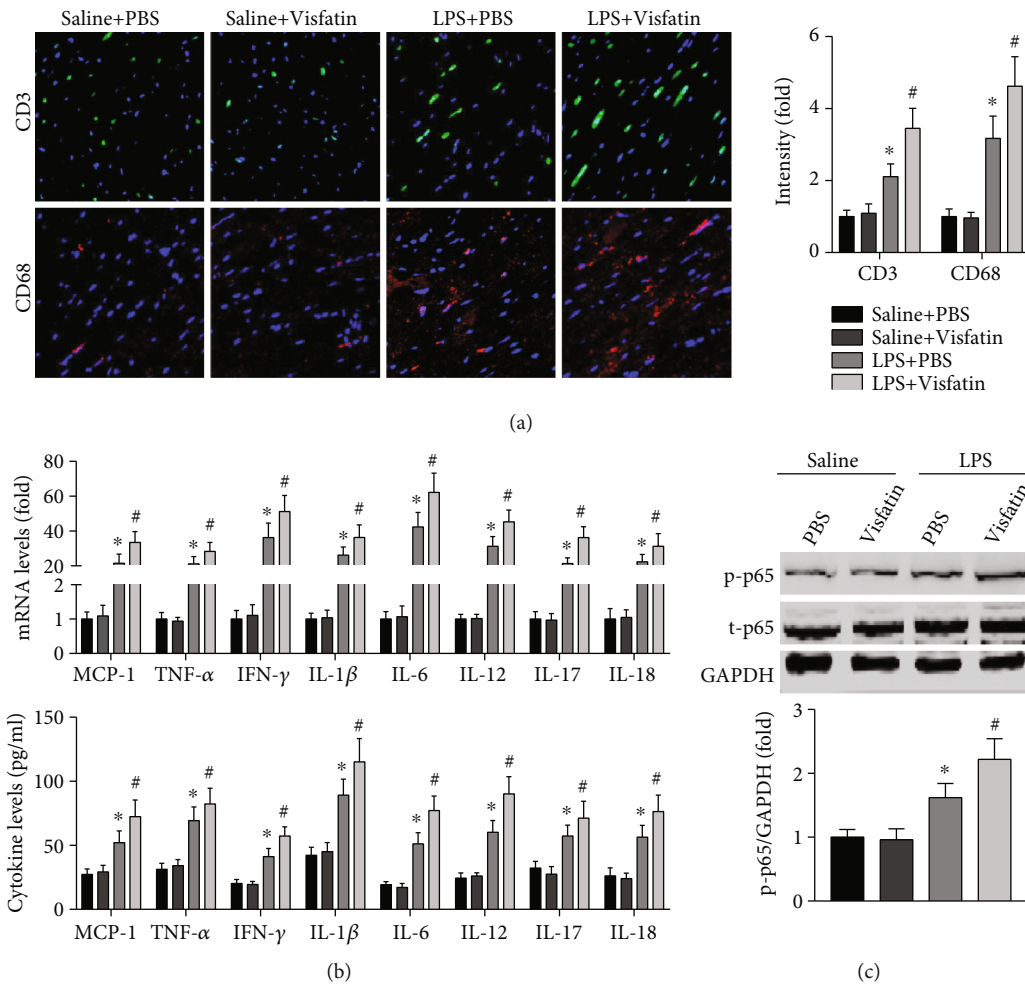


FIGURE 3: Effects of visfatin on cardiac inflammation in LPS-treated mice. (a) Cardiac CD3<sup>+</sup> cells and CD68<sup>+</sup> cells in the four groups were examined. (b) The expression of MCP-1, TNF- $\alpha$ , IFN- $\gamma$ , IL-1 $\beta$ , IL-6, IL-12, IL-17, and IL-18 in the heart and serum was detected. (c) The activation of the NF- $\kappa$ B p65 pathway was measured.  $N = 5 - 6$  in each group. \* $p < 0.05$  vs. the saline + PBS group. # $p < 0.05$  vs. the LPS + PBS group.

assay lysis buffer, and then the supernatant was collected as total protein. The concentration of each sample was determined using a BCA Protein Assay Kit (Thermo Fisher Scientific) and then quantified to the same concentration. Then, approximately 45  $\mu$ g of total protein was used to perform electrophoresis on Laemmli sodium dodecyl sulfate (SDS) polyacrylamide gels to separate proteins of different molecular weights. After transfer to Immobilon-FL PVDF membranes (Millipore), the membranes were blocked with 5% nonfat milk and then incubated with anti-NF- $\kappa$ B p65, anti-NF- $\kappa$ B p65, anti-cleaved caspase3, anti-Bcl2, and anti-GAPDH (all purchased from Abcam) antibodies at 4°C overnight. Then, the membranes were incubated with secondary antibodies and scanned using the Odyssey (LI-COR Biosciences).

**2.5. Measurement of Visfatin, Cardiac Injury Markers, and Inflammatory Cytokines.** The serum and the total protein collected from the left ventricle were diluted; mouse visfatin enzyme-linked immunosorbent assay (ELISA) kits were

used to detect circulating and cardiac visfatin levels, and creatine kinase myocardial bound (CK-MB) assay kits and lactate dehydrogenase (LDH) assay kits were used to detect CK-MB and LDH expression in both serum and supernatant. In addition, the expression levels of MCP-1, TNF- $\alpha$ , IFN- $\gamma$ , IL-1 $\beta$ , IL-6, IL-12, IL-17, and IL-18 in the serum were also detected using ELISA kits. All experimental procedures were carried out in accordance with the manufacturer's instructions.

**2.6. Histological Analysis.** The heart tissue was fixed with 4% paraformaldehyde for two days, embedded in paraffin, cut into 4-6  $\mu$ m sections, and further mounted on slides. Slides were incubated with mouse anti-visfatin, mouse anti-CD3, and anti-CD68 antibodies (all three purchased from Gene-Tex, USA) to determine the cardiac abundance of visfatin, T lymphocytes, and macrophages. Some of the slides were incubated with both anti-visfatin and anti-F4/80 antibodies to determine whether visfatin is secreted by cardiac macrophages. Apoptosis of myocardial cells was measured using



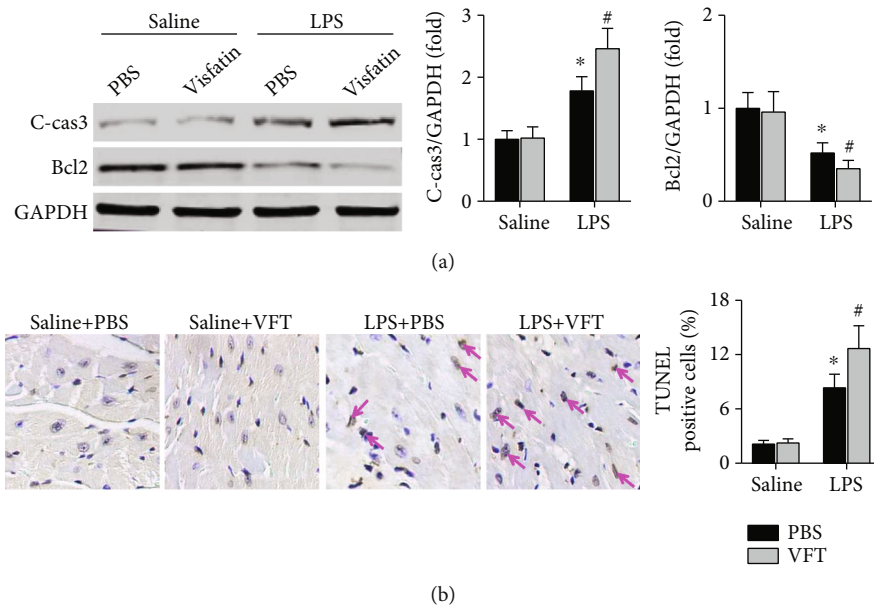


FIGURE 4: Effects of visfatin on LPS-induced myocardial cell apoptosis in mice. (a) The expression of cleaved caspase3 and Bcl2, apoptosis-related proteins, was detected. (b) TUNEL-positive cells were examined.  $N = 5 - 6$  in each group. \* $p < 0.05$  vs. the saline + PBS group. # $p < 0.05$  vs. the LPS + PBS group. VFT means visfatin.

terminal deoxynucleotidyl transferase-mediated dUTP nick end labeling (TUNEL) staining kits (Millipore, USA) according to the manufacturer's instructions.

**2.7. Data Analysis.** Data in this study are expressed as the mean  $\pm$  SD, and all data were analyzed using GraphPad Prism 7. Student's  $t$ -test was performed to analyze differences in the means of 2 groups, and one-way and two-way ANOVA was used to evaluate differences among 3 or more groups. Survival rates during the 8-day follow up were analyzed using the log-rank test.  $p < 0.05$  was considered statistically significant.

### 3. Results

**3.1. Visfatin Levels Are Increased in Septic Mice.** The ELISA results showed that compared with the saline group, treatment with LPS increased serum visfatin levels by hour 1; visfatin levels continued to increase at hour 3, peaked by hour 6, and then gradually decreased by hour 9 and hour 12 (Figure 1(a)). Similar trends in cardiac visfatin mRNA levels were observed (Figure 1(b)). The immunofluorescence staining data also showed that treatment with LPS for 6 hours significantly increased visfatin expression in cardiac macrophages (Figures 1(c) and 1(d)).

**3.2. Visfatin Aggravates LPS-Induced Cardiac Injury in Mice.** At the 8-day follow up, pretreatment with visfatin significantly increased mortality in mice with LPS-induced septicemia (Figure 2(a)). Visfatin exhibited increased expression levels in both the serum and heart in LPS-treated mice (Figures 2(b) and 2(c)). In addition, septic mice that received visfatin exhibited aggravation of cardiac dysfunction, with further increases in LVESD and further decreases in LVEF,

FS, +dp/dt, and -dp/dt, although no effects on LVEDD were observed (Figures 2(d)–2(f)).

**3.3. Visfatin Amplifies Cardiac Inflammation in LPS-Treated Mice.** Immunofluorescence staining showed that the infiltration of both CD3+ cells and CD68+ cells into the heart was significantly increased (Figure 3(a)). In addition, the mRNA and protein expression levels of inflammation-related factors, including MCP-1, TNF- $\alpha$ , IFN- $\gamma$ , IL-1 $\beta$ , IL-6, IL-12, IL-17, and IL-18, in the heart and serum were significantly increased by visfatin treatment in LPS-treated mice (Figure 3(b)). Visfatin also further elevated NF- $\kappa$ B p65 pathway phosphorylation induced by LPS (Figure 3(c)).

**3.4. Treatment with Visfatin Increases LPS-Induced Myocardial Cell Apoptosis in Mice.** Cardiac expression of cleaved caspase3, a proapoptotic protein, was increased in visfatin-pretreated septic mice compared with septic mice, while the expression of the proapoptotic protein Bcl2 was decreased (Figure 4(a)). Visfatin further increased the percentage of TUNEL-positive cells in LPS-treated mice, which indicated apoptotic myocardial cells (Figure 4(b)).

**3.5. Inhibition of the NF- $\kappa$ B p65 Pathway Improves Cardiac Dysfunction in Visfatin-Treated Septic Mice.** The mortality rate of visfatin-treated septic mice was significantly reduced by JSH-23, an inhibitor of the NF- $\kappa$ B p65 pathway (Figure 5(a)). The visfatin-mediated increase in cardiac injury markers, including CK-MB and LDH, in both the heart and serum was reversed by JSH-23 (Figures 5(b) and 5(c)). The effects of visfatin on the aggravation of LPS-induced cardiac dysfunction were also significantly improved after administration of JSH-23 (Figures 5(d)–5(f)).

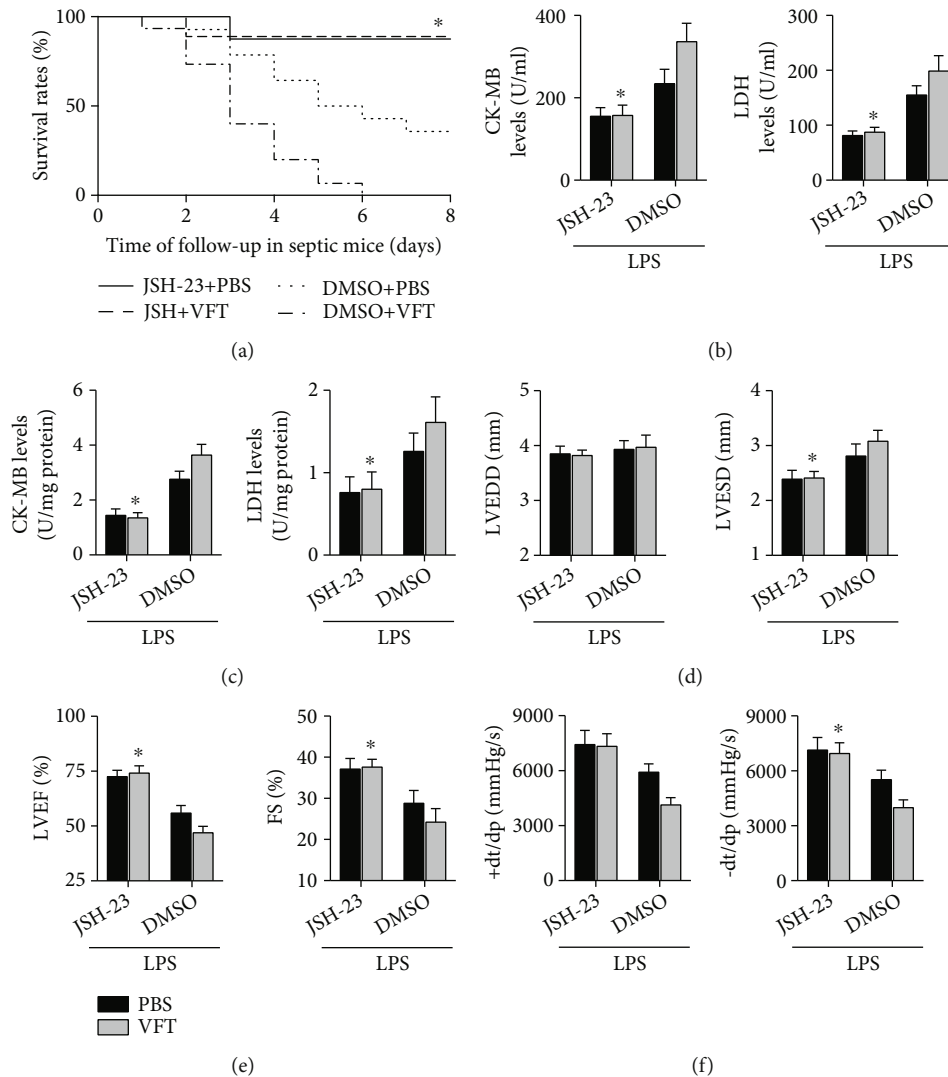


FIGURE 5: Effects of JSH-23 on LPS-induced cardiac injury and dysfunction in mice. (a) The effects of JSH-23 on the survival rates of visfatin-treated septic mice were measured,  $N = 10 - 15$  in each group. (b and c) Cardiac injury markers in the serum and heart were measured. (d-f) Cardiac structure and function in each group were measured.  $N = 5 - 10$  in each group. \* $p < 0.05$  vs. the LPS + DMSO + VFT group. VFT means visfatin.

**3.6. JSH-23 Alleviates the Cardiac Inflammatory Response and Myocardial Cell Apoptosis.** Treatment with JSH-23 decreased the activation of the NF- $\kappa$ B p65 pathway in visfatin-treated septic mice (Figure 6(a)). The expression levels of MCP-1, TNF- $\alpha$ , IFN- $\gamma$ , IL-1 $\beta$ , IL-6, IL-12, IL-17, and IL-18 were all decreased in both the heart and serum in septic mice treated with JSH-23 compared with those not treated with JSH-23 (Figure 6(b)). Fewer apoptotic cells were observed when JSH-23 was administered to visfatin-treated septic mice (Figure 6(c)).

#### 4. Discussion

As an important adipokine, visfatin has been demonstrated to be involved in the processes of a variety of cardiovascular diseases, while its role in cardiac injury in sepsis has not been reported. In this study, we found that visfatin expression was elevated in septic mice, and that visfatin may be secreted by

macrophages. Treatment with visfatin exacerbates cardiac inflammation and aggravates cardiac injury and cardiac dysfunction. These effects are reversed when the NF- $\kappa$ B p65 pathway is inhibited by JSH-23. Our study found that visfatin may amplify cardiac inflammation through the NF- $\kappa$ B p65 pathway and aggravate LPS-induced cardiac injury. Visfatin may be a potential target for the prevention of cardiac injury in sepsis in the clinic.

LPS is an important pathogenic factor in sepsis that can cause damage to a variety of tissues and organs, and its process can be regulated by visfatin. Yao et al. reported that immune cell infiltration and splenic cell apoptosis were significantly increased after LPS administration but were further aggravated after visfatin treatment [17]. Xiao et al. found that visfatin further aggravates LPS-mediated periodontal injury, exacerbates periodontitis symptoms and affects prognosis [18]. In addition, treatment with visfatin can aggravate LPS-induced intestinal injury in both rats

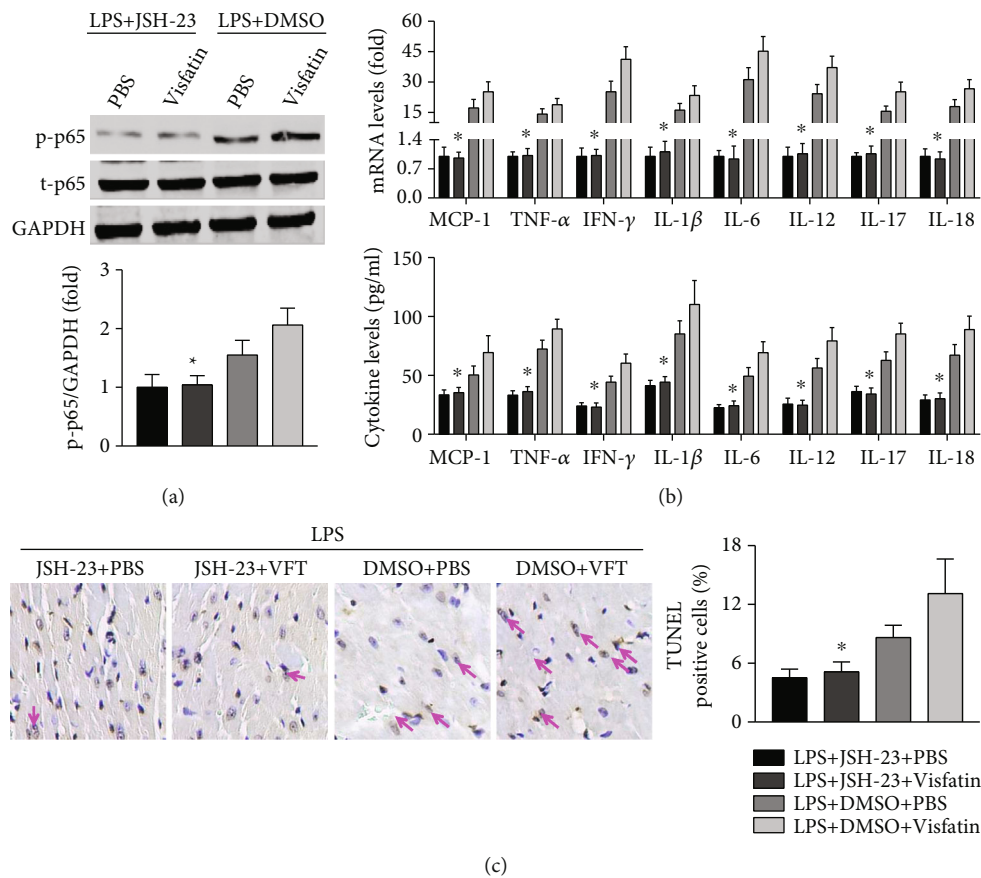


FIGURE 6: Effects of JSH-23 on cardiac inflammation and myocardial cell apoptosis. (a) Phosphorylation of NF- $\kappa$ B p65 pathway components was detected. (b) Inflammatory mediators in the heart and serum were examined. (c). The numbers of TUNEL-positive myocardial cells were quantified.  $N = 5 - 10$  in each group. \* $p < 0.05$  vs. the LPS + DMSO + VFT group.

and mice [19, 20]. These studies suggest that visfatin may aggravate LPS-induced tissue damage. In another study, Luo et al. reported that visfatin treatment unexpectedly alleviated LPS-induced acute lung injury [15]. The reason for the inconsistent results may be related to different organs. In this study, we examined the regulatory effect of visfatin on septic cardiac injury and found that visfatin further increased the mortality of mice, upregulated the expression of markers of myocardial injury in both the serum and heart, and worsened cardiac dysfunction. These results suggest that visfatin exacerbates LPS-induced cardiac injury.

Various pathological effects, such as the inflammatory response, oxidative stress, calcium overload, and ferroptosis, are involved in the development of LPS-induced tissue damage [1, 21]. Due to the poor tolerance of cardiomyocytes to the inflammatory response, an enhanced inflammatory response can activate programmed death mechanisms in cardiomyocytes, including caspase-dependent and caspase-independent pathways, leading to cardiomyocyte death and cardiac dysfunction [1]. Therefore, inflammation plays a crucial role in sepsis-induced cardiac injury. Visfatin can lead to insulin resistance, which results in the progression of diabetes, affecting lipid metabolism, which is associated with the development of obesity and the invasion of immune cells into tissues, leading to an increased inflammatory

response [15, 20, 22]. It has been widely reported that visfatin participates in sepsis-induced tissue injury by regulating the inflammatory response [1, 20–22]. Previous studies have found that the activation of hepatic stellate cells and the regulation of breast cancer by visfatin are mediated by macrophages [23, 24]. Reduction of visfatin expression can significantly reduce T lymphocyte activation, thereby improving spinal cord injury and reducing the disability rate [25]. In rheumatic diseases, visfatin can aggravate Th1/Th2 imbalance, thereby promoting disease progression and joint injury [26]. These studies suggest that both macrophages and T lymphocytes are downstream signals of visfatin and mediate the regulatory effect of visfatin on inflammatory responses. Therefore, to explain the mechanism by which visfatin regulates cardiac injury in LPS-treated mice, the regulation of inflammation by visfatin was measured. The infiltration of inflammatory cells into the heart was first detected, and the results showed that the expression of both CD3+ T lymphocytes and F4/80+ macrophages was significantly increased. The levels of inflammatory mediators were further examined, and we found that treatment with visfatin further increased the expression of a variety of proinflammatory factors. These results suggest that visfatin is involved in the regulation of sepsis-induced cardiac injury by regulating the inflammatory response.

NF- $\kappa$ B p65 is an important intracellular nuclear transcription factor, and phosphorylation is its activation mode, mainly involved in the immune response, stress response and regulation of apoptosis and other biological effects. An increasing number of studies have confirmed that NF- $\kappa$ B p65 can regulate the infiltration and differentiation of various immune cells, including macrophages and lymphocytes, into tissues and magnify the inflammatory response to participate in the regulation of tissue injury.

An increasing number of studies have confirmed that visfatin is closely related to the NF- $\kappa$ B p65 signaling pathway. In a previous study, Wang et al. found that activation of the NF- $\kappa$ B p65 signaling pathway releases IL-6 and promotes metastasis of osteosarcoma cells [27]. Kanda et al. reported that the phosphorylation of NF- $\kappa$ B p65 signaling may mediate the release of CXC chemokine ligand 8 (CXCL8), CXCL10, and CXCL20 in the presence of visfatin, which is associated with cuticle formation [28]. Decreased visfatin expression downregulated the activation of the NF- $\kappa$ B p65 pathway, and cell invasiveness was significantly reduced [29]. In addition, administration of visfatin also further activated the NF- $\kappa$ B p65 signaling pathway in LPS-treated mice and cells [30, 31]. These studies suggest that the NF- $\kappa$ B p65 pathway may be an important downstream signal of visfatin and that the NF- $\kappa$ B p65 pathway may regulate LPS-induced cardiac injury and cardiac dysfunction.

To confirm the above speculation, the small molecule compound JSH-23, a specific inhibitor of the NF- $\kappa$ B p65 signaling pathway that was reported in a previous study, was administered to visfatin-treated septic mice. The results showed that treatment with JSH-23 significantly reduced mortality rates in septic mice pretreated with visfatin at the 8-day follow up. In addition, the expression levels of cardiac injury markers and cardiac dysfunction were also reversed in mice treated with JSH-23. These results suggest that JSH-23 reverses the regulatory effect of visfatin on cardiac injury and cardiac dysfunction induced by LPS. At the same time, the phosphorylation level of NF- $\kappa$ B p65 was decreased; the levels of inflammatory markers in both the heart and serum were reduced significantly, and myocardial cell apoptosis was alleviated, suggesting that JSH-23 improved the cardiac inflammatory response and myocardial apoptosis. These results suggest that the regulatory effect of visfatin on sepsis-induced cardiac injury and cardiac dysfunction is mediated by the NF- $\kappa$ B p65 pathway. NF- $\kappa$ B p65 pathway has been reported to play an important role in the regulation of inflammatory response, and its activation can promote the release of a variety of proinflammatory factors. Therefore, the expression of a variety of cardiac injury related proinflammatory factors, including MCP-1, TNF- $\alpha$ , IFN- $\gamma$ , IL-1 $\beta$ , IL-6, IL-12, IL-17, and IL-18, were detected; the results showed that treatment with visfatin further increased these cytokines expression in LPS-induced septic mice, and these effects were abolished by JSH-23. These results suggest that visfatin may be involved in the regulation of inflammatory response through the NF- $\kappa$ B p65 pathway.

In summary, we found that visfatin may further activate the NF- $\kappa$ B p65 pathway to amplify the inflammatory response, promote myocardial cell apoptosis, and aggravate

cardiac injury and cardiac dysfunction. Visfatin may be a potential target for interventions for sepsis-induced cardiac injury.

## Data Availability

Our data is available to scientific researchers except for commercial purposes.

## Conflicts of Interest

The authors declare no potential conflict of interest.

## Authors' Contributions

Yewen Hu and Nan Wu contributed equally to this work.

## Acknowledgments

This work was supported by the Funding of the Plan of Science and Technology on Medical and Health in Zhejiang Province (Grant No. 2021KY1002); the Natural Science Foundation of Ningbo (Grant No. 2021J266); the Ningbo Province Public Welfare Project (Grant No. 20211JCGY020364); the Key Laboratory of Precision Medicine for Atherosclerotic Diseases of Zhejiang Province (Grant No. 2022E10026); the National Natural Science Foundation of China (Grant No. 81900441); the Natural Science Foundation of Zhejiang Province (Grant No. LQ19H020002).

## References

- [1] C. Lelubre and J. L. Vincent, "Mechanisms and treatment of organ failure in sepsis," *Nature Reviews. Nephrology*, vol. 14, no. 7, pp. 417–427, 2018.
- [2] Y. Huang, G. Wang, and T. Peng, "Calpain activation and organ failure in sepsis: molecular insights and therapeutic perspectives," *Shock*, vol. 56, no. 1, pp. 5–15, 2021.
- [3] A. Arfaras-Melainis, E. Polyzogopoulou, F. Triposkiadis et al., "Heart failure and sepsis: practical recommendations for the optimal management," *Heart Failure Reviews*, vol. 25, no. 2, pp. 183–194, 2020.
- [4] A. Estienne, A. Bongrani, M. Reverchon et al., "Involvement of novel adipokines, chemerin, visfatin, resistin and apelin in reproductive functions in normal and pathological conditions in humans and animal models," *International Journal of Molecular Sciences*, vol. 20, no. 18, p. 4431, 2019.
- [5] J. K. Sethei and A. Vidal-Puig, "Visfatin: the missing link between intra-abdominal obesity and diabetes?," *Trends in Molecular Medicine*, vol. 11, no. 8, pp. 344–347, 2005.
- [6] C. C. Yang, S. J. Deng, C. C. Hsu et al., "Visfatin regulates genes related to lipid metabolism in porcine adipocytes," *Journal of Animal Science*, vol. 88, no. 10, pp. 3233–3241, 2010.
- [7] C. C. Chen, T. C. Li, C. I. Li et al., "The relationship between visfatin levels and anthropometric and metabolic parameters: association with cholesterol levels in women," *Metabolism*, vol. 56, no. 9, pp. 1216–1220, 2007.
- [8] B. Kumari and U. C. S. Yadav, "Adipokine visfatin's role in pathogenesis of diabetes and related metabolic

- derangements,” *Current Molecular Medicine*, vol. 18, no. 2, pp. 116–125, 2018.
- [9] A. Wnuk, A. Stangret, M. Wątroba et al., “Can adipokine visfatin be a novel marker of pregnancy-related disorders in women with obesity?,” *Obesity Reviews*, vol. 21, no. 7, article e13022, 2020.
- [10] Q. Wan, Z. Liu, Y. Yang, and X. Cui, “Suppressive effects of berberine on atherosclerosis via downregulating visfatin expression and attenuating visfatin-induced endothelial dysfunction,” *International Journal of Molecular Medicine*, vol. 41, no. 4, pp. 1939–1948, 2018.
- [11] X. Cui, Z. Huang, L. Lou et al., “Dingxin recipe alleviates atherosclerosis injury in ApoE-knockout mice via downregulation of visfatin expression and inhibition of the visfatin-induced inflammatory response,” *Journal of Traditional Chinese Medicine*, vol. 40, no. 6, pp. 938–946, 2020.
- [12] Y. Y. Kong, G. Q. Li, W. J. Zhang et al., “Nicotinamide phosphoribosyltransferase aggravates inflammation and promotes atherosclerosis in ApoE knockout mice,” *Acta Pharmacologica Sinica*, vol. 40, no. 9, pp. 1184–1192, 2019.
- [13] M. Zheng, N. Lu, M. Ren, and H. Chen, “Visfatin associated with major adverse cardiovascular events in patients with acute myocardial infarction,” *BMC Cardiovascular Disorders*, vol. 20, no. 1, p. 271, 2020.
- [14] E. Ozal, I. Sahin, I. Bolat et al., “Visfatin levels are increased in patients with resistant hypertension and are correlated with left ventricular hypertrophy,” *Blood Pressure Monitoring*, vol. 22, no. 3, pp. 137–142, 2017.
- [15] Y. Luo, X. X. Pang, A. R. Ansari et al., “Visfatin exerts immunotherapeutic effects in lipopolysaccharide-induced acute lung injury in murine model,” *Inflammation*, vol. 43, no. 1, pp. 109–122, 2020.
- [16] S. Zhu, Y. Wang, H. Liu et al., “Thyroxine affects lipopolysaccharide-induced macrophage differentiation and myocardial cell apoptosis via the NF- $\kappa$ B p65 pathway both in vitro and in vivo,” *Mediators of Inflammation*, vol. 2019, Article ID 2098972, 10 pages, 2019.
- [17] S. Yao, C. Jiang, H. Zhang, X. Gao, Y. Guo, and Z. Cao, “Visfatin regulates Pg LPS-induced proinflammatory/prodegradative effects in healthy and inflammatory periodontal cells partially via NF- $\kappa$ B pathway,” *Biochimica et Biophysica Acta, Molecular Cell Research*, vol. 1868, no. 8, p. 119042, 2021.
- [18] K. Xiao, W. H. Zou, Z. Yang et al., “The role of visfatin on the regulation of inflammation and apoptosis in the spleen of LPS-treated rats,” *Cell and Tissue Research*, vol. 359, no. 2, pp. 605–618, 2015.
- [19] K. Xiao, Y. Zhou, H. R. Yuan et al., “The regulation mechanism of apoptosis by visfatin in the mesenteric lymph nodes of LPS-treated rats,” *Histology and Histopathology*, vol. 31, no. 9, pp. 987–1000, 2016.
- [20] X. X. Pang, A. R. Ansari, W. J. Yang et al., “Visfatin regulates inflammatory mediators in mouse intestinal mucosa through toll-like receptors signaling under lipopolysaccharide stress,” *Archivum Immunologiae et Therapiae Experimentalis (Warsz)*, vol. 69, no. 1, p. 11, 2021.
- [21] L. J. Su, J. H. Zhang, H. Gomez et al., “Reactive oxygen species-induced lipid peroxidation in apoptosis, autophagy, and ferroptosis,” *Oxidative Medicine and Cellular Longevity*, vol. 2019, Article ID 5080843, 13 pages, 2019.
- [22] M. Srinivasan, M. L. Meadows, and L. Maxwell, “Assessment of salivary adipokines resistin, visfatin, and ghrelin as type 2 diabetes mellitus biomarkers,” *Biochemistry Research International*, vol. 2018, Article ID 7463796, 5 pages, 2018.
- [23] Y. J. Heo, S. E. Choi, N. Lee et al., “CCL20 induced by visfatin in macrophages via the NF- $\kappa$ B and MKK3/6-p38 signaling pathways contributes to hepatic stellate cell activation,” *Molecular Biology Reports*, vol. 47, no. 6, pp. 4285–4293, 2020.
- [24] Y. Y. Wang, H. D. Chen, S. Lo et al., “Visfatin enhances breast cancer progression through CXCL1 induction in tumor-associated macrophages,” *Cancers*, vol. 12, no. 12, p. 3526, 2020.
- [25] S. Bruzzone, F. Fruscione, S. Morando et al., “Catastrophic NAD<sup>+</sup> depletion in activated T lymphocytes through Nampt inhibition reduces demyelination and disability in EAE,” *PLoS One*, vol. 4, no. 11, article e7897, 2009.
- [26] M. Ozgen, S. S. Koca, K. Aksoy, N. Dagli, B. Ustundag, and A. Isik, “Visfatin levels and intima-media thicknesses in rheumatic diseases,” *Clinical Rheumatology*, vol. 30, no. 6, pp. 757–763, 2011.
- [27] G. J. Wang, N. J. Shen, L. Cheng, Y. Fang, H. Huang, and K. H. Li, “Visfatin triggers the *in vitro* migration of osteosarcoma cells via activation of NF- $\kappa$ B/IL-6 signals,” *European Journal of Pharmacology*, vol. 791, pp. 322–330, 2016.
- [28] N. Kanda, C. S. Hau, Y. Tada, A. Tatsuta, S. Sato, and S. Watanabe, “Visfatin enhances CXCL8, CXCL10, and CCL20 production in human keratinocytes,” *Endocrinology*, vol. 152, no. 8, pp. 3155–3164, 2011.
- [29] S. R. Kim, H. J. Park, Y. H. Bae et al., “Curcumin down-regulates visfatin expression and inhibits breast cancer cell invasion,” *Endocrinology*, vol. 153, no. 2, pp. 554–563, 2012.
- [30] S. He, H. Zhang, Y. Lu et al., “Nampt promotes osteogenic differentiation and lipopolysaccharide-induced interleukin-6 secretion in osteoblastic MC3T3-E1 cells,” *Aging (Albany NY)*, vol. 13, no. 4, pp. 5150–5163, 2021.
- [31] I. Tam, A. Dzierżęga-Lęcznar, and K. Stępień, “Differential expression of inflammatory cytokines and chemokines in lipopolysaccharide-stimulated melanocytes from lightly and darkly pigmented skin,” *Experimental Dermatology*, vol. 28, no. 5, pp. 551–560, 2019.

## Research Article

# Exercise Preconditioning Ameliorates Cognitive Impairment in Mice with Ischemic Stroke by Alleviating Inflammation and Modulating Gut Microbiota

Heng Lv <sup>1,2</sup>, Shasha Wang <sup>2,3</sup>, Meihui Tian,<sup>1,2</sup> Liya Wang,<sup>2,3</sup> Jie Gao <sup>2,3</sup>, Qitao Zhao,<sup>2</sup> Zhaoyu Li,<sup>2</sup> Xianjie Jia <sup>1</sup> and Ying Yu <sup>2,3</sup>

<sup>1</sup>Department of Epidemiology and Statistics, School of Public Health, Bengbu Medical College, Bengbu 233000, China

<sup>2</sup>Key Laboratory of Cardiovascular and Cerebrovascular Diseases, Bengbu Medical College, Bengbu 233000, China

<sup>3</sup>Department of Physiology, School of Basic Medicine, Bengbu Medical College, Bengbu 233000, China

Correspondence should be addressed to Xianjie Jia; [xjjia@139.com](mailto:xjjia@139.com) and Ying Yu; [yuying2011@126.com](mailto:yuying2011@126.com)

Received 23 June 2022; Accepted 27 September 2022; Published 10 October 2022

Academic Editor: Dominik Skiba

Copyright © 2022 Heng Lv et al. This is an open access article distributed under the Creative Commons Attribution License, which permits unrestricted use, distribution, and reproduction in any medium, provided the original work is properly cited.

Several studies have demonstrated that exercise preconditioning is an effective means of alleviating poststroke cognitive impairment (PSCI). Mechanisms of regulating cognitive function have not been fully elucidated. Herein, the present study is aimed at exploring the effect of the microbiota-gut-inflammasome-brain axis in the process of exercise preconditioning moderating cognitive impairment after ischemic stroke. We observed that exercise preconditioning decreased infarct size, reduced the degree of neuronal damage, and alleviated cognitive impairment in mice with ischemic stroke. In addition, exercise preconditioning also reduced the expression of inflammatory cytokines, as well as NLRP3, Caspase-1, IL-18, and IL-1 $\beta$  protein expressions. Ischemic stroke could downregulate the abundance of *Roseburia* while increasing the abundance of the *Helicobacter* at the level of genus. As a comparison, exercise preconditioning increased the abundance of the *Lactobacillus*, which was beneficial for mice at the genus level. In conclusion, exercise preconditioning can improve cognitive dysfunction after ischemic stroke through alleviating inflammation and regulating the composition and diversity of the gut microbiota, which might provide a new strategy for the prevention of PSCI.

## 1. Introduction

Ischemic stroke is an emergency situation caused by reduced blood flow to the brain, which results in impairment to brain cells [1]. Poststroke cognitive impairment (PSCI) is one of the common consequences. It also is a major contributor of long-term disability and reduced quality of life. In a community-based study in China, the prevalence of PSCI was shown to be 80.97% [2]. The pathogenesis of PSCI is complicated, and there is still no effective clinical treatment [3]. Exercise preconditioning as an effective strategy has been shown experimentally to be neuroprotective in stroke survivors [4]. However, the biological mechanisms and pathways through which exercise preconditioning promotes cognitive function have not been completely clarified.

Extensive research suggested that exercise may exert a neuroprotective effect by reducing neuroinflammation [5]. Studies from both humans and animals had demonstrated that appropriate exercise delays cognitive aging and neurodegeneration [6, 7]. A study [8] published in *Nature* showed that “runner plasma,” which was collected from voluntarily running mice and injected into sedentary mice, reduced baseline neuroinflammatory gene expression and experimentally induced brain inflammation. This finding confirmed the presence of anti-inflammatory exercise factors that are metastable, target the cerebral vasculature, and are beneficial to the brain. What is more, a population-based study observed that regular exercise preconditioning was associated with fewer ischemic stroke complications and better long-term function outcomes [9].

There is substantial evidence that the pathogenesis of PSCI is also associated with inflammatory response [10]. The inflammasome is an important multiprotein complex that functions during inflammatory immune responses. Components of the inflammasome contain the NOD-like receptor pyrin domain-containing 3 (NLRP3), which is a multiprotein signaling complex containing the NLRP3 scaffold, the adaptor protein PYCARD/ASC, and Caspase-1. The interaction between these proteins can flexibly regulate the constitutive function of inflammasome, ensuring that inflammasome is activated at appropriate occasions [11]. Overactivation of inflammation is known to play a pivotal role throughout cerebral ischemia, from early injury to postischemic tissue recovery [12]. Specifically, NLRP3 is regarded as one of the predominant inflammasomes and plentifully expresses in the brain. It plays a key role in recognizing cellular damage and modulating inflammatory responses to ischemic stroke [13]. A study [14] showed that cerebral ischemia-reperfusion in mice was followed by increased infarct area and hydrocephalus content and elevated NLRP3 and Caspase-1 expression. Systemic inflammation activates the NLRP3 inflammasome, triggers neuroinflammation, and exacerbates ischemic brain injury and cognitive impairment.

In recent years, there has been an increasing interest in the role of the microbiota-gut-brain (MGB) axis in modulating the brain function [15]. The MGB axis also plays a vital role in the pathophysiology of PSCI and managing inflammatory reaction [16]. It suggests that the gut microbiota exchanges information with the central nervous system through immune, neuroendocrine, and vagal “bidirectional brain-gut signals,” affecting the host’s brain function and thus its behavior and cognitive function [17]. Furthermore, systemic low-grade chronic inflammation may be caused by dysbiosis of gut microbiota in stroke patients, which is a critical cause in the pathogenesis of PSCI [18]. Regulation of gut microbiota has been a latent target for treatment and prevention of some chronic diseases in the future. Numerous studies have indicated that the gut microbiota can be harmonized by a variety of factors such as exercise, antibiotics, infection, and diet [19–21]. Exercise can modulate the composition and diversity of gut microbiota [22]. Exercise-induced alterations in the gut microbiome are associated with corresponding physiological changes in the host, including immunity and metabolism [23]. Overgrowth of hazardous microbiota induces inflammation by altering the intestinal mucosal barrier, leading to neuroinflammation and neurodegeneration in the central nervous system [24]. Notably, recent evidence supports that the NLRP3 inflammasome has a key role to play in orchestrating host physiology and formatting the peripheral and central inflammatory/immune reactions to central neurological diseases through the release of IL-18 and IL-1 $\beta$  [25, 26]. The gut microbiota may interact with the NLRP3 inflammasome through a dynamic interaction, known as the microbiota-gut-inflammasome-brain axis [27]. Gut microbiota adopt inflammasome signal to regulate peripheral inflammatory pathways, which in turn helps to maintain brain homeostasis.

Although studies have showed that exercise has a positive effect on the gut microbiota, it is not known whether the

microbiota-gut-inflammasome-brain axis plays a role in exercise preconditioning with ischemic stroke. Therefore, the aims of the present study are as follows: (1) to investigate the effects of exercise preconditioning on the cognitive outcome of ischemic stroke and (2) to determine whether exercise preconditioning can improve cognitive function after stroke by inhibiting inflammation and regulating gut microbiota.

## 2. Materials and Methods

**2.1. Animals.** The Animal Center of Anhui Medical University (Hefei, China) provided us with 40 male C57BL/6J mice (age: 6–8 weeks; weight: 22–24 g). Mice were kept in a 12 h cycle of light/darkness, and water and food were available for free. The animal protocols were authorized by the Laboratory Animal Ethics Committee of Bengbu Medical College and were conducted in keeping with the ethical standards.

**2.2. Experiment Protocol.** C57BL/6J mice were evenly randomized into the sham operation group (Sham), the middle cerebral artery occlusion group (MCAO), the sham operation with exercise preconditioning group (EP+Sham), and the MCAO with exercise preconditioning group (EP+MCAO) ( $n = 12$  in each group). Mice in the EP+Sham group and the EP+MCAO group were kept in cages equipped with running wheels for rodents and made to exercise autonomously for 4 weeks. Mice in the Sham group and the MCAO group were maintained in conventional cages. Subsequently, the MCAO group and EP+MCAO were subjected to right brain ischemia-reperfusion operation, while the Sham group and EP+Sham group only exposed the right external carotid artery and common carotid artery via sham operation, without ischemia stroke in the right brain. After 24 h of reperfusion, the mice were stimulated to defecate by lifting their tails at hourly intervals between 9 a.m. and 12 a.m., and approximately 200 mg of feces was collected from each mouse [28]. Considering the effect of circadian rhythms on intestinal flora, all samples were collected in the same time period of days [29]. We stored the fecal pellets at  $-80^{\circ}\text{C}$  until further processing.

**2.3. Middle Cerebral Artery Occlusion (MCAO).** It was performed to induce an ischemic stroke in mice by occluding the middle cerebral artery. Mice were given anesthesia by intraperitoneal injection of sodium pentobarbital (100 mg/kg). The right common carotid artery, internal carotid artery, and external carotid artery were separated through the midline neck incision. A 30 mm long and 0.12 mm thick nylon monofilament (MSMC21B120PK50, RWD Life Science, Shenzhen, China), with its tip rounded by silica gel (4 mm in length and 0.21 mm in diameter), was inserted and left for 90 min in the internal carotid artery from the common carotid artery to the beginning of the middle cerebral artery. After 90 min, the monofilament was retracted to restore reperfusion after cerebral ischemia. Mice of the Sham group and EP+Sham group received the same procedure, except for monofilament penetration.

**2.4. Neurologic Functional Scoring.** The neurological function of mice was examined after 24 h of reperfusion with a five-level grading system according to Longa: 0, no deficits; 1, inability to extend the right paw; 2, longitudinal rotation; 3, falling to the right; and 4, inability to walk spontaneously. Mice that scored between 1 and 3 neurologically were selected for the following study, while mice that scored equal to 1 or 4 were considered unsuccessful for MCAO surgery. Our inclusion criteria were as follows: (1) a neurological score from 1 to 3 based on Longa's grading system and (2) at least 5% loss in body weight at 24 h after ischemic stroke [30]. The animals that failed to satisfy one of these criteria at 24 h poststroke were deemed spontaneously recovered and excluded.

### 2.5. Behavior Testing

**2.5.1. Novel Object Recognition Task.** An assessment of mice's nonspatial recognition memory capacity can be made through the novel object recognition (NOR) task. In this task, the day before the exact test execution, mice were habituated to the test space for 30 min to reduce stress responses [31]. In the training phase, mice were positioned in an opening field with two identical objects. For a period of 10 min, mice were asked to explore the same objects at the same distance on a familiar arena. After 1 h, the mice were set back in the same arena in front of two objects, one of which was swapped with a new object, for another 5 min. The time spent by the mice adventuring the two objects was marked. And the odor of particular mouse was removed with spraying ethanol before testing the next one. *N* (novel) was the number of times mice probe for new objects, *F* (familiar) was the number of times they explored familiar objects, and discrimination index was calculated as  $N/(N + F)$ .

**2.5.2. Y-Maze Test (Spontaneous Alternation).** The spontaneous alternation experiment is used as a method to detect spatial recognition memory capacity in rodents by exploiting their curiosity for novelty. They prefer to explore areas that they have never been to before. The test was performed in a symmetrical white Y-maze with three arms (length 20 cm × width 10 cm × height 20 cm). The mice were posed at the very end of one arm of a Y-shaped maze and permitted to move freely for a period of 8 min. A series of arm entries were visually evaluated and scored by experimenters who were blinded to the treatment. One alternation was determined as entering all three arms consecutively. The maximum number of alternations was equal to the total number of arms entered minus 2. The spontaneous alternation rate was calculated as actual number of alternations/maximum number of alternations.

**2.6. Brain Infarct Volume.** After scoring neurological function, mice were profoundly anesthetized with pentobarbital sodium (600 mg/kg) to isolate the brain quickly, and the brains were placed in a -20°C refrigerator for 15 minutes. Subsequently, the brains from Bregma +4.0 mm to 6.0 mm were sliced into five 2.0 mm thick sections. Then, the sections were stained with 2,3,5-triphenyl tetrazolium chloride solution (TTC, Sigma-Aldrich, St. Louis, Missouri, USA) in a 37°C water bath

for 30 minutes and then fixed with 4% formaldehyde for 15 minutes. The infarct area was identified by nonstaining region, while the live area should turn red. The infarct area was measured using ImageJ software. The relative infarct volume was manually calculated according to the following formula:  $\text{infarct percentage} = (\text{volume of the contralateral hemisphere} - \text{volume of the noninfarct contralateral hemisphere}) / \text{volume of the contralateral hemisphere} \times 100\%$ .

**2.7. Morphological Examination.** The mice were anesthetized and their brains were taken out after cardiac perfusion with phosphate-buffered saline (PBS) and 4% paraformaldehyde. The brains were fixed in 4% paraformaldehyde for overnight, embedded in paraffin, cut into 5 μm thick sections, and stained with hematoxylin-eosin (HE). Histomorphology changes of the right hippocampus were observed under the microscope.

**2.8. Enzyme-Linked Immunosorbent Assay (ELISA).** After 90 min of reperfusion, blood samples were gathered from venous plexus of fundus. The serum was separated by centrifugation at 3000 rpm for 15 min at 4°C and collected. The levels of IL-18 and IL-1β were examined using an IL-18 ELISA kit (Calvin Biotechnology, Suzhou, China) and an IL-1β ELISA kit (Calvin Biotechnology, Suzhou, China), following the instructions separately provided by the manufacturer. The absorbance of samples was measured at 450 nm.

**2.9. Western Blot Analysis.** The total proteins were extracted from the hippocampal region of mice, and the protein concentration was determined by BCA assay. Equivalent amounts of protein samples were sampled on a 10% SDS-PAGE gel for electrophoretic separation of the proteins, and then, the PVDF membranes were electrotransformed by constant current at 280 mA for 90 min. Subsequently, the membranes were soaked with 5% skim milk powder in TBST (Tris-buffered saline containing 1% Tween-20) for 2 h. Then, the corresponding primary antibody was added overnight at 4°C. The primary antibodies were NLRP3 (1: 1000, ab263899), Caspase-1 (1: 1000, ab179515), IL-1β (1: 1000, ab234437), IL-18 (1: 1000, ab207323), and β-actin (1: 2000, BL005B) and were purchased from Abcam (Cambridge, UK) except β-actin which was purchased from Biosharp (Anhui, China). Then, membranes were removed, rinsed 3x for 10 minutes with TBST, and incubated for 2 h at 37°C with the goat anti-rabbit IgG (1: 10000, BL003A, from Biosharp, Anhui, China), respectively. TBST was used to wash the membranes three times before they were subjected to Bio-Rad electrophoresis (Bio-Rad Laboratories, Hercules, CA, United States). Analyzing all band intensities was done using ImageJ software.

**2.10. Gut Microbiota Analysis.** The 16S rRNA method was used to detect gut microbiota as follows: genomic DNA was obtained from mouse feces using the manufacturer's designated DNA extraction kit (DNeasy PowerSoil Kit, Mo Bio, United States) and was quantified using Nanodrop. The quality of DNA extraction was confirmed by 1.2% agarose gel electrophoresis. PCR was performed using primer pairs (forward: ACTCCTACGGGAGGCAGCA; reverse:



TCGGACTACHVGGGTWTCTAAT) against the highly mutated V3-V4 region of the bacterial 16S rRNA gene. PCR amplification was performed using Pfu high fidelity DNA polymerase (TransGen Biotech), and the number of amplification cycles was strictly controlled. Then, 25  $\mu$ l of PCR product was purified by adding 0.8x volume of magnetic beads (Vazyme VAHTSTM DNA Clean Beads). PCR amplification recovery products were subjected to fluorescence quantification using the Quant-iT PicoGreen dsDNA assay kit and a microplate reader for quantification (BioTek, FLx800). Sequencing libraries were prepared using the Illumina TruSeq Nano DNA LT Library Prep Kit. Double-ended sequencing of community DNA fragments was performed using the Illumina MiSeq platform. Chimeric sequences were screened using the DADA2 method. The Greengenes and Silva databases were selected for taxonomic annotation of species on the QIIME2 (2019.4) platform.

**2.11. Statistical Analysis.** The experimental results were presented as mean  $\pm$  standard error (SEM). One-way ANOVA after Newman-Keuls test was used to analyze the data between multiple groups.  $P < 0.05$  was deemed to indicate a statistically significant difference.

### 3. Results

**3.1. Exercise Preconditioning Ameliorated Neurological Scores and Reduced Infarction Area in Mice with Ischemic Stroke.** After successful induction of focal cerebral ischemia by the MCAO method, we assessed the effect of ischemic stroke and exercise preconditioning on neurological deficits by the Longa method. The results indicated no symptoms of neurological impairment in the Sham group and EP+Sham group. In contrast, the neurological deficit scores were significantly higher in the MCAO group mice than in the Sham group ( $P < 0.01$ , Figure 1(a)). Yet, four weeks of exercise preconditioning significantly reduced the score compared with the MCAO group ( $P < 0.05$ , Figure 1(a)). These results suggest that exercise preconditioning ameliorated the neurological damage which occurs after ischemic stroke in mice. Subsequently, we evaluated the infarct size. As shown in Figures 1(b) and 1(c), there were no infarction volume in the Sham group and EP+Sham group. The infarct area significantly appeared in the ischemia groups, and a statistically significant difference was found between the MCAO group and EP+MCAO group ( $P < 0.01$ , Figures 1(b) and 1(c)). Our data pointed to the fact that exercise preconditioning ameliorates neurological scores and the infarction area due to ischemic stroke.

#### 3.2. Exercise Preconditioning Improved Cognitive Function in Mice with Ischemic Stroke

**3.2.1. Novel Object Recognition Task.** A new object recognition task was utilized for evaluating nonspatial memory capacity, which is associated with the hippocampus. When compared to the Sham group, the mice in the MCAO group spend less time navigating new objects ( $P < 0.01$ , Figure 2(a)). In contrast, this reduced ability was enhanced by the exercise preconditioning ( $P < 0.05$ , Figure 2(a)).

Ischemic stroke affects nonspatial recognition memory capacity in mice, while exercise preconditioning before ischemic stroke improves cognitive function.

**3.2.2. Y-Maze Test (Spontaneous Alternation Task).** Y-maze test of spontaneous alternation task was used to evaluate spatial memory capacity which is in connection with the hippocampus. The experimental results of Y-maze indicated that the mice in the MCAO model group had significantly reduced spontaneous alternations rate compared with the Sham group, and the difference was significant ( $P < 0.01$ , Figure 2(b)). While the mice given exercise preconditioning had increased rate of spontaneous alternations, it was remarkably higher compared to the MCAO model group ( $P < 0.05$ , Figure 2(b)), indicating that exercise preconditioning could improve the cognitive impairment caused by ischemic stroke and improve spatial memory ability.

**3.3. Exercise Preconditioning Improves the Extent of Neuronal Damage in the Hippocampus of Mice with Ischemic Stroke.** HE staining showed that hippocampal neurons of mice in the Sham groups were arranged neatly, with intact cell structure and visible nucleus. In contrast, MCAO mice exhibited significant neuronal damage with irregular cell shape, concentrated cytoplasm and nuclei, and damaged hippocampal structures. The damage was improved in the EP+MCAO group compared with the MCAO group, which indicated that exercise preconditioning could have a protective effect on brain tissue (Figure 3).

**3.4. Exercise Preconditioning Mitigated the Expression of Inflammatory Factors Caused by Ischemic Stroke.** Since the inflammatory response is involved in the pathological process of ischemic stroke, we used ELISA to observe the alteration of IL-1 $\beta$  and IL-18 after ischemic stroke and if exercise preconditioning can modulate their excretion. The IL-1 $\beta$  level was elevated in the MCAO group when compared with the Sham group, as shown in Figure 4(a). In comparison with MCAO group, the significant decrease of IL-1 $\beta$  was presented by exercise preconditioning before surgery. Our data indicated that IL-1 $\beta$  is involved in ischemic stroke and that exercise preconditioning could reduce its expression. However, the levels of IL-18 in MCAO and EP+MCAO had an increasing trend compared with Sham groups, but not statistically significant (Figure 4(b)).

**3.5. Exercise Preconditioning Reduced the Expression of NLRP3 Inflammasome and Proinflammatory Factors Induced by Ischemic Stroke.** To clarify the differences in expression of NLRP3 inflammasome and proinflammatory cytokines at the protein level among the groups, the protein expression levels of NLRP3, Caspase-1, IL-18, and IL-1 $\beta$  in ischemic brain tissue were determined (Figure 5). The protein expression levels of NLRP3, Caspase-1, IL-18, and IL-1 $\beta$  were significantly higher in the MCAO group compared with the Sham group. Exercise preconditioning reduced the expression levels of NLRP3, Caspase-1, IL-18, and IL-1 $\beta$  effectively. These findings suggested that exercise preconditioning attenuates inflammation in mice with ischemic stroke.

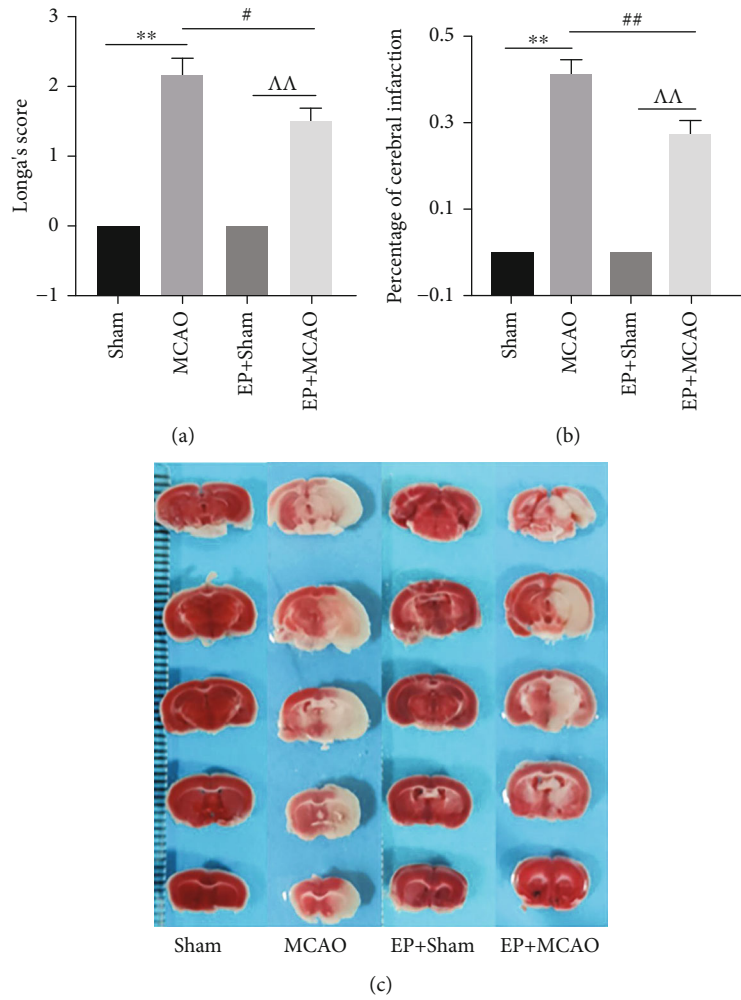


FIGURE 1: Effects of ischemic stroke and exercise preconditioning on neurological scores and infarction volume. (a) The neurological function scores of each group of mice were assessed at 24 h ( $n = 12$ ). (b) Comparison of cerebral infarct volume of the ipsilateral brain between groups ( $n = 4$ ). (c) Infarct size was determined by tetrazolium chloride (TTC) staining after cerebral ischemia-reperfusion ( $n = 4$ ), and the infarct area was identified by nonstaining region, while the live area should turn red. \*\* $P < 0.01$  vs. Sham; # $P < 0.01$  vs. MCAO; ^^ $P < 0.01$  vs. EP+Sham.

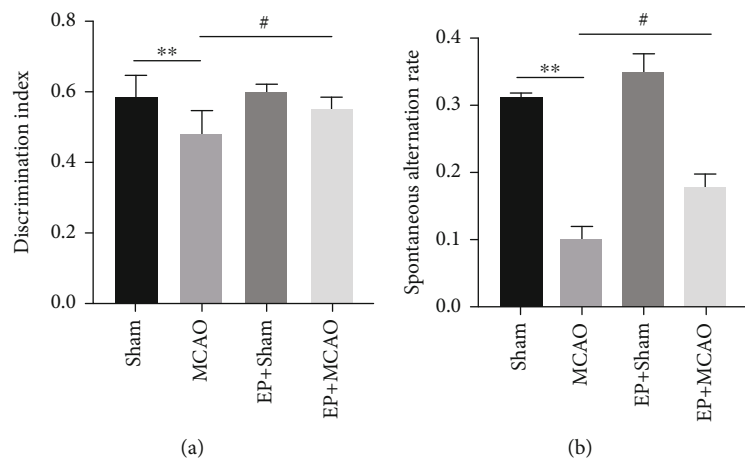


FIGURE 2: Effects of ischemic stroke and exercise preconditioning on the cognitive function of mice. (a) Discrimination index of mice in novel object recognition task ( $n = 7$ ). (b) Spontaneous alternation rate of mice in Y-maze test of spontaneous alternation ( $n = 7$ ). \*\* $P < 0.01$  vs. Sham; # $P < 0.05$  vs. MCAO.

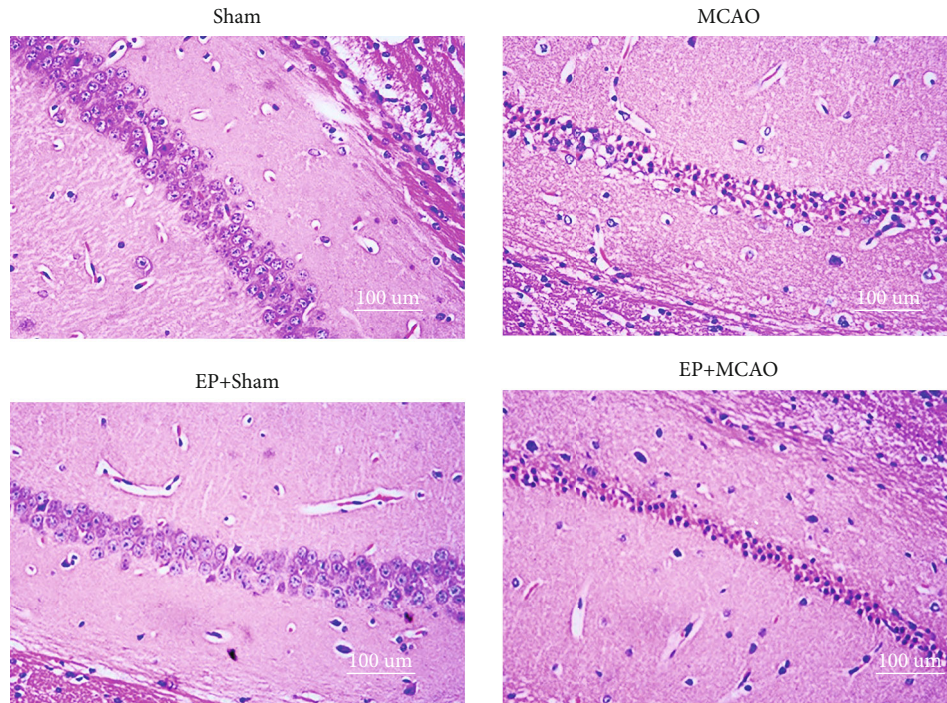


FIGURE 3: Effects of ischemic stroke and exercise preconditioning on the histopathological morphology of the hippocampal region (400x).

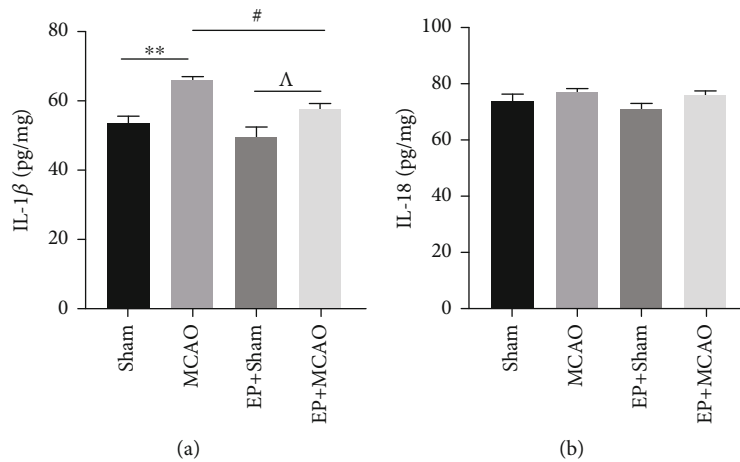


FIGURE 4: Effects of ischemic stroke and exercise preconditioning on proinflammatory cytokines in serum of each group. (a) The expression of IL-1 $\beta$  in brain tissue of mice ( $n = 8$ ). (b) The expression of IL-18 in brain tissue of mice ( $n = 8$ ). \*\* $P < 0.01$  vs. Sham; # $P < 0.05$  vs. MCAO;  $\Delta P < 0.05$  vs. EP+Sham.

**3.6. Exercise Preconditioning Regulated the Diversity and Composition of Gut Microbiota.** We used 16S rRNA gene pyrosequencing to examine the differences in gut microbiota among all groups. The 1520869 clean sequences were generated through the high-throughput pyrosequencing. Firstly, we viewed the alpha diversity which includes Chao1 and Faith's PD indices that independently represent richness and evolution-based diversity. As illustrated in Figures 6(a) and 6(b), compared to the Sham group, the MCAO group had increased the levels of Chao1 and Faith's PD indices, indicating that ischemic stroke increased the richness and diversity of the species in mice. The differences in Chao1

and Faith's PD indices between the MCAO group and the EP+MCAO group were insignificant, indicating that exercise preconditioning did not significantly affect the richness and the alpha diversity of species.

The PCoA plot was subsequently used to analyze the beta diversity, where different samples exhibited clustering or scatter distributions, and samples with similar components were placed in proximity to each other in the plot. The results showed that (Figure 6(c)) the distribution of intestinal microbiota between the Sham and MCAO group as well as between the Sham and EP+Sham group was clearly separated, indicating that ischemic stroke can not only

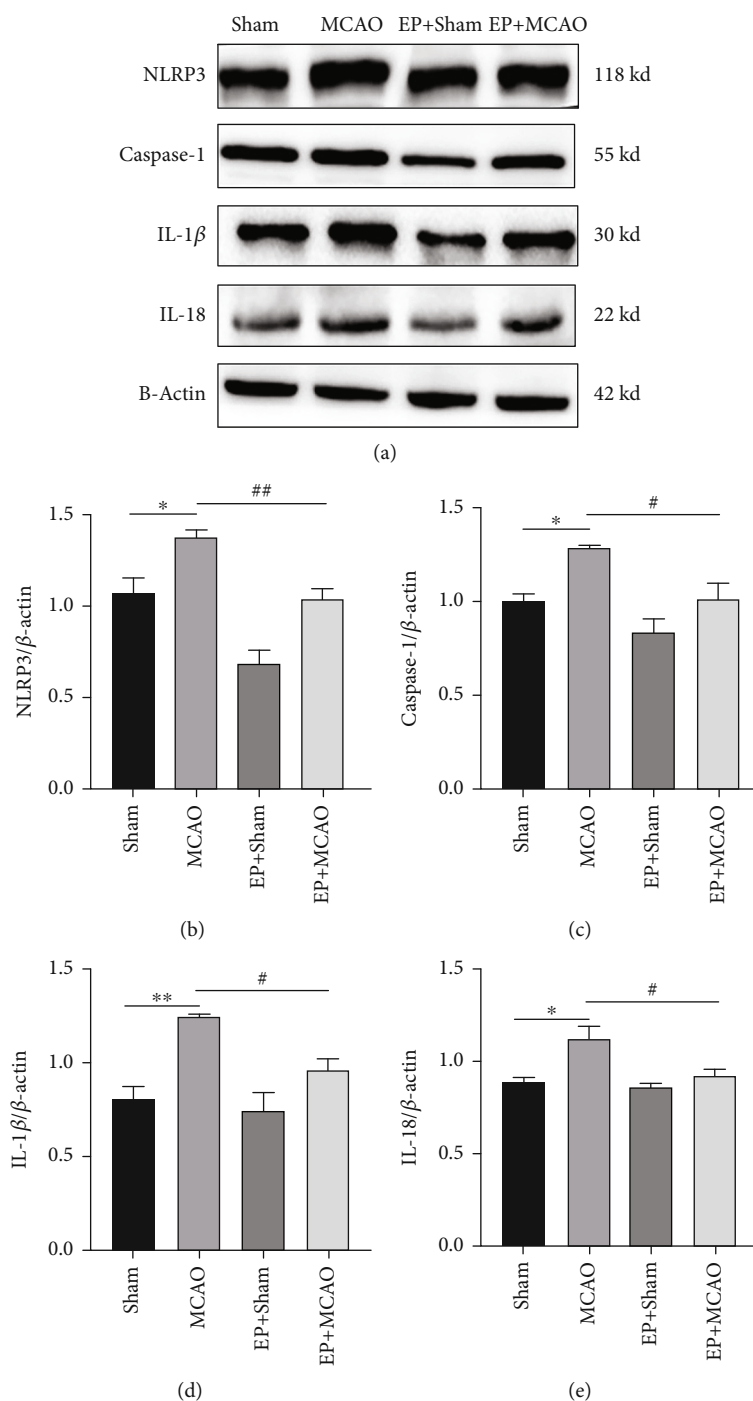


FIGURE 5: Representative western blots (a) and quantification data of NLRP3 (b), Caspase-1 (c), IL-1 $\beta$  (d), and IL-18 (e) for each group ( $n = 5$ ). \*\* $P < 0.01$  vs. Sham; # $P < 0.05$  vs. MCAO.

change the diversity of intestinal microbiota but also change the distribution structure of microbiota. Meanwhile, exercise preconditioning can also reshape the distribution of intestinal microbiota in mice.

Through clustering, we derived the relative abundance of each group of microbial communities at different taxonomic levels. Seventeen different phyla of gut microbiota were identified, with *Firmicutes* (71%), *Bacteroidetes* (16%), and *Proteobacteria* (10%) emerging as the most dominant

phyla (Figure 7). About 97% of the overall bacterial abundance was constrained to these three phyla.

Furthermore, the gut microbiota composition at the genus level was analyzed. Figure 8(a) tells the story. Hierarchical clustering analysis using the unweighted pair group method with arithmetic mean (UPGMA) showed that the majority of the samples were clustered within their own groups. Meanwhile, to find the ASV (amplicon sequence variants) with statistically significant differences between

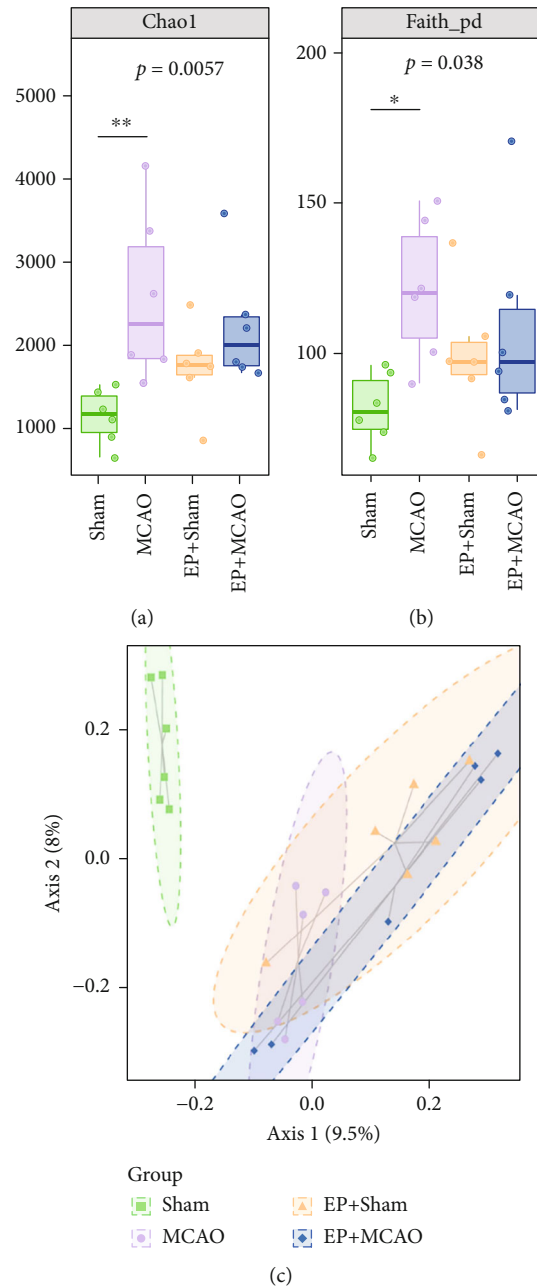


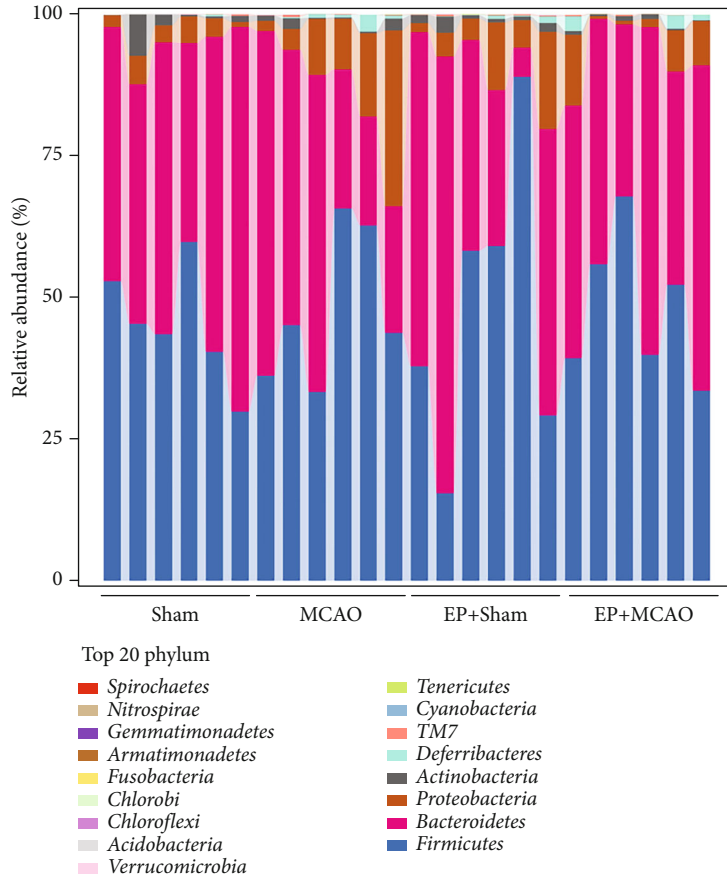
FIGURE 6: Ischemic stroke and exercise preconditioning affect the alpha and beta diversity of gut microbiota in mice ( $n = 6$ ). (a) Chao1; (b) Faith's PD; (c) PCoA analysis.

groups, we used the metagenomeSeq method to compare the samples two-by-two, called the fitFeatureModel function to fit the distribution of each ASV using a zero-inflated log-normal model, and used the fit results of this model to discriminate the significance of the differences. As shown in Figure 8(b), compared with the MCAO group, the *Helicobacter* in the Sham group was decreased and the *Roseburia* was increased. As shown in Figure 8(c), compared with the MCAO group, the *Ruminococcus* in the EP+MCAO group was decreased and the *Lactobacillus* and *Alistipes* were increased. Other ASV IDs not mentioned are not classified at the genus level.

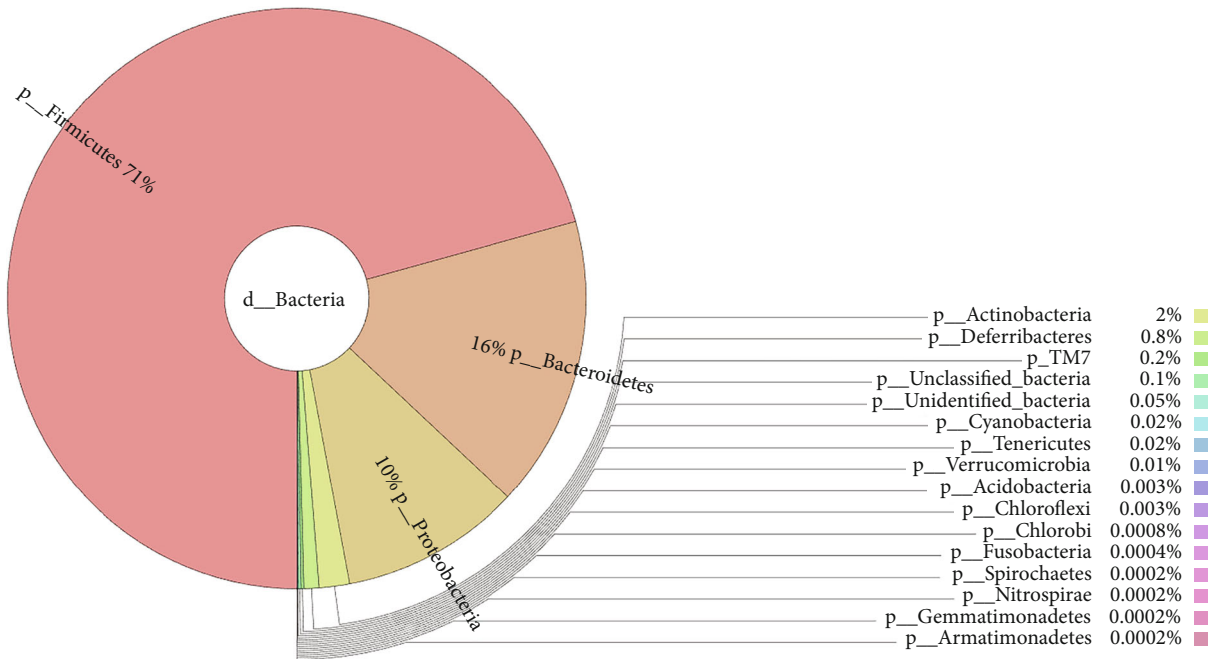
In the final analysis, LEfSe was queried for biomarkers of intergroup differences and species that differed significantly in the classification of the samples (Figure 9). Among the three differential biomarkers in terms of genus, *Akkermansia* and *Faecalibacterium* of the Sham group and *Lactococcus* of the EP+MCAO group were found.

#### 4. Discussion

In the current study, we investigated the protective effect of exercise preconditioning against cognitive impairment in ischemic stroke. We provided direct evidence that exercise

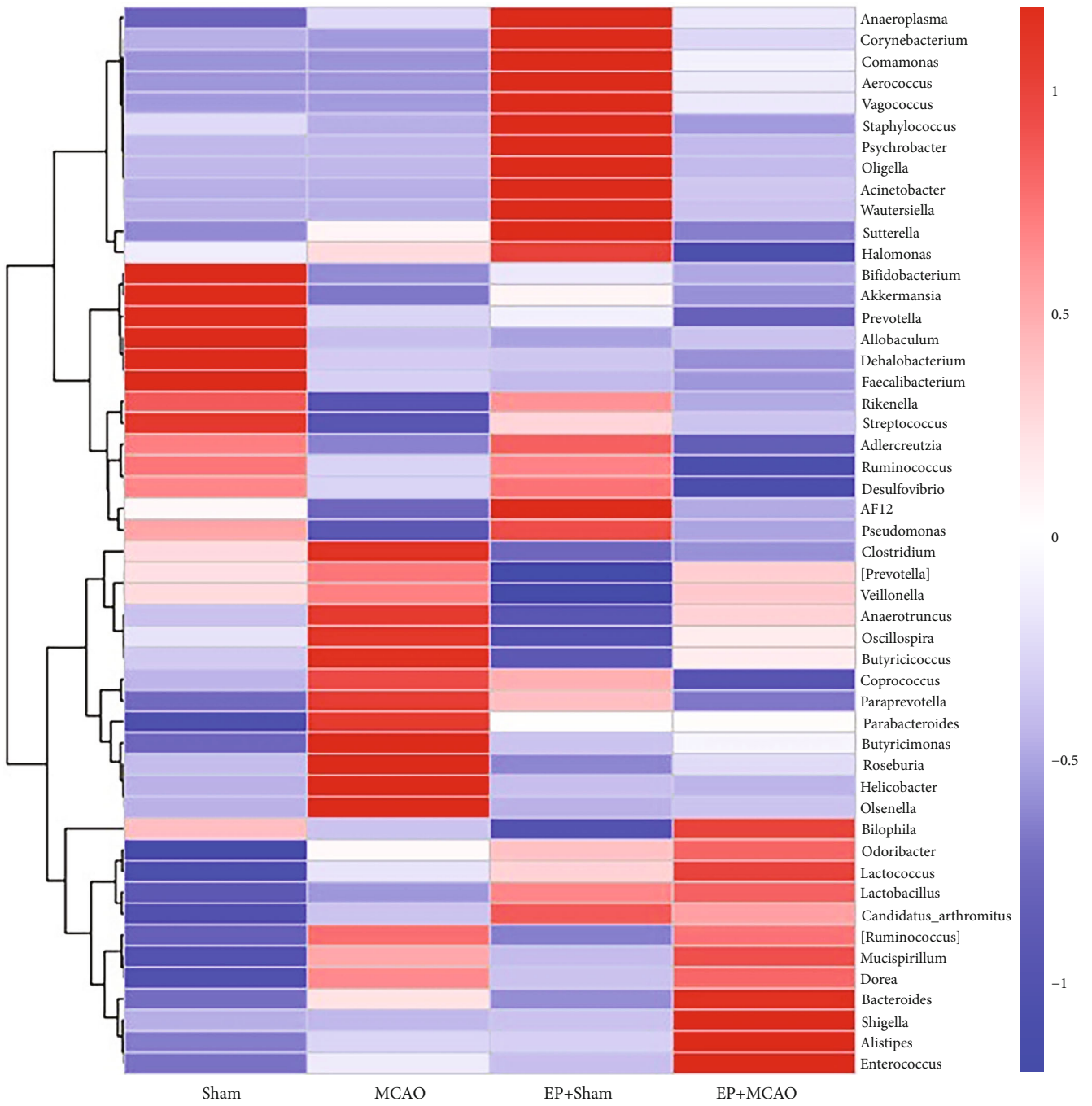


(a)



(b)

FIGURE 7: Phylum-level effects of ischemic stroke and exercise preconditioning on gut microbiota (n=6). (a) The abundance of gut microbiota at the level of phylum. (b) Interactive presentation of sample taxonomic composition at the level of phylum.



(a)

FIGURE 8: Continued.

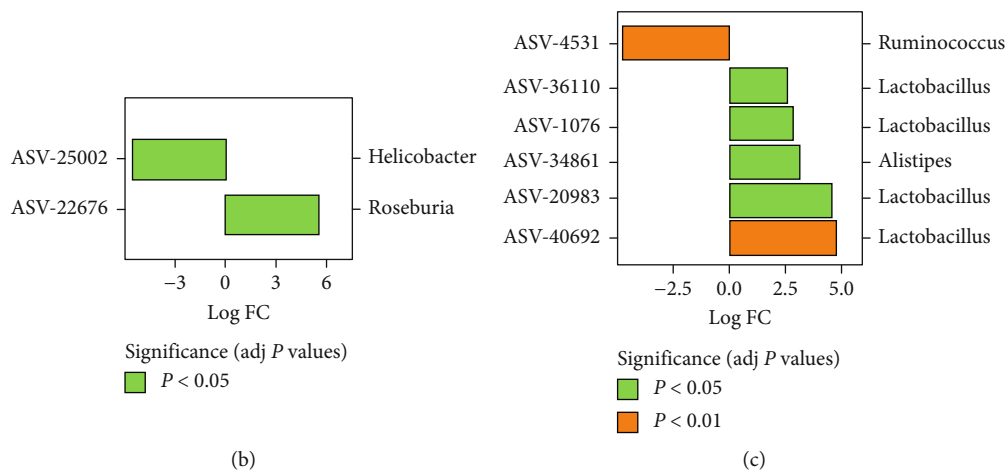


FIGURE 8: Effects of ischemic stroke and exercise preconditioning on the abundance of gut microbiota at the genus level ( $n = 6$ ). (a) The abundance of gut microbiota at the genus level. (b) Log<sub>2</sub> values of the multiple of ASV (fold change; FC) compared to the MCAO group in the Sham group, with positive values indicating upregulation, while negative values indicate downregulation. (c) Log<sub>2</sub> values of the multiple of ASV (fold change; FC) in the EP+MCAO group compared to the MCAO group, with positive values indicating upregulation, while negative values indicate downregulation.

preconditioning decreased neurological deficits, infarct size in mice subjected to ischemic stroke. In addition, after exercise preconditioning, the expression of NLRP3 inflammasome was reduced, the composition and the beta diversity of gut microbiota were remodeled, and the impairment of cognitive function was alleviated in ischemic stroke. These findings indicated that exercise preconditioning improved cognitive dysfunction after ischemic stroke through alleviating inflammation and modulating the composition and diversity of gut microbiota. According to our study, we provided a new pathophysiological viewpoint on exercise preconditioning to cognitive impairment in ischemic stroke.

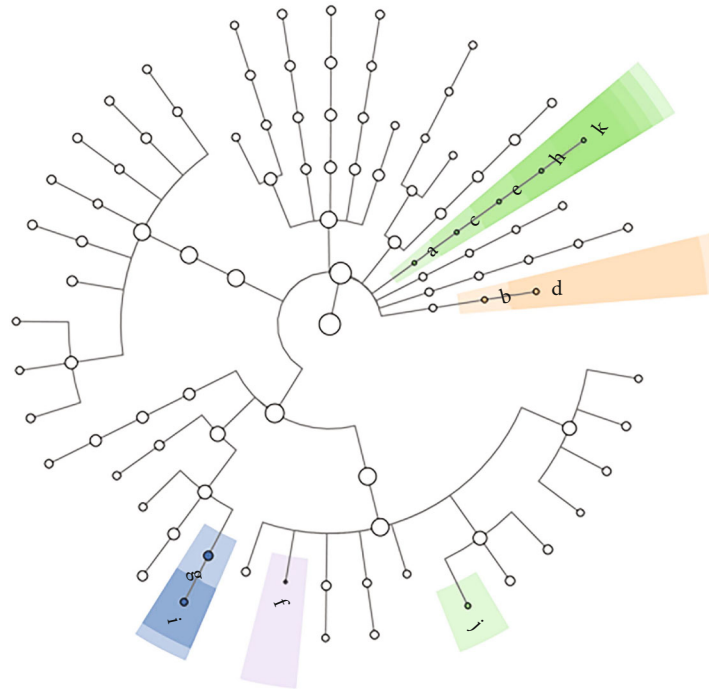
PSCI is one of the main complications after stroke, and the prognostic effect of treatment is restricted. Previous studies have shown that neuroinflammation is considered to be an important factor in PSCI [31]. Inflammasomes have been taken as therapeutic targets in human diseases [32]. The NLRP3 inflammasome is an intracellular multiprotein complexity that induces sets of proinflammatory chemokines, leading to inflammation. In the central nervous system, NLRP3 inflammasome was first reported to be activated in cortical neurons under ischemic conditions, and the expressions of NLRP3, Caspase-1, and IL-1 $\beta$  were upregulated in vitro and in vivo [33]. In our study, the levels of inflammatory factors including NLRP3, Caspase-1, and IL-1 $\beta$  were elevated in the MCAO group, demonstrating that the NLRP3 inflammasome was associated with the development of ischemic stroke. Nevertheless, the expression of IL-18 was not significantly different in the four groups. The reason is that the expression of IL-18 exhibits a delayed induction time process, starting from 24 to 48 h and peaking 6 days after ischemia [34]. Furthermore, we also observed that the cognitive function was impaired in the MCAO group of the mice, and the morphology and structure of neurons in the hippocampal region were abnormal. These results suggested that cognitive function decline in

MCAO mice is accompanied by increased inflammasome expression. In contrast, the aforementioned indices were effectively ameliorated in EP+MCAO group, which indicated that exercise preconditioning could improve the inflammatory response and cognitive impairment in ischemic stroke.

A cross-sectional study indicated that exercise preconditioning was associated with intact cognition in patients [35]. Numerous studies in animals have shown that exercise training can change the composition and functional capacity of the gut microbiota [36–40]. Similarly, population studies found that alpha diversity and relative abundance of 40 different bacterial taxa in the gut microbiota of professional athletes were significantly greater than that of sedentary controls [41]. Notably, there are few studies on the relationship between gut microbiota and PSCI. Until 2020, it was first reported that patients with PSCI had altered microbiota composition and corresponding metabolites and correlated with the degree of cognitive impairment, which suggested that gut microbiota may work essentially in the development of PSCI [42]. Therefore, we also analyzed the composition of the gut microbiota in each group. Our data showed that mice treated with MCAO had an increase in gut microbiota alpha diversity compared to the Sham group. This finding was supported by a prospective cohort study [43], showing that the gut microbiota of poststroke patients has higher alpha diversity than healthy controls. Conversely, we observed a decrease in microbial diversity in MCAO mice pretreated with 4 weeks of voluntary exercise.

We further observed that the *Helicobacter* was decreased and the *Roseburia* was increased in the Sham group compared with the MCAO group. *Helicobacter* is a member of the *Proteobacteria* phylum, which has a proinflammatory effect and is closely associated with ischemic stroke [44]. *Helicobacter* is an endotoxin-producing bacteria that can increase endotoxin and improve intestinal permeability.





- | Taxa  | Groups   |
|---|--|
| <span style="color: green;">■</span> a: p__Verrucomicrobia      | <span style="color: lightgreen;">■</span> Sham |
| <span style="color: orange;">■</span> b: c__Chloroplast         | <span style="color: purple;">■</span> MCAO     |
| <span style="color: green;">■</span> c: c__Verrucomicrobiae     | <span style="color: orange;">■</span> EP+Sham  |
| <span style="color: orange;">■</span> d: o__Streptophyta        | <span style="color: blue;">■</span> EP+MCAO    |
| <span style="color: green;">■</span> e: o__Verrucomicrobiales   |  |
| <span style="color: purple;">■</span> f: f__Christensenellaceae |  |
| <span style="color: blue;">■</span> g: f__Streptococcaceae      |  |
| <span style="color: green;">■</span> h: f__Verrucomicrobiaceae  |  |
| <span style="color: blue;">■</span> i: g__Lactococcus           |  |
| <span style="color: green;">■</span> j: g__Faecalibacterium     |  |
| <span style="color: green;">■</span> k: g__Akkermansia          |  |

(a)

FIGURE 9: Continued.

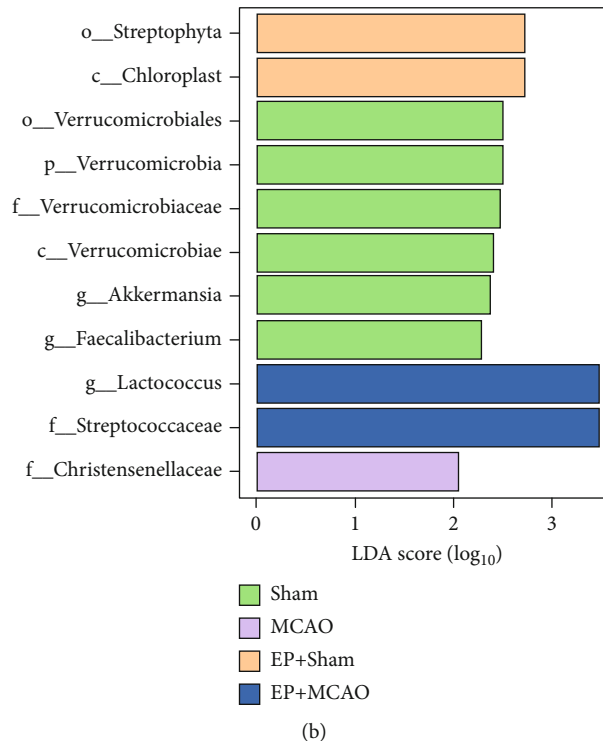


FIGURE 9: Linear discriminant analysis effect size. The biomarker of intergroup differences was found using LEfSe ( $n = 6$ ). (a) The evolutionary groupings of different species are shown. Phylum to genus (or species) is depicted by a circle radiating from the center. Small circles represent different classification levels, and the diameter of the circle represents relative abundance for each level. (b) This graph illustrates the distribution of LDA values for species. In the bar chart, the colors denote groups, while the species contributions are shown by the length of the bars.

These changes disrupted the intestinal epithelial barrier, allowing harmful substances to enter the peripheral blood. However, exercise preconditioning significantly enriched beneficial bacteria such as the *Lactobacillus* and *Alistipes* and reduced the *Ruminococcus*. Among these beneficial bacteria, *Lactobacillus* is widely recognized for the role in preserving human health and modifying immune function [45–47]. In addition, *Lactobacillus* has been reported to be protective in a rat model of ischemic stroke by inhibiting neuronal apoptosis, reducing brain infarct volume, decreasing oxidative stress, and restoring neurobehavioral deficits [48]. *Alistipes* is a relatively new genus of bacteria that can be seen as a potential SCFA (short-chain fatty acid) producer [49]. By analyzing SCFAs in the intestinal contents of rats with PSCI, researchers found that concentrations of acetic and propionic acids were lower in the early stroke than in the Sham group, and butyric and valeric acids were consistently at low level [50]. These results suggest that gut microbiota SCFA concentration is associated with the occurrence and prognosis of cognitive impairment after stroke. The mechanism behind the treatment of cerebral ischemic stroke with SCFAs may involve reducing inflammation, remodeling of the gut microbiota [44]. It has been found that intestinal SCFA levels decreased after ischemic stroke. Transplantation of SCFA-rich fecal bacteria and inhibition of inflammation are effective treatments for ischemic stroke [51]. Once the inflammatory response can be inhibited, the

progression of neurons death can be alleviated, and cognitive function can be improved after stroke. In this experiment, we found that exercise preconditioning improved poststroke cognitive impairment. We also observed that exercise preconditioning can improve cognitive dysfunction by inhibiting NLRP3 inflammasome as well as enriched *Lactobacillus* and *Alistipes* and reduced *Ruminococcus*. These findings indicated that exercise preconditioning can significantly affect the composition of the gut microbiota by adding beneficial bacteria and reducing hazardous bacteria, thereby inhibiting the activation of inflammasome and attenuating the inflammatory response in mice.

We acknowledge several important limitations to our study; firstly, there is no in-depth study of FMT (fecal microbiota transplantation) on the basis of gut microbiota. FMT has become a research hotspot in the field of basic medicine and clinical medicine and may involve several mechanisms worthy of further exploration: (1) inhibiting the expression of inflammatory factors in intestinal and brain tissues after stroke; (2) increasing the number of beneficial bacteria and restoring the normal structure of intestinal flora; and (3) promoting the expression of intestinal tight junction proteins and reducing intestinal mucosal permeability. Another limitation is that we ignored the resilience of penumbra neurons in our selection of specimens, as the number of collateral vessels that can still supply oxygen and glucose to the neurons of penumbra to prevent irreversible necrosis around

necrotic core. Finally, our inability to show certain associations may be due to insufficient sample size, rather than the absence of a true relationship.

## 5. Conclusion

In conclusion, our study suggests that exercise preconditioning can improve cognitive dysfunction after ischemic stroke by alleviating inflammation and regulating the composition and diversity of gut microbiota. The molecular mechanism may involve the inhibition of NLRP3 inflammasome-mediated inflammatory response. This evidence suggests that regulating the composition and diversity of gut microbiota and inhibiting inflammatory response through exercise preconditioning can be an efficient preventive measure in ischemic stroke.

## Data Availability

The datasets used and analyzed during the current study are available from the corresponding author upon reasonable request.

## Conflicts of Interest

The authors declared no conflicts of interest with respect to the research, authorship, and/or publication of this article.

## Authors' Contributions

Heng Lv and Shasha Wang performed the experiments and wrote the manuscript. Meihui Tian and Liya Wang performed the experiments and analyzed the data. Jie Gao, Qitao Zhao, and Zhaoyu Li performed the statistical analysis and revised the manuscript. Ying Yu and Xianjie Jia designed and supervised the study. All authors have read and approved the manuscript. Heng Lv and Shasha Wang contributed equally to this work.

## Acknowledgments

The work was supported by the Natural Science Foundation of Anhui Province (grant no. 2108085MH252), the 512 Talent Cultivation Plan of Bengbu Medical College (grant numbers by51201202 and by51201307), the Innovation and Entrepreneurship Training Program for College Students (grant no. S202110367109).


## References

- [1] K. Walter, "What is acute ischemic stroke?," *JAMA*, vol. 327, no. 9, p. 885, 2022.
- [2] N. A. Weaver, H. J. Kuijf, H. P. Aben et al., "Strategic infarct locations for post-stroke cognitive impairment: a pooled analysis of individual patient data from 12 acute ischaemic stroke cohorts," *The Lancet Neurology*, vol. 20, no. 6, pp. 448–459, 2021.
- [3] M.-Y. Ding, Y. Xu, Y. Z. Wang et al., "Predictors of cognitive impairment after stroke: a prospective stroke cohort study," *Journal of Alzheimer's Disease*, vol. 71, no. 4, pp. 1139–1151, 2019.
- [4] M.-X. Liu, L. Luo, J.-H. Fu et al., "Exercise-induced neuroprotection against cerebral ischemia/reperfusion injury is mediated via alleviating inflammasome-induced pyroptosis," *Experimental Neurology*, vol. 349, article 113952, 2022.
- [5] D. Scheffer and A. Latini, "Exercise-induced immune system response: anti-inflammatory status on peripheral and central organs," *Biochimica et Biophysica Acta (BBA) - Molecular Basis of Disease*, vol. 1866, no. 10, article 165823, 2020.
- [6] K. Do, B. T. Laing, T. Landry et al., "The effects of exercise on hypothalamic neurodegeneration of Alzheimer's disease mouse model," *PLoS One*, vol. 13, no. 1, article e0190205, 2018.
- [7] R. S. Prakash, M. W. Voss, K. I. Erickson, and A. F. Kramer, "Physical activity and cognitive vitality," *Annual Review of Psychology*, vol. 66, no. 1, pp. 769–797, 2015.
- [8] Z. De Miguel, N. Khoury, M. J. Betley et al., "Exercise plasma boosts memory and dampens brain inflammation via clusterin," *Nature*, vol. 600, no. 7889, pp. 494–499, 2021.
- [9] C. P. Wen, C. H. Liu, J. S. Jeng et al., "Pre-stroke physical activity is associated with fewer post-stroke complications, lower mortality and a better long-term outcome," *European Journal of Neurology*, vol. 24, no. 12, pp. 1525–1531, 2017.
- [10] M. Alishahi, M. Farzaneh, F. Ghaedrahmati, A. Nejabatdoust, A. Sarkaki, and S. E. Khoshnam, "NLRP3 inflammasome in ischemic stroke: as possible therapeutic target," *International Journal of Stroke*, vol. 14, no. 6, pp. 574–591, 2019.
- [11] Y. Huang, W. Xu, and R. Zhou, "NLRP3 inflammasome activation and cell death," *Cellular & Molecular Immunology*, vol. 18, no. 9, pp. 2114–2127, 2021.
- [12] J. Anrather and C. Iadecola, "Inflammation and stroke: an overview," *Neurotherapeutics*, vol. 13, no. 4, pp. 661–670, 2016.
- [13] J. Wang, M. Guo, R. Ma, M. Wu, and Y. Zhang, "Tetrandrine alleviates cerebral ischemia/reperfusion injury by suppressing NLRP3 inflammasome activation via Sirt-1," *PeerJ*, vol. 8, article e9042, 2020.
- [14] Y. Q. Li, J. X. Chen, Q. W. Li, Z. J. Xiao, T. Yuan, and Z. H. Xie, "Targeting NLRP3 inflammasome improved the neurogenesis and post-stroke cognition in a mouse model of photothrombotic stroke," *Neuroreport*, vol. 31, no. 11, pp. 806–813, 2020.
- [15] E. Quigley, "Microbiota-brain-gut axis and neurodegenerative diseases," *Current Neurology and Neuroscience Reports*, vol. 17, no. 12, p. 94, 2017.
- [16] P. Honarpisheh, R. M. Bryan, and L. D. McCullough, "Aging microbiota-gut-brain axis in stroke risk and outcome," *Circulation Research*, vol. 130, no. 8, pp. 1112–1144, 2022.
- [17] L. Zhao, L. Yang, Y. Guo, J. Xiao, J. Zhang, and S. Xu, "New insights into stroke prevention and treatment: gut microbiome," *Cellular and Molecular Neurobiology*, vol. 42, no. 2, pp. 455–472, 2022.
- [18] H. Tilg, N. Zmora, T. E. Adolph, and E. Elinav, "The intestinal microbiota fuelling metabolic inflammation," *Nature Reviews Immunology*, vol. 20, no. 1, pp. 40–54, 2020.
- [19] C. Gubert, G. Kong, T. Renoir, and A. J. Hannan, "Exercise, diet and stress as modulators of gut microbiota: implications for neurodegenerative diseases," *Neurobiology of Disease*, vol. 134, article 104621, 2020.
- [20] F. Angelucci, K. Cechova, J. Amlerova, and J. Hort, "Antibiotics, gut microbiota, and Alzheimer's disease," *Journal of Neuroinflammation*, vol. 16, no. 1, p. 108, 2019.

- [21] A. Stacy, V. Andrade-Oliveira, J. A. McCulloch et al., "Infection trains the host for microbiota-enhanced resistance to pathogens," *Cell*, vol. 184, no. 3, pp. 615–627.e17, 2021.
- [22] W. Yang, Y. Liu, G. Yang et al., "Moderate-intensity physical exercise affects the exercise performance and gut microbiota of mice," *Frontiers in Cellular and Infection Microbiology*, vol. 11, article 712381, 2021.
- [23] V. Monda, I. Villano, A. Messina et al., "Exercise modifies the gut microbiota with positive health effects," *Oxidative Medicine and Cellular Longevity*, vol. 2017, Article ID 3831972, 8 pages, 2017.
- [24] H. Wekerle, "Brain autoimmunity and intestinal microbiota: 100 trillion game changers," *Trends in Immunology*, vol. 38, no. 7, pp. 483–497, 2017.
- [25] H. Zhu, Z. Jian, Y. Zhong et al., "Janus kinase inhibition ameliorates ischemic stroke injury and neuroinflammation through reducing NLRP3 inflammasome activation via jak2/stat3 pathway inhibition," *Frontiers in Immunology*, vol. 12, article 714943, 2021.
- [26] Q. Yu, T. Zhao, M. Liu et al., "Targeting NLRP3 inflammasome in translational treatment of nervous system diseases: an update," *Frontiers in Pharmacology*, vol. 12, article 707696, 2021.
- [27] C. Pellegrini, L. Antonioli, V. Calderone, R. Colucci, M. Fornai, and C. Blandizzi, "Microbiota-gut-brain axis in health and disease: is NLRP3 inflammasome at the crossroads of microbiota-gut-brain communications?," *Progress in Neurobiology*, vol. 191, article 101806, 2020.
- [28] E. Eeckhout and A. Wullaert, "Extraction of DNA from murine fecal pellets for downstream phylogenetic microbiota analysis by next-generation sequencing," *Bio-protocol*, vol. 8, no. 3, article e2707, 2018.
- [29] C. A. Thaïss, D. Zeevi, M. Levy et al., "Transkingdom control of microbiota diurnal oscillations promotes metabolic homeostasis," *Cell*, vol. 159, no. 3, pp. 514–529, 2014.
- [30] M. A. Sayed, W. Eldahshan, M. Abdelbary et al., "Stroke promotes the development of brain atrophy and delayed cell death in hypertensive rats," *Scientific Reports*, vol. 10, no. 1, article 20233, 2020.
- [31] X. Niu, Y. Zhao, N. Yang et al., "Proteasome activation by insulin-like growth factor-1/nuclear factor erythroid 2-related factor 2 signaling promotes exercise-induced neurogenesis," *Stem Cells*, vol. 38, no. 2, pp. 246–260, 2020.
- [32] H. Kim, J. S. Seo, S. Y. Lee et al., "AIM2 inflammasome contributes to brain injury and chronic post-stroke cognitive impairment in mice," *Brain, Behavior, and Immunity*, vol. 87, pp. 765–776, 2020.
- [33] X. Zhang and X. Bi, "Post-stroke cognitive impairment: a review focusing on molecular biomarkers," *Journal of Molecular Neuroscience*, vol. 70, no. 8, pp. 1244–1254, 2020.
- [34] K. Zhou, L. Shi, Y. Wang, S. Chen, and J. Zhang, "Recent advances of the NLRP3 inflammasome in central nervous system disorders," *Journal of Immunology Research*, vol. 2016, Article ID 9238290, 9 pages, 2016.
- [35] S. Jander, M. Schroeter, and G. Stoll, "Interleukin-18 expression after focal ischemia of the rat brain: association with the late-stage inflammatory response," *Journal of Cerebral Blood Flow and Metabolism*, vol. 22, no. 1, pp. 62–70, 2002.
- [36] K. I. Erickson, C. Hillman, C. M. Stillman et al., "Physical activity, cognition, and brain outcomes: a review of the 2018 physical activity guidelines," *Medicine and Science in Sports and Exercise*, vol. 51, no. 6, pp. 1242–1251, 2019.
- [37] A. Viktorisson, E. M. Andersson, E. Lundstrom, and K. S. Sunnerhagen, "Levels of physical activity before and after stroke in relation to early cognitive function," *Scientific Reports*, vol. 11, no. 1, p. 9078, 2021.
- [38] M. Reinholdsson, T. Abzhandadze, A. Palstam, and K. S. Sunnerhagen, "A register-based study on associations between pre-stroke physical activity and cognition early after stroke (part of papsigot)," *Scientific Reports*, vol. 12, no. 1, 2022.
- [39] J. M. Allen, M. E. Berg Miller, B. D. Pence et al., "Voluntary and forced exercise differentially alters the gut microbiome in C57BL/6J mice," *Journal of Applied Physiology*, vol. 118, no. 8, pp. 1059–1066, 2015.
- [40] S. C. Campbell, P. J. Wisniewski, M. Noji et al., "The effect of diet and exercise on intestinal integrity and microbial diversity in mice," *PLoS One*, vol. 11, no. 3, article e0150502, 2016.
- [41] S. F. Clarke, E. F. Murphy, O. O'Sullivan et al., "Exercise and associated dietary extremes impact on gut microbial diversity," *Gut*, vol. 63, no. 12, pp. 1913–1920, 2014.
- [42] K. A. Romano, E. I. Vivas, D. Amador-Noguez, and F. E. Rey, "Intestinal microbiota composition modulates choline bioavailability from diet and accumulation of the proatherogenic metabolite trimethylamine-N-oxide," *mBio*, vol. 6, no. 2, article e02481, 2015.
- [43] S. M. Collins, M. Surette, and P. Bercik, "The interplay between the intestinal microbiota and the brain," *Nature Reviews. Microbiology*, vol. 10, no. 11, pp. 735–742, 2012.
- [44] Y. Liu, C. Kong, L. Gong et al., "The association of post-stroke cognitive impairment and gut microbiota and its corresponding metabolites," *Journal of Alzheimer's Disease*, vol. 73, no. 4, pp. 1455–1466, 2020.
- [45] J. S. Ayres, "Inflammasome-microbiota interplay in host physiologies," *Cell Host & Microbe*, vol. 14, no. 5, pp. 491–497, 2013.
- [46] Y. Dang, X. Zhang, Y. Zheng et al., "Distinctive gut microbiota alteration is associated with poststroke functional recovery: results from a prospective cohort study," *Neural Plasticity*, vol. 2021, Article ID 1469339, 16 pages, 2021.
- [47] L. Han, T. Li, M. Du, R. Chang, B. Zhan, and X. Mao, "Beneficial effects of *Potentilla discolor* Bunge water extract on inflammatory cytokines release and gut microbiota in high-fat diet and streptozotocin-induced type 2 diabetic mice," *Nutrients*, vol. 11, no. 3, 2019.
- [48] A. B. Hall, M. Yassour, J. Sauk et al., "A novel Ruminococcus gnavus clade enriched in inflammatory bowel disease patients," *Genome Medicine*, vol. 9, no. 1, p. 103, 2017.
- [49] S. Wanchao, M. Chen, S. Zhiguo, X. Futang, and S. Mengmeng, "Protective effect and mechanism of Lactobacillus on cerebral ischemia reperfusion injury in rats," *Brazilian Journal of Medical and Biological Research*, vol. 51, no. 7, article e7172, 2018.
- [50] B. J. Parker, P. A. Wearsch, A. C. M. Veloo, and A. Rodriguez-Palacios, "The genus *Alistipes*: gut bacteria with emerging implications to inflammation, cancer, and mental health," *Frontiers in Immunology*, vol. 11, 2020.
- [51] R. Sadler, J. V. Cramer, S. Heindl et al., "Short-chain fatty acids improve poststroke recovery via immunological mechanisms," *The Journal of Neuroscience*, vol. 40, no. 5, pp. 1162–1173, 2020.

## Research Article

# LncRNA MDRL Mitigates Atherosclerosis through miR-361/SQSTM1/NLRP3 Signaling

Ling You,<sup>1</sup> Yanjie Zheng,<sup>1</sup> Jing Yang ,<sup>1</sup> Qian Hou,<sup>1</sup> Lianxia Wang,<sup>1</sup> Yan Zhang,<sup>1</sup> Chunxia Zhao ,<sup>2</sup> and Ruiqin Xie <sup>1</sup>

<sup>1</sup>Division of Cardiology, The Second Hospital of Hebei Medical University, Shijiazhuang, China

<sup>2</sup>Institute of Hypertension and Department of Internal Medicine, Tongji Hospital, Tongji Medical College, Huazhong University of Science and Technology, Wuhan, China

Correspondence should be addressed to Chunxia Zhao; zhaocx2001@126.com and Ruiqin Xie; xieruiqin88@163.com

Received 18 April 2022; Revised 25 July 2022; Accepted 18 August 2022; Published 21 September 2022

Academic Editor: Amilia Aminuddin

Copyright © 2022 Ling You et al. This is an open access article distributed under the Creative Commons Attribution License, which permits unrestricted use, distribution, and reproduction in any medium, provided the original work is properly cited.

**Objective.** Long non-coding RNAs (lncRNAs) play many important roles in gene regulation and disease pathogenesis. Here, we sought to determine that mitochondrial dynamic related lncRNA (MDRL) modulates NLRP3 inflammasome activation and apoptosis of vascular smooth muscle cells (VSMCs) and protects arteries against atherosclerosis. **Methods.** *In vivo* experiments, we applied LDLR knockout (LDLR<sup>-/-</sup>) mice fed the high-fat diet to investigate the effects of MDRL on atherosclerosis. *In vitro* experiments, we applied mouse aortic smooth muscle cells to determine the mechanism of MDRL in abrogating NLRP3 inflammasome and inhibiting cell apoptosis through miR-361/sequosome 1 (SQSTM1) by TUNEL staining, quantitative RT-PCR, western blot, microribonucleoprotein immunoprecipitation, and luciferase reporter assay. **Results.** Downregulated MDRL and increased NLRP3 were observed in mouse atherosclerotic plaques, accompanied with the increase of miR-361. The results showed that MDRL overexpression significantly attenuated the burden of atherosclerotic plaque and facilitated plaque stability through inhibiting NLRP3 inflammasome activation and cell apoptosis, and vice versa. Mechanically, MDRL suppressed NLRP3 inflammasome activation and VSMC apoptosis via suppressing miR-361. Furthermore, miR-361 directly bound to the 3'UTR of SQSTM1 and inhibited its translation, subsequently activating NLRP3 inflammasome. Systematic delivery of miR-361 partly counteracted the beneficial effects of MDRL overexpression on atherosclerotic development in LDLR<sup>-/-</sup> mice. **Conclusions.** In summary, MDRL alleviates NLRP3 inflammasome activation and apoptosis in VSMCs through miR-361/SQSTM1/NLRP3 pathway during atherogenesis. These data indicate that MDRL and inhibition of miR-361 represent potential therapeutic targets in atherosclerosis-related diseases.

## 1. Introduction

Atherosclerosis is a leading cause of cardiovascular and cerebrovascular diseases [1]. It is widely accepted that pro-inflammatory cytokines impair endothelial function and initiate atherosclerosis. Once the initial process is completed, both biochemical and biomechanical stimuli promote plaque development and rupture [2]. The pathological mechanisms of vascular smooth muscle cell (VSMC) dysfunction include aberrant proliferation, migration, apoptosis, and differentiation. Accumulating evidence indicates that excessive apoptosis of VSMCs can drive vascular remodeling and the progression of atherosclerosis [3]. Current study demon-

strated that oxidative low-density lipoprotein (ox-LDL) caused a cascade of inflammation and VSMC apoptosis through activation of NLRP3 inflammasome [4], which triggered caspase-1-mediated cleavage of pro-interleukin (IL)-1 $\beta$  and pro-IL-18, and secreted mature forms of these mediators from cells [5]. Thus, it is urgent to explore the candidate factors mediating the inhibition of dual signaling pathways and being promising therapeutic strategies for atherosclerosis.

Numerous studies have showed that long non-coding RNAs (lncRNAs) have pivotal functions in a cell-specific manner such as chromatin stabilization, RNA processing, and protein modification [6] Cytosolic lncRNAs could act

as competing endogenous RNAs (ceRNAs), which interact with miRNAs and regulate the expression of miRNA target genes. Simion et al. [7] revealed that knockdown of VINAS attenuated atherosclerotic plaque in LDLR<sup>-/-</sup> mice through inhibition of inflammation in endothelial cells (ECs). Moreover, Ni et al. [8] found that lncRNA CARMN directly interacted with serum response factor (SRF) to regulate the phenotypic switch of VSMCs via RNA pulldown and mass spectrometry analysis, eventually aggravating atherosclerosis. Recently, Wang et al. [9] identified lncRNA MDRL (mitochondrial dynamic related lncRNA) as a key regulator of mitochondrial fission via directly binding to miR-361. In this regard, MDRL overexpression reduced myocardial infarction via suppressing mitochondrial fission and apoptosis in cardiomyocytes [9]. However, major mechanistic gaps remain in the understanding of regulatory lncRNA MDRL involved in vascular injury and atherosclerosis.

In this study, we sought to investigate the role of MDRL in the development of atherosclerosis. We also determined whether MDRL participated in the regulation of NLRP3 inflammasome and apoptosis through sponging miRNAs or proteins in VSMCs. Collectively, these findings provide further insights into lncRNA-mediated VSMC function in atherosclerosis.

## 2. Methods

**2.1. Mouse Studies.** According to the National Institutes of Health guidelines, all mice were maintained and cared for under controlled environment (21 ± 2°C and a 12-h light/dark cycle). All mouse studies performed here were approved by the Institutional Animal Care and Use Committee at the Second Hospital of Hebei Medical University. Eight-week-old male LDLR<sup>-/-</sup> mice purchased from GemPharmatech Co., Ltd. (Nanjing, China) were fed *ad libitum* with normal diet (ND) or western high-fat diet (HFD) for 12 weeks. Thereafter, mice were sacrificed to harvest the aorta tissues for the following analysis.

**2.2. Cell Culture and Cell Transfection.** HEK-293T cells from the Cell Bank at the Chinese Academy of Sciences (Shanghai, China) were cultured in Dulbecco's modified Eagle's medium (DMEM) high glucose medium (Hyclone Laboratories Inc., UT, USA) supplemented with penicillin (100 units/ml, Hyclone, USA) and fetal bovine serum (FBS, 10%, Hyclone Laboratories Inc., UT, USA), at 37°C and 5% CO<sub>2</sub> in a humidified chamber.

Mouse aortic smooth muscle cells (MSMCs) were isolated from C57BL/6J mice. Cells were maintained in DMEM containing 10% FBS and 2 mM glutamine and passaged every 3-4 days. MSMCs at Passages 2-4 were used for further study.

As shown in Table S1, silencing RNAs (siRNAs), miRNA mimics or inhibitors, and corresponding controls were designed and synthesized by Genepharma Co., Ltd. (Suzhou, China). Oligonucleotides (50 nM) were transfected into HEK-293T cells or MSMCs using Lipofectamine 3000 (Invitrogen, CA, USA) according to the manufacturer's instructions. Cells were harvested for

qRT-PCR or western blot analysis after 48 h of transfection. MDRL cDNA sequences were subcloned, and then gene expression was amplified from the lentiviral vectors. To explore the effect of MDRL on cell function and miR-361, MSMCs and HEK-293T cells were transfected and divided into four groups: scramble siRNA (MDRL-sc), MDRL-siRNA, control adenoviral, or adenoviral MDRL.

**2.3. RNAscope.** The aortas were isolated and harvested from ND or HFD-treated LDLR<sup>-/-</sup> mice to explore the expression of MDRL in normal arteries and atherosclerotic plaques. RNAscope probes of mouse MDRL and all reagents are purchased from Advanced Cell Diagnostics, Inc. (CA, USA). Paraffin-embedded tissues of mouse aortic roots underwent fixation, dehydration, embedding, cutting, and floating. Sections with a thickness of about 5 μm were deparaffinized, dehydrated, and subjected to antigen retrieval for 15 min at 90°C. After sections were treated with protease III (15 min at 40°C), probes were hybridized for 2 h at 40°C followed by a signal amplification. Subsequently, nuclei were stained with DAPI, and then we performed the signal detection using a RNAscope Multiplex Fluorescent Reagent kit. Images were captured using the Confocal laser scanning microscopy (Leica, SP8, Germany).

**2.4. Injection of Recombination Adeno-Associated Viruses (rAAVs) and miR-361.** Adeno-associated virus serotype 8 vectors for expression of the murine MDRL (rAAV-MDRL), control vectors (rAAV-CTR), scramble vectors (rAAV-scramble), and short hairpin RNA to block MDRL (rAAV-shMDRL) were synthesized by GeneChem Corporation (China). Mice were given intravenous injection of rAAV-CTR or rAAV-MDRL (1 × 10<sup>12</sup> viral genome particles) via tail vein and then fed with HFD for 12 weeks. To investigate the effect of knockdown of MDRL on atherosclerosis, LDLR<sup>-/-</sup> mice were given intravenous injection of rAAV-scramble or rAAV-shMDRL (1 × 10<sup>12</sup> viral genome particles) via tail vein and then fed with HFD for 12 weeks [10]. Similarly, miRNA non-specific control (miR-NC) or miR-361 mimics was incubated with Lipofectamine 3000 (Invitrogen, CA, USA) at room temperature for 30 minutes. Mice were injected with miR-NC or miR-361 (5 nmol) weekly for 12 weeks via tail vein as previously described [11].

**2.5. Analysis of mRNA by Quantitative RT-PCR.** Total RNA was extracted from aortic tissues and cells using TRIzol reagent (Invitrogen, USA), and reverse transcribed using PrimeScript RT Master Mix (TaKaRa, Japan). Quantitative RT-PCR (qRT-PCR) was performed with the SYBR Premix Ex Taq™ Kit (Takara, Japan) using a Light Cycler 480 II system (Roche, Switzerland). GAPDH was used as an internal control to normalize gene expression. The sequences of primers are listed in Table S1.

**2.6. Western Blot.** Briefly, aortic tissues and cells from different groups were harvested and lysed with lysis buffer containing the protease inhibitor cocktail. Then, protein was evaluated by SDS-PAGE electrophoresis and transferred to PVDF blotting membrane. The primary antibodies used as

follows: NLRP3 (15101, Cell Signaling Technology, USA), SQSTM1 (sequestosome 1, 39749, Cell Signaling Technology, USA), and  $\beta$ -tubulin (66362-1-Ig, Proteintech, USA).

**2.7. Histochemical and Immunohistochemical Staining.** Formalin-fixed, paraffin-embedded sections (5  $\mu$ m thick) of mouse hearts with aortic roots were stained with H&E staining for cap thickness, and Masson's trichrome for collagen as previously described [12]. Images were evaluated by Olympus BX50 microscope and analyzed using the NIH Image J software.

Immunohistochemical staining was performed as previously described. The sections were incubated with primary antibodies against NLRP3 (1:200, Abcam, USA) at 4°C overnight, followed by secondary antibody before staining with DAB Kit (ZSGB-BIO, China). Sections incubated with species-matched IgG alone were used as negative controls.

Quantification of atherosclerotic lesions was performed as previously reported [13]. Briefly, the heart sample containing the aortic root was embedded in OCT and frozen at -80°C. Serial 7- $\mu$ m-thick cryosections from the aortic sinus were mounted on masked slides. Then, the cryosections containing atherosclerotic plaques were quantified with Oil Red O staining following standard protocol as described. Atherosclerosis in the aortic root cryosections was quantified using Image J.

**2.8. TUNEL Assay.** Apoptosis of tissues and cells was measured by TUNEL assay. Apoptotic detection kit (Roche, Switzerland) was used to investigate DNA fragments in the nucleus in situ according to the manufacturer's instructions. Fluorescence microscopy was used to capture images. TUNEL-positive cells and total cells were counted, and the ratio was calculated.

**2.9. RNA Immunoprecipitation (RIP) Assay.** According to the manufacturer's instructions, RIP was performed using a Magna RIP RNA-Binding Protein Immunoprecipitation kit (Millipore, USA) [14]. Briefly,  $2 \times 10^7$  cell lysates were incubated with RIP immunoprecipitation buffer containing magnetic beads conjugated with anti-Ago2 antibody (ab186733, Abcam, USA) and negative control normal mouse IgG. Then, immunoprecipitated RNAs were isolated and detected using qRT-PCR to determine the enrichment of binding targets, and then the products were pulled down to agarose gel electrophoresis.

**2.10. Dual-Luciferase Reporter Gene System.** To determine the binding among non-coding RNA and mRNA, the target DNA sequence was inserted into pGL3-basic luciferase reporter vector (Promega, USA). HEK-293T cells ( $1 \times 10^5$ ) were transfected with miRNA mimics/control and luciferase plasmid together. After 48 hours of transfection, the activity of luciferase reporter was assessed through Dual-Luciferase Reporter Assay (Promega, USA). Relative luciferase activity was normalized to Renilla activity.

**2.11. Statistical Analysis.** The data were analyzed using GraphPad Prism 7.0 software (USA). All continuous variables that complied with normal distribution were presented

as the mean  $\pm$  the standard error of the mean (SEM). Experiments were performed using at least three biologically distinct replicates. Student's *t* test (two-tailed) was used for comparisons of two groups, and one-way ANOVA with Bonferroni correction was used for multiple comparisons. Significant differences were determined at  $P < 0.05$ .

### 3. Results

**3.1. MDRL Expression Was Decreased in Atherosclerotic Lesion, Accompanied with Upregulated NLRP3 Expression.** To investigate the involvement of MDRL in atherosclerosis, we initially examined the expression of MDRL in bone marrow-derived macrophages, MSMCs, and primary pulmonary endothelial cells and found that MDRL was predominantly expressed in MSMCs (Figure 1(a)). Moreover, significant decreased MDRL expression was observed in aortas isolated from HFD-fed LDLR<sup>-/-</sup> mice than ND-fed LDLR<sup>-/-</sup> mice (Figure 1(b)). Further, RNAscope results confirmed the reduced MDRL expression in HFD-fed LDLR<sup>-/-</sup> mice and also demonstrated that MDRL was presented primarily in the cytoplasm (Figures 1(c) and 1(d)). Given the NLRP3 inflammasome-mediated inflammation and pyroptosis in the regulation of atherosclerosis, we also confirmed the changes of NLRP3 during atherogenesis. Consistently, NLRP3 expression was substantially upregulated in aortas of HFD-fed LDLR<sup>-/-</sup> mice by qRT-PCR and western blot (Figures 1(e) and 1(f)).

**3.2. MDRL Regulated Atherogenesis in LDLR<sup>-/-</sup> Mice.** To determine the effect of MDRL overexpression in pathological context, LDLR<sup>-/-</sup> mice were treated with rAAV-CTR or rAAV-MDRL. Quantification of atherosclerotic plaques by hematoxylin/eosin staining indicated an increase in cap thickness in the aortic sinus of MDRL-transfected versus CTR-transfected LDLR<sup>-/-</sup> mice (Figure 2(a)). Masson staining showed increased collagen contents in LDLR<sup>-/-</sup> mice transfected with rAAV-MDRL compared to those with rAAV-CTR (Figure 2(b)). Furthermore, in comparison with control group, MDRL-transfected LDLR<sup>-/-</sup> mice developed smaller lesions in aortic sinus (Figure 2(c)). Conversely, inhibition of MDRL by rAAV-shMDRL contributed to an increase in cap thickness and collagen content of the aortic sinus (Figures 2(d) and 2(e)). Knockdown of MDRL by rAAV-shMDRL enhanced the development of atherosclerotic plaques in aortic sinus compared to rAAV-scramble-treated LDLR<sup>-/-</sup> mice (Figure 2(f)).

Since the development of atherosclerotic plaques contributed to NLRP3 activation [15], we determined the effects of MDRL on NLRP3 activation. LDLR<sup>-/-</sup> mice transfected with rAAV-MDRL displayed an approximate 62.41% reduction in the percentage of NLRP3 positive area within aortic plaques relative to control group (Figures 3(a) and 3(b)). In line with this finding, augmentation of MDRL significantly attenuated NLRP3 expression in aorta of LDLR<sup>-/-</sup> mice (Figures 3(c) and 3(d)). Immunohistochemical analyses of aortic sinus cross sections showed that, compared with control mice, those in MDRL-transfected LDLR<sup>-/-</sup> mice had reduced TUNEL-positive cells (Figures 3(e) and 3(f)). Correspondingly, serum

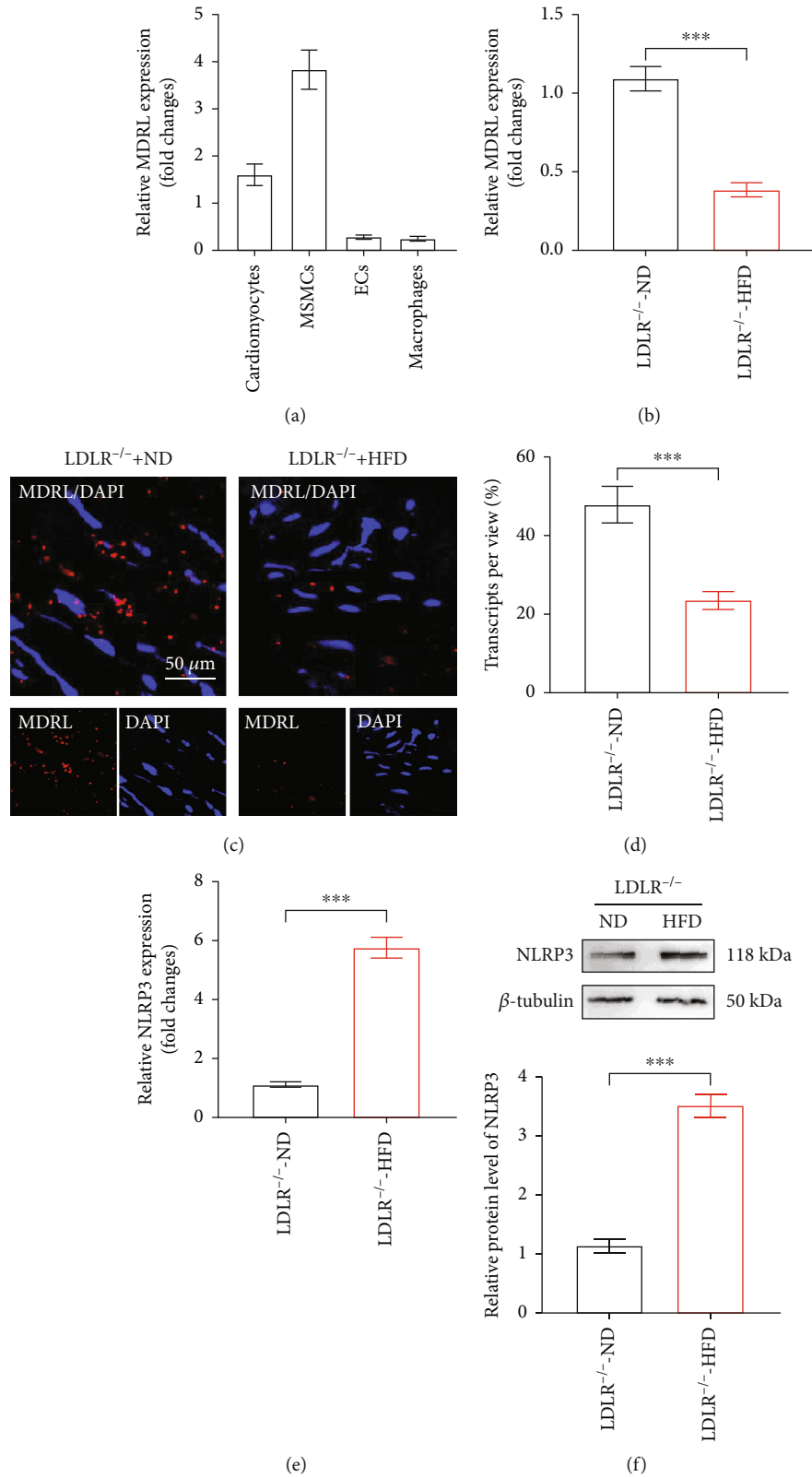


FIGURE 1: MDRL is abundant in VSMCs and decreased in atherosclerotic lesions. (a) The expression levels of lncRNA MDRL in different cell types were analyzed by qRT-PCR. \*\*\* $P < 0.001$  vs cardiomyocytes group. (b) The expression levels of MDRL in aortas of  $LDLR^{-/-}$  mice fed with normal diet (ND) or high-fat diet (HFD) were analyzed by qRT-PCR. (c) Confocal microscopy of MDRL in aortic roots of  $LDLR^{-/-}$  mice fed with ND or HFD. Scale bar: 50  $\mu$ m. (d) Quantitative analysis of MDRL transcripts in aortic roots of  $LDLR^{-/-}$  mice fed with ND or HFD. (e) The expression levels of NLRP3 in aortas of  $LDLR^{-/-}$  mice fed with ND or HFD were analyzed by qRT-PCR. (f) Representative images and quantification of NLRP3 protein in aortas of  $LDLR^{-/-}$  mice fed with ND or HFD. Data are presented as mean  $\pm$  SEM. \*\*\* $P < 0.001$  vs  $LDLR^{-/-}$ -ND group.



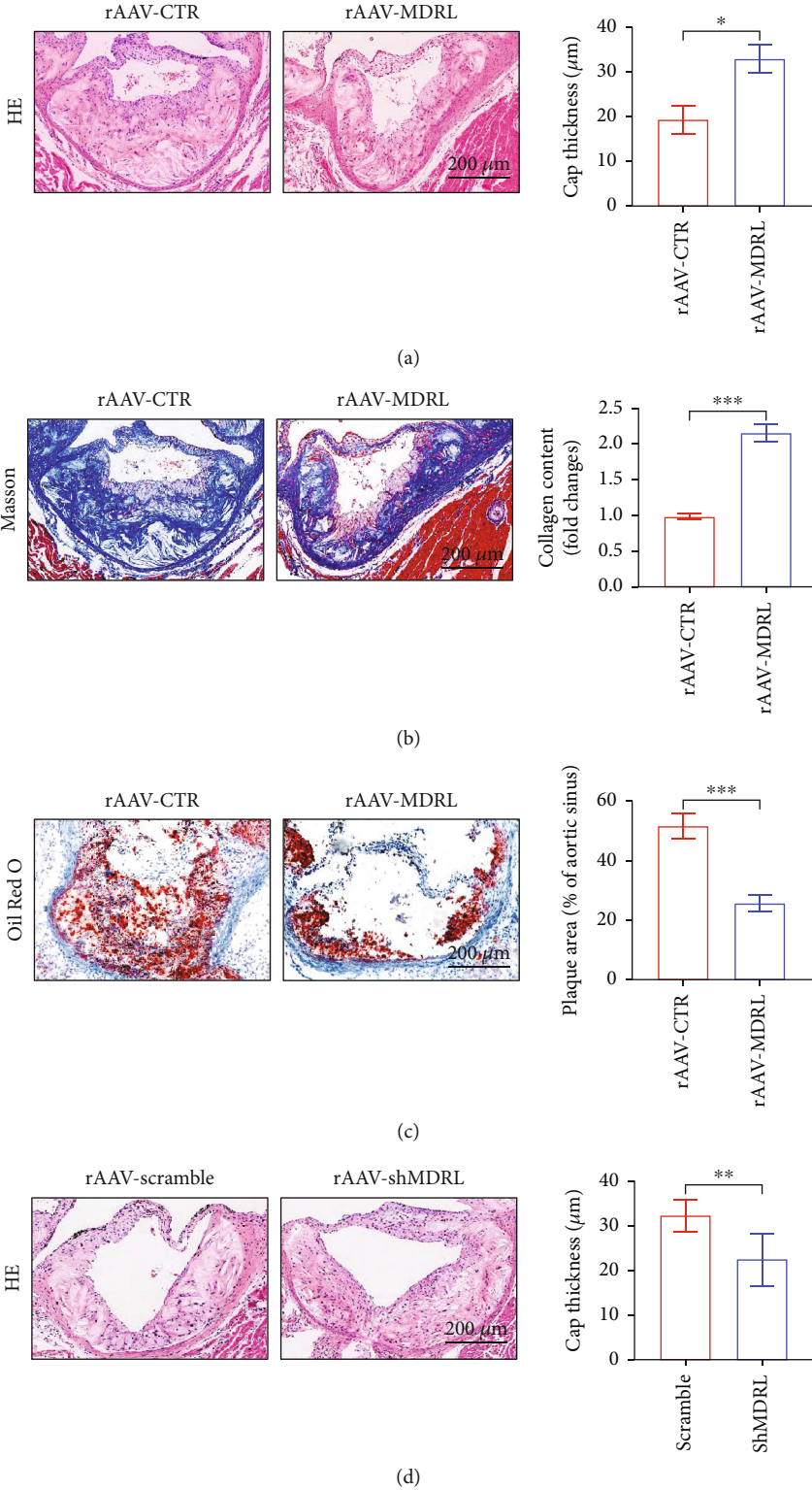


FIGURE 2: Continued.

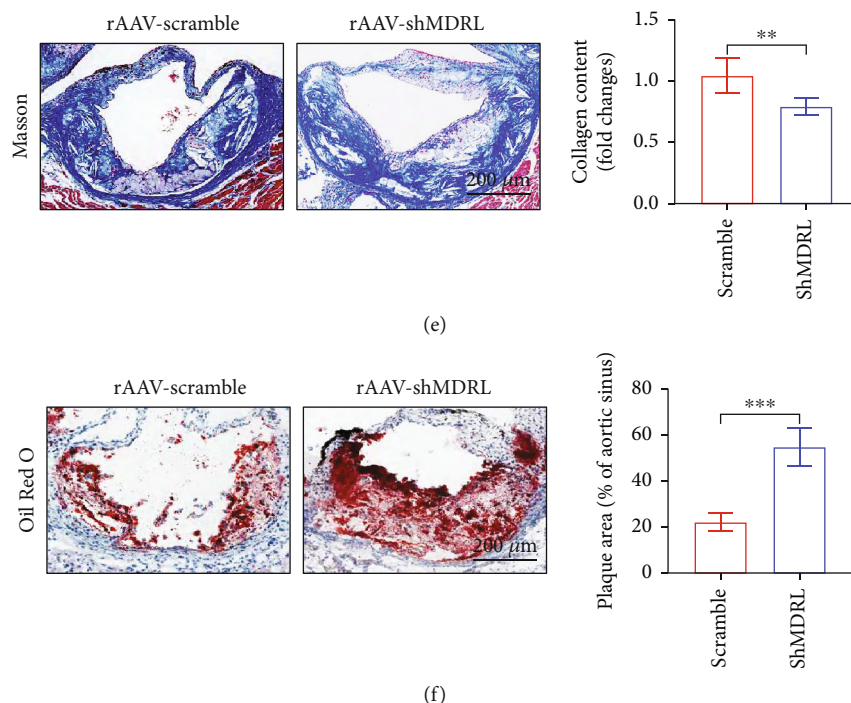


FIGURE 2: MDRL alleviates atherosclerosis in  $LDLR^{-/-}$  mice fed with HFD. (a) Representative images of HE-stained aortic roots from rAAV-CTR- or rAAV-MDRL-treated  $LDLR^{-/-}$  mice and quantification of fibrous cap thickness. (b) Representative images of Masson-stained aortic roots from rAAV-CTR- or rAAV-MDRL-treated  $LDLR^{-/-}$  mice and quantification of collagen content. (c) Representative images of Oil red O-stained aortic roots from rAAV-CTR- or rAAV-MDRL-treated  $LDLR^{-/-}$  mice and quantification of plaque area. (d) Representative images of HE-stained aortic roots from rAAV-scramble- or rAAV-shMDRL-treated  $LDLR^{-/-}$  mice and quantification of fibrous cap thickness. (e) Representative images of Masson-stained aortic roots from rAAV-scramble- or rAAV-shMDRL-treated  $LDLR^{-/-}$  mice and quantification of collagen content. (f) Representative images of Oil red O-stained aortic roots from rAAV-scramble- or rAAV-MDRL-treated  $LDLR^{-/-}$  mice and quantification of plaque area. Scale bar:  $200\ \mu\text{m}$ . Data are presented as mean  $\pm$  SEM. \* $P < 0.05$ , \*\* $P < 0.01$ , \*\*\* $P < 0.001$  vs rAAV-CTR or rAAV-scramble group.

concentration of  $IL-1\beta$  was lower in MDRL-transfected group compared to control group (Figure 3(g)). Taken together, these data suggest a protective role of MDRL against the development of atherosclerotic plaques.

**3.3. MDRL Inhibited NLRP3 Inflammasome and Apoptosis through miR-361.** To validate the effect of MDRL on NLRP3 inflammasome and apoptosis, we first evaluate the efficiency of MDRL knockdown and overexpression in MSMCs. As expected, the expression of MDRL was significantly down-regulated by siRNA (Figure 4(a)), whereas transfection with adenoviral MDRL significantly augmented MDRL expression in MSMCs (Figure 4(b)). While decreased MDRL significantly promoted MSMCs apoptosis, adenoviral MDRL resulted in a reduction of MSMCs apoptosis (Figures 4(c) and 4(d)). Moreover, knockdown of MDRL caused increased expression of NLRP3, and adenoviral MDRL mitigated NLRP3 expression in MSMCs vice versa (Figure 4(e)).

Next, we investigated whether miR-361 acted as an effector of MDRL in VSMCs and NLRP3 inflammasome activation. As shown in Figure 5(a), the expression of miR-361 was significantly increased after transfection of MDRL-siRNA in MSMCs, whereas overexpression of MDRL markedly inhibited miR-361 expression (Figure 5(b)). To explore whether MDRL as a ceRNA competitively bound to miR-361,

we transfected the miR-361 sensor luciferase reporter vector, along with MDRL-siRNA or adenoviral MDRL in HEK-293T cells. Compared with scramble siRNA group, we detected a significantly reduced luciferase activity of miR-361 sensor in MDRL-siRNA group (Figure 5(c)). By contrast, a prominent enhancement of luciferase activity was observed in adenoviral MDRL group (Figure 5(d)). We then employed biotin-conjugated pull-down assay in MSMCs, finding that miR-361 could pull down MDRL (Figure 5(e)). These data confirm that MDRL acts as an endogenous sponge lncRNA to interact with miR-361 and blocks miR-361 expression.

**3.4. MiR-361 Provoked NLRP3 Inflammasomes via Weakening SQSTM1.** To explore how miR-361 affects NLRP3 inflammasomes in VSMCs, we applied TargetScan and PicTar to the putative targets of miR-361 related to regulation of NLRP3 inflammasomes. The bioinformatic database exhibited the predicted binding site of miR-361 within the 3'UTR of SQSTM1 (Figure 6(a)). As expected, elevated miR-361 resulted in decreased expression of SQSTM1, accompanied with enhanced NLRP3 expression (Figures 6(b) and 6(c)). To confirm whether SQSTM1 was a direct target of miR-361, luciferase reporter plasmid containing the 3'UTR fragment of SQSTM1 was co-transfected with miR-361 mimics into HEK-293T cells. As illustrated

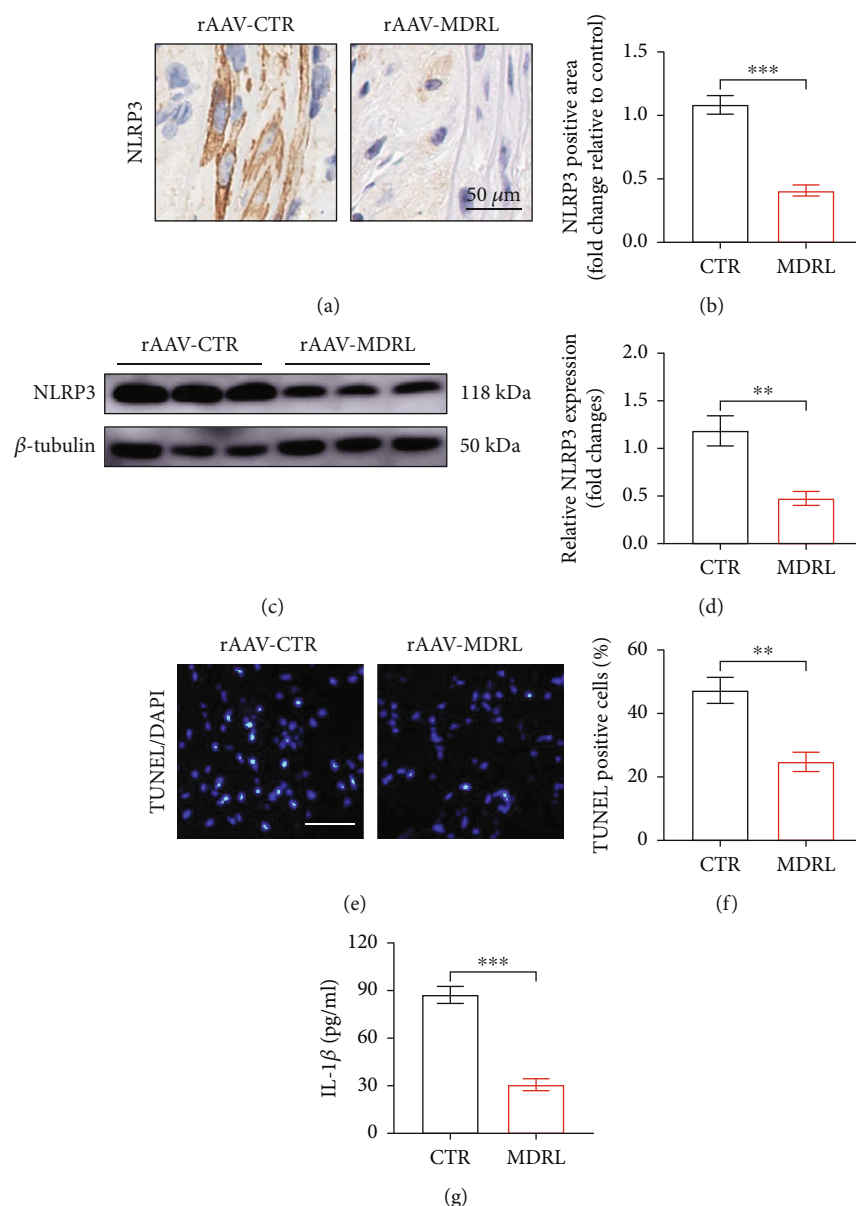


FIGURE 3: MDRL attenuates NLRP3 inflammasome and apoptosis in plaques of *LDLR*<sup>-/-</sup> mice fed with HFD. (a) Representative images of IHC staining for NLRP3 in aortic roots from rAAV-CTR- or rAAV-MDRL-treated *LDLR*<sup>-/-</sup> mice. Scale bar: 50  $\mu$ m. (b) Quantification of NLRP3 positive area in aortic roots. (c and d) Western blots showed the expression levels of NLRP3 protein in aortas from rAAV-CTR- or rAAV-MDRL-treated *LDLR*<sup>-/-</sup> mice. (e) Representative images of TUNEL staining (stained with green) in aortic roots from rAAV-CTR- or rAAV-MDRL-treated *LDLR*<sup>-/-</sup> mice. Scale bar: 50  $\mu$ m. (f) Quantification of TUNEL-positive cells in aortic roots. (g). Serum concentration of IL-1 $\beta$  from rAAV-CTR- or rAAV-MDRL-treated *LDLR*<sup>-/-</sup> mice. Data are presented as mean  $\pm$  SEM. \*\* $P < 0.01$ , \*\*\* $P < 0.001$  vs rAAV-CTR group.

in Figure 6(d), the luciferase activity of SQSTM1 3'UTR was remarkably suppressed by miR-361 mimics, whereas the luciferase activity of mutant binding sequences of SQSTM1 3'UTR was not changed. Likewise, microribonucleoprotein immunoprecipitation identified the interaction between miR-361 and SQSTM1 (Figure 6(e)). We also found that overexpression of miR-361 facilitated VSMC apoptosis detected by TUNEL staining (Figure 6(f)).

### 3.5. MiR-361 Is Required for the Inhibitory Effect of MDRL on Atherosclerotic Development in *LDLR*<sup>-/-</sup> Mice. To confirm

whether miR-361 was essential for MDRL in regulating atherosclerosis, MDRL-transfected *LDLR*<sup>-/-</sup> mice received weekly tail vein injections of miR-NC or miR-361 mimics for 12 weeks. Morphological analyses showed that *LDLR*<sup>-/-</sup> mice with both MDRL and miR-361 overexpression had thinner fibrous cap than *LDLR*<sup>-/-</sup> mice with only MDRL overexpression (Figures 7(a) and 7(b)). The collagen volume within the lesions was remarkably decreased in miR-361 overexpression mice relative to miR-NC group (Figures 7(c) and 7(d)). Compared to miR-NC group, Oil Red O staining of miR-361-transfected *LDLR*<sup>-/-</sup> mice revealed a 2-fold increase in lesion

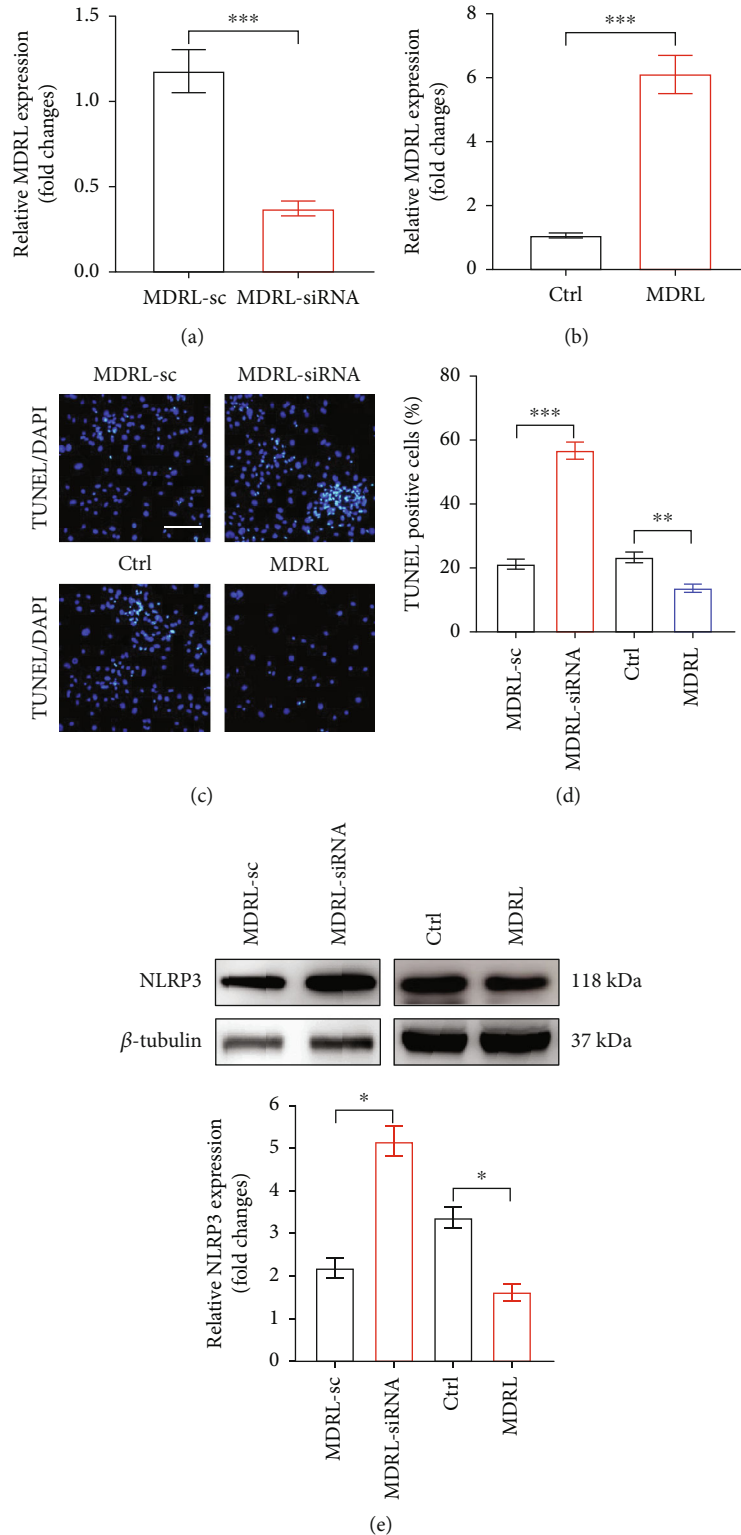


FIGURE 4: MDRL regulates NLRP3 inflammasome and apoptosis in VSMCs. (a) The expression of MDRL in MSMCs transfected with siRNA (MDRL-siRNA) or scramble (MDRL-sc) were analyzed by qRT-PCR. (b) The expression of MDRL in MSMCs transfected with adenoviral MDRL (MDRL) or control adenovirus (ctrl) was analyzed by qRT-PCR. (c) Representative images of TUNEL staining in MSMCs transfected with MDRL-sc, MDRL-siRNA, ctrl, or MDRL. Scale bar: 50  $\mu$ m. (d) Quantification of TUNEL-positive cells in MSMCs in the indicated groups. (e) Western blots showed the expression levels of NLRP3 in MSMCs in the indicated groups and quantification. The relative expression of NLRP3 was normalized to housekeeping gene  $\beta$ -tubulin in corresponding lane. Data are presented as mean  $\pm$  SEM. \*  $P < 0.05$ , \*\*  $P < 0.01$ , \*\*\*  $P < 0.001$  vs MDRL-sc or ctrl group.

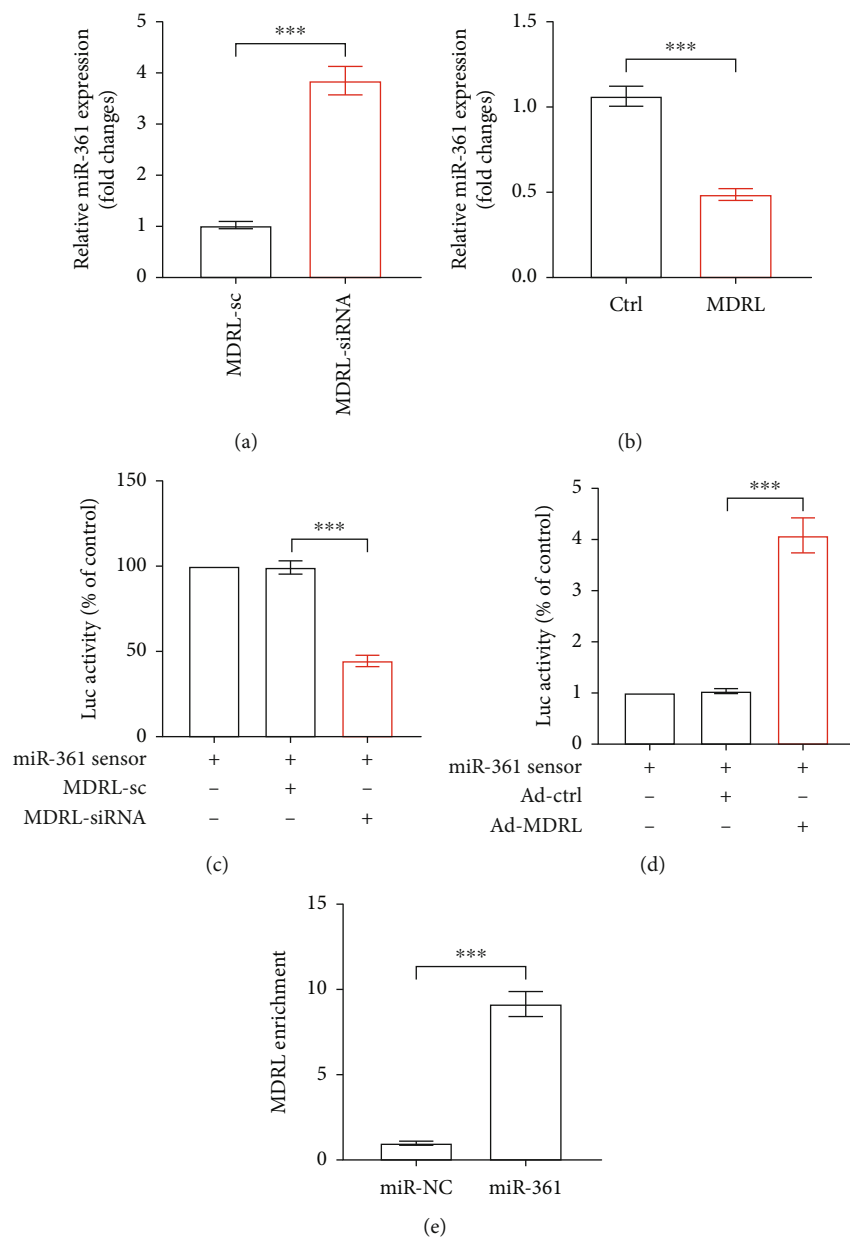


FIGURE 5: MDRL acts as an endogenous sponge to miR-361. (a) The expression levels of miR-361 in MSMCs transfected with siRNA (MDRL-siRNA) or scramble (MDRL-sc) were analyzed by qRT-PCR. (b) The expression levels of miR-361 in MSMCs transfected with adenoviral MDRL (MDRL) or control adenovirus (ctrl) were analyzed by qRT-PCR. (c) Luciferase activities were measured in HEK-293T cells transfected miR-361 sensor luciferase reporter vector, along with MDRL-siRNA or MDRL-sc. (d) Luciferase activities were measured in HEK-293T cells transfected miR-361 sensor luciferase reporter vector, along with ctrl or MDRL. (e) MDRL binds to miR-361. Biotin-conjugated pulldown assay and qRT-PCR were performed in MSMCs. Data are presented as mean  $\pm$  SEM.  $^{**}P < 0.001$  vs MDRL-sc or ctrl or miR-361 sensor group.

area at the level of the aortic sinus (Figures 7(e) and 7(f)). These data support our hypothesis that MDRL exerts its effect on atherosclerotic development via suppression of miR-361.

#### 4. Discussion

Our study reveals that MDRL plays an important role in the development of atherosclerosis. We indicate that MDRL is downregulated in atherosclerotic plaques of LDLR<sup>-/-</sup> mice. More importantly, overexpression of MDRL alleviates the

burdens of plaque and stabilizes plaques. Our *in vitro* mechanistic study shows that VSMC-enriched lncRNA MDRL regulates VSMC apoptosis and inflammation via interplaying with miR-361/SQSTM1 and suppressing NLRP3 inflammasome.

It is accepted that lncRNA confers pleiotropic functions, directly interacting and mediating expression and functionality of DNA, other non-coding RNAs, and proteins. Accumulating studies highlight that lncRNAs participate in atherogenesis and dysfunction of VSMCs [16–18]. For

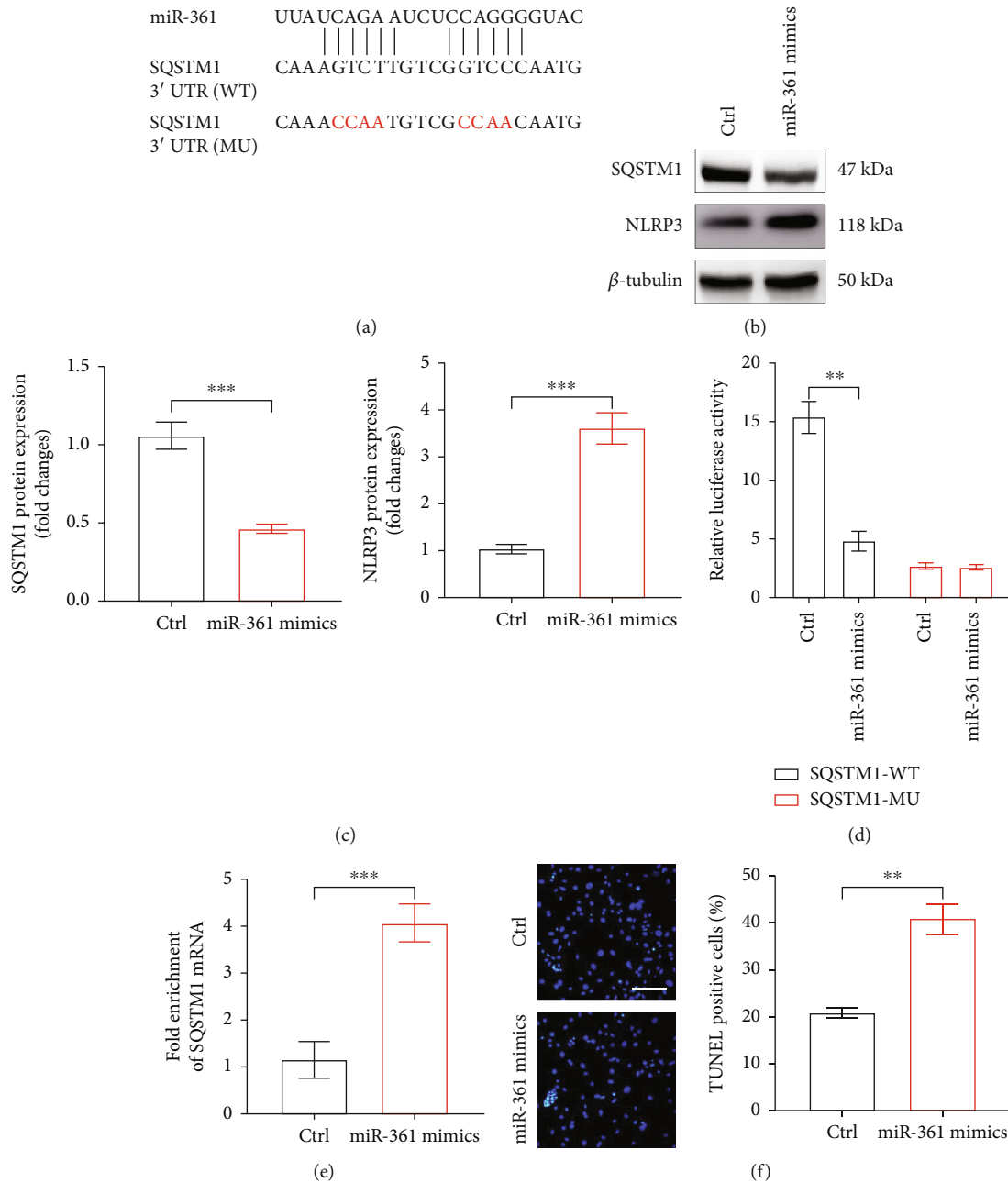


FIGURE 6: miR-361 binds to SQSTM1 and suppresses SQSTM1/NLRP3. (a) The putative targeting site of SQSTM1 and miR-361 was predicted by Targetscan and PicTar. (b) SQSTM1 and NLRP3 protein expression in MSMCs transfected with miR-361 mimics or control (ctrl). (c) Quantification of SQSTM1 and NLRP3 protein expression on western blots. (d) Luciferase activities were measured in HEK-293T cells transfected with SQSTM1-WT or SQSTM1-MU luciferase reporter vector, along with ctrl or miR-361 mimics. (e) MiR-361 binds to MDRL. Biotin-conjugated pulldown assay and qRT-PCR were performed in MSMCs. (f) Representative images of TUNEL staining in MSMCs transfected with ctrl or miR-361 mimics, and quantification of TUNEL-positive cells. Scale bar: 50  $\mu$ m. Data are presented as mean  $\pm$  SEM. \*\*\* $P$  < 0.001 vs ctrl group.

instance, lncRNA CARMN was reported to be abundant in VSMCs and involved in the formation of atherosclerotic plaques, while knockdown of CARMN mitigated VSMC proliferation, migration, and differentiation [8]. In our present study, we identified a novel mechanism through which lncRNA MDRL represses VSMC apoptosis and retards the progression of atherosclerosis. MDRL was initially described to be highly expressed in cardiomyocytes but reduced upon

the condition of anoxia followed by reoxygenation [9]. Moreover, MDRL was able to attenuate mitochondrial fission and apoptosis of cardiomyocytes through targeting miR-361 and miR-484 and inhibited the infarct size in mice of ischemia/reperfusion model [9]. Therefore, despite possessing multiple functions, MDRL is likely to confer cardioprotection and atheroprotection. Another important finding of our study was that MDRL alleviated VSMC apoptosis via

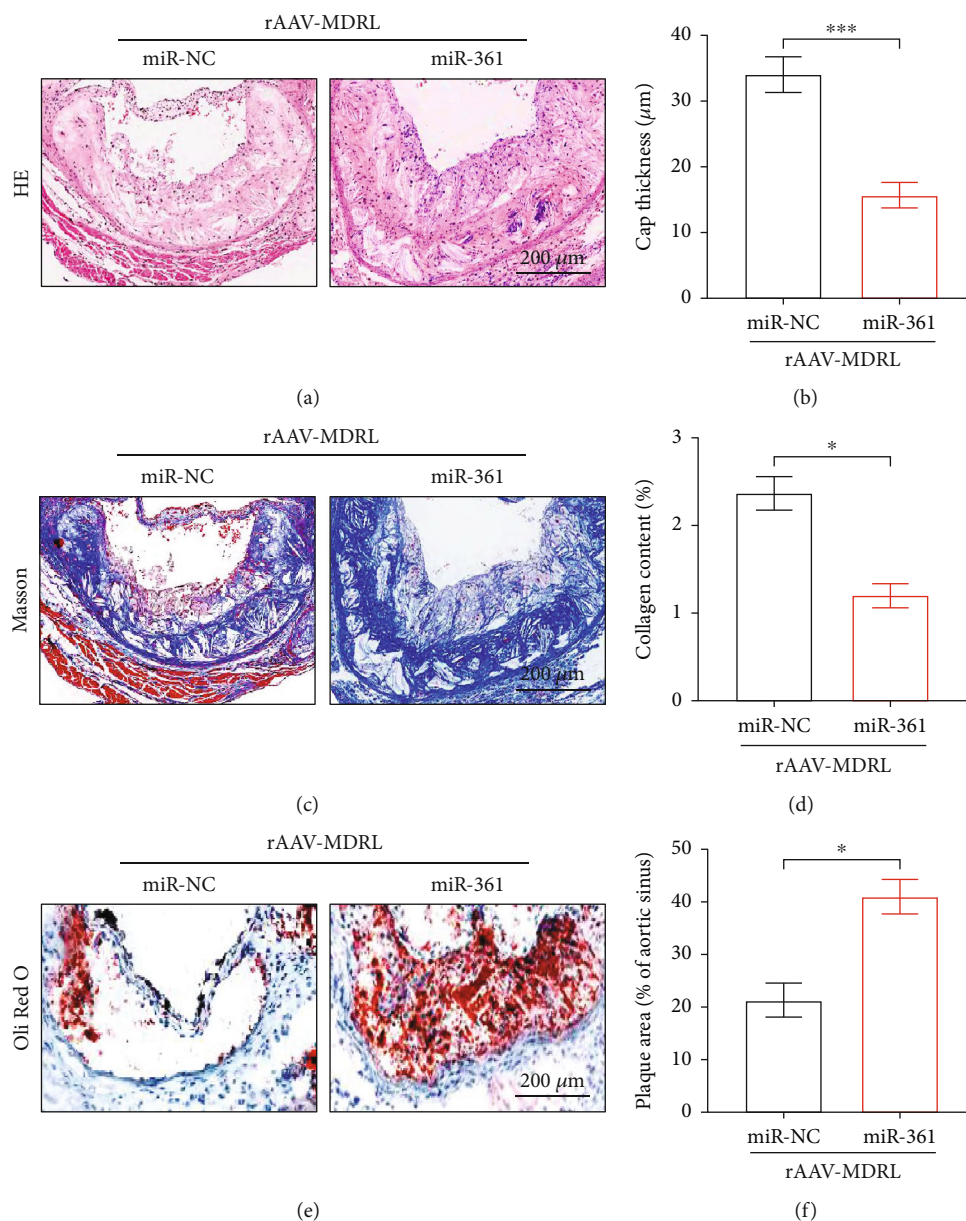


FIGURE 7: Overexpression of miR-361 counteracts the protective effect of MDRL against atherosclerosis. (a) Representative images of HE-stained aortic roots from control miRNA (miR-NC) or miR-361-treated LDLR<sup>-/-</sup> mice after intravenous injection of rAAV-MDRL. (b) Quantification of fibrous cap thickness. (c) Representative images of Masson-stained aortic roots from miR-NC or miR-361-treated LDLR<sup>-/-</sup> mice. (d) Quantification of collagen content. (e) Representative images of Oil red O-stained aortic roots from miR-NC or miR-361-treated LDLR<sup>-/-</sup> mice. (f) Quantification of plaque area. Scale bar: 200  $\mu\text{m}$ . Data are presented as mean  $\pm$  SEM. \*  $P < 0.05$  vs miR-NC group.

reducing NLRP3 inflammasomes. As the predominant cells in plaques and tunica media of the vessels, VSMCs are essential for the maintenance of artery structure and function [19]. Apart from phenotypic switching, VSMCs appear to possess universal effects, such as proliferation and apoptosis, which are implicated in vascular remodeling, aortic aneurysm, and atherosclerosis [20, 21]. In this regard, loss and alteration of VSMCs in atherosclerotic plaques exert detrimental effects, causing fibrous cap thinning, necrotic core formation, and plaque rupture [21, 22].

On the other hand, lncRNAs are frequently emerged as ceRNAs for miRNAs. In cardiovascular diseases, Huang

et al. [23] reported that the ceRNA network constituted by lncRNA PVT1, miR-3127-5p, and NCKAP1L was involved in the formation of aortic aneurysm. Another study suggested that lncRNA CDKN2B-AS1 as a ceRNA competitively bound to miR-126-5p to upregulate PTPN7, accelerating VSMC apoptosis [24]. Similarly, our findings recognized SQSTM1 as an effector of MDRL/miR-361 ceRNA activity. Previous studies demonstrated that miR-361 functioned as a regulator in glioma aerobic glycolysis and proliferation [25]. In addition, systematic delivery of miR-361 impeded glioma development through suppressing UBR5 [26]. In contrast with these phenomena, our study

showed that effective delivery of miR-361 partly offset the protective effect of MDRL on the development of atherosclerosis. These contradictory results are probable to account for the cell-specific potency of miR-361 in cancer cells and VSMCs.

NLRP3 inflammasomes centrally integrate multiple signal inputs in different types of cells and in the pathogenesis of atherosclerosis [27]. In atherogenesis, NLRP3 serves as an important responder to danger signals, including reactive oxygen species, ox-LDL, and cholesterol crystals [28]. NLRP3 inflammasomes drive caspase-1 cleavage, IL-1 $\beta$ , and IL-18 maturation and secretion, causing inflammation and pyroptosis [29]. Additionally, activation of NLRP3 inflammasome provoked high mobility group box 1 secretion, promoting VSMC-derived foam cell formation and accelerating atherosclerosis [30]. Current evidence corroborated previous observations supporting a translational strategy for blockage of caspase-1 to prevent VSMC pyroptosis and atherogenesis [31]. There were few known miRNAs targeting assemble and activation of NLRP3 inflammasomes, while hypermethylated miR-145 induced NLRP3 inflammasome through CD137/NFATc1 pathway [32]. Our study demonstrated that MDRL negatively regulates NLRP3 inflammasome via interacting with miR-361 and SQSTM1. Indeed, SQSTM1 served as a bona fide direct target of miR-361 in VSMCs. SQSTM1, nominated p62, is defined as a potent selective autophagy receptor, also engaged in the ubiquitin-proteasome system, cellular metabolism, and apoptosis [33]. Correspondingly, SQSTM1 was reported to interplay with NLRP3 in macrophages, which in turn exerted SQSTM1-dependent autophagic degradation of NLRP3 and inactivation of NLRP3 inflammasomes [34]. Combined with these data, the molecular action of SQSTM1 provides further insight to the relevance of MDRL and miR-361 to activation of NLRP3 inflammasomes and VSMC apoptosis.

## 5. Conclusion

Collectively, the results of our study indicate that the lncRNA MDRL abrogates miR-361 expression, thereby inhibiting VSMC apoptosis via suppression of SQSTM1-dependent NLRP3 inflammasome and consequently retarding atherosclerotic development. These findings establish a new mechanism for controlling gene expression during atherogenesis, providing new insights into lncRNA and miRNA-controlled cellular mechanism.

## Data Availability

The data that support the findings of this study are available upon request from the corresponding authors.

## Ethical Approval

The animal study was approved by the Animal Care and Use Committees of The Second Hospital of Hebei Medical University.

## Conflicts of Interest

The authors declare that the research was conducted in the absence of any commercial or financial relationships that could be construed as a potential conflict of interest.

## Authors' Contributions

LY and RX conceived the presented idea and prepared the manuscript. CX revised the manuscript. LY, YZ, and LW performed the animal study. LY, JY, and YZ performed the cellular and molecular experiments. QH conducted the statistical analysis. RX drafted the final version of the manuscript. All authors contributed to the article and approved the submitted version.

## Acknowledgments

This work was supported by Hebei Natural Science Foundation (Grant No. H2020206037).

## Supplementary Materials

Table S1. Information of primers. (*Supplementary Materials*)

## References

- [1] P. Libby, P. M. Ridker, and G. K. Hansson, "Progress and challenges in translating the biology of atherosclerosis," *Nature*, vol. 473, no. 7347, pp. 317–325, 2011.
- [2] A. E. Mullick, K. Soldau, W. B. Kiosses, T. A. Bell 3rd, P. S. Tobias, and L. K. Curtiss, "Increased endothelial expression of Toll-like receptor 2 at sites of disturbed blood flow exacerbates early atherogenic events," *The Journal of Experimental Medicine*, vol. 205, no. 2, pp. 373–383, 2008.
- [3] C. Espinosa-Diez, V. Mandi, M. Du, M. Liu, and D. Gomez, "Smooth muscle cells in atherosclerosis: clones but not carbon copies," *JVS-Vascular Science*, vol. 2, pp. 136–148, 2021.
- [4] Z. Yan, Z. Qi, X. Yang et al., "The NLRP3 inflammasome: multiple activation pathways and its role in primary cells during ventricular remodeling," *Journal of Cellular Physiology*, vol. 236, no. 8, pp. 5547–5563, 2021.
- [5] B. Bai, Y. Yang, Q. Wang et al., "NLRP3 inflammasome in endothelial dysfunction," *Cell Death & Disease*, vol. 11, no. 9, p. 776, 2020.
- [6] L. Statello, C. J. Guo, L. L. Chen, and M. Huarte, "Gene regulation by long non-coding RNAs and its biological functions," *Nature Reviews. Molecular Cell Biology*, vol. 22, no. 2, pp. 96–118, 2021.
- [7] V. Simion, H. Zhou, J. B. Pierce et al., "LncRNA VINAS regulates atherosclerosis by modulating NF- $\kappa$ B and MAPK signaling," *Insight*, vol. 5, no. 21, 2020.
- [8] H. Ni, S. Haemmig, Y. Deng et al., "A smooth muscle cell-enriched Long noncoding RNA regulates cell plasticity and atherosclerosis by interacting with serum response factor," *Arteriosclerosis, Thrombosis, and Vascular Biology*, vol. 41, no. 9, pp. 2399–2416, 2021.
- [9] K. Wang, T. Sun, N. Li et al., "MDRL lncRNA regulates the processing of miR-484 primary transcript by targeting miR-361," *PLoS Genetics*, vol. 10, no. 7, article e1004467, 2014.



- [10] A. Jungmann, B. Leuchs, J. Rommelaere, H. A. Katus, and O. J. Muller, "Protocol for efficient generation and characterization of adeno-associated viral vectors," *Human Gene Therapy Methods*, vol. 28, no. 5, pp. 235–246, 2017.
- [11] X. Sun, S. He, A. K. M. Wara et al., "Systemic delivery of microRNA-181b inhibits nuclear factor- $\kappa$ B activation, vascular inflammation, and atherosclerosis in apolipoprotein E-deficient mice," *Circulation Research*, vol. 114, no. 1, pp. 32–40, 2014.
- [12] Y. W. Hu, F. X. Guo, Y. J. Xu et al., "Long noncoding RNA NEXN-AS1 mitigates atherosclerosis by regulating the actin-binding protein NEXN," *The Journal of Clinical Investigation*, vol. 129, no. 3, pp. 1115–1128, 2019.
- [13] N. Villa-Roel, K. Ryu, L. Gu et al., "Hypoxia inducible factor 1 $\alpha$  inhibitor PX-478 reduces atherosclerosis in mice," *Atherosclerosis*, vol. 344, pp. 20–30, 2022.
- [14] W. J. Caspary, R. Langenbach, B. W. Penman, C. Crespi, B. C. Myhr, and A. D. Mitchell, "The mutagenic activity of selected compounds at the TK locus: rodent vs. human cells," *Mutation Research*, vol. 196, no. 1, pp. 61–81, 1988.
- [15] Y. H. Chan and D. P. Ramji, "Probing inflammasome activation in atherosclerosis," *Methods in Molecular Biology*, vol. 2419, pp. 313–331, 2022.
- [16] F. Fasolo, H. Jin, G. Winski et al., "Long noncoding RNA MIAT controls advanced atherosclerotic lesion formation and plaque destabilization," *Circulation*, vol. 144, no. 19, pp. 1567–1583, 2021.
- [17] D. Y. Li, A. Busch, H. Jin et al., "H19 induces abdominal aortic aneurysm development and progression," *Circulation*, vol. 138, no. 15, pp. 1551–1568, 2018.
- [18] M. Du, C. Wang, L. Yang et al., "The role of long noncoding RNA Nron in atherosclerosis development and plaque stability," *Iscience*, vol. 25, no. 3, article 103978, 2022.
- [19] S. S. Wang, C. Wang, and H. Chen, "MicroRNAs are critical in regulating smooth muscle cell mineralization and apoptosis during vascular calcification," *Journal of Cellular and Molecular Medicine*, vol. 24, no. 23, pp. 13564–13572, 2020.
- [20] H. Lu, W. Du, L. Ren et al., "Vascular smooth muscle cells in aortic aneurysm: from genetics to mechanisms," *Journal of the American Heart Association*, vol. 10, no. 24, article e023601, 2021.
- [21] M. O. J. Grootaert, M. Moulis, L. Roth et al., "Vascular smooth muscle cell death, autophagy and senescence in atherosclerosis," *Cardiovascular Research*, vol. 114, no. 4, pp. 622–634, 2018.
- [22] M. C. Clarke, N. Figg, J. J. Maguire et al., "Apoptosis of vascular smooth muscle cells induces features of plaque vulnerability in atherosclerosis," *Nature Medicine*, vol. 12, no. 9, pp. 1075–1080, 2006.
- [23] Y. Huang, L. Ren, J. Li, and H. Zou, "Long non-coding RNA PVT1/microRNA miR-3127-5p/NCK-associated protein 1-like axis participates in the pathogenesis of abdominal aortic aneurysm by regulating vascular smooth muscle cells," *Bioengineered*, vol. 12, no. 2, pp. 12583–12596, 2021.
- [24] J. Li, J. Chen, F. Zhang et al., "LncRNA CDKN2B-AS1 hinders the proliferation and facilitates apoptosis of ox-LDL-induced vascular smooth muscle cells via the ceRNA network of CDKN2B-AS1/miR-126-5p/PTPN7," *International Journal of Cardiology*, vol. 340, pp. 79–87, 2021.
- [25] N. Long, L. Chu, J. Jia et al., "CircPOSTN/miR-361-5p/TPX2 axis regulates cell growth, apoptosis and aerobic glycolysis in glioma cells," *Cancer Cell International*, vol. 20, no. 1, p. 374, 2020.
- [26] J. Jia, Z. Ouyang, M. Wang et al., "MicroRNA-361-5p slows down gliomas development through regulating UBR5 to elevate ATMIN protein expression," *Cell Death & Disease*, vol. 12, no. 8, p. 746, 2021.
- [27] M. B. Olsen, I. Gregersen, O. Sandanger et al., "Targeting the inflammasome in cardiovascular disease," *JACC: Basic to Translational Science*, vol. 7, no. 1, pp. 84–98, 2022.
- [28] P. Duewell, H. Kono, K. J. Rayner et al., "NLRP3 inflammasomes are required for atherogenesis and activated by cholesterol crystals," *Nature*, vol. 464, no. 7293, pp. 1357–1361, 2010.
- [29] M. Westerterp, P. Fotakis, M. Ouimet et al., "Cholesterol efflux pathways suppress inflammasome activation, NETosis, and atherogenesis," *Circulation*, vol. 138, no. 9, pp. 898–912, 2018.
- [30] R. Wang, W. Wu, W. Li et al., "Activation of NLRP3 inflammasome promotes foam cell formation in vascular smooth muscle cells and atherogenesis via HMGB1," *Journal of the American Heart Association*, vol. 7, no. 19, article e008596, 2018.
- [31] Y. Li, X. Niu, H. Xu et al., "VX-765 attenuates atherosclerosis in ApoE deficient mice by modulating VSMCs pyroptosis," *Experimental Cell Research*, vol. 389, no. 1, article 111847, 2020.
- [32] W. Zhong, B. Li, Y. Xu et al., "Hypermethylation of the microRNA 145 promoter is the key regulator for NLRP3 inflammasome-induced activation and plaque formation," *JACC: Basic to Translational Science*, vol. 3, no. 5, pp. 604–624, 2018.
- [33] A. V. Kumar, J. Mills, and L. R. Lapierre, "Selective autophagy receptor p62/SQSTM1, a pivotal player in stress and aging," *Frontiers in Cell and Development Biology*, vol. 10, article 793328, 2022.
- [34] W. Wang, Y. Qin, H. Song et al., "Galectin-9 targets NLRP3 for autophagic degradation to limit inflammation," *Journal of Immunology*, vol. 206, no. 11, pp. 2692–2699, 2021.

## Research Article

# GJD Modulates Cardiac/Vascular Inflammation and Decreases Blood Pressure in Hypertensive Rats

Shadi A. D. Mohammed <sup>1</sup>, Hanxing Liu,<sup>1</sup> Salem Baldi,<sup>2</sup> Pingping Chen,<sup>3</sup> Fang Lu,<sup>3</sup> and Shumin Liu <sup>3</sup>

<sup>1</sup>Graduate School of Heilongjiang University of Chinese Medicine, Harbin, 150040 Heilongjiang, China

<sup>2</sup>Research Center of Molecular Diagnostics and Sequencing, Axbio Biotechnology (Shenzhen) co., Ltd., Gaoxin South 7th Road, Yuehai Street, Nanshan District, Shenzhen, China

<sup>3</sup>Institute of Traditional Chinese Medicine, Heilongjiang University of Chinese Medicine, Harbin, 150040 Heilongjiang, China

Correspondence should be addressed to Shumin Liu; keji-liu@163.com

Received 1 June 2022; Revised 19 July 2022; Accepted 12 August 2022; Published 17 September 2022

Academic Editor: Dominik Skiba

Copyright © 2022 Shadi A. D. Mohammed et al. This is an open access article distributed under the Creative Commons Attribution License, which permits unrestricted use, distribution, and reproduction in any medium, provided the original work is properly cited.

Gedan Jiangya decoction (GJD) (aqueous ethanol extract), a traditional Chinese medicine formula which contain six botanical drugs (*Uncaria rhynchophylla* (Miq.) Miq., *Salvia miltiorrhiza* Bunge, *Pueraria lobata* (Willd.) Ohwi, *Eucommia ulmoides* Oliv., *Prunella vulgaris* L., and *Achyranthes bidentata* Blume) was designed to treat hypertension; however, the underlying mechanism of action is unclear. This study aimed to determine the mechanisms of action of GJD in the treatment of hypertension in spontaneously hypertensive rats (SHR). Male SHRs were randomly divided into five groups: GJD doses were low (1.36 g/kg/d), medium (2.72 g/kg/d), and high (5.44 g/kg/d), captopril (13.5 mg/kg/d), and SHR groups, with Wistar-Kyoto rats (WKY) serving as the control. Every rat was gavaged once a day. The ALC-NIBP, a noninvasive blood pressure device, measured systolic (SBP) and diastolic (DBP) blood pressures. Six weeks following treatment, all rats were anesthetized. The blood samples were obtained from the abdominal aorta and then serum isolated to assess endothelin-1 and angiotensin II, interleukin-1beta, interleukin-6, and TNF-alpha. The left ventricular and thoracic aortas were taken for HE staining, immunohistochemistry, RT-qPCR, and western blot examination. Following GJD therapy, SBP and DBP were significantly lowered, as were serum levels of endothelin-1 and angiotensin II. The thickness of the left ventricular and thoracic aorta walls reduced, as did type I collagen, type III collagen, and alpha-SMA expression in the left ventricular and aortic tissues. The GJD treatment significantly reduced serum levels of the inflammatory markers interleukin-1beta, interleukin-6, and TNF-alpha. Furthermore, interleukin-1 beta, interleukin-6, TNF-alpha, TAK1, and NF- $\kappa$ B/p65 levels were significantly reduced in left ventricular and aortic tissues, whereas I $\kappa$ B-alpha levels were significantly elevated. GJD has a dose-dependent effect on all parameters. In conclusion, GJD has been shown to lower blood pressure, improve cardiovascular remodeling, and reduce inflammation via regulating NF- $\kappa$ B in SHRs.

## 1. Introduction

Hypertension is the leading cause of cardiovascular disease-related morbidity and mortality worldwide [1]. Globally, the prevalence of SBP levels more than 110 mm Hg has increased over the past three decades; in 2015, the number of fatalities and disability-adjusted life years (DALYs) was 10 million and 212 million, respectively, representing a 1.4-fold increase since 1990 [1]. One million persons from 44

low and middle income countries were studied; 17.5% were hypertensive; 39.2% were diagnosed with high blood pressure; and 29.9% were treated, yet only 10.3% had their hypertension under control [2]. Uncontrolled hypertension is associated with a higher risk of cardiovascular disease death [3, 4]. Furthermore, people with hypertension have a higher chance of developing cardiovascular disease (CVD) throughout their lives, and the onset of CVD morbidity occurs five years earlier in those with hypertension

TABLE 1: Primer pairs list used in RT-qPCR.

Gene	Forward primer (5'-3')	Reverse primer (5'-3')
IL1B (interleukin-1 beta)	CCCTGAACTCAACTGTGAAATAGCA	CCCAAGTCAAGGGCTTGAA
IL6 (interleukin-6)	TTGGGACTGATGTTGTTG	TGTGGGTGGTATCCTCTGT
TNF (TNF-alpha)	TCAGTTCCATGGCCCAGAC	GTTGTCTTTGAGATCCATGCCATT
COL1A1 (type I collagen)	CCTGCCGATGTCGCTATCC	TTGCCTTCGCCCCCTGAG
COL3A1 (type III collagen)	AGATGCTGGTGCTGAGAAG	TGGAAAGAAGTCTGAGGAAGG
ACTA2 (alpha-SMA)	TTCGTGACTACTGCTGAGCG	CTGTCAGCAATGCCTGGGTA
MAP3K7 (TAK1)	AGCAGAAACGACAAGGCACT	CAGCGAGACAGTGGATTTGA
NFKBIA (IkB-alpha)	CCCTGGAAAATCTTCAGACG	ACAAGTCCACGTTTCCTTTGG
RELA(p65)	GACCTGGAGCAAGCCATTAG	CACTGTCACCTGGAAGCAGA
GAPDH	TGCACCACCAACTGCTTAG	GATGCAGGGATGATGTTC

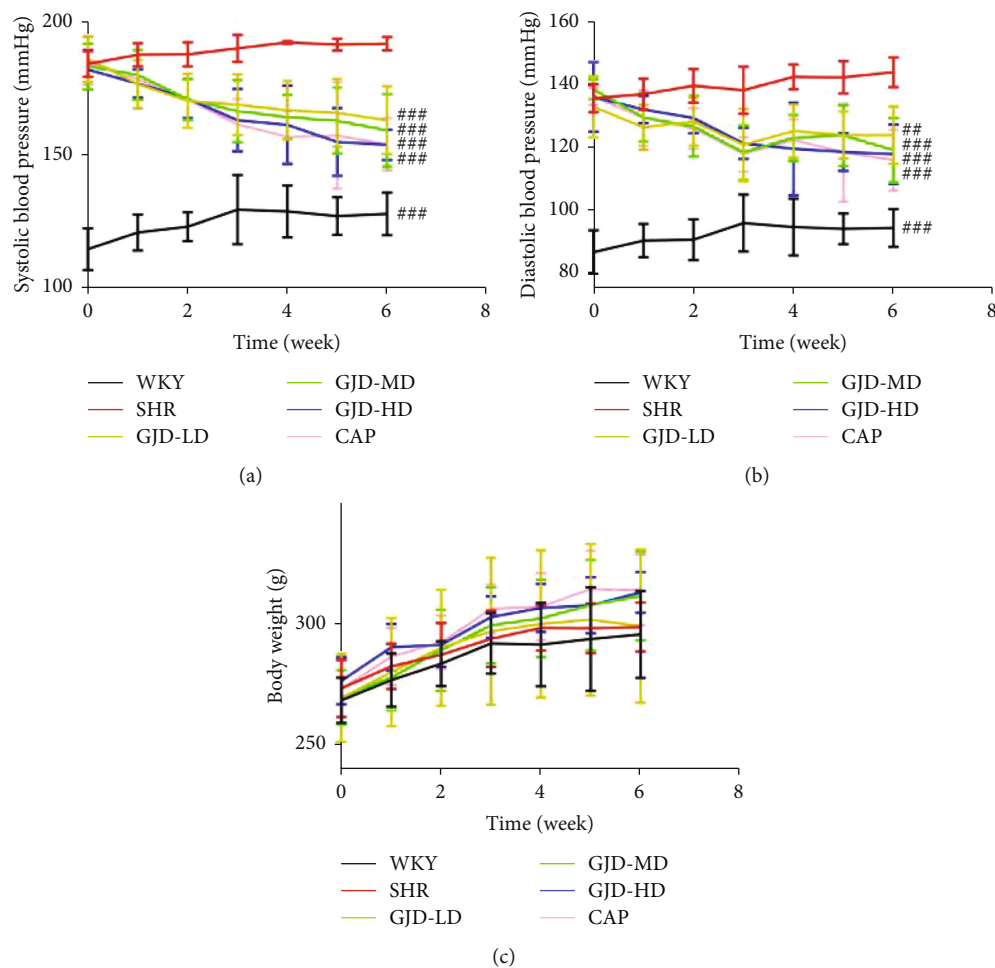


FIGURE 1: Effect of GJD on systolic and diastolic blood pressures and body weight. (a) SBP, (b) DBP, and (c) body weight. WKY indicates the WKY control group, SHR indicates the SHR Model group, GJD-LD indicates the SHR treated with GJD at a low dose, GJD-MD indicates the SHR treated with GJD at a medium dose, GJD-HD indicates the SHR treated with GJD at a high dose, and CAP indicates SHR treated with captopril. Data are means  $\pm$  SD,  $n = 7$ . \* $P < 0.05$ , \*\* $P < 0.01$ , \*\*\* $P < 0.001$  vs. SHR group.

compared to those with normal blood pressure [5, 6]. Over 2.54 million people in China died in 2017 due to hypertension-related disorders, with about 69% of those deaths attributable to stroke, 54% to ischemic heart disease, and 41% to other forms of cardiovascular disease, according

to a study by the Chinese Center for Disease Control and Prevention (CCDC) [7].

Despite the availability of effective hypertension drug therapy, there has been a rise in hypertension-related cardiovascular mortality, as seen by current US statistics, in the

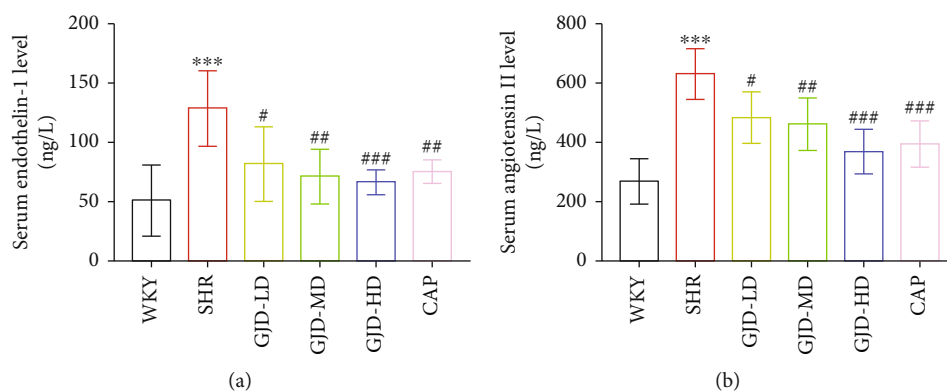


FIGURE 2: Serum level of endothelin-1 and angiotensin II. WKY indicates the WKY control group, SHR indicates the SHR model group, GJD-LD indicates the SHR treated with GJD at a low dose, GJD-MD indicates the SHR treated with GJD at a medium dose, GJD-HD indicates the SHR treated with GJD at a high dose, and CAP indicates SHR treated with captopril. Data are means  $\pm$  SD,  $n = 7$ . \* $P < 0.05$ , \*\* $P < 0.01$ , \*\*\* $P < 0.001$  vs. WKY group, # $P < 0.05$ , ## $P < 0.01$ , ### $P < 0.001$  vs. SHR group.

decreased percentage of persons with controlled hypertension from 53.8% in 2013 to 2014 to 43.7% from 2017 to 2018 [8]. Furthermore, among Chinese individuals with hypertension, 46.9% were aware of their disease, 40.7% were taking prescribed western antihypertensive medication, and only 15.3% had their hypertension under control [9]. This might be partly due to the numerous medications available not effectively targeting the necessary pathways, as well as counter-regulatory mechanisms generated by these therapies limiting their blood pressure (BP)-lowering effect. As a result, new therapeutic methods are desperately required. Thus, traditional Chinese medicine can provide different treatment methods according to the cause and the response of the body, and multicomponent, multitarget, and multipathway pharmacological action properties have shown consistent therapeutic advantages on chronic difficult disorders, attracting increasing worldwide interest [10]; [11, 12]. Finding effective drugs for treating hypertension from traditional Chinese medicine has become a major technique in developing innovative antihypertension medications.

Cardiovascular remodeling and inflammation are essential in hypertensive target organ damage's etiology and adaptive mechanism [13, 14]. Several studies have shown that the activation of the nuclear factor- $\kappa$ B (NF- $\kappa$ B) pathway results in an upregulation of inflammatory factors such as interleukin-1 beta, interleukin-6, and tumor necrosis factor- $\alpha$  [15, 16]. Hypertension may be treated with TCM that have anti-inflammatory effects and the potential to stop hypertensive cardiovascular remodeling. This study investigates the possible mechanism of GJD, for which a Chinese patent publication number (No.: CN114246896A) was previously applied, but the underlying mechanism has not yet been entirely detailed. GJD includes six botanical drugs, namely, *Uncaria rhynchophylla* (Miq.) Miq. [Rubiaceae] (Gouteng), *Salvia miltiorrhiza* Bunge [Lamiaceae] (Danshen), *Pueraria lobata* (Willd.) Ohwi [Fabaceae] (Gegen), *Eucommia ulmoides* Oliv. [Eucommiaceae] (Duzhong), *Prunella vulgaris* L. [Lamiaceae] (Xiakucao), and *Achyranthes bidentata* Blume [Amaranthaceae] (Niuxi). *Uncaria rhynchophylla* is a

component of the Chinese crude medication Gouteng, which is extensively used to cure various conditions such as anti-inflammatory, decreased hypertension, and cardiac fibrosis [17]; [18]. Pharmacological effects on the cardiovascular system from *Salvia miltiorrhiza*, *Pueraria lobata*, and *Eucommia ulmoides* include anti-inflammatory, endothelium protecting, antioxidative, vasodilatory, and myocardial protective effects [19, 20]; [21]. Modern pharmacological investigations have demonstrated that *Prunella vulgaris* and *Achyranthes bidentata* offer cardiovascular therapeutic effects such as blood pressure reduction, anti-inflammatory, and antioxidant properties [22, 23].

Due to the major role of inflammation in hypertension and cardiovascular remodeling, we propose that GJD reduces hypertension-related inflammation and might be utilized as an antihypertensive medication to minimize cardiovascular remodeling. This study aimed to observe whether GJD may be utilized as a new antihypertensive medicine by evaluating its effects on heart and aorta remodeling and inflammation via NF- $\kappa$ B regulation in SHR.

## 2. Materials and Methods

**2.1. Plant Material and Extraction.** The following GJD botanical drugs included in the study: *Uncaria rhynchophylla* (Miq.) Miq. (Lot No. 20200901), 10 g; *Salvia miltiorrhiza* Bunge, (Lot No. 20191001) 25 g; *Pueraria lobata* (Willd.) Ohwi (Lot No. 20191001) 30 g; *Eucommia ulmoides* Oliv. (Lot No. 20190901), 15 g; *Prunella vulgaris* L. (Lot No. 20190701) 15 g; and *Achyranthes bidentata* Blume (Lot No. 20200901) 20 g were purchased from Heilongjiang Xiushengtang Pharmaceutical Co., Ltd.

*Salvia miltiorrhiza*, *Pueraria lobata*, *Eucommia ulmoides*, *Prunella vulgaris*, and *Achyranthes bidentata* were mixed with a 60% aqueous ethanol solution at a material-liquid ratio of 1 g dissolved in 10 ml, soaked for 30 minutes, heated and refluxed the soaking solution for 1.5 hours (keeping the solution slightly boiling during the reflux process), and then filtered through six layers of degreasing gauze.

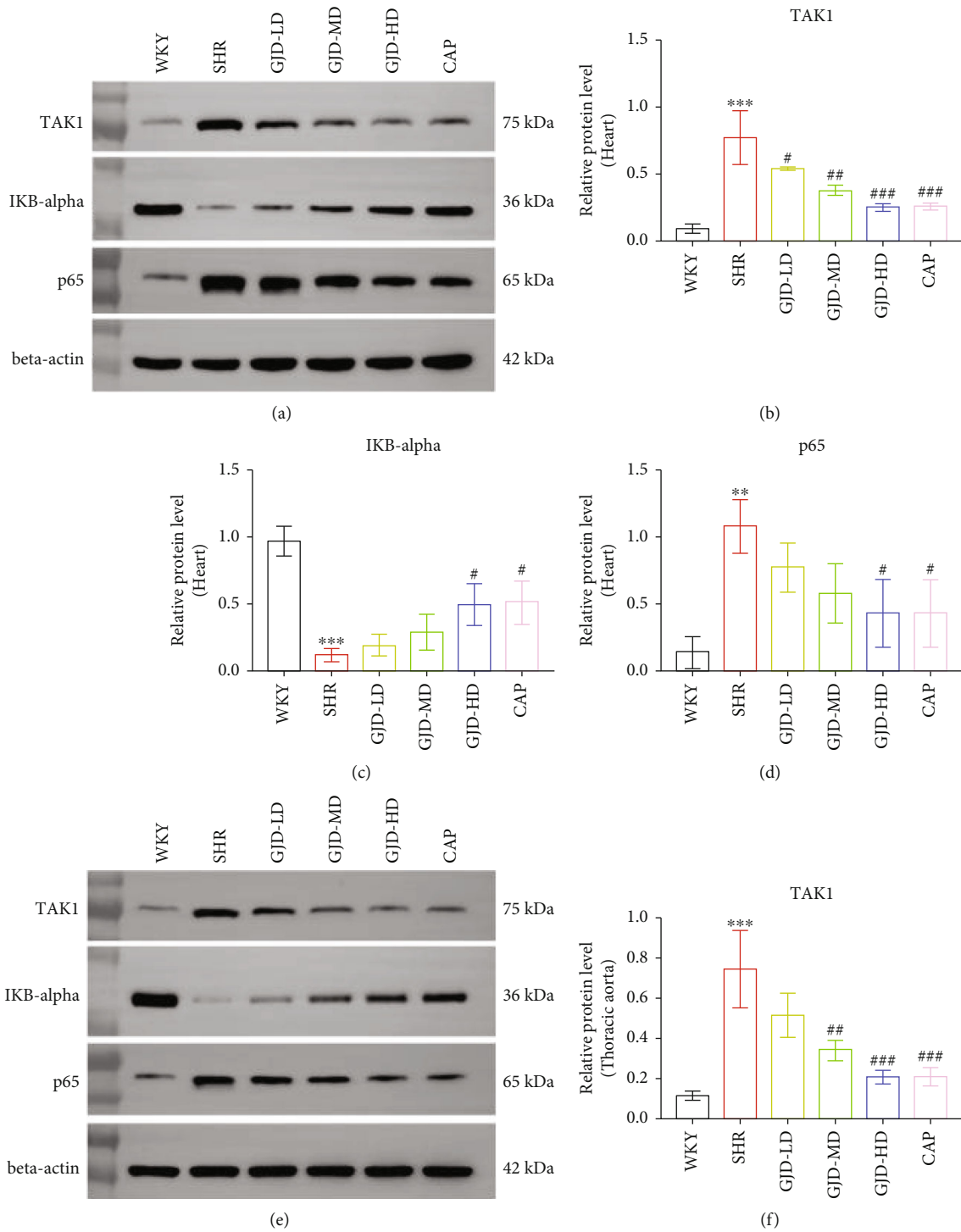


FIGURE 3: Continued.

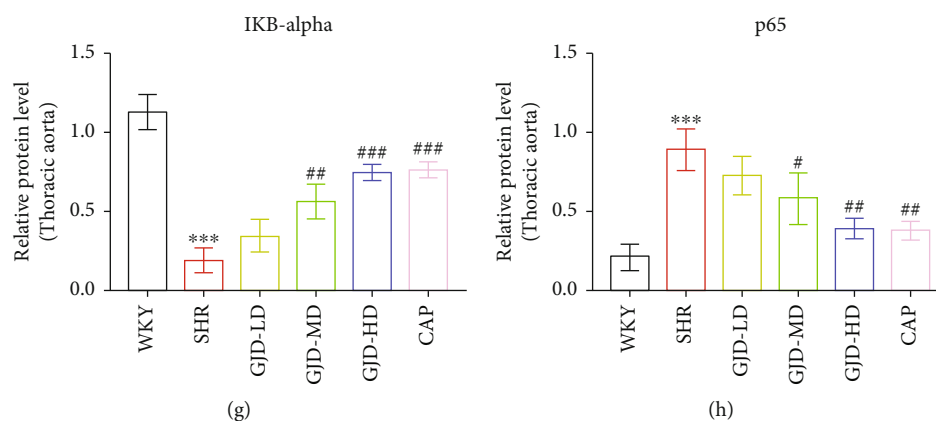


FIGURE 3: Effect of GJD on the expression of TAK1, IκB-alpha, and p65. The expression of TAK1, IκB-alpha, and p65 in the left ventricular and aorta was examined by western blot. (a) The left ventricular expression of TAK1, IκB-alpha, and p65, and (b) the aorta expression of TAK1, IκB-alpha, and p65. The bar charts indicate relative protein levels referenced to  $\beta$ -actin. WKY indicates the WKY control group, SHR indicates the SHR model group, GJD-LD indicates the SHR treated with GJD at a low dose, GJD-MD indicates the SHR treated with GJD at a medium dose, GJD-HD indicates the SHR treated with GJD at a high dose, and CAP indicates SHR treated with captopril. Data are means  $\pm$  SD.  $n = 3$ . \* $P < 0.05$ , \*\* $P < 0.01$ , \*\*\* $P < 0.001$  vs. WKY group. # $P < 0.05$ , ## $P < 0.01$ , ### $P < 0.001$  vs. SHR group.

The components were then filtered after being subjected to a 1.5-hour period of reheating and refluxing with 10 times their original volume of 60% aqueous ethanol solution. After that, we combined the two filtrates, distilled the ethanol under reduced pressure using a rotary evaporator, and dried the solution under reduced pressure and vacuum to get extracts powder of *Salvia miltiorrhiza*, *Pueraria lobata*, *Eucommia ulmoides*, *Prunella vulgaris*, and *Achyranthes bidentata*. Similarly, *Uncaria rhynchophylla* was soaked in a 70% aqueous ethanol solution in a 1g: 10ml ratio for 0.5 hour, heated to 65~75°C, and soaked again for 2 hours. *Uncaria rhynchophylla* was also filtered through six layers of degreasing gauze and soaked in 10 times the amount of 70% aqueous ethanol solution for 2 hours. The two filtrates were then combined, distilled the ethanol under reduced pressure using a rotary evaporator, and then dried under reduced pressure and vacuumed to obtain extracts powder of *Uncaria rhynchophylla*. Finally, two extracts were mixed to obtain GJD powder.

**2.2. Animal.** Under the experimental animal approval license number SYXK (Hei)2018-007, a total of 35 SHR and 7 Wistar Kyoto (WKY) control male rats (Vital River Laboratory Animal Technology Co., Ltd., Beijing), 10 weeks of age (body weight  $250 \pm 10$  g), were utilized in the investigation. Throughout the experiment, all rats had unrestricted access to normal chow and tap water ad libitum, and they were kept in a room with a regulated temperature ( $21 \pm 3^\circ\text{C}$ ), humidity ( $50 \pm 6\%$ ), and lighting (12 h/12 h light-dark cycle). The study protocol was authorized by the Heilongjiang University of Chinese Medicine's Animal Care and Use Committee (Approval number: 2020031203).

**2.3. Groups, Drug Doses, and Blood Pressure Measurement.** After one week of acclimatization period, the 35 SHR were randomly assigned into the following 5 groups, each containing 7 rats: model group (SHR), the low dose of GJD

group (GJD-LD) gavage of GJD (1.36 g/kg/d), the medium dose of GJD group (GJD-MD) gavage of GJD (2.72 g/kg/d), the high dose of GJD group (GJD-HD) gavage of GJD (5.44 g/kg/d), and captopril group (CAP): gavage of captopril (13.5 mg/kg/d Meilun Biotechnology Co., Ltd., Dalian). The GJD doses were dissolved in 1 ml of distilled water (every rat was gavaged 1 ml once time a day), and the control group (WKY) and model group (SHR) were gavaged with an equivalent volume (1 ml) of distilled water every day (at 8 a.m. feeding the rats and at 9 a.m. gastric gavage).

Body weight, systolic, and diastolic blood pressure (SBP and DBP) were measured every week. The systolic and diastolic blood pressures were measured with the tail-cuff method using ALC-NIBP, a noninvasive blood pressure system from Shanghai Alcott Biotechnology Co., Ltd., China. BP measurement was performed first, then gavaging, and the measurements were taken three times per rat, and an average value was reported. After 6 weeks, the rats were euthanized with sodium pentobarbital (45 mg/kg, intraperitoneally), and then, the blood samples were taken from the abdominal artery and immediately centrifuged at 1176 g for 15 minutes at  $4^\circ\text{C}$  and stored at  $-80^\circ\text{C}$ . The hearts were retrieved and cleaned in normal saline before being dried using filter paper. The atrium's free walls, major blood arteries, and right ventricle were removed along the atrioventricular junction, and the hearts' left ventricles were obtained. The left ventricular mass index (LVMI) was determined to measure thickening of the left ventricular as follows:  $\text{LVMI} = \text{left ventricular weight (mg)}/\text{body weight (g)}$ . The left ventricular and thoracic aorta parts were frozen and kept at  $-80^\circ\text{C}$  for subsequent western blot and RT-qPCR analyses. In addition, sliced sections of the left ventricular and thoracic aorta were fixed in 4% paraformaldehyde for HE staining and immunohistochemistry analysis.

**2.4. ELISA Measurement of Endothelin-1, Angiotensin II, and Inflammatory Factors in Serum.** The ELISA kits were used to

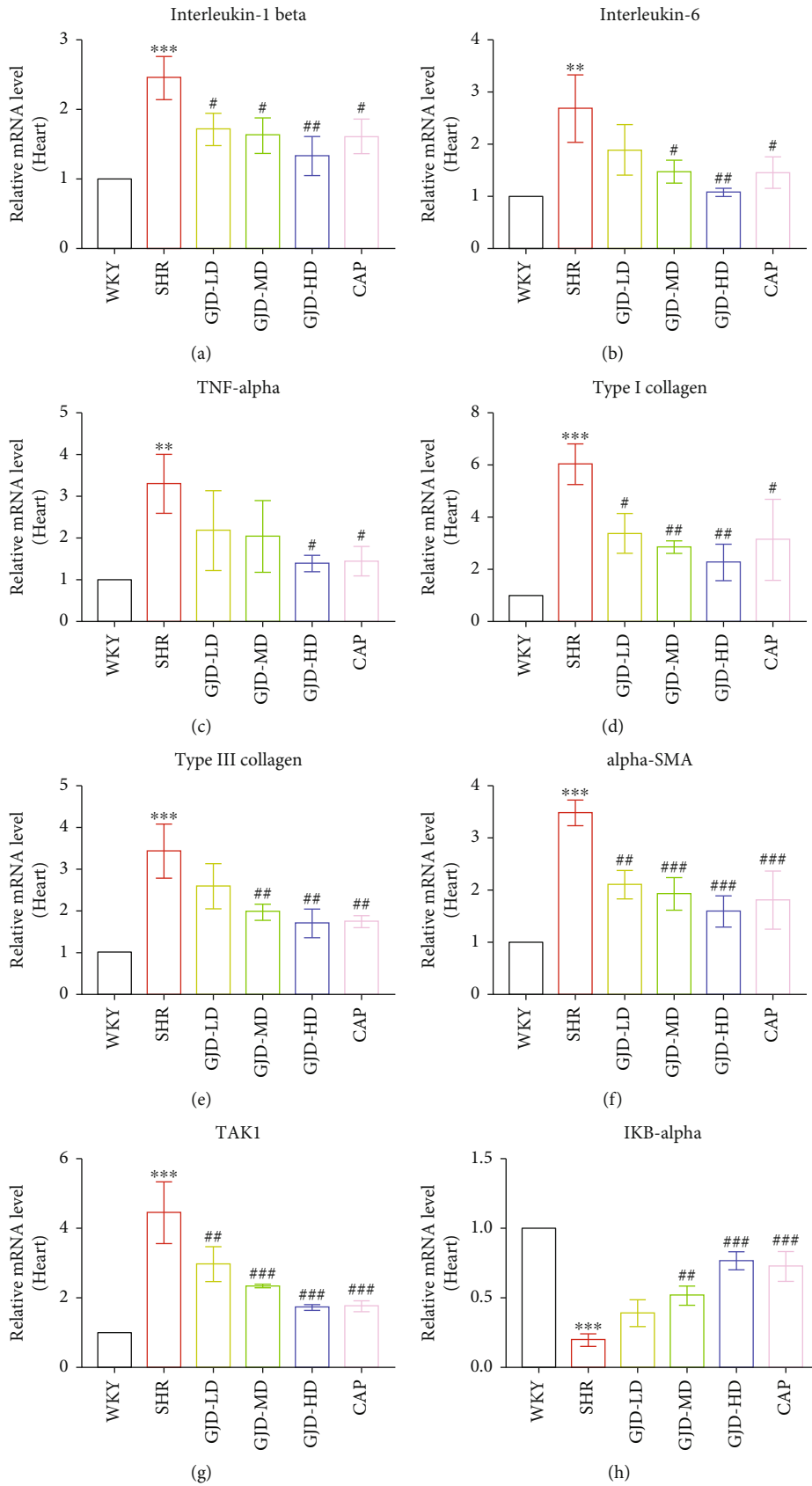


FIGURE 4: Continued.

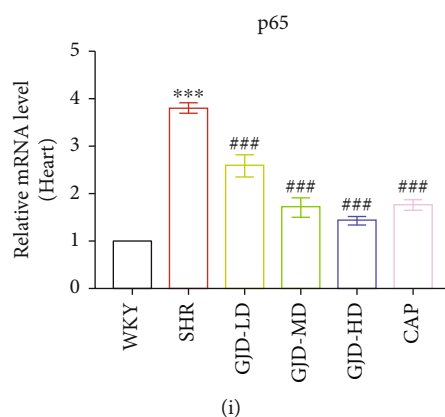


FIGURE 4: Effects of GJD on mRNA expression of interleukin -1 beta, interleukin-6, TNF-alpha, type I collagen, type III collagen, and alpha-SMA in the left ventricular. (a) Interleukin-1 beta, (b) interleukin-6, (c) TNF-alpha, (d) type I collagen, (e) type III collagen, (f) alpha-SMA, (g) TAK1, (h) IκB-alpha, and (i) p65. WKY indicates the WKY control group, SHR indicates the SHR model group, GJD-LD indicates the SHR treated with GJD at a low dose, GJD-MD indicates the SHR treated with GJD at a medium dose, GJD-HD indicates the SHR treated with GJD at a high dose, and CAP indicates SHR treated with captopril. Data are means ± SD,  $n = 3$ . \* $P < 0.05$ , \*\* $P < 0.01$ , \*\*\* $P < 0.001$  vs. WKY group, # $P < 0.05$ , ## $P < 0.01$ , ### $P < 0.001$  vs. SHR group.

assess serum levels of interleukin-1 beta (Nanjing Jiancheng Bioengineering Institute, Nanjing, China, Serial number: H002), interleukin-6 (Nanjing Jiancheng Bioengineering Institute, Nanjing, China, Serial number: H007-1-2), TNF-alpha (Nanjing Jiancheng Bioengineering Institute, Nanjing, China, Serial number: H052-1), endothelin-1 (Nanjing Jiancheng Bioengineering Institute, Nanjing, China, Serial number: H093), and angiotensin II (Nanjing Jiancheng Bioengineering Institute, Nanjing, China, Serial number: H185). All kit procedures were completed in line with the company's instructions.

**2.5. Western Blot.** The total protein was obtained from the thoracic aorta and left ventricular of three rats selected randomly using RIPA lysis buffer with PMSF and phosphatase inhibitor (Servicebio, China). Protein concentration was measured using a BCA protein detection kit (Servicebio, China). SDS-PAGE separated the whole protein, which was subsequently transferred to 0.45 μM on the PVDF membrane (Servicebio, China). The membrane was sealed with 5% nonfat milk for 1 hour at room temperature before being incubated with the primary antibody overnight at 4°C. The membrane was then washed three times with TBST, incubated for one hour at room temperature with a secondary antibody, and the protein was identified using an ECL reagent (Servicebio, China). Primary antibodies include TAK1 (GB11564, 1: 1,000, Servicebio, China), IκB-alpha (GB13212-1, 1:1,000, Servicebio, China), p65 (GB11997, 1:1,000, Servicebio, China), and β-actin (GB15001, 1: 2,000, Servicebio, China).

**2.6. HE Staining.** Fresh tissues were taken from thoracic aorta and left ventricle, fixed in 4% paraformaldehyde at 4°C for 24 hours, and then dehydrated. After drying and embedding in paraffin, the fixed tissue was cut into 5-micron thick slices and stained with hematoxylin and eosin. Using an Eclipse Ci-L (Nikon, Japan) optical microscope to

select the target area of the tissue for 20× imaging, try to fill the whole field of vision with the tissue. At least three 200× visual fields were randomly selected from each slice and observed under a microscope. HE-stained slides were evaluated by two veterinary pathologists to identify abnormalities.

**2.7. Immunohistochemistry.** The tissue sections were deparaffinized with xylene and then dehydrated using a graded alcohol series (put the sections into BioDewax and clear solution I for 15 minutes–BioDewax and clear solution II for 15 minutes–BioDewax and clear solution III for 15 minutes–absolute ethanol I for 5 minutes–absolute ethanol II for 5 minutes–85% alcohol for 5 minutes–75% alcohol for 5 minutes–rinsed in distilled water). To block endogenous peroxidase activity, the sections were incubated in 3% H<sub>2</sub>O<sub>2</sub> for 25 minutes at room temperature in the dark and then washed with phosphate-buffered saline (PBS). Sections were blocked for 30 minutes at room temperature before being incubated overnight at 4°C with diluted primary antibodies (interleukin-1 beta, interleukin-6, TNF-alpha, type I collagen, type III collagen, and alpha-SMA). After washing in phosphate buffered saline, the sections were incubated for 50 minutes with the matching secondary antibodies. Then, 3,3-diaminobenzidine (DAB, Servicebio, China) was used as a chromogen, and slices were counterstained with hematoxylin. Dehydration and mounting are accomplished by soaking the section in a series of solvents until it is dehydrated and transparent, as follows: 75% alcohol for 5 minutes, 85% alcohol for 5 minutes, absolute ethanol I for 5 minutes, anhydrous ethanol II for 5 minutes, n-butanol for 5 minutes, and xylene I for 5 minutes. SweSuper clean BioMount medium was then used to mount the sections. Primary antibodies used for detection were against interleukin-1 beta (bs-0812R, 1:100, Bioss, China), interleukin-6 (GB11117, 1:200, Servicebio, China), TNF-alpha (GB11188, 1:200, Servicebio, China), type I collagen (GB11022-3, 1:800, Servicebio, China), type III collagen



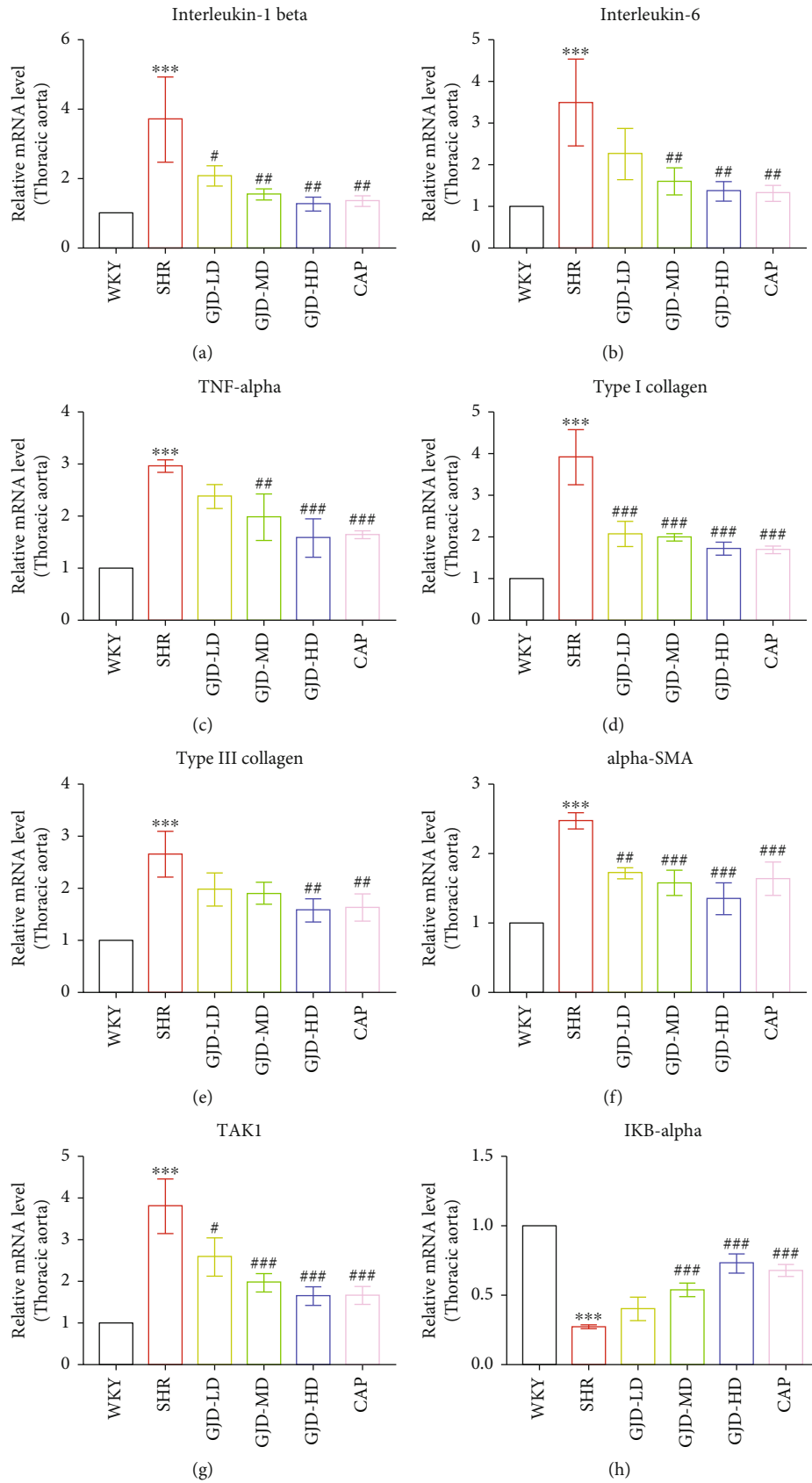


FIGURE 5: Continued.

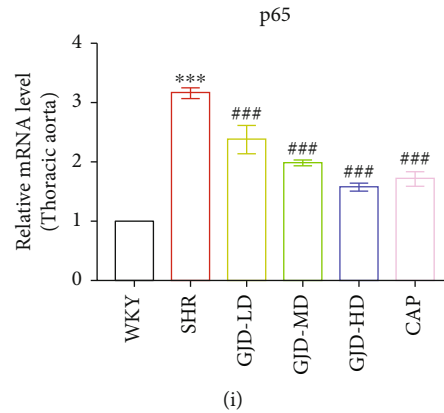


FIGURE 5: Effects of GJD on mRNA expression of interleukin-1 beta, interleukin-6, TNF-alpha, type I collagen, type III collagen, and alpha-SMA in the thoracic aorta. (a) Interleukin-1 beta, (b) interleukin-6, (c) TNF-alpha, (d) type I collagen, (e) type III collagen, (f) alpha-SMA, (g) TAK1, (h) I $\kappa$ B-alpha, and (i) p65. WKY indicates the WKY control group, SHR indicates the SHR model group, GJD-LD indicates the SHR treated with GJD at a low dose, GJD-MD indicates the SHR treated with GJD at a medium dose, GJD-HD indicates the SHR treated with GJD at a high dose, and CAP indicates SHR treated with captopril. Data are means  $\pm$  SD.  $n = 3$ . \* $P < 0.05$ , \*\* $P < 0.01$ , \*\*\* $P < 0.001$  vs. WKY group, # $P < 0.05$ , ## $P < 0.01$ , ### $P < 0.001$  vs. SHR group.

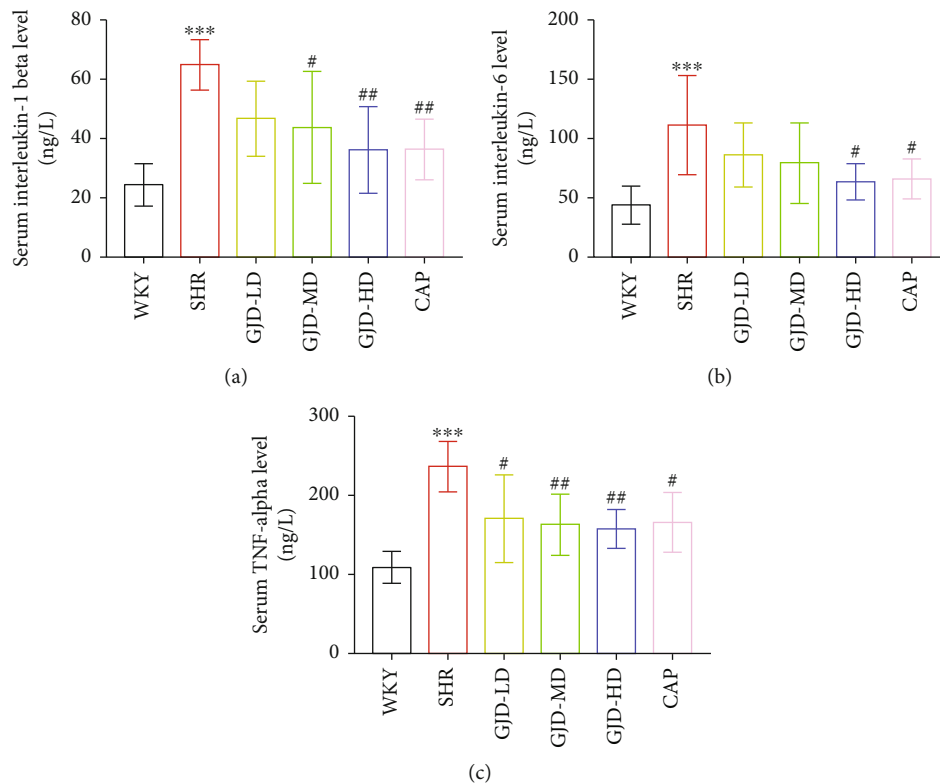


FIGURE 6: Serum level of interleukin-1 beta, interleukin-6, and TNF-alpha in each group. (a) endothelin-1, (b) angiotensin II, (c) interleukin-1 beta, (d) interleukin-6, and (e) TNF-alpha. WKY indicates the WKY control group, SHR indicates the SHR model group, GJD-LD indicates the SHR treated with GJD at a low dose, GJD-MD indicates the SHR treated with GJD at a medium dose, GJD-HD indicates the SHR treated with GJD at a high dose, and CAP indicates SHR treated with captopril. Data are means  $\pm$  SD,  $n = 7$ . \* $P < 0.05$ , \*\* $P < 0.01$ , \*\*\* $P < 0.001$  vs. WKY group, # $P < 0.05$ , ## $P < 0.01$ , ### $P < 0.001$  vs. SHR group.

(GB111629, 1:250, Servicebio, China), and alpha-SMA (GB111364, 1:300, Servicebio, China). All the above antibodies are rabbit polyclonal antibodies. The Eclipse Ci-L light microscope was used to randomly select the target area

of the tissue for  $200\times$  imaging. Image pro plus 6.0 analysis software is used to measure the integrated optical density (IOD) values in three visual field slices of each slice with the pixel area as the standard unit.

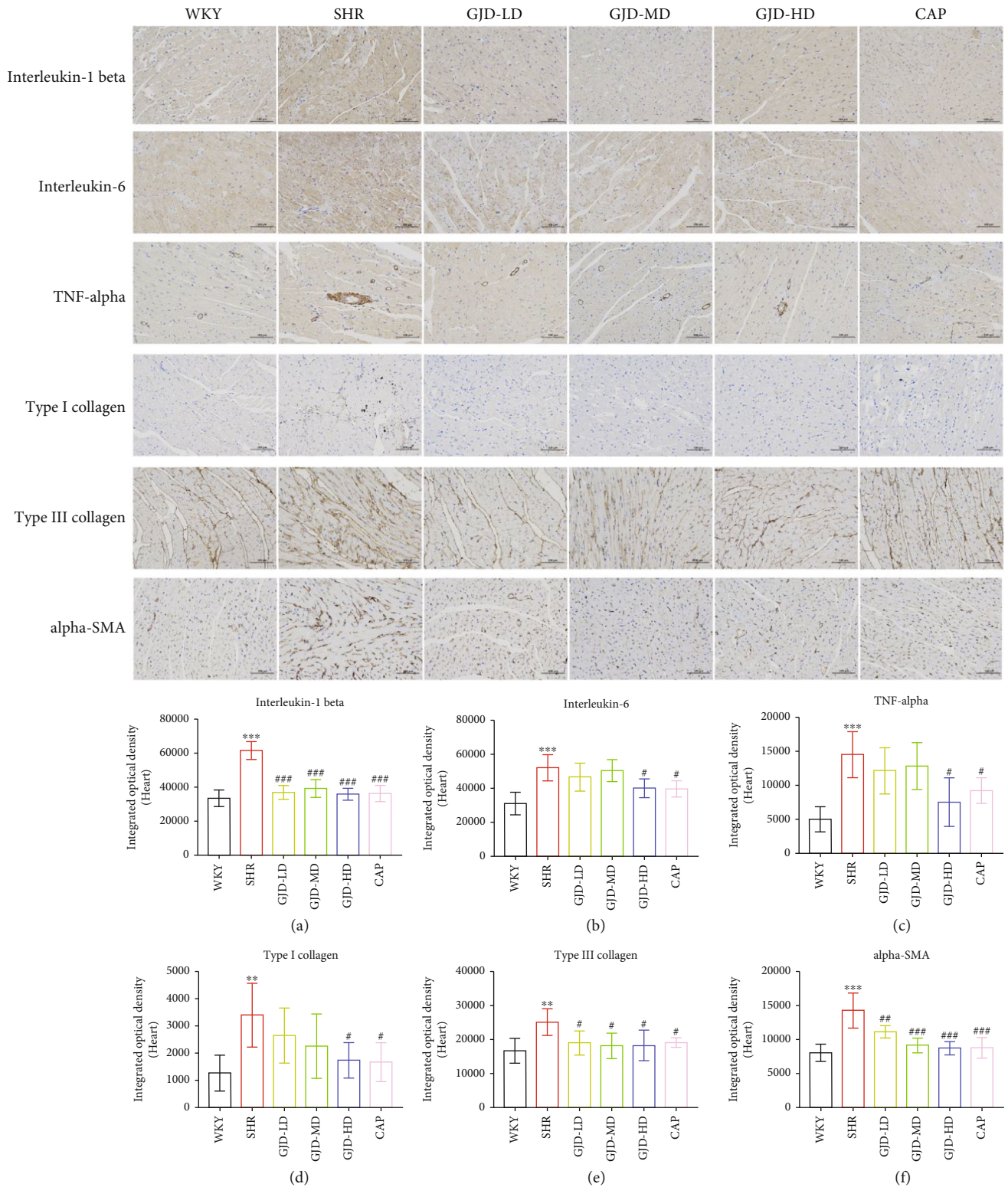


FIGURE 7: In the left ventricular, immunohistochemistry sections and quantification of protein expressions of interleukin-1 beta, interleukin-6, TNF-alpha, type I collagen, type III collagen, and alpha-SMA. (A) Interleukin-1 beta, (B) interleukin-6, (C) TNF-alpha, (D) type I collagen, (E) type III collagen, and (F) alpha-SMA. The images were taken at a magnification of  $\times 200$ . Scale bar =  $100 \mu\text{m}$ . WKY indicates the WKY control group, SHR indicates the SHR model group, GJD-LD indicates the SHR treated with GJD at a low dose, GJD-MD indicates the SHR treated with GJD at a medium dose, GJD-HD indicates the SHR treated with GJD at a high dose, and CAP indicates SHR treated with captopril. Data are means  $\pm$  SD.  $n = 7$ . \* $P < 0.05$ , \*\* $P < 0.01$ , \*\*\* $P < 0.001$  vs. WKY group, # $P < 0.05$ , ## $P < 0.01$ , ### $P < 0.001$  vs. SHR group.

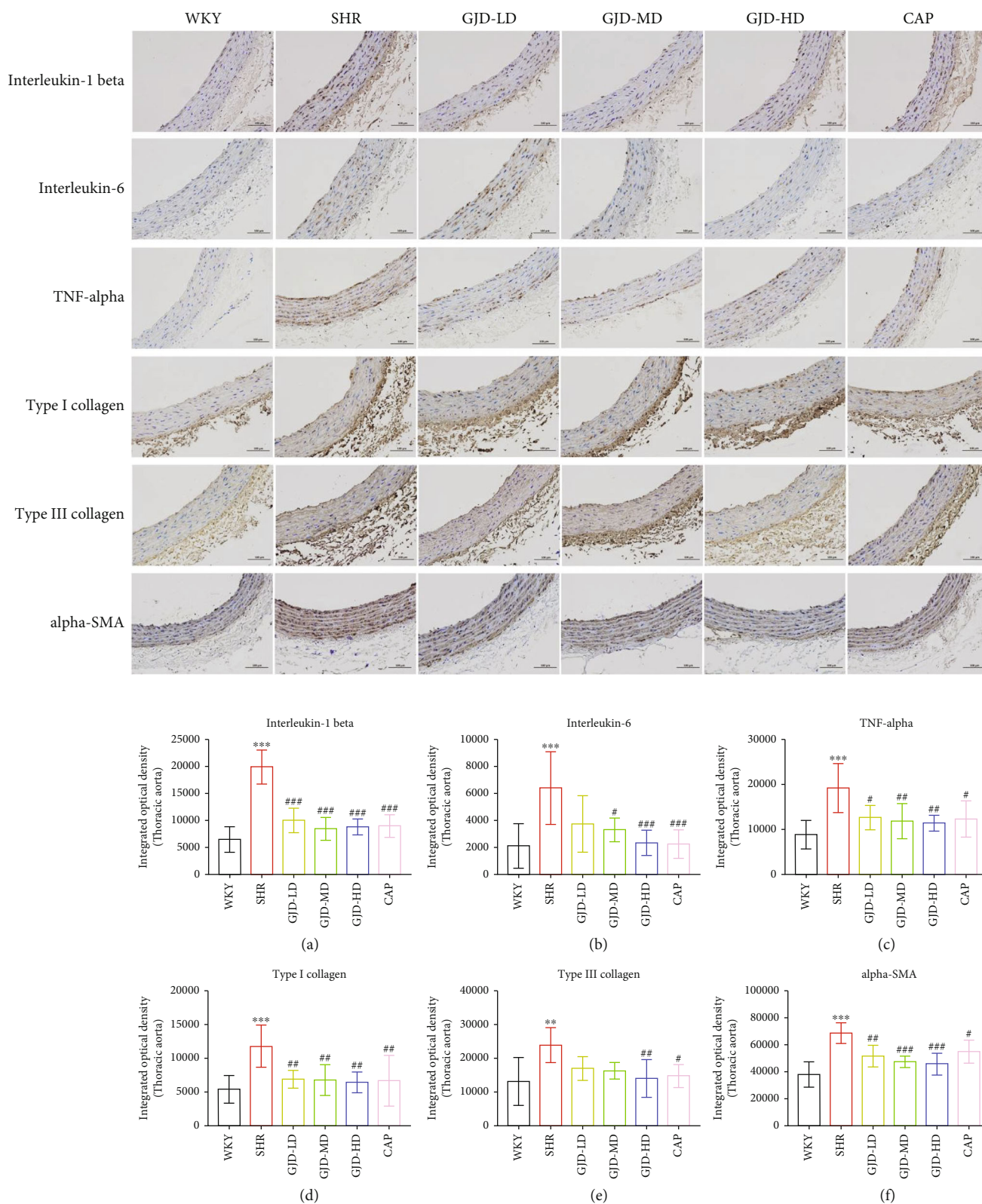


FIGURE 8: In the thoracic aorta, immunohistochemistry sections and quantification of protein expressions of interleukin -1 beta, interleukin-6, TNF-alpha, type I collagen, type III collagen, and alpha-SMA. (A) Interleukin-1 beta, (B) interleukin-6, (C) TNF-alpha, (D) type I collagen, (E) type III collagen, and (F) alpha-SMA. The images were taken at a magnification of  $\times 200$ . Scale bar =  $100 \mu\text{m}$ . WKY indicates the WKY control group, SHR indicates the SHR model group, GJD-LD indicates the SHR treated with GJD at a low dose, GJD-MD indicates the SHR treated with GJD at a medium dose, GJD-HD indicates the SHR treated with GJD at a high dose, and CAP indicates SHR treated with captopril. Data are means  $\pm$  SD.  $n = 7$ . \* $P < 0.05$ , \*\* $P < 0.01$ , \*\*\* $P < 0.001$  vs. WKY group, # $P < 0.05$ , ## $P < 0.01$ , ### $P < 0.001$  vs. SHR group.

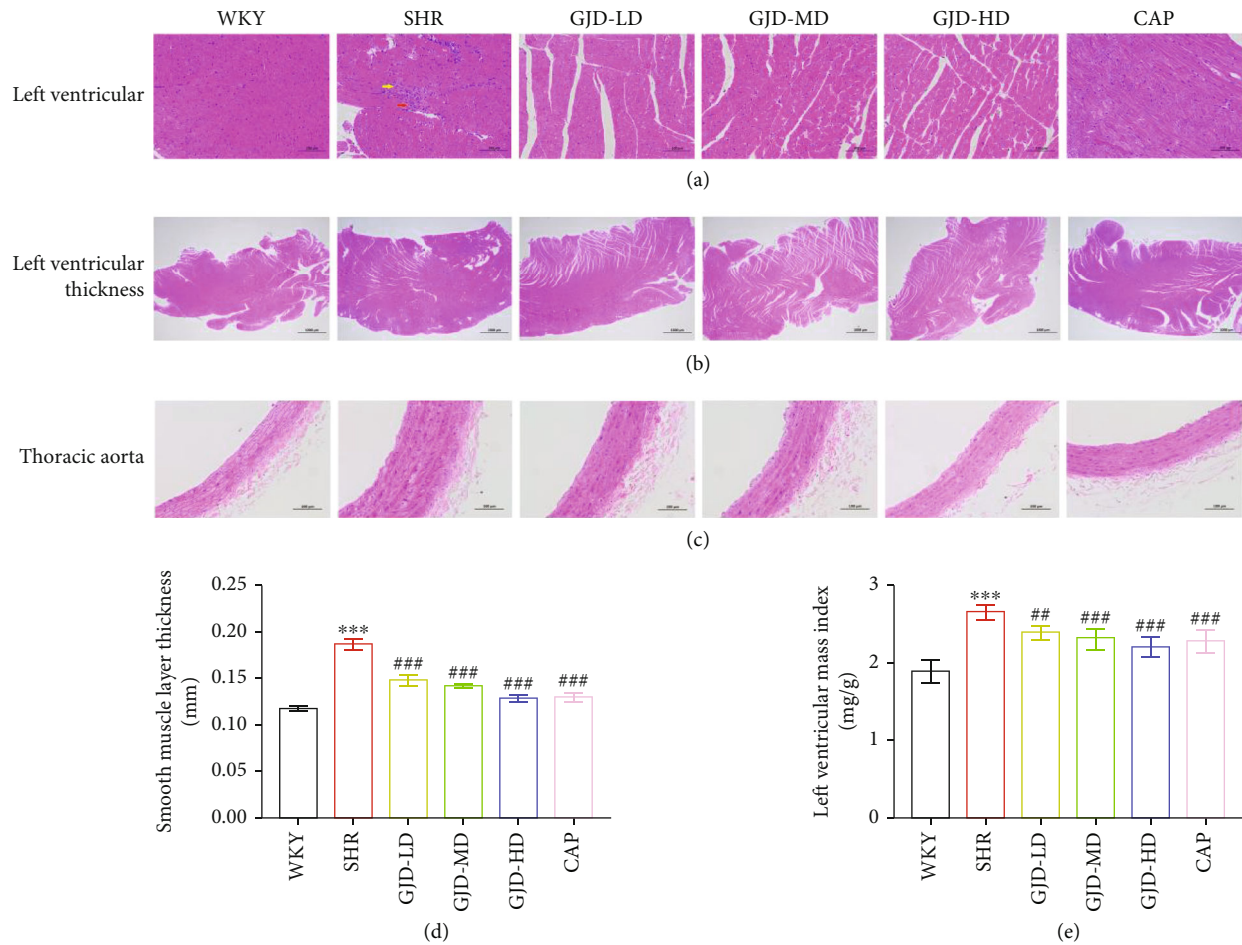


FIGURE 9: Effect of GJD on cardiovascular remodeling and histology of left ventricular and thoracic aorta of SHR after 6-week treatment by GJD. (a) HE staining Left ventricular (magnification of  $\times 200$ , scale bar  $100 \mu\text{m}$ ). (b) Ventricular wall (magnification of  $\times 20$ , scale bar  $1000 \mu\text{m}$ ). (c) HE staining of thoracic aorta (magnification of  $\times 200$ , scale bar  $100 \mu\text{m}$ ). (d) Smooth muscle layer thickness. (e) LVMI. Partial myocardial fibrosis necrosis was replaced by hyperplastic connective tissue with punctate lymphocytic infiltration (red arrows) in the SHR group. WKY indicates the WKY control group, SHR indicates the SHR model group, GJD-LD indicates the SHR treated with GJD at a low dose, GJD-MD indicates the SHR treated with GJD at a medium dose, GJD-HD indicates the SHR treated with GJD at a high dose, and CAP indicates SHR treated with captopril. Data are means  $\pm$  SD,  $n = 7$ . \* $P < 0.05$ , \*\* $P < 0.01$ , \*\*\* $P < 0.001$  vs. WKY group. # $P < 0.05$ , ## $P < 0.01$ , ### $P < 0.001$  vs. SHR group.

**2.8. Quantitative Real-Time Polymerase Chain Reaction (RT-qPCR).** The total RNA was extracted from the left ventricular and thoracic aorta tissues of three rats selected at random using Trizol reagent (Takara), reversed transcription into cDNA using the primescripttm RT Kit (Takara), and then subjected to real-time PCR reaction using TB Green® Premix Ex Taq™ II (Tli RNaseH Plus) (Takara), and the gene expression level was quantified using QuantStudio™3 real-time PCR system. After a hot start ( $42^\circ\text{C}$  2 min and  $4^\circ\text{C}$  5 min) ( $37^\circ\text{C}$  15 min,  $85^\circ\text{C}$  5 s, and  $4^\circ\text{C}$  5 min), amplification was performed (stage 1 Repts 1 ( $95.0^\circ\text{C}$  and 0.30 min), stage 2 Repts 40 ( $95.0^\circ\text{C}$ , 0.05 min,  $60.0^\circ\text{C}$ , 0.34 min), and stage 3 Repts 1 ( $95.0^\circ\text{C}$ , 0.15 min,  $60.0^\circ\text{C}$  1.00 min,  $95.0^\circ\text{C}$ , 0.15 min). The data was calculated and analyzed using the  $2^{-\Delta\Delta\text{Ct}}$  technique, and GAPDH acted as an internal control. Table 1 shows the primers used for PCR amplification.

**2.9. Statistical Analysis.** In this study, all data are presented as mean  $\pm$  standard deviation (SD), and they were statistically analyzed using Graphpad Prism 7. Statistical differences were assessed using one-way ANOVA with Tukey's multiple comparisons as a post hoc test. Statistical significance was defined as  $P < 0.05$ .

### 3. Results

**3.1. The Effect of GJD on Blood Pressure.** After 6 weeks of GJD gavage therapy, both systolic and diastolic blood pressures are significantly reduced, as seen in Figures 1(a) and 1(b). The systolic blood pressure was in the WKY ( $128.34 \text{ mm Hg}$ ), SHR ( $191.79 \text{ mm Hg}$ ), GJD-LD ( $163.45 \text{ mm Hg}$ ), GJD-MD ( $159.40 \text{ mm Hg}$ ), GJD-HD ( $153.84 \text{ mm Hg}$ ), and CAP group ( $154.26 \text{ mm Hg}$ ), while

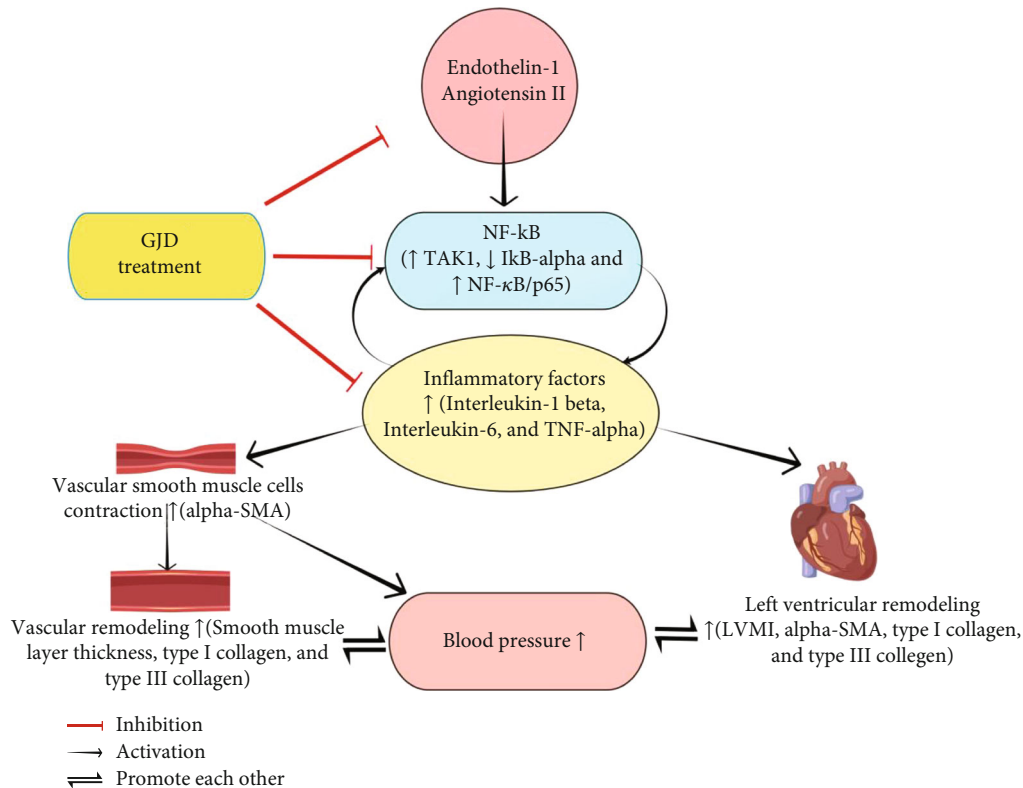


FIGURE 10: Flowchart of possible mechanisms of GJD attenuates hypertension and cardiovascular remodeling through inhibition NF- $\kappa$ B, created by FigDraw.

the diastolic blood pressure in the WKY (94.44 mm Hg), SHR (143.86 mm Hg), GJD-LD (124.20 mm Hg), GJD-MD (119.18 mm Hg), GJD-HD (117.86 mm Hg), and CAP group (116.13 mm Hg). The rats in GJD-HD experienced the highest decrease in systolic and diastolic blood pressures (Figures 1(a) and 1(b)), but there were no substantial differences between the GJD-HD and CAP groups. We also observed no differences in body weight across groups (Figure 1(c)).

**3.2. Effects of GJD on Endothelin-1 and Angiotensin II.** After 6 weeks of gavage treatment, we measured the serum's endothelin-1 and angiotensin II levels. The level of endothelin-1 and angiotensin II in the GJD-LD, GJD-MD, GJD-HD, and CAP groups was considerably lower than in the model group (Figures 2(a) and 2(b)). Both endothelin-1 and angiotensin II levels were decreased significantly in the GJD-HD group (Figures 2(a) and 2(b)).

**3.3. GJD's Effect on Nuclear Factor Kappa B.** After six weeks of therapy, we measured TAK1, p65, and I $\kappa$ B-alpha proteins in the left ventricular and thoracic aorta. TAK1 and P65 levels in SHR increased significantly in comparison to the WKY group; however, I $\kappa$ B-alpha levels declined significantly. In the left ventricular, TAK1 decreased significantly in the GJD-LD, GJD-MD, GJD-HD, and CAP groups compared to the SHR group, while p65 decreased significantly in the GJD-HD and CAP groups in comparison to the SHR group, but the lowered level of p65 in GJD-LD and

GJD-MD was not significant. While I $\kappa$ B-alpha increased significantly in the GJD-HD and CAP groups, it did not increase significantly in the GJD-LD and GJD-MD groups (Figure 3(a)).

The expression of p65 and TAK1 in the thoracic aorta of SHRs in the GJD-MD, GJD-HD, and CAP groups was considerably lower than in the SHR group, however, the decrease in GJD-LD was not statistically significant. Conversely, the level of I $\kappa$ B-alpha in the aorta of SHRs in the GJD-MD, GJD-HD, and CAP groups was significantly higher than in the SHR group; however the increased in GJD-LD was not significant (Figure 3(b)). The rats in the GJD-HD group had the highest elevation in I $\kappa$ B-alpha levels, as well as the lowest levels of TAK1 and p65 (Figure 3(b)).

The Real-time PCR also examined TAK1, I $\kappa$ B-alpha, and p65 mRNA expression in the left ventricular and thoracic aorta. As shown in Figures 4 and 5(g)–5(i), the mRNA expressions of p65 and TAK1 were decreased significantly in the left ventricular and thoracic aorta of SHRs in the GJD-LD, GJD-MD, GJD-HD, and CAP groups in comparison to those in the SHR group, whereas the level of I $\kappa$ B-alpha was significantly higher in both the left ventricular and aorta of SHRs in the GJD-MD, GJD-HD and CAP groups compared to those in SHR group, however, the decrease in GJD-LD was not significant.

**3.4. GJD's Effect on Inflammatory Cytokines.** After six weeks of gavage therapy, the levels of the markers of inflammation interleukin-1 beta, interleukin-6, and TNF-alpha were

significantly reduced in the SHR's serum in the GJD-LD, GJD-MD, GJD-HD, and CAP groups in comparison to the SHR group (Figures 6(a)–6(c)). The rats in the GJD-HD group exhibited a significant decrease in the markers of inflammation interleukin-1 beta, interleukin-6, and TNF-alpha (Figures 6(a)–6(c)), whereas there were no significant differences between the GJD-HD and the CAP groups.

Furthermore, we assessed the expression of interleukin-1 beta, interleukin-6, and TNF-alpha in the left ventricular and aorta by immunohistochemistry. In the left ventricle, the interleukin-1 beta, interleukin-6, and TNF-alpha expression in the model group (SHR) were markedly higher than WKY group. In comparison to the SHR group, all GJD groups had significantly lower interleukin-1 beta expression, but the low and medium dosages have no significant decrease in interleukin-6 and TNF-alpha expression in the left ventricle (Figures 7(a)–7(c)). The rats in the GJD-HD group had the greatest decrease in markers of inflammation interleukin-1 beta, interleukin-6, and TNF-alpha, while there were no differences between the GJD-HD group and the CAP group (Figures 7(a)–7(c)). In addition, in the aorta, the interleukin-1 beta, interleukin-6, and TNF-alpha expression in the SHR group were significantly higher than WKY group (Figures 8(a)–8(c)). In comparison with the SHR group, GJD-MD and GJD-HD groups had significantly lower interleukin-1 beta, interleukin-6, and TNF-alpha expression; however, GJD-LD only decreased interleukin-1 beta and TNF-alpha expression markedly, but the interleukin-6 did not decrease significantly in this group.

The real-time PCR was also performed to examine interleukin-1 beta, interleukin-6, and TNF-alpha mRNA expression in the left ventricular and aorta. As shown in Figures 4(a)–4(c), interleukin-1 beta, interleukin-6, and TNF-alpha are decreased in the left ventricular of SHRs in the GJD-LD, GJD-MD, and GJD-HD in comparison to those in the SHR group (IL-1 beta decreased significantly in all treatment group; however, the GJD-MD, and GJD-HD significantly reduced the interleukin-6, but the TNF-alpha only significantly decreased in GJD-HD). The rats in the GJD-HD group had the greatest significant decrease in interleukin-1 beta, interleukin-6, and TNF-alpha in the left ventricular (Figures 4(a)–4(c)). In the aorta, interleukin-1 beta, interleukin-6, and TNF-alpha expression reduced in all GJD groups (interleukin-1 beta decreased significantly in all treatment groups; however, interleukin-6 and TNF-alpha reduced significantly in both GJD-MD and GJD-HD) (Figures 5(a)–5(c)). The rats in the GJD-HD group had the greatest significantly decreased mRNA expression of interleukin-1 beta, interleukin-6, and TNF-alpha in the thoracic aorta, while no significant differences were identified between the GJD-HD group and CAP group (Figures 5(a)–5(c)).

**3.5. GJD's Effects on Cardiovascular Remodeling.** Based on the findings of left ventricular and thoracic aorta HE staining following six weeks of gavage administration, when compared with the WKY group, the heart tissue from SHRs showed significant thickening of the ventricular wall by an increase in LVMI, partial myocardial fiber necrosis, accom-

panied by fibrosis and mild inflammation. It was observed that after therapy, LVMI are reduced to a greater extent in the GJD-LD, GJD-MD, GJD-HD, and CAP groups than in the SHR group, and there is no necrosis or fibrosis in these groups as shown in Figures 9(a), 9(b), and 9(e). Neither the GJD-LD nor the GJD-MD groups showed any signs of necrosis or fibrosis, and the distinction between the two groups was unclear. Groups GJD-HD and CAP both showed no signs of necrosis or fibrosis, and the difference between them was not apparent (Figure 9(a)).

As shown in Figures 9(c) and 9(d), we measure the thoracic aorta thickness, and it is lower in the GJD-LD, GJD-MD, GJD-HD, and CAP groups than in the SHR group. GJD and CAP groups significantly suppressed the development of aortic hypertrophy compared to the SHR group. The rats in the GJD-HD group had the highest decrease in thoracic aorta wall thickness (Figures 9(c) and 9(d)). Additionally, the immunohistochemistry and RT-qPCR analysis indicated that the expression of type I collagen, type III collagen, and alpha-SMA in the left ventricular and thoracic aorta was significantly decreased in GJD's groups than SHR group, but there were no differences between CAP and GJD-HD groups (Figures 4(d)–4(f), 5(d)–5(f), 6(d)–6(f), 7(d)–7(f) and 8(d)–8(f)). The possible mechanisms of GJD attenuate hypertension and cardiovascular remodeling (Figure 10).

## 4. Discussion

In this research, we investigated the efficacy of GJD in treating hypertension. SHRs were treated with various dosages of GJD, and the efficacies were assessed on numerous parameters. This research will provide new concepts and theoretical foundations for managing hypertensive related target organ remodeling. In this research, we examined how blood pressure changed following GJD therapy. We observed that the following six weeks of GJD gavage therapy at GJD-LD, GJD-MD, and GJD-HD doses significantly reduced SBP and DBP. We observed that GJD-HD had the largest decrease in SBP and DBP after six weeks of treatment. Angiotensin II and endothelin-1 are the main vasoconstrictors in hypertension pathogenesis [24–26]. Moreover, numerous studies found that increased Ang II and ET-1 activated NF- $\kappa$ B signaling pathway [27–30]. Here, after therapy with GJD groups, the serum's levels of endothelin-1 and angiotensin II were significantly reduced, with GJD-HD having the most significant reduction.

Several studies have implicated the nuclear factor-kappa B (NF- $\kappa$ B) pathway in the pathogenesis of hypertensive cardiovascular disease through its role in the transcriptional activation of inflammatory markers [15, 31, 32]; [33, 34]. Signal-induced degradation of I $\kappa$ B proteins initiates NF- $\kappa$ B activation [35, 36], which happens primarily through phosphorylation and activation of a kinase termed I $\kappa$ B kinase (IKK). TAK1 causes degradation of I $\kappa$ B via the I $\kappa$ B kinase (IKK) and nuclear factor (NF) kappa B (NF- $\kappa$ B) signaling pathways [37]; [38, 39]. With the degradation of I $\kappa$ B, the NF- $\kappa$ B complex is free to enter the nucleus and trigger the expression of certain genes that have NF- $\kappa$ B DNA-binding

sites nearby [40–42]. Rodríguez-Iturbe B et al. showed that long-term suppression of this proinflammatory transcription factor could prevent hypertension in this model, confirming the early increase in NF- $\kappa$ B activation in the SHR [43].

The inflammatory markers interleukin-1 beta, interleukin-6, and tumor necrosis factor alpha were all secreted at higher rates after NF-kappaB activation [44–46]. Recent studies have shown that interleukin-1beta, interleukin-6, and TNF- alpha are all elevated in high blood pressure, suggesting that these inflammatory markers may play a role in the pathogenesis of hypertension [7, 47–49]; [50]. Numerous studies have shown that nuclear factor (NF)-kappaB (NF- $\kappa$ B) signaling is crucial in inflammation and cardiovascular diseases [33, 34, 51, 52]. Many major CVD, including hypertension, are caused by abnormal vascular smooth muscle cells (VSMC) contraction, migration, and proliferation [53–55]. The primary component of the artery's medial layer is VSMC [54]. These cells contract to control blood vessel tone (constriction/dilation), hence controlling blood flow and pressure [56, 57]. VSMC may also secrete molecules, which allows for the creation and repair of extracellular matrix proteins as well as the modulation of vascular wall structure [58]. Strong expression of several marker genes, such as alpha-SMA, SM22, and calponin, is characteristic of contractile VSMC, which are nonproliferative and fully differentiated [59, 60]. In brief, VSMC contraction is caused by alpha-SMA, the major and particular isoform of actin produced in VSMC [54, 55]. In mice, a deficiency of alpha-SMA can result in reduced VSMC contractility and then hypotension [61, 62]. Hence, the ability of VSMC to differentiate and contract depends on the expression level of gene that serves as marker for these cells. Numerous studies have shown that inflammatory indicators, which are activated by NF-KB, cause vascular smooth muscle cells (VSMC) to become more contractile and, thus, are responsible for elevations in blood pressure. In the Choi S study, it shows that the TNF $\alpha$ -induced VSMC phenotypic alteration and vasodilatory dysfunction were blocked by NF- $\kappa$ B inhibition [63]. Data suggested that IL-1B treatment elevated proinflammatory genes through an NF- $\kappa$ B-dependent pathway, and initial observations suggested a connection between inflammation/IL-1B and its associated proteins and alterations in the phenotypic of smooth muscle cells in systemic arterial hypertension [64, 65]. In this research, the same is found that NF- $\kappa$ B induced the inflammatory markers interleukin-1 beta, interleukin-6, and TNF-alpha which upregulates the alpha-SMA expression and that a sign of VSMC contraction in SHR group may lead to increase blood pressure, while the downregulation of alpha-SMA expression levels in GJD groups suggests that GJD has the capacity to prevent VSMC differentiation from the proliferative type. As a result, GJD may be functionally relevant for lowering blood pressure by decreasing the contractile phenotype of VSMCs.

Furthermore, the proinflammatory cytokines have been linked to pathological cardiac hypertrophy [66]. Many studies over the last two decades have shown that IL-1 $\beta$ , IL-6, and TNF- $\alpha$  are intimately linked to cardiac fibrosis, patho-

logical cardiac remodeling, and cardiac hypertrophy [67–70], and the inflammatory cytokines induced following the activation of the nuclear factor- $\kappa$ B (NF- $\kappa$ B) pathway [71] [44]. Therefore, inhibition of the NF- $\kappa$ B pathway might be a means to decrease inflammation led to attenuate cardiac remodeling. In the study of Miguel-Carrasco JL, it is demonstrated that captopril reduces inflammation in the left ventricle of hypertensive rats and suggests that NF- $\kappa$ B-driven inflammatory reactivity may be responsible for this impact by inactivating of NF-B-dependent proinflammatory factors [34]. Our study also showed that GJD decreased hypertrophy of the left ventricle by inhibiting NF- $\kappa$ B-related inflammatory markers.

Increase in wall thickness of the aorta and the thickening of the ventricular wall are hallmark features of hypertension-induced widespread cardiovascular remodeling [72–74]. Vascular remodeling in hypertension comprises alterations to smooth muscle cells in the artery wall, as well as endothelial cells, elastin, and collagen levels [75]. These vascular remodeling characteristics in hypertension are typically associated with a renin-angiotensin-aldosterone system imbalance, endothelial cell (EC) dysfunction, contractile properties, and phenotypic switching of VSMC, as well as extracellular matrix (ECM) reorganization and inflammation throughout the entire vessel wall [53]. In addition, myofibroblasts are differentiated from cardiac fibroblasts by myocardial injury, and the expression of alpha-SMA signals effective transformation into a phenotype with a high capacity to synthesize extracellular matrix proteins [76, 77], and the fibrillary proteins which are the primary components of the cardiac extracellular matrix are type I collagen and type III collagen, which are considered as indicators of fibrosis in fibroblasts and then remodeling [76, 78]. For that type I collagen, type III collagen and alpha-SMA expression promote thoracic and left ventricular remodeling [79–82]. The *Salvia miltiorrhiza* active ingredients have the effect of reducing the alpha-SMA expression, collagen, and ET-1, thereby reducing the vessel wall thickness [83]. Icariside II may reduce the formation of alpha-SMA and type I collagen/type III collagen in SHR via the MMP/TIMP-1 and TGF-b1/Smad2,3/p-p38 signaling pathways, according to the findings of Fu's study [84]. Here, GJD therapy decreased arterial wall thickness and ventricular wall thickening in SHR, and type I collagen, type III collagen, and alpha-SMA levels in the thoracic aorta and left ventricle were significantly reduced following GJD therapy.

NF- $\kappa$ B signaling activation may enhance the expression of inflammatory markers in the SHR thoracic aorta and left ventricle leading to hypertension and cardiovascular remodeling. GJD administration inhibited this change, suggesting that inflammatory component control through NF- $\kappa$ B activation may be implicated in GJD's cardiovascular protective impact on SHR rats.

## 5. Conclusion

In conclusion, GJD may reduce blood pressure and improve left ventricular and aortic remodeling in a SHR model of hypertension by inhibiting inflammatory factors through



NF- $\kappa$ B. Our data indicated that GJD might be used as an antihypertensive agent and provides scientific basis for further pharmacological studies and clinical applications. This study has some limitations, such as the need to fully evaluate the active ingredients in the GJD and then extract the active ingredients to investigate further its impact on treating hypertension, and the GJD's regulatory mechanisms for improving hypertension symptoms in SHR models should be investigated further by assessing mRNA, ncRNA, and protein levels. In addition, we did not follow up on blood pressure measurements after withdrawal or with long-term treatment in this study; further researches are needed to assess the efficacy of GJD after withdrawal and long-term therapy.

## Abbreviations

GJD: Gedan Jiangya decoction  
 SBP: Systolic blood pressure  
 DBP: Diastolic blood pressure  
 SHR: Spontaneously hypertensive rats  
 WKY: Wistar-Kyoto rats  
 P65: NF- $\kappa$ B/p65  
 TAK1: Transforming growth factor b-activated kinase 1  
 VSMC: Vascular smooth muscle cells  
 TCM: Traditional Chinese medicine.

## Data Availability

All data generated or analyzed during this study have been deposited in the documents [Supplementary Data 1 and Supplementary Data 2]. Further enquiries can be directed to the corresponding author.

## Conflicts of Interest

The authors declare that they have no conflicts of interest.

## Authors' Contributions

Shadi A.D. Mohammed, Hanxing Liu, and Shumin Liu conceived and designed this study. Shadi A.D. Mohammed and Hanxing Liu conducted the experiment, statistical analysis, and wrote the manuscript. Salem Baldi, Ping-ping Chen, and Fang Lu revised the manuscript and provided valuable suggestions for the research. All authors approved the final version of the manuscript.

## Supplementary Materials

The supplementary materials which include all data used in this study in Supplementary Data 1 and western blot in Supplementary Data 2. (*Supplementary Materials*)

## References

- [1] D. W. Jones, P. K. Whelton, N. Allen et al., "Management of stage 1 hypertension in adults with a low 10-year risk for cardiovascular disease: filling a guidance gap: a scientific statement from the American Heart Association," *Hypertension*, vol. 77, no. 6, pp. e58–e67, 2021.
- [2] P. Geldsetzer, J. Manne-Goehler, M. E. Marcus et al., "The state of hypertension care in 44 low-income and middle-income countries: a cross-sectional study of nationally representative individual-level data from 1\*1 million adults," *The Lancet*, vol. 394, no. 10199, pp. 652–662, 2019.
- [3] F. Bragg, J. Halsey, Y. Guo et al., "Blood pressure and cardiovascular diseases in Chinese adults with type 2 diabetes: a prospective cohort study," *The Lancet Regional Health - Western Pacific*, vol. 7, article 100085, 2021.
- [4] Y. Qi, X. Han, D. Zhao et al., "Long-term cardiovascular risk associated with stage 1 hypertension defined by the 2017 ACC/AHA hypertension guideline," *Journal of the American College of Cardiology*, vol. 72, no. 11, pp. 1201–1210, 2018.
- [5] M. H. Forouzanfar, P. Liu, G. A. Roth et al., "Global burden of hypertension and systolic blood pressure of at least 110 to 115 mm hg, 1990-2015," *JAMA*, vol. 317, no. 2, pp. 165–182, 2017.
- [6] E. Rapsomaniki, A. Timmis, J. George et al., "Blood pressure and incidence of twelve cardiovascular diseases: lifetime risks, healthy life-years lost, and age-specific associations in 1\*25 million people," *The Lancet*, vol. 383, no. 9932, pp. 1899–1911, 2014.
- [7] L. Deng, W. Liu, Q. Xu et al., "Tianma Gouteng decoction regulates oxidative stress and inflammation in AngII-induced hypertensive mice via transcription factor EB to exert anti-hypertension effect," *Biomedicine & Pharmacotherapy*, vol. 145, article 112383, 2022.
- [8] D. Pugh and N. Dhaun, "Hypertension and vascular Inflammation," *Hypertension*, vol. 77, no. 1, pp. 190–192, 2021.
- [9] Z. Wang, Z. Chen, L. Zhang et al., "Status of hypertension in China," *Circulation*, vol. 137, no. 22, pp. 2344–2356, 2018.
- [10] L. He, Y. Liu, K. Yang et al., "The discovery of Q-markers of Qiliqiangxin capsule, a traditional Chinese medicine prescription in the treatment of chronic heart failure, based on a novel strategy of multi-dimensional "radar chart" mode evaluation," *Phytomedicine*, vol. 82, article 153443, 2021.
- [11] H. Li, "Advances in anti hepatic fibrotic therapy with traditional Chinese medicine herbal formula," *Journal of Ethnopharmacology*, vol. 251, article 112442, 2020.
- [12] X. Xiong, X. Yang, Y. Liu, Y. Zhang, P. Wang, and J. Wang, "Chinese herbal formulas for treating hypertension in traditional Chinese medicine: perspective of modern science," *Hypertension Research*, vol. 36, no. 7, pp. 570–579, 2013.
- [13] F. Lin, X. Huang, F. Xing et al., "“\_Semen Brassicae\_” reduces thoracic aortic remodeling, inflammation, and oxidative damage in spontaneously hypertensive rats," *Biomedicine & Pharmacotherapy*, vol. 129, article 110400, 2020.
- [14] X. Wu, A. Shen, L. Bao et al., "Qingda granules attenuate hypertensive cardiac remodeling and inflammation in spontaneously hypertensive rats," *Biomedicine & Pharmacotherapy*, vol. 129, article 110367, 2020.
- [15] A. Fiordelisi, G. Iaccarino, C. Morisco, E. Coscioni, and D. Sorriento, "NFkappaB is a key player in the crosstalk between inflammation and cardiovascular diseases," *International Journal of Molecular Sciences*, vol. 20, no. 7, p. 1599, 2019.
- [16] H. Yu, L. Lin, Z. Zhang, H. Zhang, and H. Hu, "Targeting NF- $\kappa$ B pathway for the therapy of diseases: mechanism and clinical study," *Signal Transduction and Targeted Therapy*, vol. 5, no. 1, p. 209, 2020.

- [17] L. Xie, T. Wang, S. Lin et al., "Uncaria rhynchophylla attenuates angiotensin II-induced myocardial fibrosis via suppression of the RhoA/ROCK1 pathway," *Biomedicine & Pharmacotherapy*, vol. 146, article 112607, 2022.
- [18] Q. Zhang, J. J. Zhao, J. Xu, F. Feng, and W. Qu, "Medicinal uses, phytochemistry and pharmacology of the genus *Uncaria*," *Journal of Ethnopharmacology*, vol. 173, pp. 48–80, 2015.
- [19] X. He, J. Wang, M. Li et al., "Eucommia ulmoides Oliv.: ethnopharmacology, phytochemistry and pharmacology of an important traditional Chinese medicine," *Journal of Ethnopharmacology*, vol. 151, no. 1, pp. 78–92, 2014.
- [20] J. Ren, L. Fu, S. H. Nile, J. Zhang, and G. Kai, "Salvia miltiorrhiza in treating cardiovascular diseases: a review on its pharmacological and clinical applications," *Frontiers in Pharmacology*, vol. 10, p. 753, 2019.
- [21] Z. Zhang, T. N. Lam, and Z. Zuo, "Radix Puerariae: an overview of its chemistry, pharmacology, pharmacokinetics, and clinical use," *Journal of Clinical Pharmacology*, vol. 53, no. 8, pp. 787–811, 2013.
- [22] Y. Bai, B. Xia, W. Xie et al., "Phytochemistry and pharmacological activities of the genus *Prunella*," *Food Chemistry*, vol. 204, pp. 483–496, 2016.
- [23] H.-X. Kuang, Q.-H. Wang, L. Yang et al., "Investigation of radix achyranthis bidentatae phytochemistry and pharmacology," *Journal of Traditional Chinese Medicine*, vol. 5, no. 1, p. 50, 2019.
- [24] A. Dushpanova, S. Agostini, E. Ciofini et al., "Gene silencing of endothelial von Willebrand factor attenuates angiotensin II-induced endothelin-1 expression in porcine aortic endothelial cells," *Scientific Reports*, vol. 6, no. 1, article 30048, 2016.
- [25] Y. J. Lin, C. F. Kwok, C. C. Juan et al., "Angiotensin II enhances endothelin-1-induced vasoconstriction through upregulating endothelin type a receptor," *Biochemical and Biophysical Research Communications*, vol. 451, no. 2, pp. 263–269, 2014.
- [26] Y. Lv, W. Zhao, L. Yu, J. G. Yu, and L. Zhao, "Angiotensin-converting enzyme gene D/I polymorphism in relation to endothelial function and endothelial-released factors in Chinese women," *Frontiers in Physiology*, vol. 11, p. 951, 2020.
- [27] J. M. Kim, H. S. Heo, Y. M. Ha et al., "Mechanism of Ang II involvement in activation of NF- $\kappa$ B through phosphorylation of p65 during aging," *Age (Dordrecht, Netherlands)*, vol. 34, no. 1, pp. 11–25, 2012.
- [28] D. N. Muller, R. Dechend, E. M. Mervaala et al., "NF-kappaB inhibition ameliorates angiotensin II-induced inflammatory damage in rats," *Hypertension*, vol. 35, no. 1, pp. 193–201, 2000.
- [29] E. L. Schiffrin, "Role of endothelin-1 in hypertension and vascular disease," *American Journal of Hypertension*, vol. 14, no. 11, pp. S83–S89, 2001.
- [30] S. H. Wilson, R. D. Simari, and A. Lerman, "The effect of endothelin-1 on nuclear factor kappa B in macrophages," *Biochemical and Biophysical Research Communications*, vol. 286, no. 5, pp. 968–972, 2001.
- [31] K. W. Choy, D. Murugan, X. F. Leong, R. Abas, A. Alias, and M. R. Mustafa, "Flavonoids as natural anti-inflammatory agents targeting nuclear factor-kappa B (NF $\kappa$ B) signaling in cardiovascular diseases: a mini review," *Frontiers in Pharmacology*, vol. 10, p. 1295, 2019.
- [32] H. Haybar, S. Shahrabi, H. Rezaeeyan, R. Shirzad, and N. Saki, "Endothelial cells: from dysfunction mechanism to pharmacological effect in cardiovascular disease," *Cardiovascular Toxicology*, vol. 19, no. 1, pp. 13–22, 2019.
- [33] H. Li, Y. Shi, X. Wang et al., "Piceatannol alleviates inflammation and oxidative stress via modulation of the Nrf2/HO-1 and NF- $\kappa$ B pathways in diabetic cardiomyopathy," *Chemico-Biological Interactions*, vol. 310, article 108754, 2019.
- [34] J. L. Miguel-Carrasco, S. Zambrano, A. J. Blanca, A. Mate, and C. M. Vázquez, "Captopril reduces cardiac inflammatory markers in spontaneously hypertensive rats by inactivation of NF- $\kappa$ B," *Journal of Inflammation (Lond)*, vol. 7, no. 1, p. 21, 2010.
- [35] M. J. Bloom, S. D. Saksena, G. P. Swain, M. S. Behar, T. E. Yankeelov, and A. G. Sorace, "The effects of IKK-beta inhibition on early NF-kappa-B activation and transcription of downstream genes," *Cellular Signalling*, vol. 55, pp. 17–25, 2019.
- [36] K. Iwai, "Diverse roles of the ubiquitin system in NF- $\kappa$ B activation," *Biochimica et Biophysica Acta*, vol. 1843, no. 1, pp. 129–136, 2014.
- [37] A. A. Ajibade, H. Y. Wang, and R. F. Wang, "Cell type-specific function of TAK1 in innate immune signaling," *Trends in Immunology*, vol. 34, no. 7, pp. 307–316, 2013.
- [38] K. C. Chen and S. H. Juo, "MicroRNAs in atherosclerosis," *The Kaohsiung Journal of Medical Sciences*, vol. 28, no. 12, pp. 631–640, 2012.
- [39] S. J. Watkins, G. M. Borthwick, R. Oakenfull, A. Robson, and H. M. Arthur, "Angiotensin II-induced cardiomyocyte hypertrophy *in vitro* is TAK1-dependent and Smad2/3-independent," *Hypertension Research*, vol. 35, no. 4, pp. 393–398, 2012.
- [40] A. A. Beg, S. M. Ruben, R. I. Scheinman, S. Haskill, C. A. Rosen, and A. S. Baldwin Jr., "I kappa B interacts with the nuclear localization sequences of the subunits of NF-kappa B: a mechanism for cytoplasmic retention," *Genes & Development*, vol. 6, no. 10, pp. 1899–1913, 1992.
- [41] F. Christian, E. L. Smith, and R. J. Carmody, "The regulation of NF- $\kappa$ B subunits by phosphorylation," *Cell*, vol. 5, no. 1, 2016.
- [42] I. M. Verma, J. K. Stevenson, E. M. Schwarz, D. Van Antwerp, and S. Miyamoto, "Rel/NF-kappa B/I kappa B family: intimate tales of association and dissociation," *Genes & Development*, vol. 9, no. 22, pp. 2723–2735, 1995.
- [43] B. Rodriguez-Iturbe, A. Ferrebuz, V. Vanegas, Y. Quiroz, S. Mezzano, and N. D. Vaziri, "Early and sustained inhibition of nuclear factor-kappaB prevents hypertension in spontaneously hypertensive rats," *The Journal of Pharmacology and Experimental Therapeutics*, vol. 315, no. 1, pp. 51–57, 2005.
- [44] J. P. Cardinale, S. Sriramula, N. Mariappan, D. Agarwal, and J. Francis, "Angiotensin II-induced hypertension is modulated by nuclear factor- $\kappa$ B in the paraventricular nucleus," *Hypertension*, vol. 59, no. 1, pp. 113–121, 2012.
- [45] D. G. Harrison, T. J. Guzik, H. E. Lob et al., "Inflammation, immunity, and hypertension," *Hypertension*, vol. 57, no. 2, pp. 132–140, 2011.
- [46] H. Nagoshi, Y. Uehara, F. Kanai et al., "Prostaglandin D2 inhibits inducible nitric oxide synthase expression in rat vascular smooth muscle cells," *Circulation Research*, vol. 82, no. 2, pp. 204–209, 1998.
- [47] A. Agita and M. T. Alsagaff, "Inflammation, immunity, and hypertension," *Acta Medica Indonesiana*, vol. 49, no. 2, pp. 158–165, 2017.
- [48] Q. N. Dinh, G. R. Drummond, C. G. Sobey, and S. Chrissobolis, "Roles of inflammation, oxidative stress, and

- vascular dysfunction in hypertension,” *BioMed Research International*, vol. 2014, Article ID 406960, 11 pages, 2014.
- [49] E. C. Murray, R. Nosalski, N. MacRitchie et al., “Therapeutic targeting of inflammation in hypertension: from novel mechanisms to translational perspective,” *Cardiovascular Research*, vol. 117, no. 13, pp. 2589–2609, 2021.
- [50] Y. Wang, Y. Li, Y. Wu et al., “5TNF- $\alpha$  and IL-1 $\beta$  neutralization ameliorates angiotensin II-induced cardiac damage in male mice,” *Endocrinology*, vol. 155, no. 7, pp. 2677–2687, 2014.
- [51] Z. Gan, D. Huang, J. Jiang, Y. Li, H. Li, and Y. Ke, “Captopril alleviates hypertension-induced renal damage, inflammation, and NF- $\kappa$ B activation,” *Brazilian Journal of Medical and Biological Research*, vol. 51, no. 11, article e7338, 2018.
- [52] X. Jing, T. Jiang, L. Dai et al., “Hypoxia-induced autophagy activation through NF- $\kappa$ B pathway regulates cell proliferation and migration to induce pulmonary vascular remodeling,” *Experimental Cell Research*, vol. 368, no. 2, pp. 174–183, 2018.
- [53] Z. Cai, Z. Gong, Z. Li, L. Li, and W. Kong, “Vascular extracellular matrix remodeling and hypertension,” *Antioxidants & Redox Signaling*, vol. 34, no. 10, pp. 765–783, 2021.
- [54] P. Fan, B. Han, M. Feng et al., “Functional and proteomic investigations reveal major royal jelly protein 1 associated with anti-hypertension activity in mouse vascular smooth muscle cells,” *Scientific Reports*, vol. 6, no. 1, article 30230, 2016.
- [55] R. Jones, M. Jacobson, and W. Steudel, “Alpha-smooth-muscle actin and microvascular precursor smooth-muscle cells in pulmonary hypertension,” *American Journal of Respiratory Cell and Molecular Biology*, vol. 20, no. 4, pp. 582–594, 1999.
- [56] M. Chiong, P. Morales, G. Torres et al., “Influence of glucose metabolism on vascular smooth muscle cell proliferation,” *VASA*, vol. 42, no. 1, pp. 8–16, 2013.
- [57] S. K. Michael, H. K. Surks, Y. Wang et al., “High blood pressure arising from a defect in vascular function,” *Proceedings of the National Academy of Sciences of the United States of America*, vol. 105, no. 18, pp. 6702–6707, 2008.
- [58] A. Cecchetti, S. Rocchiccioli, C. Boccardi, and L. Citti, “Vascular smooth-muscle-cell activation: proteomics point of view,” *International Review of Cell and Molecular Biology*, vol. 288, pp. 43–99, 2011.
- [59] Z. Chen, J. Wu, C. Yang et al., “DiGeorge syndrome critical region 8 (DGCR8) protein-mediated microRNA biogenesis is essential for vascular smooth muscle cell development in mice,” *The Journal of Biological Chemistry*, vol. 287, no. 23, pp. 19018–19028, 2012.
- [60] M. Chiong, B. Cartes-Saavedra, I. Norambuena-Soto et al., “Mitochondrial metabolism and the control of vascular smooth muscle cell proliferation,” *Frontiers in Cell and Development Biology*, vol. 2, p. 72, 2014.
- [61] D. M. Milewicz, J. R. Østergaard, L. M. Ala-Kokko et al., “De novo ACTA2 mutation causes a novel syndrome of multisystemic smooth muscle dysfunction,” *American Journal of Medical Genetics. Part A*, vol. 152A, no. 10, pp. 2437–2443, 2010.
- [62] L. A. Schildmeyer, R. Braun, G. Taffet et al., “Impaired vascular contractility and blood pressure homeostasis in the smooth muscle alpha-actin null mouse,” *The FASEB Journal*, vol. 14, no. 14, pp. 2213–2220, 2000.
- [63] S. Choi, M. Park, J. Kim et al., “TNF- $\alpha$  elicits phenotypic and functional alterations of vascular smooth muscle cells by miR-155-5p-dependent down-regulation of cGMP-dependent kinase 1,” *The Journal of Biological Chemistry*, vol. 293, no. 38, pp. 14812–14822, 2018.
- [64] M. R. Alexander, M. Murgai, C. W. Moehle, and G. K. Owens, “Interleukin-1 $\beta$  modulates smooth muscle cell phenotype to a distinct inflammatory state relative to PDGF-DD via NF- $\kappa$ B-dependent mechanisms,” *Physiological Genomics*, vol. 44, no. 7, pp. 417–429, 2012.
- [65] A. E. Postlethwaite, R. Raghov, G. P. Stricklin, H. Poppleton, J. M. Seyer, and A. H. Kang, “Modulation of fibroblast functions by interleukin 1: increased steady-state accumulation of type I procollagen messenger RNAs and stimulation of other functions but not chemotaxis by human recombinant interleukin 1 alpha and beta,” *The Journal of Cell Biology*, vol. 106, no. 2, pp. 311–318, 1988.
- [66] C. J. Oldfield, T. A. Duhamel, and N. S. Dhalla, “Mechanisms for the transition from physiological to pathological cardiac hypertrophy,” *Canadian Journal of Physiology and Pharmacology*, vol. 98, no. 2, pp. 74–84, 2020.
- [67] J. G. Cannon, “Inflammatory cytokines in nonpathological states,” *News in Physiological Sciences*, vol. 15, pp. 298–303, 2000.
- [68] B. Coles, C. A. Fielding, S. Rose-John, J. Scheller, S. A. Jones, and V. B. O’Donnell, “Classic interleukin-6 receptor signaling and interleukin-6 trans-signaling differentially control angiotensin II-dependent hypertension, cardiac signal transducer and activator of transcription-3 activation, and vascular hypertrophy in vivo,” *The American Journal of Pathology*, vol. 171, no. 1, pp. 315–325, 2007.
- [69] G. C. Meléndez, J. L. McLarty, S. P. Levick, Y. Du, J. S. Janicki, and G. L. Brower, “Interleukin 6 mediates myocardial fibrosis, concentric hypertrophy, and diastolic dysfunction in rats,” *Hypertension*, vol. 56, no. 2, pp. 225–231, 2010.
- [70] M. Sun, M. Chen, F. Dawood et al., “Tumor necrosis factor- $\alpha$  mediates cardiac remodeling and ventricular dysfunction after pressure overload state,” *Circulation*, vol. 115, no. 11, pp. 1398–1407, 2007.
- [71] E. Vellaichamy, M. L. Khurana, J. Fink, and K. N. Pandey, “Involvement of the NF-kappa B/matrix metalloproteinase pathway in cardiac fibrosis of mice lacking guanylyl cyclase/natriuretic peptide receptor A,” *The Journal of Biological Chemistry*, vol. 280, no. 19, pp. 19230–19242, 2005.
- [72] W. S. Aronow, “Hypertension and left ventricular hypertrophy,” *Annals of Translational Medicine*, vol. 5, no. 15, p. 310, 2017.
- [73] V. J. Dzau, G. H. Gibbons, R. Morishita, and R. E. Pratt, “New perspectives in hypertension research,” *Potentials of vascular biology. Hypertension*, vol. 23, pp. 1132–1140, 1994.
- [74] N. F. Renna, N. de Las Heras, and R. M. Miatello, “Pathophysiology of vascular remodeling in hypertension,” *International Journal of Hypertension*, vol. 2013, Article ID 808353, 7 pages, 2013.
- [75] Y. Zhuge, J. Zhang, F. Qian et al., “Role of smooth muscle cells in cardiovascular disease,” *International Journal of Biological Sciences*, vol. 16, no. 14, pp. 2741–2751, 2020.
- [76] D. Fan, A. Takawale, J. Lee, and Z. Kassiri, “Cardiac fibroblasts, fibrosis and extracellular matrix remodeling in heart disease,” *Fibrogenesis & Tissue Repair*, vol. 5, no. 1, p. 15, 2012.
- [77] V. V. Petrov, R. H. Fagard, and P. J. Lijnen, “Stimulation of collagen production by transforming growth factor-beta1 during differentiation of cardiac fibroblasts to myofibroblasts,” *Hypertension*, vol. 39, no. 2, pp. 258–263, 2002.
- [78] J. M. Muñoz-Félix, N. Perretta-Tejedor, N. Eleno, J. M. López-Novoa, and C. Martínez-Salgado, “ALK1 heterozygosity

increases extracellular matrix protein expression, proliferation and migration in fibroblasts," *Biochimica et Biophysica Acta*, vol. 1843, no. 6, pp. 1111–1122, 2014.

- [79] Y. Chen, S. Li, Y. Guo et al., "Astaxanthin attenuates hypertensive vascular remodeling by protecting vascular smooth muscle cells from oxidative stress-induced mitochondrial dysfunction," *Oxidative Medicine and Cellular Longevity*, vol. 2020, Article ID 4629189, 19 pages, 2020.
- [80] X. Li, L. Li, W. Lei et al., "Traditional Chinese medicine as a therapeutic option for cardiac fibrosis: pharmacology and mechanisms," *Biomedicine & Pharmacotherapy*, vol. 142, article 111979, 2021.
- [81] L. Schirone, M. Forte, S. Palmerio et al., "A review of the molecular mechanisms underlying the development and progression of cardiac remodeling," *Oxidative Medicine and Cellular Longevity*, vol. 2017, Article ID 3920195, 16 pages, 2017.
- [82] N. Zhou, J. J. Lee, S. Stoll et al., "Inhibition of SRF/myocardin reduces aortic stiffness by targeting vascular smooth muscle cell stiffening in hypertension," *Cardiovascular Research*, vol. 113, no. 2, pp. 171–182, 2017.
- [83] J. Zhang, S. J. An, J. Q. Fu et al., "Mixed aqueous extract of salvia miltiorrhiza reduces blood pressure through inhibition of vascular remodelling and oxidative stress in spontaneously hypertensive rats," *Cellular Physiology and Biochemistry*, vol. 40, no. 1-2, pp. 347–360, 2016.
- [84] S. Fu, Y. Li, Y. Wu, Y. Yue, and D. Yang, "Icariside II improves myocardial fibrosis in spontaneously hypertensive rats by inhibiting collagen synthesis," *The Journal of Pharmacy and Pharmacology*, vol. 72, no. 2, pp. 227–235, 2020.

## Research Article

# Anti-Inflammatory Activity of *Ferula assafoetida* Oleo-Gum-Resin (Asafoetida) against TNF- $\alpha$ -Stimulated Human Umbilical Vein Endothelial Cells (HUVECs)

Leila Mobasheri,<sup>1,2</sup> Mohsen Khorashadizadeh,<sup>3,4</sup> Hossein Safarpour,<sup>3</sup> Maryam Mohammadi,<sup>5</sup> Gholamreza Anani Sarab <sup>2,3</sup> and Vahid Reza Askari <sup>6,7,8</sup>

<sup>1</sup>Student Research Committee, Birjand University of Medical Sciences, Birjand, Iran

<sup>2</sup>Department of Medical Immunology, Faculty of Medicine, Birjand University of Medical Sciences, Birjand, Iran

<sup>3</sup>Cellular and Molecular Research Center, Birjand University of Medical Sciences, Birjand, Iran

<sup>4</sup>Department of Medical Biotechnology, Faculty of Medicine, Birjand University of Medical Sciences, Birjand, Iran

<sup>5</sup>Department of Medical Immunology, Faculty of Medicine, Shahed University of Medical Sciences, Tehran, Iran

<sup>6</sup>Applied Biomedical Research Center, Mashhad University of Medical Sciences, Mashhad, Iran

<sup>7</sup>Department of Pharmaceutical Sciences in Persian Medicine, School of Persian and Complementary Medicine, Mashhad University of Medical Sciences, Mashhad, Iran

<sup>8</sup>International UNESCO Center for Health-Related Basic Sciences and Human Nutrition, Mashhad University of Medical Sciences, Mashhad, Iran

Correspondence should be addressed to Gholamreza Anani Sarab; [ghansa@yahoo.com](mailto:ghansa@yahoo.com) and Vahid Reza Askari; [askariv@mums.ac.ir](mailto:askariv@mums.ac.ir)

Received 19 May 2022; Revised 12 July 2022; Accepted 18 August 2022; Published 31 August 2022

Academic Editor: Azizah Ugusman

Copyright © 2022 Leila Mobasheri et al. This is an open access article distributed under the Creative Commons Attribution License, which permits unrestricted use, distribution, and reproduction in any medium, provided the original work is properly cited.

Inflammation is the body's biological reaction to endogenous and exogenous stimuli. Recent studies have demonstrated several anti-inflammatory properties of *Ferula* species. In this paper, we decided to study the anti-inflammatory effect of ethanolic extract of *Ferula assafoetida* oleo-gum-resin (asafoetida) against TNF- $\alpha$ -stimulated human umbilical vein endothelial cells (HUVECs). HUVECs were cultured in a flat-bottom plate and then treated with ethanolic extract of asafoetida (EEA, 0-500  $\mu$ g/ml) and TNF- $\alpha$  (0-100 ng/ml) for 24 h. We used the MTT test to assess cell survival. In addition, the LC-MS analysis was performed to determine the active substances. HUVECs were pretreated with EEA and then induced by TNF- $\alpha$ . Intracellular reactive oxygen species (ROS) and adhesion of peripheral blood mononuclear cells (PBMCs) to HUVECs were evaluated with DCFH-DA and CFSE fluorescent probes, respectively. Gene expression of intercellular cell adhesion molecule-1 (ICAM-1), vascular cell adhesion molecule 1 (VCAM-1), and E-selectin and surface expression of ICAM-1 protein were measured using real-time PCR and flow cytometry methods, respectively. While TNF- $\alpha$  significantly increased intracellular ROS formation and PBMC adhesion to TNF- $\alpha$ -induced HUVECs, the pretreatment of HUVECs with EEA (125 and 250  $\mu$ g/ml) significantly reduced the parameters. In addition, EEA pretreatment decreased TNF- $\alpha$ -induced mRNA expression of VCAM-1 and surface protein expression of ICAM-1 in the target cells. Taken together, the results indicated that EEA prevented ROS generation, triggered by TNF- $\alpha$ , and inhibited the expression of VCAM-1 and ICAM-1, leading to reduced PBMC adhesion. These findings suggest that EEA can probably have anti-inflammatory properties.

## 1. Introduction

Inflammation is the body's protective response against interior or foreign stimulators, which causes pain and tissue damage. When inflammation becomes chronic, it can lead to various conditions, including asthma, allergic reactions, cancer, cardiovascular diseases, thrombosis, and autoimmune disorders [1, 2].

Endothelial cells (E.C.s) are the essential modulators in vascular inflammation, and their dysfunction is associated with the induction and expansion of many chronic inflammatory problems [3]. Activation of E.C.s at the inflammatory site leads to the upregulation of endothelial cell adhesion molecules (ECAMs), which include vascular cell adhesion molecule 1 (VCAM-1), intercellular adhesion molecule 1 (ICAM-1), and E-selectin (CD62E) [4, 5]. Also, leukocyte migration following ECAM expression causes tissue and organ dysfunction by secreting inflammatory cytokines and chemokines, including tumour necrosis factor- $\alpha$  (TNF- $\alpha$ ) and interleukin- (IL-) 1 $\beta$ , 6, and 8 [6, 7]. Furthermore, there is considerable evidence that TNF- $\alpha$  can trigger oxidative stress via increasing reactive oxygen species (ROS). ROS is reduced metabolites of oxygen that keep their oxidising abilities. Studies show that the expression quantity of VCAM-1 and ICAM-1 are directly connected to intracellular ROS synthesis [5, 8–10]. Therefore, suppression of ROS generation and ECAM expression can be a helpful medicinal approach for controlling vasculitis [11].

Corticosteroids and nonsteroidal anti-inflammatory drugs (NSAIDs) are common treatments that prevent chronic inflammation by reducing the production and secretion of TNF- $\alpha$ , IL-1 $\beta$ , ROS, and nitric oxide (NO) from the inflammatory cells [12]. However, patients may be affected by adverse effects of corticosteroids and NSAIDs, such as stomach pain and ulcers, kidney failure, Cushing's syndrome, high blood pressure, diabetes, fragile bones, and vulnerability to infections [13, 14]. Therefore, new compounds with minimal adverse effects tend to be detected and launched.

Herbal medicines and extracts have been commonly used for many years due to their possessing active compounds that might provide a valuable platform for drug discovery [2, 15]. For example, *assafoetida* is an oleo-gum-resin derived by cutting the stems and roots of the different *Ferula* species, such as *F. assafoetida* L. (as the main source), *F. foetida*, *F. rubricaulis*, *F. rigidula*, *F. alliacea*, *F. narthex*, *F. latisecta*, and *F. lutensis*, scattered in southern and eastern Iran [16, 17].

Asafoetida is renowned due to its pharmaceutical effects in Iranian folk medicine. It has traditionally been used as an antispasmodic, antihelmintic, anticancer, carminative, antiasthmatic, antiepileptic, and analgesic agent worldwide [2, 18]. In addition, *assafoetida* has long been used as a treatment for inflammation, and several anti-inflammatory properties have been discovered. Bagheri et al. demonstrated the antinociceptive and anti-inflammatory activities of *Ferula assafoetida* in chronic and acute pain and paw oedema in mice [19, 20]. In a double-blind study, *assafoetida* improved inflammation in irritable colon disease [21]. Another study showed the effects of asafoetida for reducing and healing inflammatory markers and cartilage impairment triggered by rheumatoid arthritis in rats [22]. This evidence provides dependable rea-

sons for assessing *assafoetida*'s effects on reducing inflammation and identifying the possible mechanisms involved in this action. Our main objective of the research is to explore the inhibitory efficacy of ethanolic extract of *Ferula assafoetida* oleo-gum-resin or asafoetida (EEA) on TNF- $\alpha$ -stimulated human umbilical vein endothelial cells (HUVECs).

## 2. Materials and Methods

**2.1. Materials.** 5-Carboxy-fluorescein diacetate N-succinimidyl ester (CFSE) was purchased from Santa Cruz (sc-214315, Santa Cruz, CA, USA). 2,7-Dichlorofluorescein diacetate (DCFH-DA) and (4,5-dimethyl-2-thiazolyl)-2,5-diphenyltetrazolium bromide (MTT) were purchased from Sigma (D6883 and M2128, respectively, Sigma-Aldrich, St. Louis, MO, USA). RiboEx solution (301-001, GeneAll), cDNA Synthesis Kit (K1621, Thermo Fisher Scientific, CA, USA), and Ficoll with a density of 1.078 g/ml were bought from G.E. Healthcare (17-5442-02, G.E. Healthcare, Chicago, IL, USA). PE-conjugated ICAM-1 and PE-isotype control were from eBiosciences (12-0549-42 and 12-4714-42, respectively, eBioscience, Thermo Fisher Scientific, CA, USA). Trypsin, penicillin, and streptomycin (P/S), foetal bovine serum (FBS), and DMEM high-glucose medium were purchased all from GIBCO (Grand Island, NY, USA). Dimethyl sulphoxide (DMSO) was purchased from Amresco (Solon, OH, USA).

**2.2. Preparation of EEA by Maceration.** *Ferula assafoetida* oleo-gum-resin was gathered from the Tabas Region (Southern Khorasan, Iran). The voucher specimen was confirmed in the Herbarium of the School of Pharmacy, University of Medical Sciences, Mashhad, Iran (voucher number: 13257). Thirty-five grams of dried *Ferula assafoetida* oleo-gum-resin was macerated in 70% ethanol and was kept in a shaker incubator (28°C, 145 rpm) for two days. Afterwards, the solution was filtrated through Whatman filter no. 4, then it was centrifuged, and the supernatant was obtained. The remaining solution was dried at 37°C, weighed, and kept at -80°C throughout the study.

**2.3. Cell Culture and Condition.** HUVECs were gifted by Dr. M.R. Ardeshty-Lajimi (Shahid Beheshti University of Medical Sciences, Tehran, Iran). DMEM high-glucose medium enriched by 10% v/v FBS and 1% v/v penicillin-streptomycin was provided for cells to achieve the confluence at 37°C in a wet atmosphere under 5% v/v CO<sub>2</sub>.

**2.4. Cell Viability Assessment.** Cell viability was measured by the MTT test. HUVECs (1 × 10<sup>4</sup> cells/well in 96-well plates) were saved in supplemented media for 24 h. One day later, culture media were exchanged with 200  $\mu$ l serum-free culture medium consisting of different concentrations of EEA (0, 31, 62, 125, 250, and 500  $\mu$ g/ml) and TNF- $\alpha$  (TNF- $\alpha$ ) that was cloned as previously described [23] in various concentrations (0, 0.1, 1, 10, and 100 ng/ml) for 24 h. The next day, 20  $\mu$ l of MTT (5 mg/ml) was applied to each well and was stored at 37°C for another 4 h. Finally, the wells were emptied and filled with 100  $\mu$ l of DMSO to dissolve formazan crystals. The absorbance of the solubilised formazan was read out at 570 and 630 nm using Epoch Microplate

TABLE 1: Primer sequences.

Gene	Forward primer (5' to 3')	Reverse primer (5' to 3')	PCR product size (bp)
E-selectin	TCAAGTGTGAGCAAATTGTGAAC	ATTCTCCAGAGGACATACACTGC	174
ICAM-1	AGCTTCGTGTCCTGTATGGC	CTGGCACATTGGAGTCTGCT	96
VCAM-1	ATGTCAATGTTGCCCCAGCA	ACAGGATTTTCGGAGCAGGA	119
$\beta$ -actin	TGGGCATCCACGAAACTAC	GATCTCCTTCTGCATCCTGT	137

PCR: polymerase chain reaction; ICAM-1: intercellular adhesion molecular 1; VCAM-1: vascular cell adhesion protein 1.

Spectrophotometer (Biotek Instrument, USA). The incubated cells in the control medium were regarded as 100% viable.

**2.5. PBMC Adhesion Assay.** In order to check the potency of the TNF- $\alpha$  in the induction of ECAMs on the cell surface of HUVECs, we performed a cell adhesion assay using peripheral blood mononuclear cells (PBMC). HUVECs were seeded in a 96-well plate ( $1 \times 10^4$  cells/well) and were incubated until reaching confluence. The cells were then stimulated with 10, 20, and 40 ng/ml of TNF- $\alpha$  for 6, 12, and 18 h, respectively. The PBMCs were isolated from peripheral blood as described elsewhere [24] and were labelled with CFSE (1 mM) for 15 minutes at 37°C. The PBMCs were centrifuged at 1200 *g* for 5 min and washed twice with PBS (1 $\times$ ) to remove free CFSE. The HUVECs were washed with PBS (1 $\times$ ), and then 50  $\mu$ l of labelled PBMC suspension ( $2 \times 10^6$  cells/ml) was added to each well and incubated for another 1 h. The plate was washed with PBS (1 $\times$ ) to remove unattached PBMCs. Then, each well was filled with 100  $\mu$ l PBS and was examined with an inverted fluorescent microscope (Olympus IX70, Japan), while photos were taken using a digital camera (Olympus DP-12, Japan). After that, the cells were lysed with 0.25% Triton X-100, and the fluorescence intensity of the lysed cells was measured at the 485 nm excitation and 535 nm emissions using a fluorescence microplate reader (Cytation 3, BioTeck, USA).

The inhibitory effect of EEA on TNF- $\alpha$ -induced PBMC adhesion was evaluated on HUVECs as pretreatment with EEA at two concentrations (125 and 250  $\mu$ g/ml) in starved media containing 1% *v/v* FBS for 6 h, followed by TNF- $\alpha$  stimulation at the optimal time.

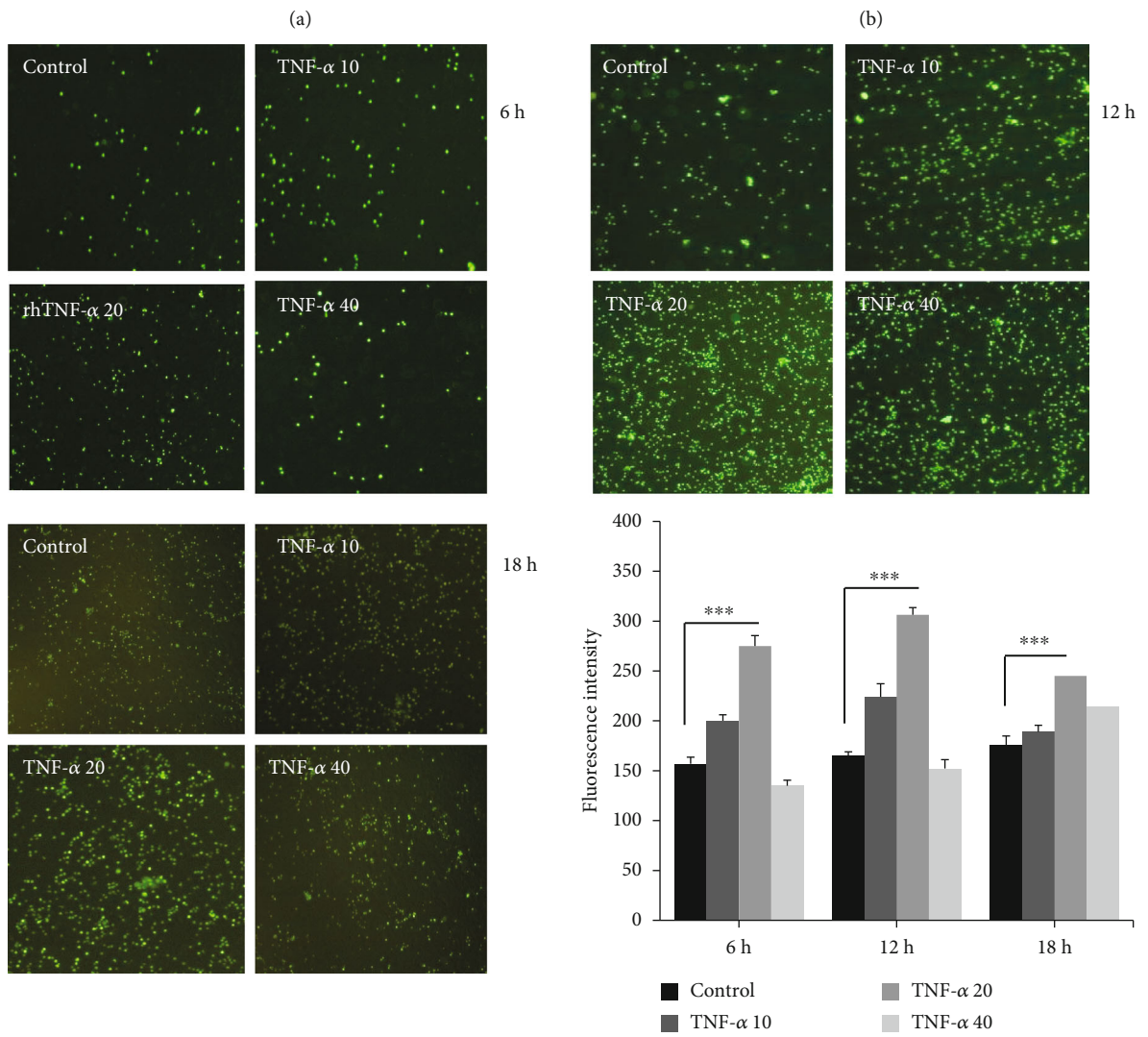
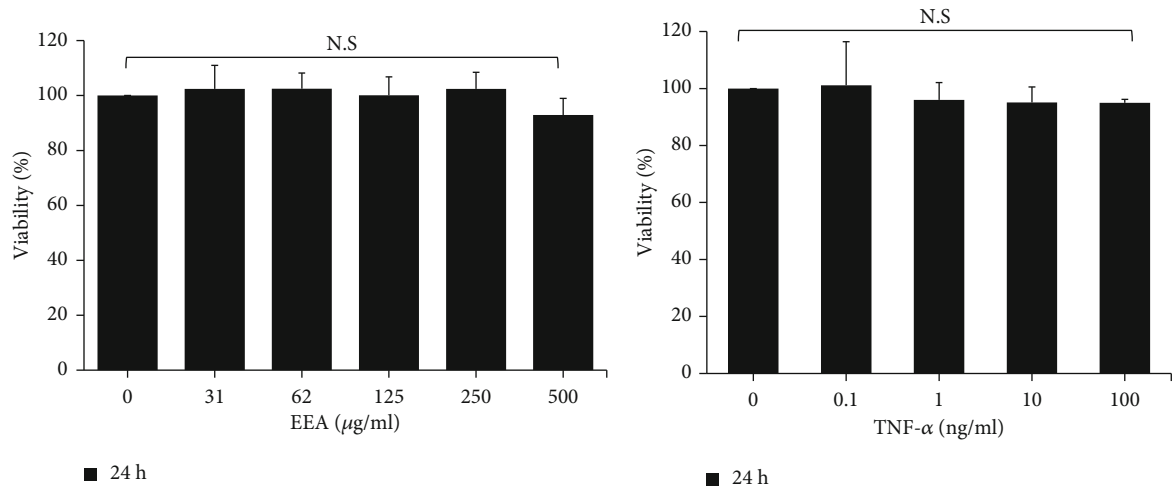
**2.6. Intracellular ROS Assay.** The effects of TNF- $\alpha$  on intracellular ROS production in HUVECs were evaluated using the DCFH-DA protocol. First, the HUVECs ( $2 \times 10^5$  cells/well) were cultured in a 12-well plate until confluency was reached. Then, the cells were treated with 10, 20, and 40 ng/ml of TNF- $\alpha$  for 12 h. Next, the media were discarded, and the cells were washed twice with PBS (1 $\times$ ) and incubated with DCFH-DA (10  $\mu$ M) for 20 min in the incubator. Then, the wells were washed to remove unused DCFH-DA, and then they were filled with PBS (100  $\mu$ L/well). Next, the cells were analyzed using an inverted fluorescent microscope, and photos were taken with a digital camera. Finally, the cells were lysed with 0.25% Triton X-100, and the fluorescence intensity of the lysed cells was determined at 485 nm excitation and 535 nm emissions via a fluorescence microplate reader.

The inhibitory impact of EEA on TNF- $\alpha$ -induced ROS production was evaluated through the pretreatment of HUVECs with EEA at two concentrations (125 and 250  $\mu$ g/ml) in starved media for 6 h, followed by TNF- $\alpha$  stimulation at optimal time and concentration.

**2.7. Gene Expression Assessment Using Real-Time PCR.** After the treatment of HUVECs under various conditions, total RNA was extracted by the RiboEx solution. The samples were harvested with 1 ml of solution specific for RNA extraction as instructed by the manufacturer. First, total RNA concentration and its purity were quantified. Then, complementary DNA was prepared with the RevertAid First-Strand cDNA Synthesis Kit following the guidance of the producer. For real-time PCR, amplification of the E-selectin, ICAM-1, and VCAM-1 was performed on the ABI Step-One Real-Time PCR system using SYBR Green qPCR Master Mix (A325402, Ampliqon, Denmark) according to the instructions of the manufacturer. The amplification procedures included an initial denaturation for 15 min at 95°C, denaturation for 15 s at 95°C, primer annealing for 15 s at 60°C, and extension for 30 s at 72°C, with a melting curve temperature range from 60°C to 95°C. The number of PCR cycles was set at 40 for all the reactions. Primer sequences have shown in Table 1.

**2.8. Detection of ICAM-1 through Flow Cytometry.** HUVECs were first treated with or without EEA at the required concentrations for 6 h, followed by TNF- $\alpha$  stimulation (20 ng/ml) for 12 h. After treatments, HUVECs were harvested using PBS-EDTA (10 mM), washed with PBS, and resuspended in 100  $\mu$ l binding buffer. Samples were then subjected to 5  $\mu$ l pretitrated PE-conjugated ICAM-1 antibody. The related PE-labeled isotype was used as a control. The cells were washed after 30 min incubation at 4°C in the dark, and surface expressions of ICAM-1 were detected by flow cytometry (Sysmex-partec, Cube 6).

**2.9. Liquid Chromatography-Mass Spectrometry (LC-MS) Analysis of *Ferula assafoetida* Extract.** The liquid chromatography-mass spectrometry (LC-MS) analysis was performed in an Agilent 1200 series liquid chromatography coupled with Agilent 6410 triple quadrupole mass spectrometer [25, 26]. Liquid chromatography separation was performed on an Agilent Eclipse plus C18 ( $2.1 \times 100$  mm  $\times$  3.5  $\mu$ m) column. The flow rate was set at 0.4 ml/min, and the mobile phase consisted of (A) water+0.1% formic acid and (B) methanol+0.1% formic acid. The gradient programs were as follows: 0.0-1.0 min 10% B, 1.0-40 min from 10% to 100% (B), 40.0-42.0 min 100% (B), and 42.0-50 min from 100% to 10%



(c)

FIGURE 1: Continued.



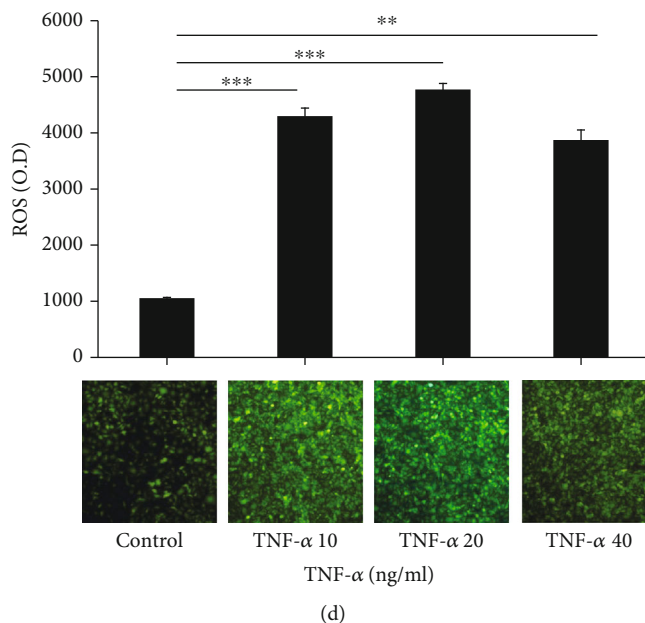


FIGURE 1: Cell viability, cell adhesion, and intracellular ROS production assay. (a) Effect of EEA on the viability of HUVECs that were treated at various EEA concentrations (0, 31, 62, 125, 250, and 500  $\mu\text{g/ml}$ ) for 1 day. MTT test determined HUVECs' viability. The cell viability did not show significant differences up to 500  $\mu\text{g/ml}$ . (b) HUVECs were treated at various TNF- $\alpha$  amounts (0, 0.1, 1, 10, and 100 ng/ml) for 24 h followed by an MTT reagent to evaluate cell viability. The difference was not statistically significant in cell viability at different concentrations. (c) HUVECs were treated under different TNF- $\alpha$  levels (10, 20, and 40 ng/ml) for 6, 12, and 18 h, and a PBMC adhesion assay was carried out. (d) Cells were treated with distinct concentrations of TNF- $\alpha$  (10, 20, and 40 ng/ml) for half a day, and intracellular ROS production was assessed. Stimulation with TNF- $\alpha$  at 20 ng/ml significantly increased the PBMC adhesion and ROS production after 12 h. Every value is entered as the mean  $\pm$  S.D. from at least separate triple tests. \*\* $p < 0.001$  and \*\*\* $p < 0.0001$  versus control. N.S.: not significant.

(B). The mass spectra were acquired from 100 to 1000 within 50 minutes of scan time. The positive electrospray ionisation (ESI) mode was applied for the mass spectrometer. Mass feature extraction of the acquired LC-MS data and maximum detection of peaks was done using the *MZmine* analysis software package, version 2.3.

**2.10. Statistical Analysis.** All values have been evaluated with version 16.0 SPSS software (SPSS Inc., Chicago, IL, USA). The reports were provided as the mean  $\pm$  S.D. for each condition of at least three independent experiments and checked for using the parametric or nonparametric *post hoc* analysis. In addition, the raw data of flow cytometry and real-time PCR were analyzed with the FSC Express 5 and Rest 2009 software, respectively. Thus, one-way variance analysis (ANOVA) and the Tukey test were carried out to investigate group variations. Statistically, significant differences have been taken into account at  $p < 0.05$ , 0.01, and 0.001.

### 3. Results

**3.1. Determining Cell Viability, PBMC Adhesion, and Intracellular ROS Production of HUVECs.** First of all, the cytotoxicity impact of EEA on HUVECs was tested using the MTT assay after 24 h treatment. The EEA had no significant effects on cells' viability up to 500  $\mu\text{g/ml}$  (Figure 1(a)). Then, we evaluated the cytotoxicity of our produced TNF- $\alpha$  on HUVECs. As shown in Figure 1(b), there was no change in cell viability

of HUVECs at utilised concentration ranges from 0.1-100 ng/ml, suggesting that TNF- $\alpha$  was not directly toxic to the HUVECs.

After that, we decided to evaluate the efficacy of TNF- $\alpha$  by analyzing its ability to stimulate PBMC adhesion and intracellular ROS production in HUVECs. As illustrated in Figure 1(c), the adhesion of PBMCs to HUVECs was significantly increased by 20 ng/ml TNF- $\alpha$  in all conditions compared to their controls (\*\* $p < 0.0001$ ), with the most considerable rise at 12 h. Moreover, the treatment of HUVECs with indicated TNF- $\alpha$  concentrations for 12 hours showed a significant ROS production increase, which the 20 ng/ml TNF- $\alpha$  was better than other concentrations of TNF- $\alpha$  (Figure 1(d)).

**3.2. EEA Inhibits TNF- $\alpha$ -Induced Intracellular ROS Production and Adhesion of PBMCs-HUVECs.** We investigated whether EEA can attenuate TNF- $\alpha$ -induced ROS production. HUVECs were pretreated with EEA at defined concentrations for 6 h and then stimulated with TNF- $\alpha$  (20 ng/ml) for another 12 h. As shown in Figure 2(a), EEA reduced considerably TNF- $\alpha$ -mediated intracellular ROS production in HUVECs at both concentrations of 125 (\* $p < 0.01$ ) and 250  $\mu\text{g/ml}$  (\*\* $p < 0.0001$ ). Since the increase of intracellular ROS is an effective inducer of cell adhesion molecules, we investigated the impacts of EEA on PBMC adhesion to TNF- $\alpha$ -activated HUVECs. The findings exhibited that EEA pretreatment with 250  $\mu\text{g/ml}$  significantly diminished PBMCs-HUVECs adhesion (\*\* $p < 0.01$ , Figure 2(b)).

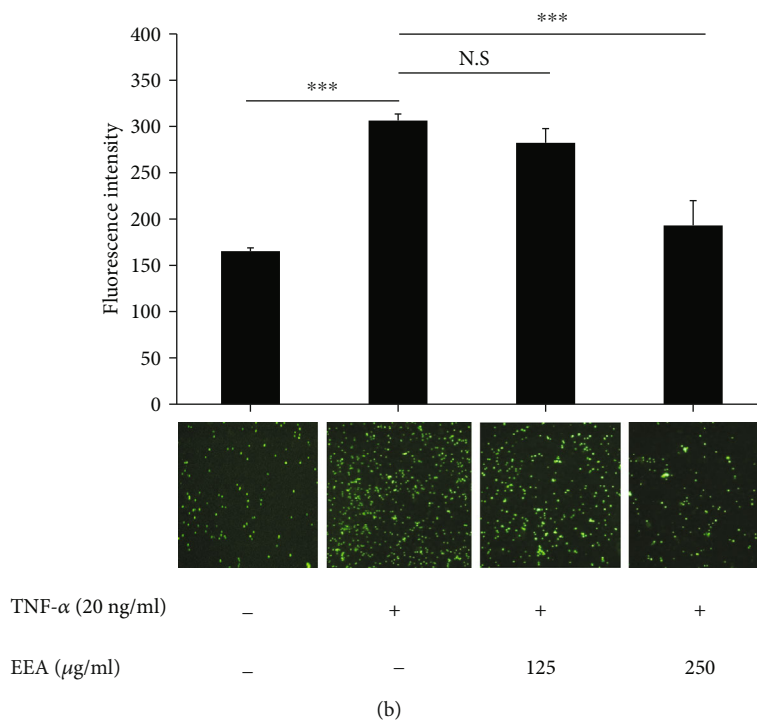
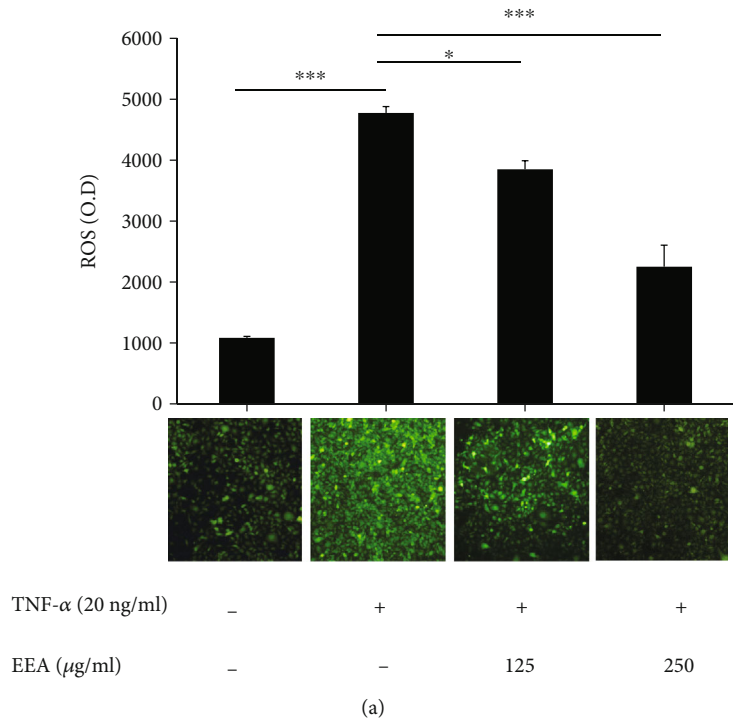
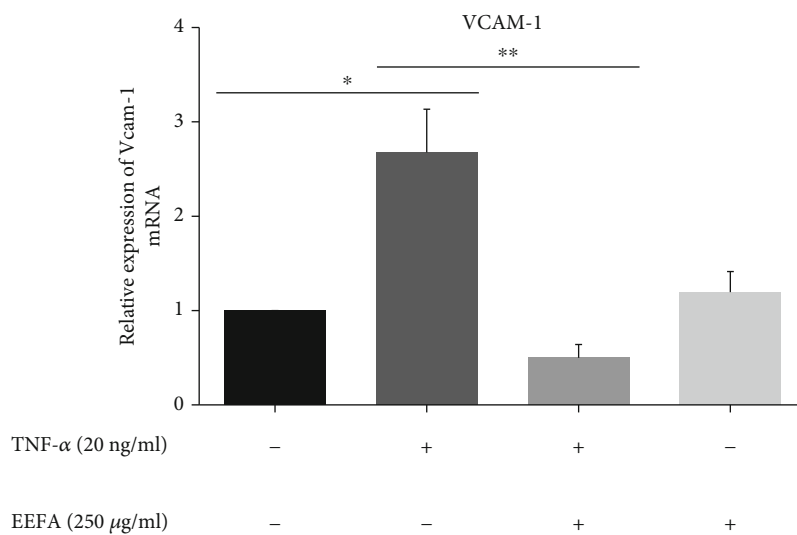


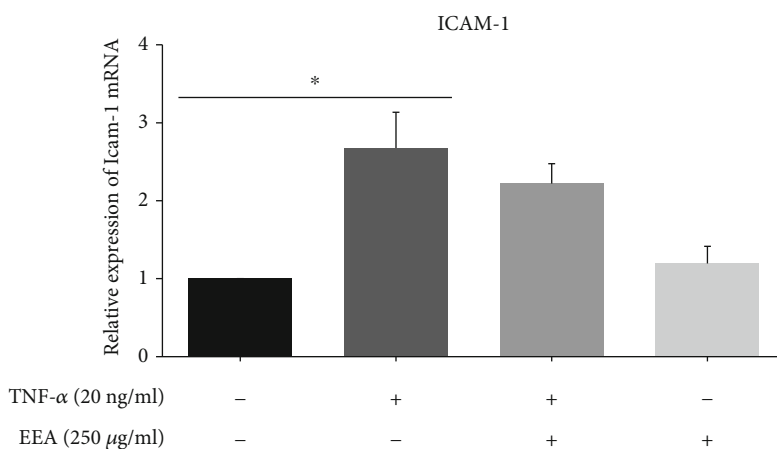
FIGURE 2: EEA reduces TNF- $\alpha$ -stimulated ROS production and PBMC adhesion to HUVECs. Target cells were incubated with two concentrations of EEA (125 and 250  $\mu\text{g/ml}$ ) for 6 h, followed by treatment along with TNF- $\alpha$  (20 ng/ml) for 12 h. (a) DCFH-DA probes assessed ROS production. Fluorescent microscopy showed decreased ROS production in *Assafoetida* pretreatment. (b) The adhesive function of PBMCs for HUVECs was assessed. Fluorescent microscopy showed decreased adhesion in EEA pretreatment. The data reflects the mean  $\pm$  SD ( $N = 3$ ). \* $p < 0.01$  and \*\*\* $p < 0.0001$  opposed to control and TNF- $\alpha$ -treated groups. N. S: not significant.

**3.3. EEA Inhibits TNF- $\alpha$ -Induced ECAM mRNA Expression in HUVECs.** Real-time PCR explorations have been done to examine the VCAM-1, ICAM-1, and E-selectin mRNA expression in activated HUVECs. Pretreatment of HUVECs

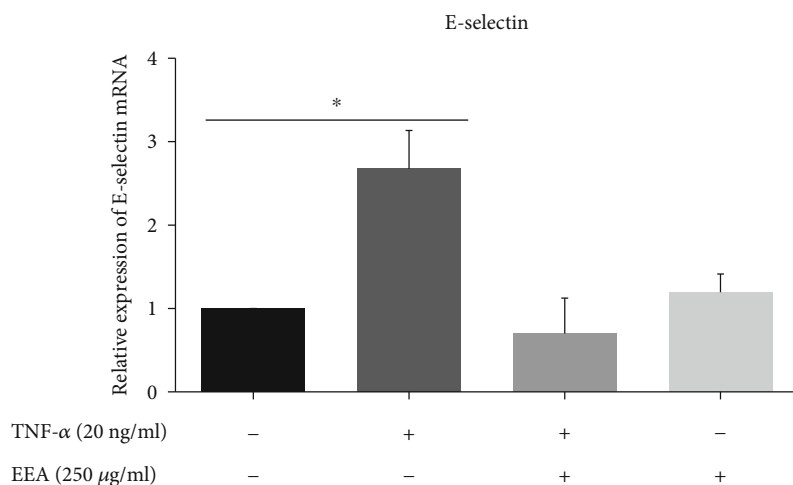
with EEA (250  $\mu\text{g/ml}$ ) for 6 h decreased VCAM-1, ICAM-1, and E-selectin gene expression parallel to the TNF- $\alpha$  stimulated group. But this decrease was just significant in VCAM-1 expression (\*\* $p < 0.001$ ) (Figure 3).



(a)



(b)



(c)

FIGURE 3: Impact of EEA on ECAM expression in HUVECs activated by TNF- $\alpha$  through real-time PCR. (a, b, c) TNF- $\alpha$  (20 ng/ml) across 12 h raises VCAM-1, ICAM-1, and E-selectin expression. TNF- $\alpha$ -induced expression of VCAM-1, ICAM-1, and E-selectin decreased with 250  $\mu$ g/ml of EEA for 6 h, but this reduction was not statistically meaningful except in the expression of VCAM-1. Numbers are presented as a normalised VCAM-1, ICAM-1, and E-selectin mRNA to  $\beta$ -actin mRNA, schemed in bar diagrams, and have been shown as mean  $\pm$  S.D. \* $p$  < 0.01 concerning the control group and \*\* $p$  < 0.001 relatives to the TNF- $\alpha$ -treated group that were calculated by *one-way ANOVA*.

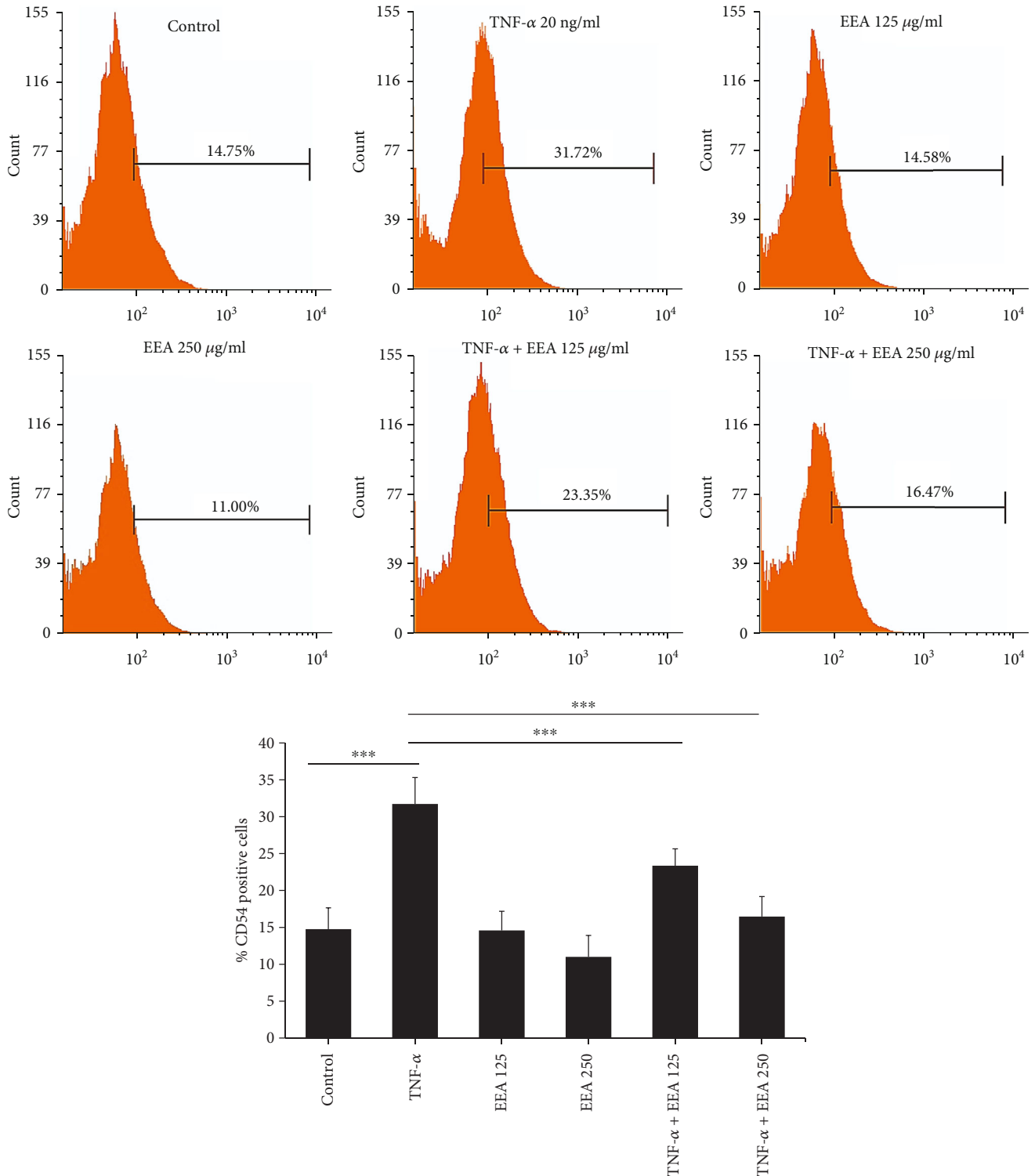


FIGURE 4: The outcome of EEA upon on surface expression of ICAM-1 in TNF- $\alpha$ -stimulated HUVECs by flow cytometry. At first, HUVECs were treated with or without *Assafoetida* (125 and 250  $\mu$ g/ml) for 6 h, and after that, activated with TNF- $\alpha$  (20 ng/ml) for 12 h. TNF- $\alpha$  increases ICAM-1 expression, but *Assafoetida* inhibits its expression explicitly. The parameters are reported as the mean  $\pm$  S.D. for at least three separate experiments. \*\*\* $p < 0.0001$  compared with the control and TNF- $\alpha$ -treated groups.

3.4. EEA Suppresses TNF- $\alpha$ -Induced ICAM-1 Surface Protein Expression on HUVECs. Since ICAM-1 is a crucial prerequisite for PBMCs-HUVECs adherence, we studied the effects of EEA on its protein surface distribution by flow cytometry.

The findings represented that ICAM-1 protein expression (Figure 4) was deficient in unstimulated cells, and TNF- $\alpha$  (20 ng/ml) enhanced its surface aggregation. In contrast, EEA (125 and 250  $\mu$ g/ml) significantly reduced the expression

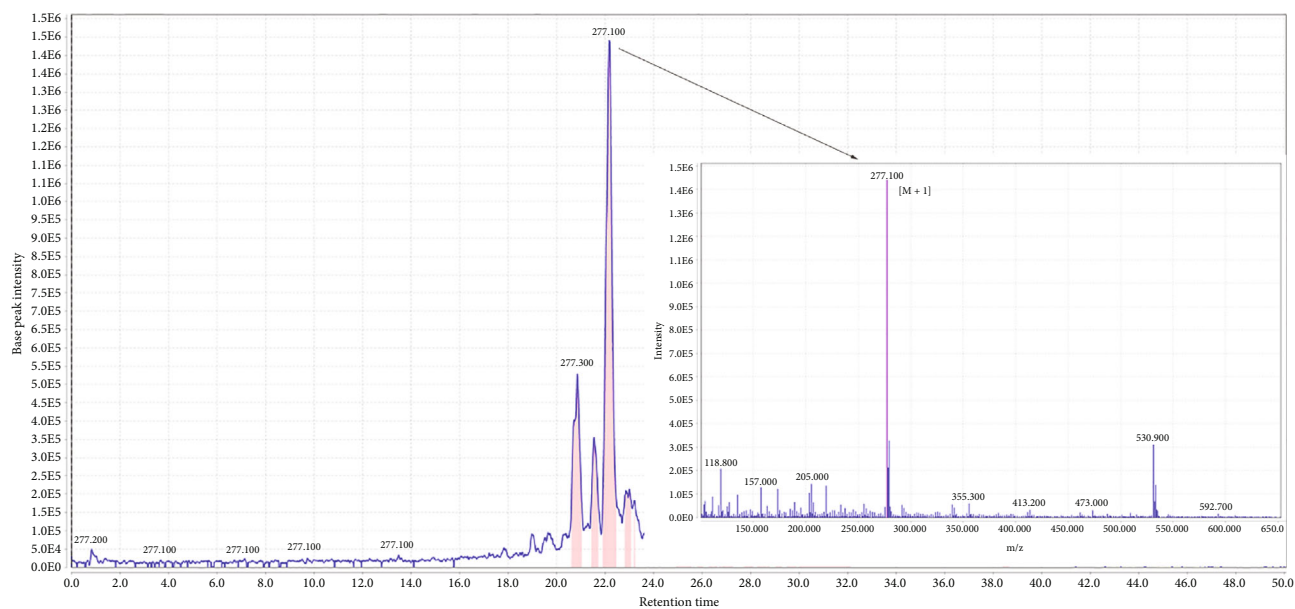
TABLE 2: Peak assignment of metabolites in the hydroethanol extract of *Ferula assafoetida* using LC-MS in the positive mode.

Peak no.	Compound identification	$t_R$ (min)	$[M + 1]$ (m/z)	Ref.
1	Assafoetidin	35.9	383.3	[16]
2	Umbelliprenin	39.4	367.4	[16]
3	Assafoetidinol A	33.0	399.3	[16]
4	Methyl galbanate	40.5	413.3	[16]
5	2-Butyl 1-propenyl disulfide	34.7	163.1	[16]
6	2-Butyl 3-(methylthio)-2-propenyl disulfide	24.3	209.0	[16]
7	1-Methylthio-1-propene	31.1	103.8	[16]
8	Methyl-1-propenyl disulfide	34.6	120.9	[16]
9	S-Methylpropanethioate	33.3	104.9	[16]
10	Dimethyl trisulfide	33.6	126.9	[16]
11	2-Butyl methyl disulfide	33.9	137.0	[16]
12	Dipropyl disulfide	29.3	151.0	[16]
13	2-Butyl vinyl disulfide	34.7	149.1	[16]
14	Methyl 1-(methylthio)propyl disulfide	29.3	169.1	[16]
15	1-(Methylthio)propyl 1-propenyl disulfide	20.8	194.9	[16]
16	Asadisulfide	22.2	277.1	[16]
17	Di-2-butyl trisulfide	33.1	211.1	[16]
18	Di-2-butyl tetrasulfide	34.4	243.2	[16]
19	Foetisulfide A	23.9	225.1	[16]
20	Foetisulfide C	19.1	241.1	[16]
21	Ligupersin A	36.5	397.3	[16]
22	8-Acetoxy-5-hydroxyumbelliprenin	34.4	441.2	[16]
23	Galbanic acid	33.0	399.3	[42]
24	7-Oxocallitric acid	40.1	329.4	[42]
25	Picealactone C	39.9	327.4	[42]
26	15-Hydroxy-6-en-dehydroabiatic acid	39.4	315.4	[42]
27	Taraxacin	34.4	243.2	[42]
28	Fetidone A	23.5	233.1	[42]
29	Fetidone B	23.8	235.1	[42]
30	Falcarinolone	31.0	259.2	[42]
31	Luteolin 7-b-D-glucopyranoside	40.8	449.3	[42]
32	Epi-samarcandin	35.7	401.2	[42]
33	Epi-conferdione	39.1	395.3	[42]

of ICAM-1 protein in TNF- $\alpha$ -stimulation HUVECs (\*\* $p < 0.0001$ ) for both cases, Figure 4).

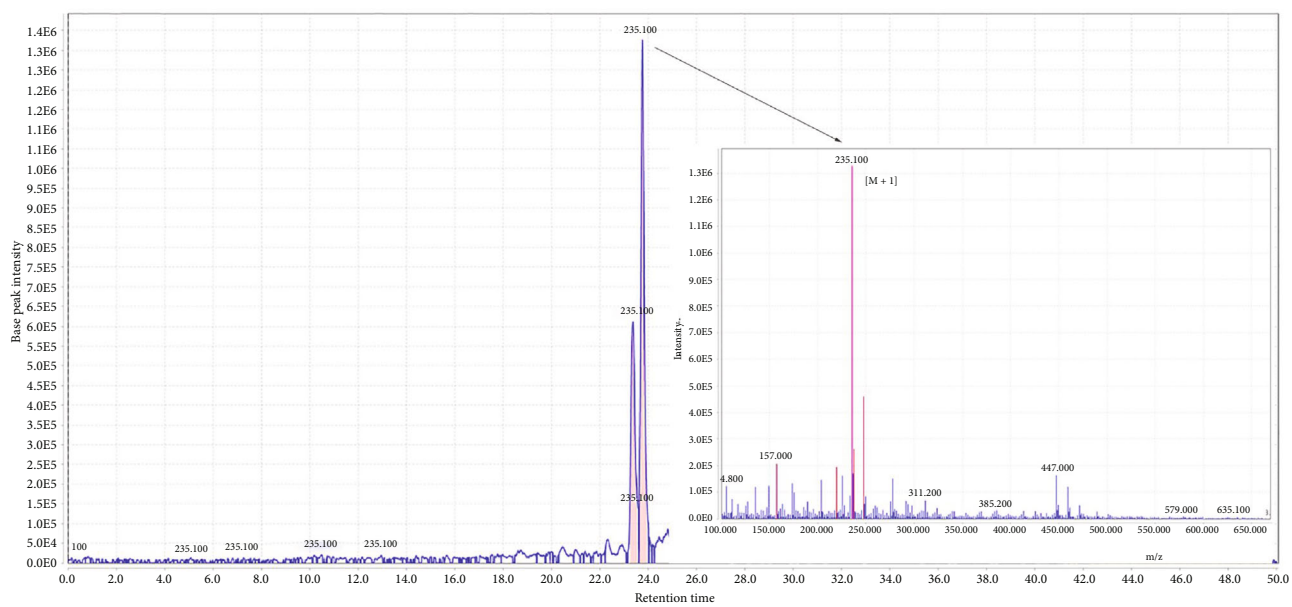
**3.5. LC-MS Analysis of *Ferula assafoetida* Extract.** Experimentally, 33 compounds were characterised in the hydroethanol extract of *Ferula assafoetida*, which is a rich source of xanthenes, flavonoid-glycosides, isoflavones, and other derivatives. The identified compounds are represented in Table 2. The total ion chromatogram of *Ferula assafoetida* extract and the examples of extracted ion chromatograms from the total ion chromatogram and its related mass are shown in Figure 5. The MS spectral data were compared with the reported compounds in some previous literature. Most of the compounds detected in the *F. assafoetida* extracts have been

previously reported in *Ferula* species. In addition, some coumarins (ligupersin A), sesquiterpenes (taraxacin, fetidone A, and fetidone B), and sesquiterpene coumarins (assafoetidin, umbelliprenin, assafoetidinol A, methyl galbanate, 8-acetoxy-5-hydroxyumbelliprenin, galbanic acid, epi-samarcandin, and epi-conferdione) were detected in *Ferula assafoetida* extract. Some sulfur-containing compounds (2-butyl 1-propenyl disulphide, 2-butyl 3-(methylthio)-2-propenyl disulphide, 1-methylthio-1-propene, methyl-1-propenyl disulphide, S-methylpropanethioate, dimethyl trisulfide, 2-butyl methyl disulphide, dipropyl disulphide, 2-butyl vinyl disulphide, methyl 1-(methylthio) propyl disulphide, 1-(methylthio) propyl 1-propenyl disulphide, asadisulfide, di-2-butyl trisulfide, di-2-butyl tetrasulfide, foetisulfide A, and



(a)

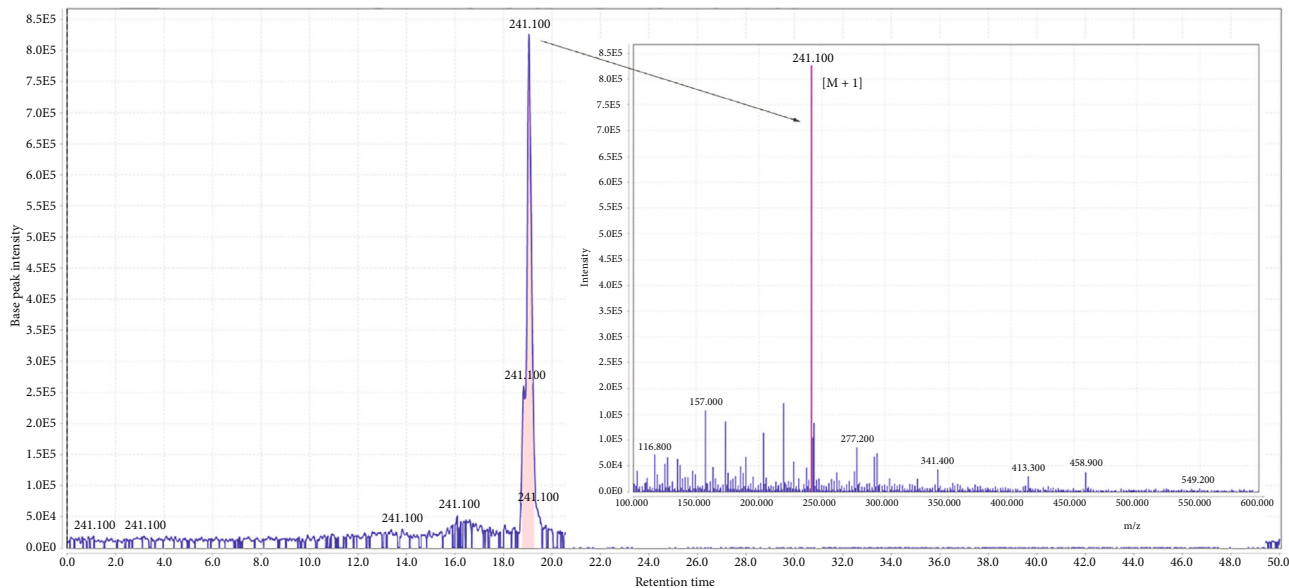
XIC (base peak), m/z: 235.100 - 235.200



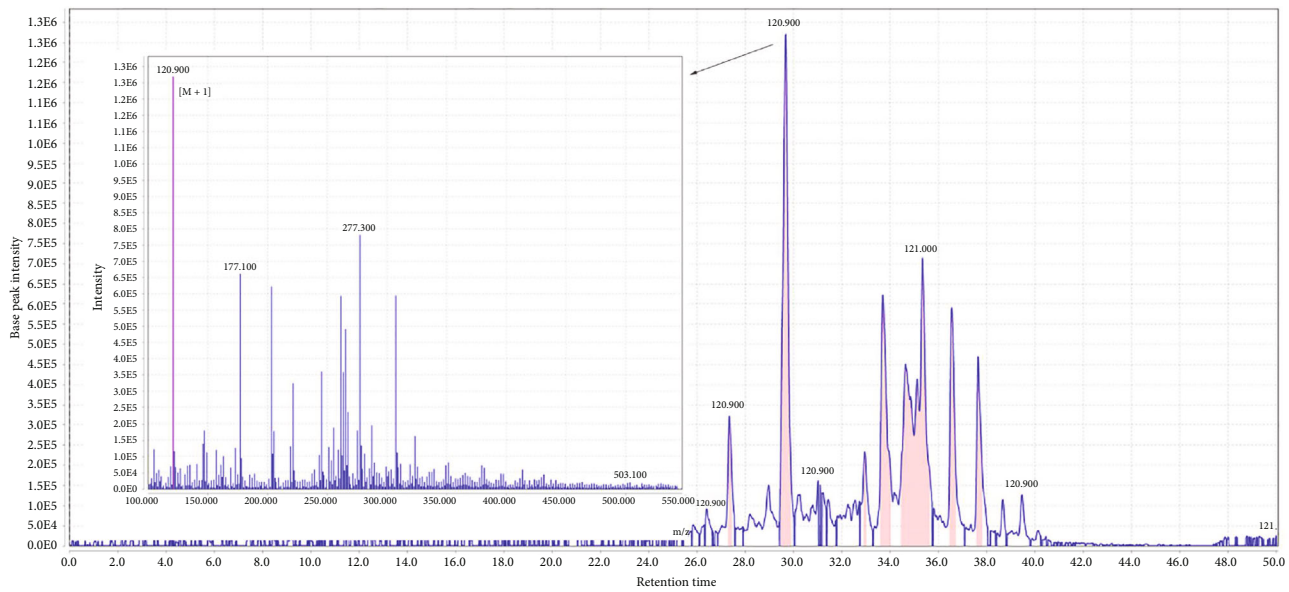
■ Chromatogram 235.100 m/z  
— 40008151306-1.mzdata (1).xml

(b)

FIGURE 5: Continued.



(c)



(d)

FIGURE 5: Continued.

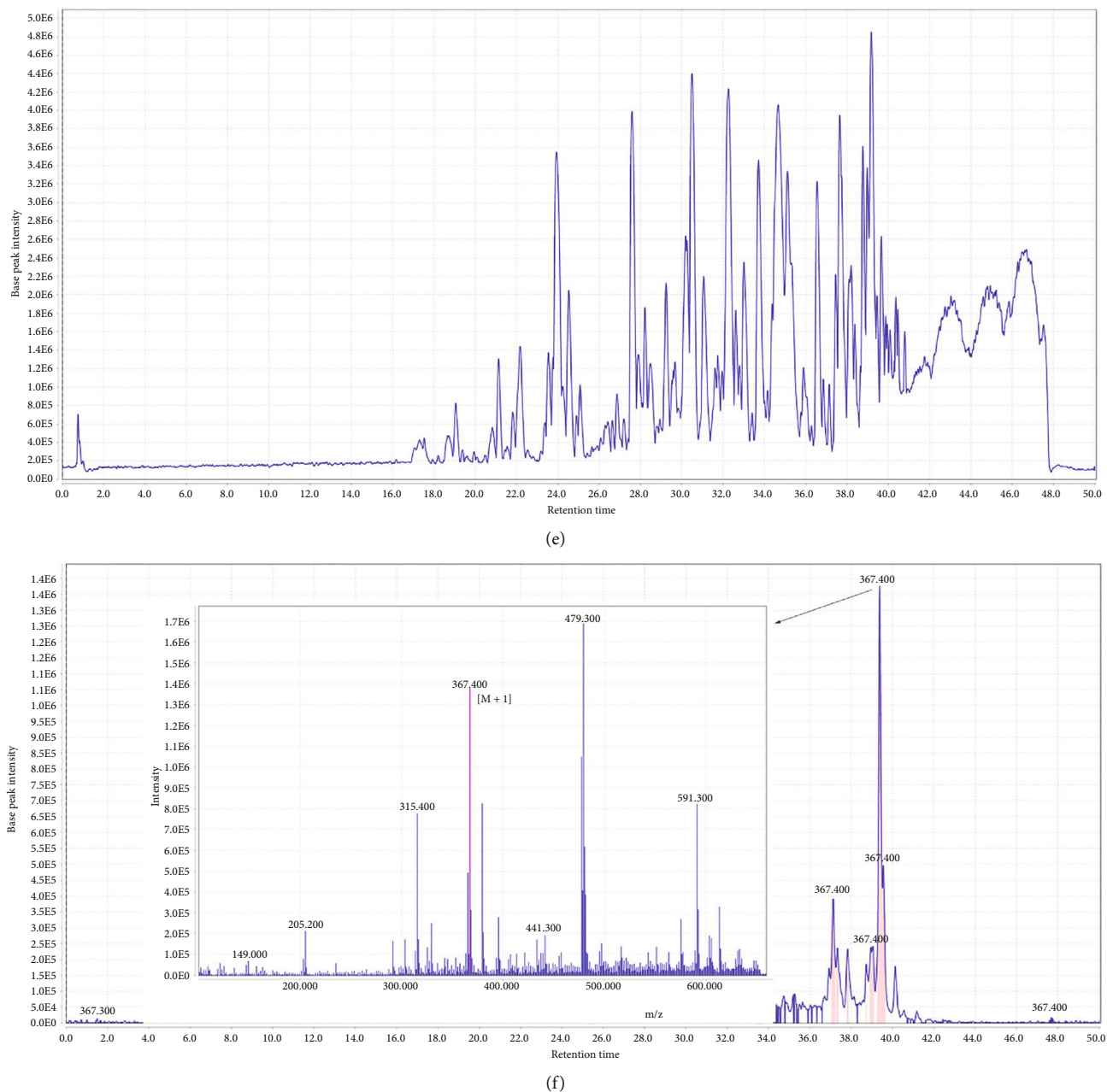


FIGURE 5: (a) The total ion chromatogram of *Ferula assafoetida* extract. (b) Chromatogram of umbelliprenin and corresponding mass adduct,  $[M + 1]$ , at  $m/z$  367.4. (c) Chromatogram of foetisulfide C and corresponding mass adduct,  $[M + 1]$ , at  $m/z$  241.1. (d) Chromatogram of fetidone B and corresponding mass adduct,  $[M + 1]$ , at  $m/z$  235.1. (e) Chromatogram of asadisulfide and corresponding mass adduct,  $[M + 1]$ , at  $m/z$  277.3. (f) Chromatogram of methyl-1-propenyl disulfide and corresponding mass adduct,  $[M + 1]$ , at  $m/z$  120.09.

foetisulfide C), diterpenes (7-oxocallitric acid, picealactone C, and 15-hydroxy-6-en-dehydroabiatic acid), and acetylenes (falcarinolone) were also identified.

#### 4. Discussion

Inflammation is a complex of interconnected mechanisms in reacting to various biological, chemical, and physical stimuli. Chronic inflammation can cause tissue damage and inflammatory illnesses, e.g., arthritis, atherosclerosis, and cancer. The leukocytes' movement to the inflammatory lesion and the cre-

ation of proinflammatory cytokines and chemokines are the main steps in developing chronic inflammatory diseases [27]. These events occur if E.C.s induced by proinflammatory mediators, like  $TNF-\alpha$ , that stimulate ECAMs through the  $TNF/TNF-\alpha$  receptor signalling cascade and ROS production [28–30]. Hence, inhibition of ROS generation and ECAM expression will be a helpful curative approach for treating vascular inflammatory disorders [31].

To the best of our knowledge, this is the first research to consider the *F. assafoetida* extract's anti-inflammatory activity on a  $TNF-\alpha$  model of inflammation of the HUVECs.  $TNF-\alpha$  is



used in several studies with different concentrations to examine the anti-inflammatory activity of multiple compounds [32]. At this point, we induced inflammation with TNF- $\alpha$ , the most crucial proinflammatory cytokine, in a nontoxic concentration that could particularly increase PBMC adhesion levels and ECAM expression. In line with these findings, preceding experiments indicated that TNF- $\alpha$  enhanced ROS formation, monocyte adhesion, and ECAM expression [33, 34], supporting our results.

To provide a good vision for picking the working concentrations, we first carried out a cytotoxicity analysis based on a wide variety of the EEA concentrations on HUVECs. We found that the extract did not have any cytotoxicity in such cells at concentrations lower than 500  $\mu\text{g/ml}$ . We also observed that EEA at only 250  $\mu\text{g/ml}$  of EEA significantly inhibited both ROS levels and PBMC adhesion on TNF- $\alpha$ -stimulated HUVECs, indicating the inhibitory actions of EEA on the high level of ROS and PBMC adhesion. The LC-MS analysis revealed the existence of 33 different compounds in this plant, including foetisulfide A, foetisulfide C, fetidone B, assafoetidin, umbelliprenin, and others, which may have a role in the inflammation-induced action. In this context, some studies demonstrated that luteolin and coumarin, as important constituents of the asafoetida, suppress ROS formation and reduce monocyte adhesion to TNF- $\alpha$ -stimulated HUVECs [35, 36]. Khaghanzadeh and colleagues revealed that umbelliprenin, a sesquiterpene coumarin, induces anti-inflammatory responses via an increase in the secretion of anti-inflammatory cytokines in the sera and splenocytes of mice [37]. Kohno et al. have shown that methyl galbanate derived from *Ferula szowitsiana* decreased NO generation and iNOS mRNA expression and somewhat reduced COX-2 mRNA expression in LPS/IFN-stimulated RAW264.7 cells [38]. As expected, the EEA significantly suppressed the expression of TNF- $\alpha$ -induced VCAM-1 gene and ICAM-1 protein in our research. Also, EEA decreased the ICAM-1 gene expression but was insignificant. Transcription, translation, and protein turnover are all required for cellular activity. The participation of those factors to protein levels is being debated, as transcript levels and cognate protein levels do not always correlate due to different timings, points of action, translational regulation, and protein degradation regulation, all of which are required in controlling steady-state protein abundances [39]. Breakdown of mRNA includes transcript length, ribosome density, biased codon use, and G.C. content of the third spot in codons, enhancing protein burst creation [40, 41].

A study in 2013 by Ahmadvand et al. showed that asafoetida is rich in natural antioxidant compounds such as eremophilene and  $\delta$ -cadinene that inhibit monocytes-endothelial cell adhesion through suppressing VCAM-1 expression [19]. Furthermore, it was found that *assafoetida* contains different compounds, such as phenolic compounds, flavonoids, and compounds containing sulfur, diterpene, and sesquiterpenes [42, 43]. In 1995, Gerritsen et al. showed that some flavonoid compounds declined the expression of ICAM-1, VCAM-1, and E-selectin genes and decreased their surface expression on TNF- $\alpha$ -induced HUVECs [44]. Furthermore, in a study by Motai (2004), sesquiterpene coumarins inhibit NO development and inducible NO synthase expression of LPS-

induced murine macrophage-like cell line (RAW 264.7), suggesting the anti-inflammatory effect of *Ferula fukanensis* [45].

Moreover, several studies carried out in 2004 showed that various kinds of natural antioxidant compounds, including flavonoids and polyphenolic compounds, inhibit monocyte adhesion in E.C.s [46, 47]. Therefore, according to all evidence, we hypothesised that *F. assafoetida* and its compounds might exhibit anti-inflammatory effects. Nevertheless, more experiments are necessary to identify the effects of the components of *F. assafoetida* and their anti-inflammatory activity in ex vivo and in vivo studies.

## 5. Conclusion

Since asafoetida has strong anti-inflammatory properties mentioned in various studies, we assessed EEA's possible anti-inflammatory molecular mechanisms. TNF- $\alpha$  can trigger kinase cascade pathways in the cell and induces NF- $\kappa\text{B}$  in the nucleus, causing transcription and expression of adhesion genes on the cell surface. EEA via decreasing ROS generation, VCAM-1 gene expression, ICAM-1 protein expression, and leukocyte adhesion might inhibit inflammation in HUVECs. This research offers substantial proof that supports the therapeutic value of asafoetida from *Ferula assafoetida* is a new applicant for the prevention and cure of chronic inflammatory diseases, such as atherosclerotic diseases, in humans. However, further work is required to explain these promising features.

## Abbreviations

TNF- $\alpha$ :	Tumour necrosis factor-alpha
EEA:	Ethanol extract of asafoetida oleo-gum-resin
HUVECs:	Human umbilical vein endothelial cells
TNFR:	Tumour necrosis factor receptor
PBMCs:	Peripheral blood mononuclear cells
ROS:	Reactive oxygen species
VCAM-1:	Vascular cell adhesion protein-1
ICAM-1:	Intercellular adhesion molecule-1
E.C.s:	Endothelial cells
ECAMs:	Endothelial cell adhesion molecules
NSAIDs:	Nonsteroidal anti-inflammatory drugs
NO:	Nitric oxide
CFSE:	5-Carboxy-fluorescein diacetate N-succinimidyl ester
DCFH-DA:	2,7-Dichlorofluorescein diacetate
MTT:	(4,5-Dimethyl-2-thiazolyl)-2,5-diphenyltetrazolium bromide
FBS:	Foetal bovine serum
DMSO:	Dimethyl sulphoxide.

## Data Availability

The data used to support the findings of this study are available on reasonable requests.

## Conflicts of Interest

The authors verify no competing interests.

## Authors' Contributions

L.M., M.K., and VRA carried out the experiment, wrote the manuscript, and analyzed the data. H.S. helped to supervise the project. MM helped on carrying out the investigation. GAS and M.K. supervised the project. All authors discussed the results and commented on the manuscript.

## Acknowledgments

We acknowledged the Birjand University of Medical Sciences for financially supporting this research project. This work was supported by the Vice-Chancellor for Research and Technology at the Birjand University of Medical Sciences (grant number: 455590).

## References

- [1] L. Chen, H. Deng, H. Cui et al., "Inflammatory responses and inflammation-associated diseases in organs," *Oncotarget*, vol. 9, no. 6, pp. 7204–7218, 2018.
- [2] V. R. Askari, A. Alavinezhad, V. B. Rahimi, S. A. Rezaee, and M. H. Boskabady, "Immuno-modulatory effects of methanolic extract of *Ferula szowitsiana* on isolated human Th<sub>1</sub>/Th<sub>2</sub>/T<sub>reg</sub> cytokines levels, and their genes expression and nitric oxide production," *Cytokine*, vol. 138, article 155387, 2021.
- [3] C. Cerutti and A. J. Ridley, "Endothelial cell-cell adhesion and signaling," *Experimental Cell Research*, vol. 358, no. 1, pp. 31–38, 2017.
- [4] W. O. Vitoria, L. S. Thomé, L. Kanashiro-Galo et al., "Upregulation of intercellular adhesion molecule-1 and vascular cell adhesion molecule-1 in renal tissue in severe dengue in humans: effects on endothelial activation/dysfunction," *Revista da Sociedade Brasileira de Medicina Tropical*, vol. 52, 2019.
- [5] V. R. Askari, V. Baradaran Rahimi, A. Assaran, M. Iranshahi, and M. H. Boskabady, "Evaluation of the anti-oxidant and anti-inflammatory effects of the methanolic extract of *Ferula szowitsiana* root on PHA-induced inflammation in human lymphocytes," *Drug and Chemical Toxicology*, vol. 43, no. 4, pp. 353–360, 2020.
- [6] I. M. Fenyo and A. V. Gafencu, "The involvement of the monocytes/macrophages in chronic inflammation associated with atherosclerosis," *Immunobiology*, vol. 218, no. 11, pp. 1376–1384, 2013.
- [7] A. Lazzaro, G. De Girolamo, V. Filippi et al., "The interplay between host defense, infection, and clinical status in septic patients: a narrative review," *International Journal of Molecular Sciences*, vol. 23, no. 2, p. 803, 2022.
- [8] J. M. Cook-Mills, M. E. Marchese, and H. Abdala-Valencia, "Vascular cell adhesion molecule-1 expression and signaling during disease: regulation by reactive oxygen species and antioxidants," *Antioxidants & Redox Signaling*, vol. 15, no. 6, pp. 1607–1638, 2011.
- [9] J. Kim, S. Lee, J. Park, and Y. Yoo, "TNF- $\alpha$ -induced ROS production triggering apoptosis is directly linked to Romo1 and Bcl-X<sub>L</sub>," *Cell Death and Differentiation*, vol. 17, no. 9, pp. 1420–1434, 2010.
- [10] J. Checa and J. M. Aran, "Reactive oxygen species: drivers of physiological and pathological processes," *Journal of Inflammation Research*, vol. 13, pp. 1057–1073, 2020.
- [11] D. Preiss and N. Sattar, "Vascular cell adhesion molecule-1: a viable therapeutic target for atherosclerosis?," *International Journal of Clinical Practice*, vol. 61, no. 4, pp. 697–701, 2007.
- [12] V. B. Rahimi, V. R. Askari, R. Shirazinia et al., "Protective effects of hydro-ethanolic extract of *Terminalia chebula* on primary microglia cells and their polarization (M<sub>1</sub>/M<sub>2</sub> balance)," *Multiple Sclerosis and Related Disorders*, vol. 25, pp. 5–13, 2018.
- [13] A. L. Buchman, "Side effects of corticosteroid therapy," *Journal of Clinical Gastroenterology*, vol. 33, no. 4, pp. 289–294, 2001.
- [14] C. Sostres, C. J. Gargallo, M. T. Arroyo, and A. Lanás, "Adverse effects of non-steroidal anti-inflammatory drugs (NSAIDs, aspirin and coxibs) on upper gastrointestinal tract," *Best Practice & Research. Clinical Gastroenterology*, vol. 24, no. 2, pp. 121–132, 2010.
- [15] A. G. Atanasov, S. B. Zotchev, V. M. Dirsch, and C. T. Supuran, "Natural products in drug discovery: advances and opportunities," *Nature Reviews Drug Discovery*, vol. 20, no. 3, pp. 200–216, 2021.
- [16] M. Iranshahi and M. Iranshahi, "Traditional uses, phytochemistry and pharmacology of asafoetida (*Ferula assafoetida* oleo-gum-resin)—a review," *Journal of Ethnopharmacology*, vol. 134, no. 1, pp. 1–10, 2011.
- [17] F. Farhadi, J. Asili, M. Iranshahi, and M. Iranshahi, "NMR-based metabolomic study of asafoetida," *Fitoterapia*, vol. 139, article 104361, 2019.
- [18] M. Mohammadhosseini, A. Venditti, S. D. Sarker, L. Nahar, and A. Akbarzadeh, "The genus *Ferula*: ethnobotany, phytochemistry and bioactivities - a review," *Industrial Crops and Products*, vol. 129, pp. 350–394, 2019.
- [19] H. Ahmadvand, H. Amiri, Z. Dehghani Elmi, and S. Bagheri, "Chemical composition and antioxidant properties of *Ferula assafoetida* leaves essential oil," *Iranian Journal of Pharmacology and Therapeutics*, vol. 12, no. 2, pp. 52–57, 2014.
- [20] S. M. Bagheri, S. T. Hedesh, A. Mirjalili, and M. H. Dashti-r, "Evaluation of anti-inflammatory and some possible mechanisms of antinociceptive effect of *Ferula assafoetida* oleo gum resin," *Journal of Evidence-Based Complementary & Alternative Medicine*, vol. 21, no. 4, pp. 271–276, 2016.
- [21] V. W. Rahlfs and P. Mossinger, "Asa foetida bei Colon irritabile," *Deutsche Medizinische Wochenschrift*, vol. 104, no. 4, pp. 140–143, 1979.
- [22] C. M. Mahdavi, M. Tehranipour, and S. N. Mahdavi, "Effect of asafoetida resin hydroalcoholic extract on experimental rheumatoid arthritis in rat," *Pajouhesh Dar Pezeshki*, vol. 40, no. 4, pp. 172–177, 2017.
- [23] H. Safarpour, S. B. Banadkoki, Z. Keshavarzi et al., "Expression analysis and ATR-FTIR characterization of the secondary structure of recombinant human TNF- $\alpha$  from *Escherichia coli* SHuffle<sup>®</sup> T7 Express and BL21 (DE3) cells," *International Journal of Biological Macromolecules*, vol. 99, pp. 173–178, 2017.
- [24] U. Repnik, M. Knezevic, and M. Jeras, "Simple and cost-effective isolation of monocytes from buffy coats," *Journal of Immunological Methods*, vol. 278, no. 1-2, pp. 283–292, 2003.
- [25] P. Rahmanian-Devin, H. Rakhshandeh, V. Baradaran Rahimi et al., "Intraperitoneal lavage with *Crocus sativus* prevents postoperative-induced peritoneal adhesion in a rat model: evidence from animal and cellular studies," *Oxidative Medicine and Cellular Longevity*, vol. 2021, Article ID 5945101, 22 pages, 2021.

- [26] A. Jaafari, V. Baradaran Rahimi, N. Vahdati-Mashhadian et al., "Evaluation of the therapeutic effects of the hydroethanolic extract of *Portulaca oleracea* on surgical-induced peritoneal adhesion," *Mediators of Inflammation*, vol. 2021, Article ID 8437753, 18 pages, 2021.
- [27] J. M. Bennett, G. Reeves, G. E. Billman, and J. P. Sturmberg, "Inflammation—nature's way to efficiently respond to all types of challenges: implications for understanding and managing "The epidemic" of chronic diseases," *Frontiers in Medicine*, vol. 5, 2018.
- [28] T. P. Rao, T. Okamoto, N. Akita, T. Hayashi, N. Kato-Yasuda, and K. Suzuki, "Amla (*Embllica officinalis* Gaertn.) extract inhibits lipopolysaccharide-induced procoagulant and pro-inflammatory factors in cultured vascular endothelial cells," *The British Journal of Nutrition*, vol. 110, no. 12, pp. 2201–2206, 2013.
- [29] H. Blaser, C. Dostert, T. W. Mak, and D. Brenner, "TNF and ROS crosstalk in inflammation," *Trends in Cell Biology*, vol. 26, no. 4, pp. 249–261, 2016.
- [30] M. Mittal, M. R. Siddiqui, K. Tran, S. P. Reddy, and A. B. Malik, "Reactive oxygen species in inflammation and tissue injury," *Antioxidants & Redox Signaling*, vol. 20, no. 7, pp. 1126–1167, 2014.
- [31] S. Wongrakpanich, A. Wongrakpanich, K. Melhado, and J. Rangaswami, "A comprehensive review of non-steroidal anti-inflammatory drug use in the elderly," *Aging and Disease*, vol. 9, no. 1, pp. 143–150, 2018.
- [32] P. Zhou, S. Lu, Y. Luo et al., "Attenuation of TNF- $\alpha$ -induced inflammatory injury in endothelial cells by ginsenoside Rb1 via inhibiting NF- $\kappa$ B, JNK and p38 signaling pathways," *Frontiers in Pharmacology*, vol. 8, p. 464, 2017.
- [33] E. N. Lee, Y. W. Choi, H. K. Kim et al., "Chloroform extract of aged black garlic attenuates TNF- $\alpha$ -induced ROS generation, VCAM-1 expression, NF- $\kappa$ B activation and adhesiveness for monocytes in human umbilical vein endothelial cells," *Phytotherapy Research*, vol. 25, no. 1, pp. 92–100, 2011.
- [34] D. Jeon, S. J. Kim, and H. S. Kim, "Anti-inflammatory evaluation of the methanolic extract of *Taraxacum officinale* in LPS-stimulated human umbilical vein endothelial cells," *BMC Complementary and Alternative Medicine*, vol. 17, no. 1, p. 508, 2017.
- [35] S. Tranchina, S. Bernasconi, E. Dejana, and A. Del Maschio, "Inhibition of human monocyte adhesion to endothelial cells by the coumarin derivative, cloricromene," *British Journal of Pharmacology*, vol. 111, no. 2, pp. 575–581, 1994.
- [36] F. Xia, C. Wang, Y. Jin et al., "Luteolin protects HUVECs from TNF- $\alpha$ -induced oxidative stress and inflammation via its effects on the Nox4/ROS-NF- $\kappa$ B and MAPK pathways," *Journal of Atherosclerosis and Thrombosis*, vol. 21, no. 8, pp. 768–783, 2014.
- [37] N. Khaghanzadeh, A. Samiei, Z. Mojtahedi, M. Ramezani, M. Hosseinzadeh, and A. Ghaderi, "Umbelliprenin induced both anti-inflammatory and regulatory cytokines in C57/BL6 mice," *Iranian Journal of Basic Medical Sciences*, vol. 20, no. 7, pp. 829–834, 2017.
- [38] S. Kohno, T. Murata, A. Sugiura et al., "Methyl galbanate, a novel inhibitor of nitric oxide production in mouse macrophage RAW264. 7 cells," *Journal of Natural Medicines*, vol. 65, no. 2, pp. 353–359, 2011.
- [39] C. P. Moritz, T. Mühlhaus, S. Tenzer, T. Schulenburg, and E. Friauf, "Poor transcript-protein correlation in the brain: negatively correlating gene products reveal neuronal polarity as a potential cause," *Journal of Neurochemistry*, vol. 149, no. 5, pp. 582–604, 2019.
- [40] S. Kim and C. Jacobs-Wagner, "Effects of mRNA degradation and site-specific transcriptional pausing on protein expression noise," *Biophysical Journal*, vol. 114, no. 7, pp. 1718–1729, 2018.
- [41] B. Neymotin, V. Ettore, and D. Gresham, "Multiple transcript properties related to translation affect mRNA degradation rates in *Saccharomyces cerevisiae*," *Genetics*, vol. 6, no. 11, pp. 3475–3483, 2016.
- [42] A. Amalraj and S. Gopi, "Biological activities and medicinal properties of *Asafoetida*: a review," *Journal of Traditional and Complementary Medicine*, vol. 7, no. 3, pp. 347–359, 2017.
- [43] P. Mahendra and S. Bisht, "*Ferula asafoetida*: traditional uses and pharmacological activity," *Pharmacognosy Reviews*, vol. 6, no. 12, pp. 141–146, 2012.
- [44] M. E. Gerritsen, W. W. Carley, G. E. Ranges et al., "Flavonoids inhibit cytokine-induced endothelial cell adhesion protein gene expression," *The American Journal of Pathology*, vol. 147, no. 2, pp. 278–292, 1995.
- [45] T. Motai and S. Kitanaka, "Sesquiterpene coumarins from *Ferula fukanensis* and nitric oxide production inhibitory effects (2)," *Chemical and Pharmaceutical Bulletin*, vol. 52, no. 10, pp. 1215–1218, 2004.
- [46] J.-S. Choi, Y.-J. Choi, S.-H. Park, J.-S. Kang, and Y.-H. Kang, "Flavones mitigate tumor necrosis factor- $\alpha$ -induced adhesion molecule upregulation in cultured human endothelial cells: role of nuclear factor- $\kappa$ B," *The Journal of Nutrition*, vol. 134, no. 5, pp. 1013–1019, 2004.
- [47] A. Ludwig, M. Lorenz, N. Grimbo et al., "The tea flavonoid epigallocatechin-3-gallate reduces cytokine-induced VCAM-1 expression and monocyte adhesion to endothelial cells," *Biochemical and Biophysical Research Communications*, vol. 316, no. 3, pp. 659–665, 2004.

## Research Article

# Vaspin Alleviates Sepsis-Induced Cardiac Injury and Cardiac Inflammation by Inhibiting Kallikrein 7 in Mice

Na Yin,<sup>1</sup> Fuze Pan,<sup>2</sup> Lingyue Qiu,<sup>2,3</sup> Zicong Yang,<sup>2</sup> Rixin Xiong,<sup>2</sup> Lei Shi,<sup>2</sup> Ying Shi,<sup>2</sup> Ning Wu,<sup>2</sup> Kui Wu,<sup>2</sup> Qingkuan Li,<sup>2</sup> Daojun Wen,<sup>2</sup> Qili Huang,<sup>2</sup> Yuyan Zhang,<sup>2</sup> Yuhong Mi ,<sup>1</sup> and Qingwei Ji <sup>2</sup>

<sup>1</sup>Emergency Critical Care Center, Beijing Anzhen Hospital, Capital Medical University, Beijing, China

<sup>2</sup>Department of Cardiology, The People's Hospital of Guangxi Zhuang Autonomous Region, Nanning, China

<sup>3</sup>Institute of Cardiovascular Sciences, Guangxi Academy of Medical Sciences, Nanning, China

Correspondence should be addressed to Yuhong Mi; myhicu@163.com and Qingwei Ji; jqw124@163.com

Received 10 April 2022; Revised 10 June 2022; Accepted 15 June 2022; Published 15 July 2022

Academic Editor: Dominik Skiba

Copyright © 2022 Na Yin et al. This is an open access article distributed under the Creative Commons Attribution License, which permits unrestricted use, distribution, and reproduction in any medium, provided the original work is properly cited.

**Background.** Vaspin is an important adipokine that is involved in cardiovascular diseases. This study is aimed at investigating whether vaspin participates in sepsis-induced cardiac injury and explored the possible mechanism. **Methods.** First, cecal ligation and puncture (CLP) and lipopolysaccharide (LPS) were used to establish a mouse model of sepsis, and cardiac vaspin expression was examined. In addition, after pretreatment with vaspin or phosphate-buffered saline (PBS), wild-type (WT) mice underwent CLP to establish a septic model and received sham as a control. Finally, WT mice and kallikrein 7 (KLK7<sup>-/-</sup>) mice were underwent CLP with or without vaspin pretreatment. **Results.** Mice that underwent CLP and were administered LPS exhibited increased vaspin expression in both the heart and serum compared with sham- or saline-treated mice. In CLP mice, pretreatment with vaspin reduced mortality and alleviated the expression of cardiac injury markers and cardiac dysfunction. In addition, vaspin reduced the cardiac levels of CD45<sup>+</sup> cells and CD68<sup>+</sup> cells, alleviated the cardiac inflammatory response, and reduced cardiomyocyte apoptosis. The protective effects of vaspin on CLP mice were masked by the deletion of KLK7, which was demonstrated to be a downstream signal of vaspin. **Conclusions.** Vaspin alleviates cardiac inflammation and plays a protective role in sepsis-induced cardiac injury by reducing KLK7 expression.

## 1. Introduction

Sepsis is a systemic inflammatory syndrome caused by the invasion of pathogenic microorganisms in the body that affects approximately 18 million people every year and leads to 14,000 deaths every day [1]. The process of sepsis is often accompanied by the release of lipopolysaccharide (LPS), which leads to the activation of a variety of immune cells and a variety of pathological reactions [2, 3]. Then, it causes tissue and organ injury and failure, which is an important cause of death in patients, among which heart failure is the most important cause of death due to sepsis [2, 3]. Therefore, it is critical to identify potential intervention targets to prevent sepsis-induced cardiac injury and cardiac dysfunction.

Vaspin, also known as SerpinA12, is a member of the Serpin family of serine protease inhibitors [4]. Vaspin is an adipokine that is mainly derived from visceral fat cells and can be expressed in a variety of tissues, such as the heart, kidney, brain, gastrointestinal tract, and pancreas [5]. Inflammation, high glucose, and other pathological conditions can promote the synthesis and secretion of vaspin, and vaspin can alleviate the inflammatory response in tissues and organs by inhibiting kallikrein 7 (KLK7), which was the first discovered downstream signaling pathway [6].

Numerous studies have shown an association between vaspin and the progression of cardiovascular diseases. Treatment with vaspin can significantly protect against methylglyoxaldehyde-induced apoptosis in human umbilical vein endothelial cells and delay high glucose-induced

vascular smooth muscle cell proliferation and migration [7, 8]. Vaspin is increased in coronary artery disease (CAD) patients and positively correlates with the severity of CAD [9, 10]. Vaspin is also increased in atherosclerotic mice and reverses atherosclerosis progression in ApoE<sup>-/-</sup> mice by alleviating inflammation [10–12]. However, it remains unclear whether vaspin plays a role in sepsis-induced cardiac injury, and we examined this question using mice with cecal ligation and puncture- (CLP-) induced sepsis in this study.

## 2. Experimental Materials and Methods

**2.1. Mice and Sepsis Model.** Wild-type (WT) mice and kallikrein 7 knockout (KLK7<sup>-/-</sup>) mice on a C57BL/6 background were purchased from GemPharmatech Co., Ltd. (Jiangsu, China). Male WT mice and KLK7<sup>-/-</sup> mice aged 10 weeks were used in this study. First, WT mice were subjected to CLP or stimulated with LPS (10 mg/kg, Sigma) to establish a mouse model of sepsis as described in previous studies [13, 14]. Six hours later, vaspin expression was analyzed, while WT mice underwent a sham operation or were administered saline as a control ( $n = 5$  for each group, part 1). Additionally, before being subjected to CLP or a sham operation, WT mice were pretreated with PBS or vaspin (0.1  $\mu$ g/kg, PeproTech) for 30 minutes as previously described [15], and then, the effects of vaspin on cardiac injury were detected ( $n = 10 - 12$  in each group); some mice were observed for 8 days to determine the survival rates in each group (part 2). Third, WT mice and KLK7<sup>-/-</sup> mice underwent CLP or sham for the analysis of cardiac inflammation ( $n = 5$  in each group, part 3). Finally, WT mice and KLK7<sup>-/-</sup> mice were pretreated with vaspin or PBS and then underwent CLP and observed for 6 hours or 8 days to determine whether vaspin affects sepsis-induced cardiac injury and survival rates by regulating KLK7 ( $n = 10 - 13$  in each group, part 4). The treatment of mice and the establishment of the sepsis model are shown in Figure 1. This study was approved by our institution's Ethics Committee (approval no. Cardiac2020-01-122).

**2.2. Implementation of CLP.** CLP was performed as described in previous studies [16, 17]. Briefly, WT mice or KLK7<sup>-/-</sup> mice were pretreated with vaspin or PBS, anesthetized with 2% isoflurane inhalation, and laid flat on a preheated operating table. The abdominal hair was removed, 75% ethanol was used to disinfect the skin, and the abdominal skin was dissected to expose the abdominal cavity. The cecum was ligated at half the distance between the distal pole and the base of the cecum and then punctured once from the mesenteric end in the antimesenteric direction using a 26 G needle. Finally, the abdominal skin was sutured and disinfected, and the mice were placed in an incubator at 28°C for resuscitation.

**2.3. Examination of Cardiac Function.** After 6 hours of CLP or sham operation, the mice were anesthetized as described above and placed flat on the operating table. A MyLab™30CV ultrasound system ( Esaote SpA, Genoa,

Italy) consisting of a 10 MHz linear array ultrasonic transducer was used to collect data related to left ventricular (LV) structure and function, including LV end-systolic diameter (LVESD), LV end-diastolic diameter (LVEDD), ejection fraction (EF), and fractional shortening (FS). A Millar Pressure Volume system containing a microtip catheter transducer (Millar, Inc.) was used to collect the LV signals. The microtip catheter transducer was inserted into the left ventricle via the right carotid artery, and information on the maximal slope of the systolic pressure increment (+dp/dt max) and diastolic pressure decrement (-dp/dt max) were recorded on a beat-by-beat basis.

**2.4. Analysis of Cardiac Injury Markers.** Blood samples were collected and centrifuged to obtain serum. The levels of cardiac injury markers, including lactate dehydrogenase (LDH) and myocardial-bound creatine kinase (CK-MB), were examined using LDH assay kits and CK-MB assay kits (both purchased from Njjcbio Biotechnology, China), respectively, according to the manufacturer's instructions.

**2.5. Western Blot Analysis.** The frozen LV tissue was ground, lysed with lysis buffer, and further lysed by ultrasound. Total protein was obtained by centrifugation, the supernatants were collected, and all samples were quantified using a BCA protein quantification kit (Thermo Fisher Scientific, USA) and adjusted to the same concentration. Total protein was separated by molecular weight by electrophoresis using 10% Laemmli sodium dodecyl sulfate (SDS) polyacrylamide gels and transferred to Immobilon-FL PVDF membranes (Millipore, USA). After blocking with 3% BSA for 1 hour, the membranes were incubated with rabbit antimouse vaspin (1:1000), rabbit antimouse KLK7 (1:1000), rabbit antimouse nuclear factor-kappa B p65 (1:1000), rabbit antimouse nuclear factor-kappa B (NF- $\kappa$ B) p-p65 (1:500), rabbit antimouse Bax (1:1000), rabbit antimouse Bcl2 (1:500), and rabbit antimouse GAPDH (1:2000, all monoclonal antibodies were purchased from Abcam, UK) overnight (9 hours) to examine target protein expression. After incubation at room temperature for 1 hour with the secondary antibody, the membranes were scanned using an Odyssey system.

**2.6. Real-Time Quantitative Polymerase Chain Reaction (RT-qPCR).** LV tissue was lysed in TRIzol reagent (Roche, Germany), total RNA was extracted, and the concentration of each sample was determined. Two micrograms of total RNA from each sample was reverse transcribed into cDNA using a reverse transcription kit (Roche, Germany) according to the manufacturer's instructions. Then, the forward primer, reverse primer, and LightCycler 480 SYBR Green Master Mix (Roche, Germany) were used for PCR amplification to measure the expression of target genes, including interleukin-6 (IL-6), IL-17, tumor necrosis factor  $\alpha$  (TNF- $\alpha$ ), interferon  $\gamma$  (IFN- $\gamma$ ), and monocyte chemoattractant protein-1 (MCP-1). Target gene expression was normalized to GAPDH. The RT-qPCR primer sequences were as described in our previous study [18].

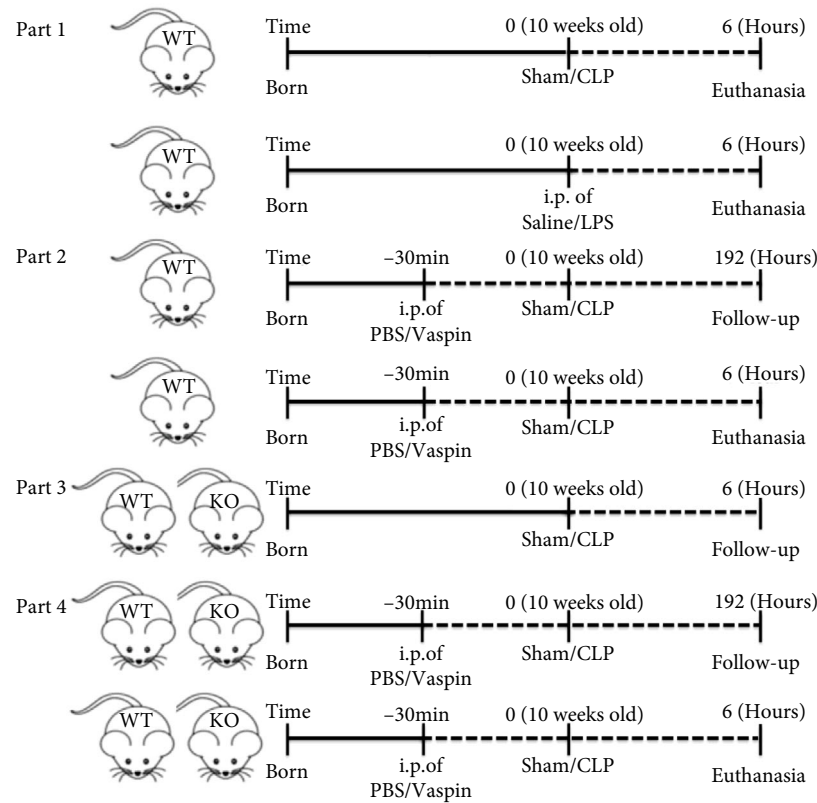


FIGURE 1: Establishment and pretreatment of the mouse sepsis model.

**2.7. Histological Analysis.** Hearts were fixed in 4% neutral paraformaldehyde for 4 days. After paraffin embedding, the hearts were cut to a thickness of  $4\ \mu\text{m}$  and then transferred and fixed on slides. The slides were incubated with anti-CD45 and anti-CD68 antibodies (both purchased from GeneTex, USA) to examine the levels of cardiac leukocytes and macrophages. Apoptotic cells in the left ventricle were examined by terminal deoxynucleotidyl transferase-mediated dUTP nick end labeling (TUNEL) staining (Millipore, USA) using a commercially available kit according to the manufacturer's instructions. In addition, cardiomyocytes were incubated with anticlaved caspase3 (Abcam, UK) to examine the effects of vaspin on cardiomyocyte apoptosis.

**2.8. Cell Studies and Analysis.** Cardiomyocytes were isolated as previously described [19]. Briefly, WT mice and *KLK7*<sup>-/-</sup> mice aged 8 weeks were euthanized, the chest cavity was exposed, and the hearts were quickly collected. The hearts were rinsed with phosphate-buffered saline (PBS), and the left ventricle was further isolated, gently prepared into  $1\ \text{mm}^3$  fragments, and then digested with mixed enzymes, including EDTA buffer, perfusion buffer, and collagenase buffer (7:3:40, triple purchase from Servicebio, China). After being passed through a  $100\ \mu\text{m}$  filter, the cells underwent 4 sequential rounds of gravity settling, and then, 3 intermediate calcium reintroduction buffers were used to gradually restore the calcium concentration to physiological levels. Then, WT cardiomyocytes and *KLK7*<sup>-/-</sup> cardiomyocytes were obtained.

RPMI 1640 medium (Gibco, USA) with 10% fetal bovine serum was used to culture the cardiomyocytes. First, WT cardiomyocytes were pretreated with PBS or vaspin (80 ng/ml, PeproTech, USA) and then administered saline or LPS ( $1\ \mu\text{mol/ml}$ , Sigma, USA) [13, 20]. Additionally, WT and *KLK7*<sup>-/-</sup> cardiomyocytes were pretreated with vaspin or PBS and then stimulated with LPS. All cardiomyocytes were cultured for 24 hours, the culture medium was changed once every 8 hours, and both vaspin and LPS were added again. Cleaved caspase-3 expression was examined as described above.

**2.9. Statistical Analysis.** All data in this study were analyzed using GraphPad Prism 8 software and are presented as the mean  $\pm$  SD. Differences between 2 groups or multiple groups were compared using Student's *t* test or one- two-way ANOVA, respectively. The log-rank test was used to analyze the differences in the survival rates among the four groups at follow-up. A value of  $p < 0.05$  was considered statistically significant.

### 3. Results

**3.1. Vaspin Expression Is Increased in Septic Mice.** In the CLP-induced mouse model of sepsis, cardiac and serum vaspin levels were, respectively, increased 0.98-fold and 1.33-fold compared with those in sham mice (Figures 2(a) and 2(b)). And the magnitude of increase was 0.79-fold and 1.19-fold in the LPS-induced mouse sepsis model (Figures 2(c) and 2(d)).

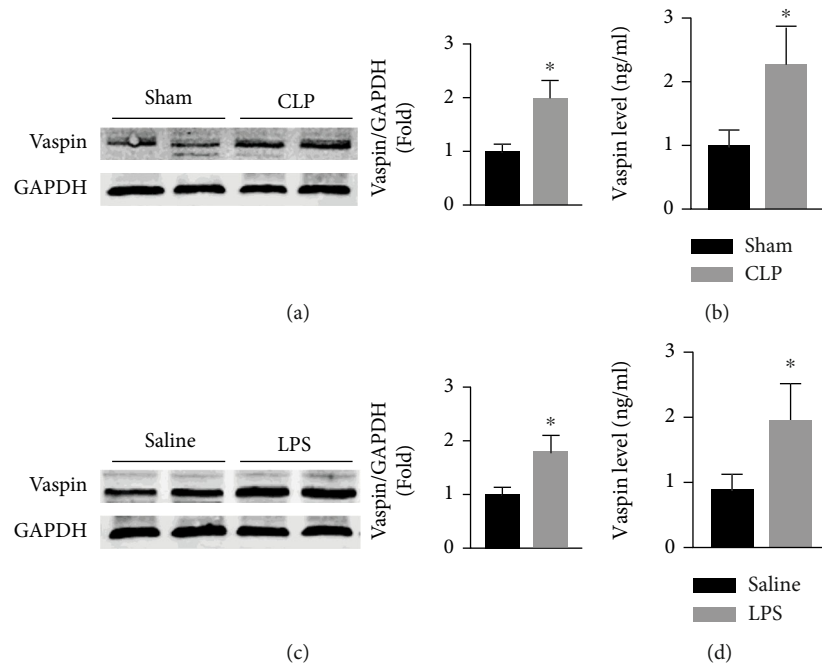


FIGURE 2: Effects of sepsis on vaspin expression in mice. Cardiac (a) and serum (b). Vaspin expression in sham and CLP mice (Student's *t* test). Cardiac (c) and serum (d). Vaspin levels in saline- and LPS-treated mice (Student's *t* test).  $N = 6$  in each group. \* $p < 0.05$  vs. the sham or saline group.

**3.2. Treatment with Vaspin Alleviates Cardiac Injury and Cardiac Dysfunction in CLP-Induced Septic Mice.** During the 8-day follow-up, pretreatment with vaspin did not affect the survival rates of sham mice but improved the survival rates of septic mice (CLP + PBS group: 30.0% vs. CLP + vaspin group: 80.8%, Figure 3(a)). Vaspin decreased cardiac KLK7 expression for 49% in sham and for 57% in CLP mice (Figure 3(b)). In addition, vaspin decreased LDH levels for 38% and reduced CK-MB levels for 29.7% in septic mice that underwent CLP for 5 days (Figure 3(c)). Furthermore, treatment with vaspin alleviated sepsis-induced cardiac dysfunction, as indicated by reductions in LVEDD, LVESD, +dp/dt max, and -dp/dt max, as well as increases in LVEF and FS (Figures 2(d) and 2(e)).

**3.3. Vaspin Alleviates Sepsis-Induced Cardiac Inflammation in Mice.** The effects of vaspin on inflammation were investigated, and the results showed that pretreatment with vaspin decreased the cardiac infiltration of CD45+ cells and CD68+ cells (Figure 4(a)). The expression levels of various inflammatory markers, including MCP-1, IL-6, IL-17, TNF- $\alpha$ , and IFN- $\gamma$ , were decreased by approximately 45-70% after vaspin treatment (Figure 4(b)). In addition, vaspin decreased the phosphorylation of NF- $\kappa$ B p65 in septic mice (Figure 4(c)).

**3.4. Vaspin Protects against Cardiomyocyte Apoptosis in Septic Mice.** Cardiomyocyte apoptosis was then examined, and the results showed that treatment with vaspin increased cardiac expression levels of Bcl2 for 88% in septic mice but decreased Bax expression for 34% (Figure 5(a)). Reduced

levels of cleaved caspase3 were observed in LPS-stimulated WT cardiomyocytes when vaspin was added in vitro (Figure 5(b)). Pretreatment also decreased the number of TUNEL-positive cardiac cells in septic mice (CLP + PBS group:  $9.42 \pm 2.43$  vs. CLP + vaspin group:  $3.67 \pm 0.64$ , Figure 5(c)).

**3.5. KLK7 Knockout Mediates the Effects of Vaspin on Sepsis-Induced Cardiac Injury and Cardiac Dysfunction.** The effects of vaspin on the survival rates of KLK7 $^{-/-}$  mice were examined, and the results showed that none mice died in septic KLK7 $^{-/-}$  mice with or without vaspin treatment, and vaspin had no effects on the survival rates of KLK7 $^{-/-}$  mice (Figure 6(a)). Vaspin did not affect cardiac injury marker expression in KLK7 $^{-/-}$  mice (Figure 6(b)). The regulatory effects of vaspin on cardiac function were also evident in septic KLK7 $^{-/-}$  mice (Figures 6(c) and 6(d)).

**3.6. KLK7 Deficiency Masks the Anti-Inflammatory and Protective Effects of Vaspin on Septic Mice.** Cardiac inflammation was examined, and the results showed that KLK7 knockout significantly improves cardiac inflammation response in septic mice, but still higher than the sham +KLK7 $^{-/-}$  group (as the supplemental Figure S1). While treatment with vaspin did not decrease the number of CD45+ cells or CD68+ cells in the hearts of septic KLK7 $^{-/-}$  mice (Figure 7(a)). Pretreatment with vaspin did not affect the cardiac expression of MCP-1, IL-6, IL-17, TNF- $\alpha$ , or IFN- $\gamma$  in CLP mice (Figure 7(b)). No changes in cleaved caspase3- or TUNEL-positive cell percentages were observed in vaspin-treated KLK7 $^{-/-}$  mice (TUNEL levels,

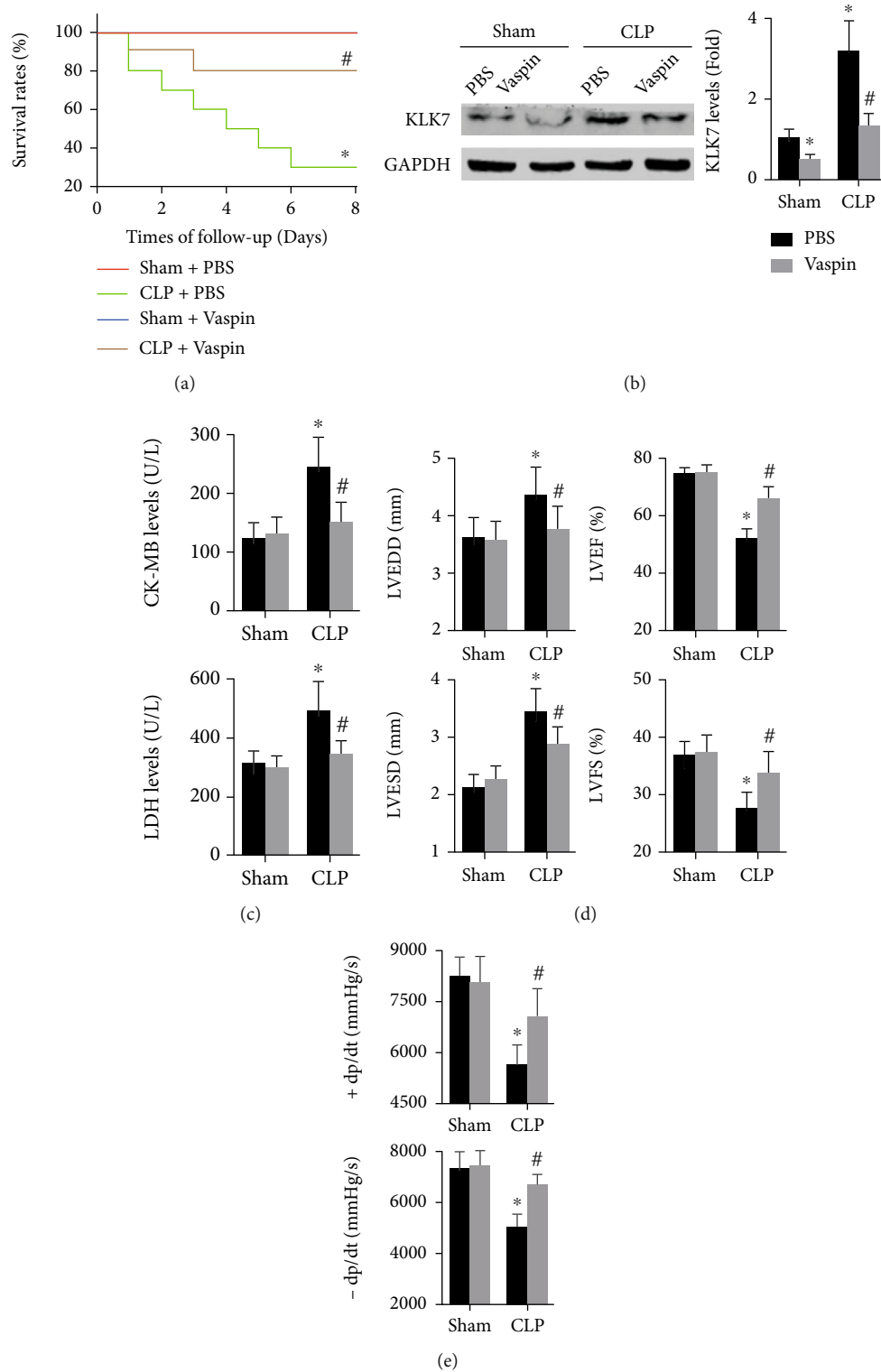


FIGURE 3: Effects of vaspin on survival rates and cardiac dysfunction in CLP mice. (a) The survival rates in each group were examined during the 8-day follow-up (log-rank test). (b) Cardiac KLK7 expression in the four groups was measured (two-way ANOVA). (c) Serum levels of CK-MB and LDH in all groups were analyzed (two-way ANOVA). (d, e) Cardiac structural and functional data were examined, including LVEDD, LVESD, LVEF, FS, +dp/dt max, and -dp/dt max (two-way ANOVA).  $N = 5 - 10$  in each group. \* $p < 0.05$  vs. the sham + PBS group. # $p < 0.05$  vs. the CLP + PBS group.



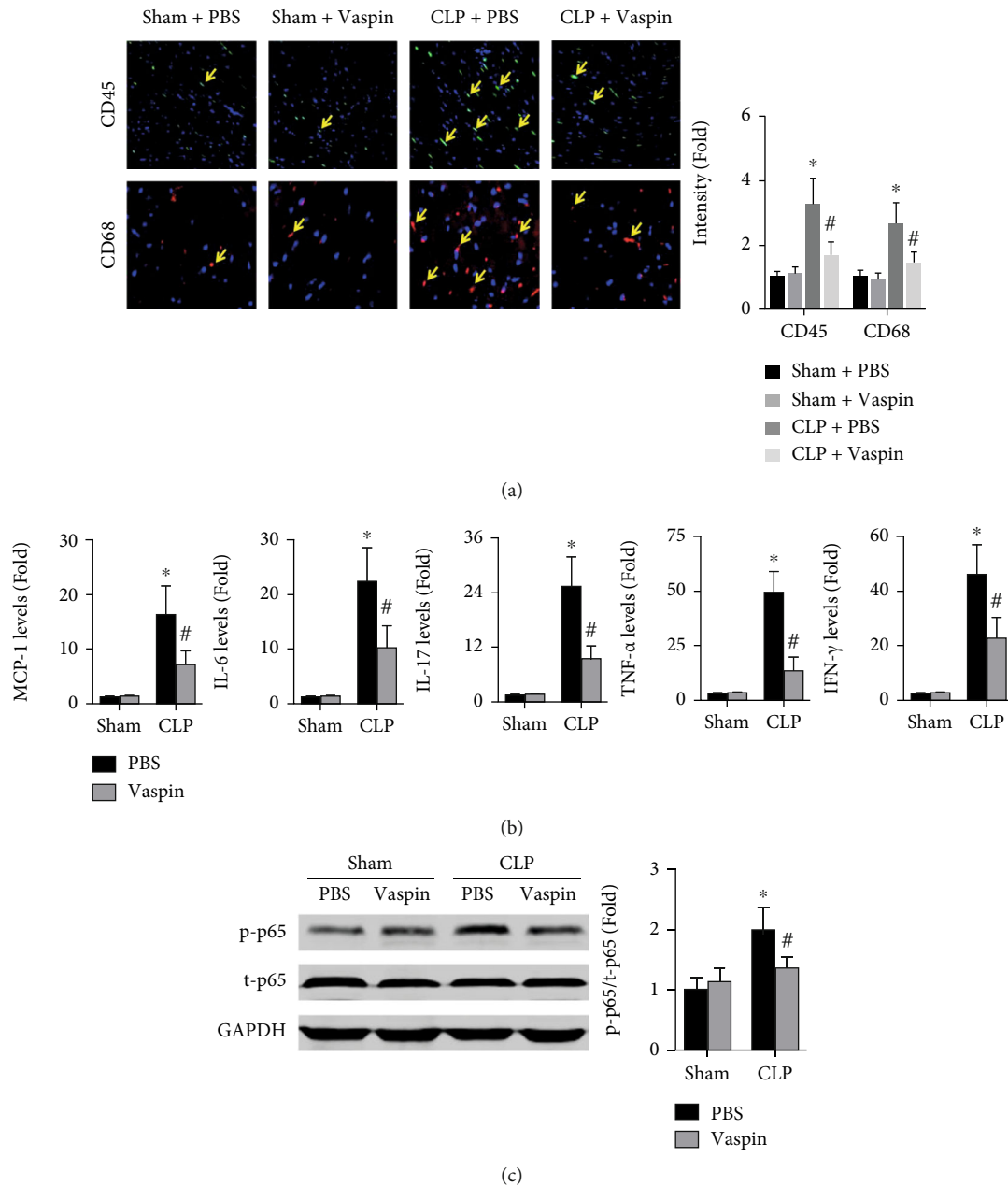


FIGURE 4: Effects of vaspin on sepsis-induced cardiac inflammation in mice. (a) Cardiac CD45+ cells and CD68+ cells in each group were examined (two-way ANOVA). (b) Cardiac mRNA expression levels of MCP-1, IL-6, IL-17, TNF- $\alpha$ , and IFN- $\gamma$  were measured (two-way ANOVA). (c) The phosphorylation of NF- $\kappa$ B p65 in each group (two-way ANOVA). Blue, green, and red indicate nuclei, CD45-positive cells, and CD68-positive cells, respectively.  $N = 5$  in each group. \* $p < 0.05$  vs. the sham + PBS group. # $p < 0.05$  vs. the CLP + PBS group.

CLP + KLK7 -/- + PBS group:  $3.11 \pm 0.45$  vs. CLP + KLK7 -/- + vaspin group:  $2.98 \pm 0.31$ , Figures 7(c) and 7(d)).

#### 4. Discussion

In this study, we examined the regulatory role of the adipokine vaspin in cardiac injury induced by sepsis and focused on the inflammatory response in the heart to elucidate the mechanism. We showed for the first time that vaspin alleviates cardiac inflammation, reduces cardiomyocyte apoptosis, improves cardiac injury, and increases the

survival rates of septic mice. These effects were masked when KLK7 was knocked out. Our findings suggest that vaspin can reduce sepsis-induced cardiac inflammation, alleviate sepsis-induced cardiac injury, and improve cardiac function by inhibiting KLK7 expression. Vaspin may be a therapeutic target for the prevention and treatment of cardiac injury in clinical sepsis.

Sepsis is a major public health problem worldwide and is a systemic inflammatory response syndrome caused by the invasion of bacteria and other pathogenic microorganisms in the body [21, 22]. The cell wall of gram-negative bacteria

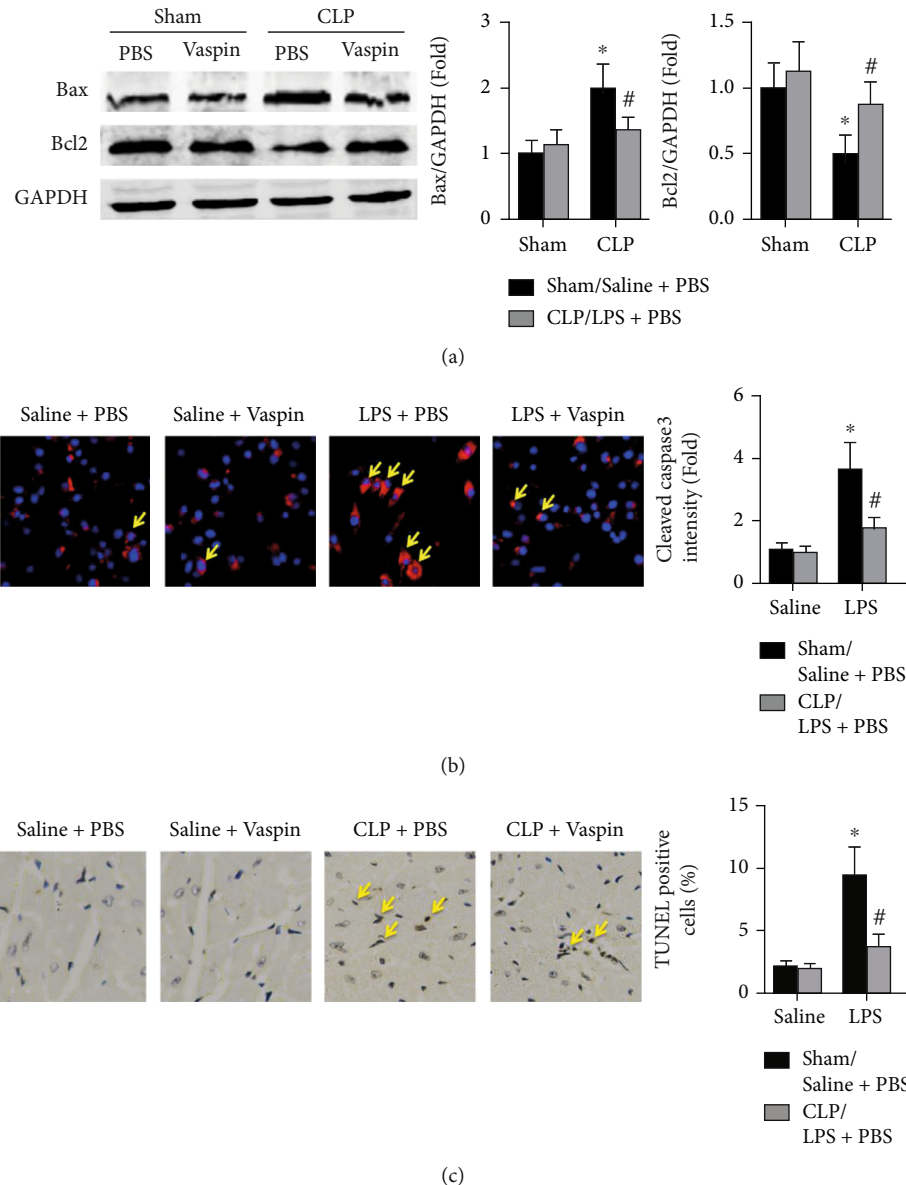


FIGURE 5: Effects of vaspin on cardiomyocyte apoptosis in septic mice. (a) Protein expression levels of cardiac Bax and Bcl2 were examined (two-way ANOVA). (b) Cleaved caspase-3 expression in LPS-induced cardiomyocytes was analyzed (two-way ANOVA). Blue and red spots indicate the nucleus and cleaved caspase-3. (c) TUNEL-positive cells in each group were determined (two-way ANOVA).  $N = 5$  in each group. \* $p < 0.05$  vs. the sham + PBS or saline + PBS group. # $p < 0.05$  vs. the CLP + PBS or LPS + PBS group.

contains LPS, which can be released into the blood after infection and lead to inflammatory reactions, oxidative stress, coagulation dysfunction, immune system activation, and other pathological processes and then induce tissue and organ injury, which suggests that LPS is the initiating factor in the occurrence and development of sepsis [22, 23]. In addition, a previous study reported that circulating vaspin levels were increased in septic patients [24]. Thus, in this study, mice underwent CLP to induce abdominal infection and simulate clinical sepsis, while intraperitoneal injection of LPS was used to simulate the release of LPS from the cell walls of gram-negative bacteria. Therefore, mice underwent CLP and were administered LPS to establish sepsis models, and vaspin expression was examined to deter-

mine the effect of CLP on vaspin expression. The results showed that the expression of cardiac vaspin was significantly increased in CLP- and LPS-treated mice. These findings suggest that vaspin may be involved in sepsis-induced cardiac injury, while the effects of vaspin on cardiac injury need to be further determined. In subsequent experiments, we examined the effects of vaspin on mortality and cardiac injury in CLP-induced septic mice, and the results showed that pretreatment with vaspin significantly increased the survival rate, decreased the expression of multiple markers of cardiac injury, and improved cardiac dysfunction. These results suggest that vaspin was compensatorily increased to protect against sepsis-induced cardiac injury. Just as B-type natriuretic peptide (BNP), which can play a vein dilating

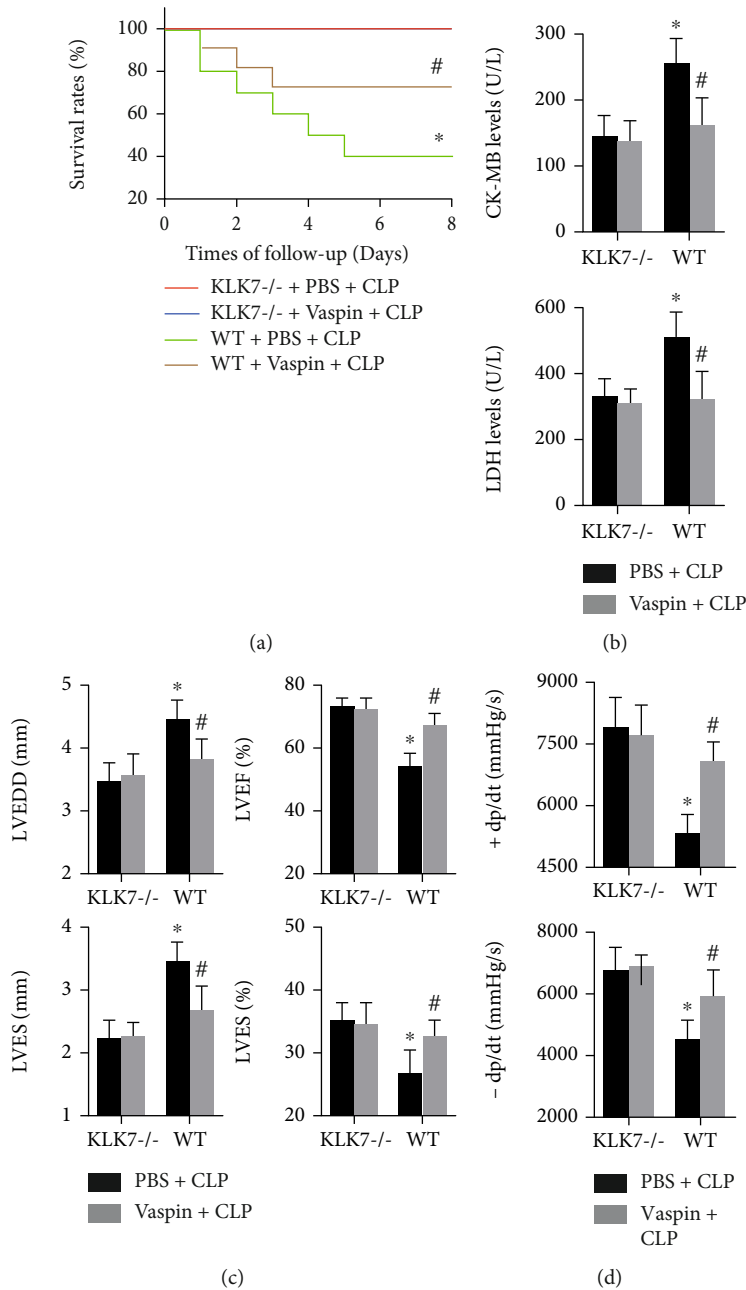


FIGURE 6: Effects of KLK7 deficiency on sepsis-induced cardiac injury in mice. (a) The survival rates of septic WT mice and KLK7<sup>-/-</sup> mice were measured (log-rank test). (b) CK-MB and LDH concentrations in serum were examined (two-way ANOVA). (c, d) Cardiac structure and function were measured (two-way ANOVA).  $N = 5$  in each group. \* $p < 0.05$  vs. the WT + PBS + CLP group. # $p > 0.05$  vs. the KLK7<sup>-/-</sup> + PBS + CLP group.

and diuretic role, is compensatory increased in heart failure and beneficial in improving symptoms, BNP-related drugs are used in the treatment of clinical chronic heart failure [25].

In sepsis patients and mice, it was found that the levels of various immune cells in the blood, including leukocytes, monocytes, and macrophages, were significantly increased. In addition, these immune cells gradually infiltrate the heart and become activated, thus releasing multiple factors and amplifying the cardiac inflammatory response [26–28]. These findings suggest that inflammation plays an important

role in the progression of sepsis, although other pathological factors, including oxidative stress and vascular injury, are involved in sepsis progression. Therefore, to investigate the mechanism by which vaspin protects against sepsis-induced cardiac injury, cardiac inflammation in each group of mice was investigated. The results showed that vaspin significantly reduced the levels of cardiac leukocytes and macrophages and downregulated the expression of several proinflammatory factors. These results suggest that vaspin alleviates sepsis-induced cardiac dysfunction by reducing cardiac inflammation.

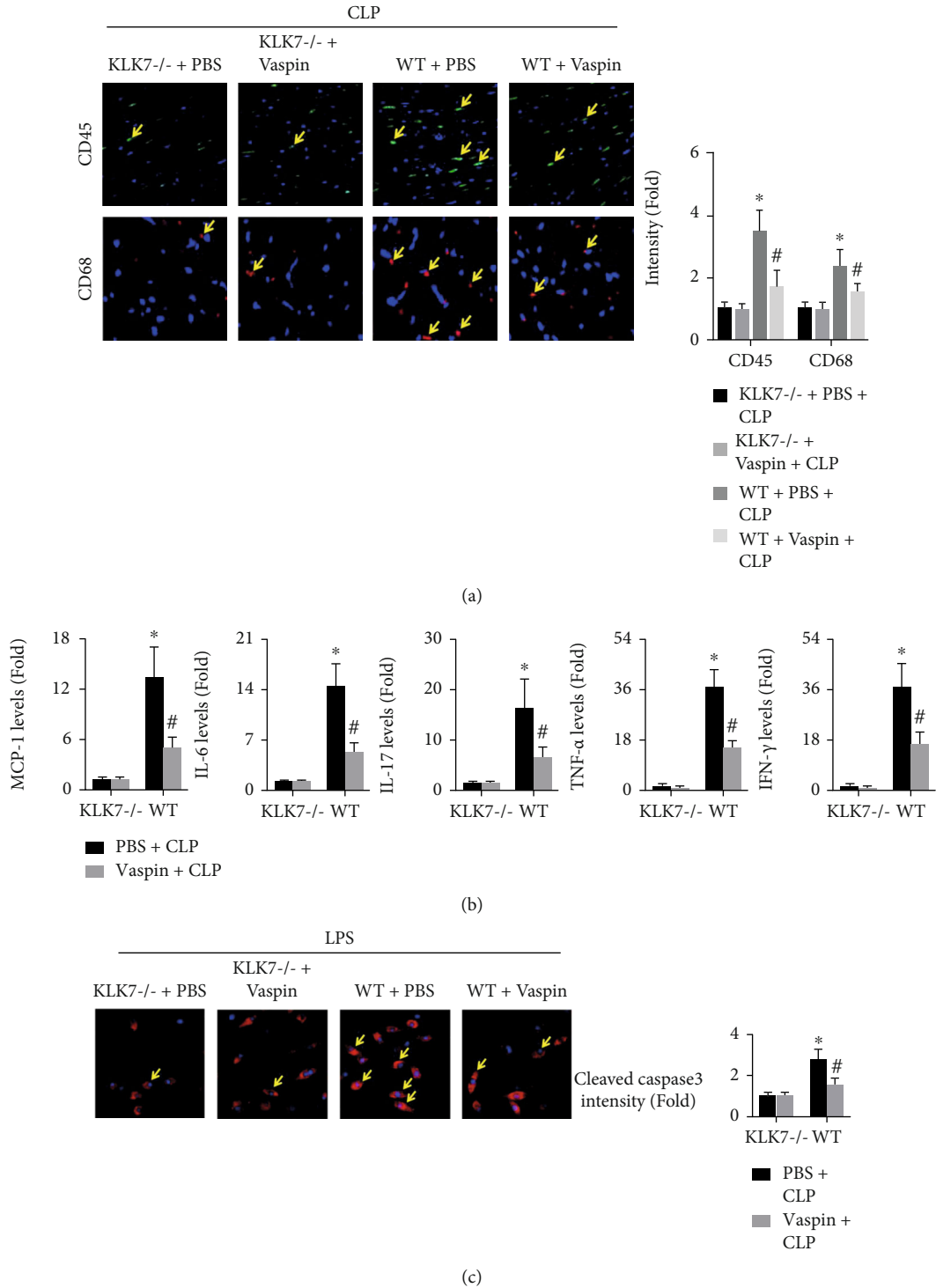
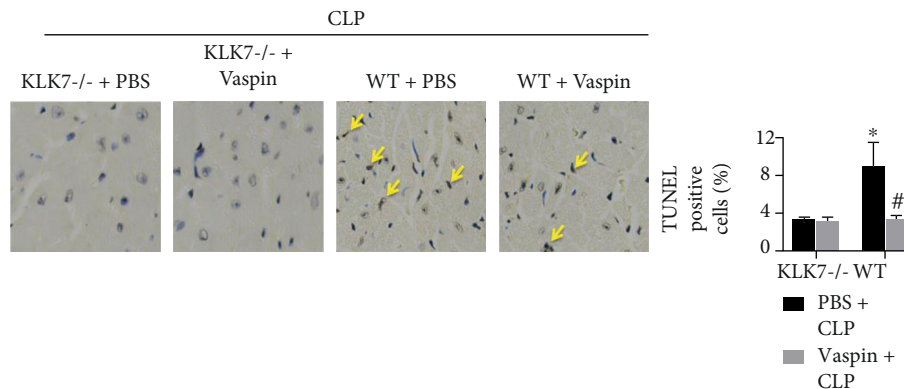


FIGURE 7: Continued.



(d)

FIGURE 7: Effects of KLK7 deletion on cardiac inflammation and cardiomyocyte apoptosis in septic mice. (a, b) Levels of CD45+ cells and CD68+ cells, as well as the levels of the proinflammatory cytokines MCP-1, IL-6, IL-17, TNF- $\alpha$ , and IFN- $\gamma$  in the heart (two-way ANOVA). Blue, green, and red indicate nuclei, CD45-positive cells, and CD68-positive cells, respectively. (c) The expression of cleaved caspase3 in LPS-treated WT cardiomyocytes and KLK7<sup>-/-</sup> cardiomyocytes was analyzed (two-way ANOVA). Blue and red spots indicate the nucleus and cleaved caspase3, respectively. (d) The number of TUNEL-positive cardiac cells was quantified (two-way ANOVA). \* $p < 0.05$  vs. the WT + PBS + CLP or WT + PBS + LPS group. <sup>ns</sup> $p > 0.05$  vs. the KLK7<sup>-/-</sup> + PBS + CLP or KLK7<sup>-/-</sup> + PBS + LPS group.

The antiapoptotic protein Bcl2 is present in the outer mitochondrial membrane, while the proapoptotic protein Bax is present in the cytoplasm. Their expression maintains a balance, and these proteins antagonize each other, which is essential for maintaining normal cell morphology and function [29]. In response to certain factors, the expression of Bax is increased and translocates and inserts into the outer mitochondrial membrane to form large channels; moreover, the expression of Bcl2 is inhibited, and the stability of the mitochondrial membrane is damaged [30]. Cytochrome C and other proapoptotic factors are released to activate caspase3 and initiate the caspase cascade, leading to programmed cell death [29–31]. Cardiomyocytes have low tolerance for the inflammatory response, and an enhanced inflammatory response can initiate the caspase cascade, leading to excessive apoptosis in cardiomyocytes, which can lead to cardiac injury and an excessive decline in cardiac function. Vaspin reduces sepsis-mediated cardiac inflammation. To further explain the mechanism, we examined the effect of vaspin on myocardial apoptosis. The results showed that vaspin treatment significantly reversed the imbalance in Bax/Bcl2 expression and reduced the proportion of Caspase3 expression and TUNEL-positive cells. These results suggest that vaspin alleviates cardiac injury and cardiac dysfunction and may be related to protecting against cardiomyocyte apoptosis.

KLK7 is a member of the tissue kallikrein-releasing enzyme gene family and can be expressed in a variety of tissues and organs. Studies have shown that KLK7 is involved in the progression of multiple systemic diseases, including skin diseases, tumors, and prostatitis [32]. KLK7 is the first downstream signal of vaspin, and vaspin can significantly decrease KLK7 expression, thus inhibiting its downstream signal and ameliorating various diseases [6]. In addition, previous studies have found that vaspin was a valuable predictor of heart failure hospitalization during patients with acute myocardial infarction [33]. Our results also found that

treatment with vaspin improved cardiac dysfunction, but whether this effect is mediated by KLK7 is still unclear. We further found that cardiac KLK7 levels were significantly inhibited in sham mice and CLP mice after vaspin pretreatment, suggesting that vaspin may be more likely involved in regulating sepsis-induced cardiac injury related to KLK7. Therefore, the regulatory effect of vaspin on sepsis progression was examined in KLK7<sup>-/-</sup> mice. The results showed that KLK7 knockout improves inflammation response, but still higher than the sham+KLK7<sup>-/-</sup> group. And vaspin-mediated regulation of survival, cardiac dysfunction, cardiac inflammation, and myocardial apoptosis in septic mice was masked by KLK7 knockout. These results suggest that vaspin-mediated regulation of sepsis-induced cardiac injury is mediated by KLK7.

In summary, our data showed for the first time that vaspin alleviates cardiac inflammation and protects against cardiomyocyte apoptosis by inhibiting KLK7 expression and alleviates sepsis-induced myocardial injury and cardiac dysfunction. Vaspin/KLK7 axis may be a potential therapeutic agent for treating septic cardiac injury, and KLK7 may play an even more important role.

## Data Availability

We confirm that all the data in our study could be freely available to scientists, except for commercial purposes.

## Conflicts of Interest

The authors declare no potential conflicts of interest.

## Authors' Contributions

Na Yin is the first author of this work.

## Acknowledgments

This work was supported by the National Natural Science Foundation of China (no. 81770472 to Dr. Qingwei Ji).

## Supplementary Materials

Supplemental S1: effects of KLK7 deletion on sepsis-induced cardiac inflammation. mRNA expression levels of MCP-1, IL-6, IL-17, TNF- $\alpha$ , and IFN- $\gamma$  were detected.  $N = 6$  in each group. \* $p < 0.05$  vs. the CLP + WT group. # $p < 0.05$  vs. the Sham + KLK7-/- group. (*Supplementary Materials*)

## References

- [1] T. van der Poll, F. L. van de Veerdonk, B. P. Scicluna, and M. G. Netea, "The immunopathology of sepsis and potential therapeutic targets," *Nature Reviews. Immunology*, vol. 17, no. 7, pp. 407–420, 2017.
- [2] M. Cecconi, L. Evans, M. Levy, and A. Rhodes, "Sepsis and septic shock," *Lancet*, vol. 392, no. 10141, pp. 75–87, 2018.
- [3] M. W. Merx and C. Weber, "Sepsis and the heart," *Circulation*, vol. 116, no. 7, pp. 793–802, 2007.
- [4] P. Kurowska, E. Mlyczyńska, M. Dawid et al., "Review: vaspin (SERPINA12) expression and function in endocrine cells," *Cell*, vol. 10, no. 7, p. 1710, 2021.
- [5] J. Weiner, K. Zieger, J. Pippel, and J. T. Heiker, "Molecular mechanisms of vaspin action - from adipose tissue to skin and bone, from blood vessels to the brain," *Advances in Experimental Medicine and Biology*, vol. 1111, pp. 159–188, 2019.
- [6] J. T. Heiker, N. Klötting, P. Kovacs et al., "Vaspin inhibits kallikrein 7 by serpin mechanism," *Cellular and Molecular Life Sciences*, vol. 70, no. 14, pp. 2569–2583, 2013.
- [7] C. H. Jung, W. J. Lee, J. Y. Hwang et al., "Vaspin increases nitric oxide bioavailability through the reduction of asymmetric dimethylarginine in vascular endothelial cells," *PLoS One*, vol. 7, no. 12, article e52346, 2012.
- [8] H. Li, W. Peng, J. Zhuang et al., "Vaspin attenuates high glucose-induced vascular smooth muscle cells proliferation and chemokinesis by inhibiting the MAPK, PI3K/Akt, and NF- $\kappa$ B signaling pathways," *Atherosclerosis*, vol. 228, no. 1, pp. 61–68, 2013.
- [9] S. H. Choi, S. H. Kwak, Y. Lee et al., "Plasma vaspin concentrations are elevated in metabolic syndrome in men and are correlated with coronary atherosclerosis in women," *Clinical Endocrinology*, vol. 75, no. 5, pp. 628–635, 2011.
- [10] P. Zahradka, "Inhibition of NADPH oxidase by vaspin may prevent progression of atherosclerosis," *Acta Physiologica*, vol. 209, no. 3, pp. 195–198, 2013.
- [11] R. Dimova and T. Tankova, "The role of vaspin in the development of metabolic and glucose tolerance disorders and atherosclerosis," *BioMed Research International*, vol. 2015, Article ID 823481, 7 pages, 2015.
- [12] Y. Lin, J. Zhuang, H. Li et al., "Vaspin attenuates the progression of atherosclerosis by inhibiting ER stress-induced macrophage apoptosis in apoE-/- mice," *Molecular Medicine Reports*, vol. 13, no. 2, pp. 1509–1516, 2016.
- [13] W. Liang, J. Li, C. Bai et al., "Interleukin-5 deletion promotes sepsis-induced M1 macrophage differentiation, deteriorates cardiac dysfunction, and exacerbates cardiac injury via the NF- $\kappa$ B p65 pathway in mice," *BioFactors*, vol. 46, no. 6, pp. 1006–1017, 2020.
- [14] S. Zhu, Y. Wang, H. Liu et al., "Thyroxine affects lipopolysaccharide-induced macrophage differentiation and myocardial cell apoptosis via the NF- $\kappa$ B p65 pathway both in vitro and in vivo," *Mediators of Inflammation*, vol. 2019, Article ID 2098972, 10 pages, 2019.
- [15] W. Li, D. Qi, L. Chen et al., "Vaspin protects against lipopolysaccharide-induced acute respiratory distress syndrome in mice by inhibiting inflammation and protecting vascular endothelium via PI3K/Akt signal pathway," *Nan Fang Yi Ke Da Xue Xue Bao*, vol. 38, no. 3, pp. 283–288, 2018.
- [16] D. Rittirsch, M. S. Huber-Lang, M. A. Flierl, and P. A. Ward, "Immunodesign of experimental sepsis by cecal ligation and puncture," *Nature Protocols*, vol. 4, no. 1, pp. 31–36, 2009.
- [17] J. Zhang, Z. Yang, Z. Liang et al., "Anti-interleukin-16 neutralizing antibody treatment alleviates sepsis-induced cardiac injury and dysfunction via the nuclear factor erythroid-2 related factor 2 pathway in mice," *Oxidative Medicine and Cellular Longevity*, vol. 2021, Article ID 6616422, 11 pages, 2021.
- [18] J. Ye, Q. Ji, J. Liu et al., "Interleukin 22 promotes blood pressure elevation and endothelial dysfunction in angiotensin II-treated mice," *Journal of the American Heart Association*, vol. 6, no. 10, article e005875, 2017.
- [19] M. Ackers-Johnson, P. Y. Li, A. P. Holmes, S. M. O'Brien, D. Pavlovic, and R. S. Foo, "A simplified, langendorff-free method for concomitant isolation of viable cardiac myocytes and nonmyocytes from the adult mouse heart," *Circulation Research*, vol. 119, no. 8, pp. 909–920, 2016.
- [20] S. Liu, X. Li, Y. Wu et al., "Effects of vaspin on pancreatic  $\beta$  cell secretion via PI3K/Akt and NF- $\kappa$ B signaling pathways," *PLoS One*, vol. 12, no. 12, article e0189722, 2017.
- [21] M. Huang, S. Cai, and J. Su, "The pathogenesis of sepsis and potential therapeutic targets," *International Journal of Molecular Sciences*, vol. 20, no. 21, p. 5376, 2019.
- [22] L. Liu and B. Sun, "Neutrophil pyroptosis: new perspectives on sepsis," *Cellular and Molecular Life Sciences*, vol. 76, no. 11, pp. 2031–2042, 2019.
- [23] K. Dickson and C. Lehmann, "Inflammatory response to different toxins in experimental sepsis models," *International Journal of Molecular Sciences*, vol. 20, no. 18, p. 4341, 2019.
- [24] M. C. Motal, D. A. Klaus, D. Leberher-Eichinger et al., "Increased plasma vaspin concentration in patients with sepsis: an exploratory examination," *Biochemia Medica*, vol. 25, no. 1, pp. 90–96, 2015.
- [25] C. A. Wasywich, G. A. Whalley, and R. N. Doughty, "Brain natriuretic peptide in the contemporary management of congestive heart failure," *Expert Review of Cardiovascular Therapy*, vol. 3, no. 1, pp. 71–84, 2005.
- [26] P. Bhattacharjee, D. P. Edelson, and M. M. Churpek, "Identifying patients with sepsis on the hospital wards," *Chest*, vol. 151, no. 4, pp. 898–907, 2017.
- [27] M. D. Font, B. Thyagarajan, and A. K. Khanna, "Sepsis and septic shock - basics of diagnosis, pathophysiology and clinical decision making," *The Medical Clinics of North America*, vol. 104, no. 4, pp. 573–585, 2020.
- [28] E. Kyriazopoulou and E. J. Giamarellos-Bourboulis, "Monitoring immunomodulation in patients with sepsis," *Expert Review of Molecular Diagnostics*, vol. 21, no. 1, pp. 17–29, 2021.
- [29] X. Wang, B. Zhang, R. Xia, and Q. Jia, "Inflammation, apoptosis and autophagy as critical players in vascular dementia,"

*European Review for Medical and Pharmacological Sciences*, vol. 24, no. 18, pp. 9601–9614, 2020.

- [30] P. Zhong, D. Quan, J. Peng et al., “Role of CaMKII in free fatty acid/hyperlipidemia-induced cardiac remodeling both in vitro and in vivo,” *Journal of Molecular and Cellular Cardiology*, vol. 109, pp. 1–16, 2017.
- [31] J. Ye, Y. Huang, B. Que et al., “Interleukin-12p35 knock out aggravates doxorubicin-induced cardiac injury and dysfunction by aggravating the inflammatory response, oxidative stress, apoptosis and autophagy in mice,” *eBioMedicine*, vol. 35, pp. 29–39, 2018.
- [32] M. Avgeris and A. Scorilas, “Kallikrein-related peptidases (KLKs) as emerging therapeutic targets: focus on prostate cancer and skin pathologies,” *Expert Opinion on Therapeutic Targets*, vol. 20, no. 7, pp. 801–818, 2016.
- [33] X. Zhou, Y. Chen, Y. Tao, W. Zhang, W. Xu, and X. Lu, “Serum vaspin as a predictor of adverse cardiac events in acute myocardial infarction,” *Journal of the American Heart Association*, vol. 8, no. 2, article e010934, 2019.

## Research Article

# Heat Shock Protein 27 Levels Predict Myocardial Inhomogeneities in Hemodialysis Patients

Andrzej Jaroszyński <sup>1</sup>, Todd T. Schlegel,<sup>2,3</sup> Jerzy Mosiewicz,<sup>4</sup> Renata Stępień,<sup>1</sup> and Wojciech Dąbrowski<sup>5</sup>

<sup>1</sup>Collegium Medicum, Jan Kochanowski University of Kielce, Kielce, Poland

<sup>2</sup>Department of Molecular Medicine and Surgery, Karolinska Institute, Stockholm, Sweden

<sup>3</sup>Nicollier-Schlegel SARL, 1270 Trélex, Switzerland

<sup>4</sup>Department of Internal Medicine, Medical University of Lublin, Lublin, Poland

<sup>5</sup>Department of Anaesthesiology and Intensive Therapy, Medical University of Lublin, 20-954 Lublin, Poland

Correspondence should be addressed to Andrzej Jaroszyński; jaroszynskiaj@interia.pl

Received 18 April 2022; Accepted 6 May 2022; Published 19 May 2022

Academic Editor: Simon Kennedy

Copyright © 2022 Andrzej Jaroszyński et al. This is an open access article distributed under the Creative Commons Attribution License, which permits unrestricted use, distribution, and reproduction in any medium, provided the original work is properly cited.

**Background.** Sudden cardiac death (SCD) is the single major cause of death in hemodialysis (HD) patients. QRS-T angle is an established marker of global repolarization heterogeneity associated with electrical instability and SCD. Heat shock protein 27 (HSP27) plays an important, protective role against noxious factors in the cardiovascular (CV) system. This study is aimed at assessing whether low HSP27 is associated with myocardial inhomogeneities in HD patients, as expressed by increases in the spatial QRS-T angle. **Methods.** Clinical data and biochemical, echocardiographic, and electrocardiographic parameters were evaluated in 182 HD patients. Patients were split into normal and abnormal QRS-T angle groups. **Results.** Patients with abnormally high QRS-T angles were older and had higher prevalence of diabetes as well as myocardial infarction, higher left ventricular mass index (LVMI) and C-reactive protein, worse oxidant/antioxidant status, and lower ejection fraction and HSP27. Multiple regression analysis revealed that abnormal QRS-T values were independently, negatively associated with serum HSP27 and positively associated with LVMI. **Conclusions.** Low HSP27 levels are associated with increased heterogeneity of myocardial action potential, as expressed by increased spatial QRS-T angle.

## 1. Introduction

Renal registry data shows that sudden cardiac death (SCD) is the single major cause of death in hemodialysis (HD) patients, accounting for approximately 26% of all mortality [1]. The pathogenesis of SCD in HD patients is complex, multifactorial, and not completely understood. Additionally, clear differences in terms of the pathophysiology and cause of SCD exist between HD patients and the general population [1–4].

The QRS-T angle is the spatial angle between the three-dimensional vectorcardiographic representation of QRS complex and T-wave loops (ventricular repolarization and depolarization). The QRS-T angle is an established marker

of global repolarization heterogeneity associated with electrical instability and SCD [5–10]. Well-documented evidence exists that QRS-T angle is a sensitive, powerful, and reliable risk stratifier for cardiac events and especially for SCD in the general population and in various clinical settings [5, 6, 11–14], including HD patients [7, 8, 15–19].

Heat shock proteins (HSP) are chaperone proteins that protect cells against noxious factors and interact with other proteins to facilitate normal cellular functions. Heat shock protein 27 (HSP27) is a part of the HSP family playing an important role in cardiovascular (CV) system. HSP27 is both a biomarker of CV disease and a potential therapeutic target [20–23]. Evidence exists that HSP27 functions as an antioxidant, exerts cytoprotective effects, inhibits apoptosis, and



attenuates myocardial injury [20, 21, 23–26]. Recent studies suggest that HSP27 acts as a linking molecule influencing CV mortality in HD patients [23, 24].

The purpose of this study was to assess whether low levels of HSP27 in HD patients are associated with heterogeneity of myocardial action potential as expressed by QRS-T angle.

## 2. Materials and Methods

**2.1. Patients.** This analysis was performed using digital ECG recordings collected as part of a recently published study that investigated the role of HSP27 in the prediction of cardiac mortality in HD patients [27]. Patient characteristics, inclusion/exclusion criteria, and protocols for this study have previously been described in details [27]. In brief, 202 HD patients qualified for the study underwent ECG recordings, echocardiography, and blood sampling. The study was performed in accordance with the Declaration of Helsinki and was approved by institutional review board—“Bioethical Committee of Medical University of Lublin” (KE-0254/125/2011).

**2.2. Biochemical Variables.** Biochemical routine tests including electrolytes, hemoglobin, creatinine, urea, phosphates, C-reactive protein (CRP), total protein, albumin, intact parathormone (PTH), lipid profile, and troponin T were measured in all patients by automated analyzers. Both serum total antioxidant capacity (TAC) and total oxidant capacity (TOC) were evaluated by using colorimetric methods (Immundiagnostik AG, Germany), as previously described in detail [27]. Serum HSP27, NT-proBNP, and oxidized LDL (oxLDL) were measured by the ELISA method (Biomedica). All measurements were performed the day after the dialysis session.

**2.3. Echocardiographic Examination.** All echocardiographic measurements were performed by a cardiologist who was blinded to patients’ clinical data according to the American Society of Echocardiography recommendations as described previously. LVH was diagnosed when LVMI exceeded 130 g/m<sup>2</sup> in males or 110 g/m<sup>2</sup> in females [28].

**2.4. Electrocardiography Recordings.** Surface 12-lead resting ECG was recorded in each patient using a Cardiax device (IMED Co Ltd, Budapest, Hungary). ECGs were recorded in an electrically shielded and noise-proof room with subjects lying in the horizontal position after at least 5 min rest. All ECGs were obtained the day after the dialysis session, when data for all other tests were also obtained. The 10 s recordings were automatically averaged to a single beat and transformed into three orthogonal leads using the inverse Dower method. The projections of the maximum vectors of QRS and T-waves in the frontal, transverse, and left sagittal planes and on the X-, Y-, and Z-axes were then obtained. Next, the spatial QRS-T angle values were automatically calculated from the maximum spatial QRS and T vectors. An abnormal spatial QRS-T angle was defined as a spatial QRS-T angle >116 degrees for females and >130 degrees for males [29].

**2.5. Statistical Analysis.** Statistical analysis was performed using Statistica Version 10 as described in detail previously [27]. Due to the inability to estimate population size in our previous study [27], no calculation of the sample size was also performed in the present study [27]. All available HD patients from a previous study for whom an ECG was available were included. Linear regression analysis was carried out by using the Pearson or Spearman test, as appropriate. Nonnormally distributed data were transformed logarithmically prior to analysis. For further analysis, patients were divided into normal and abnormal QRS-T groups. Significance of differences between QRS-T angle groups was assessed using a Student *t*-test. In order to estimate the potential influence of various factors on QRS-T, multiple stepwise regression analysis was carried out. The model included parameters that showed differences with  $p < 0.05$  between normal and abnormal QRS-T groups. Receiver operating characteristics (ROC) curves were constructed to determine optimal cut-off points for HSP27 in predicting abnormal QRS-T values. Probability values of  $p < 0.05$  were accepted as significant.

## 3. Results and Discussion

**3.1. Results.** From 202 HD patients included in the original study, digital ECGs were unavailable or unreadable in 20 patients. The remaining 182 subjects were included in the present study.

The causes of end-stage failure were as follows: diabetes mellitus ( $n = 77$ ), glomerulonephritis ( $n = 38$ ), hypertensive nephropathy ( $n = 18$ ), polycystic kidney disease ( $n = 7$ ), obstructive nephropathy ( $n = 5$ ), chronic pyelonephritis ( $n = 5$ ), and unknown/unsure ( $n = 32$ ).

The mean  $\pm$  SD value of the QRS-Tangle in HD patients was  $104.8 \pm 25.3$ , with statistically higher values in the abnormal QRS-T group ( $150.3 \pm 12.8$ ) than in the normal QRS-T group ( $76.9 \pm 21.7$ ;  $p < 0.001$ ). Subjects in the abnormal QRS-T group were older ( $p = 0.011$ ) and had higher prevalence of both prior infarction ( $p < 0.001$ ) and diabetes ( $p = 0.001$ ). With regard to echocardiographic parameters, patients with abnormal QRS-T had higher LVMI and lower LVEF than patients with normal QRS-T ( $p < 0.001$  in both cases). Regarding biochemical indices, patients with abnormal QRS-T had marginally higher troponin T levels, but significantly higher CRP ( $p = 0.021$ ) as well as TOC and oxLDL levels ( $p < 0.001$  in both), and lower TAC levels ( $p = 0.018$ ). The demographic, clinical, and biochemical data of the studied groups are shown in Table 1. Significant relations were found between QRS-T angle and HSP27 ( $r = -0.612$ ,  $p < 0.001$ ) (Figure 1), QRS-T angle and oxLDL ( $r = 0.571$ ,  $p < 0.001$ ), QRS-T angle and TOC ( $r = 0.548$ ,  $p < 0.001$ ), and QRS-T angle and TAC ( $r = -0.489$ ,  $p < 0.001$ ).

The results of multiple regression analysis showed that QRS-Tangle values were independently and inversely associated with HSP-27 levels and independently and positively associated with both TOC and LVMI (Table 2).

The ROC analysis of HSP27 as a predictor of abnormal QRS-T showed an AUC of 0.643 with sensitivity and specificity of 0.645 and 0.611, respectively. The optimal cut-off

TABLE 1: Basic demographic data and clinical and biochemical data of patients.

Parameter	All patients <i>n</i> = 182	Abnormal QRS-T <i>n</i> = 54	Normal QRS-T <i>n</i> = 128	<i>p</i>
Age (years)	70.8 ± 7.64	73.1 ± 7.78	69.1 ± 7.76	0.011
HD vintage (months)	58.04 ± 25.89	59.32 ± 25.12	57.61 ± 25.77	0.406
MI (%)	31.9	44.4	26.6	<0.001
Diabetes mellitus (%)	52.2	61.1	48.4	0.001
Hypertension (%)	81.8	83.3	81.2	0.213
Smoking	19.2	18.5	19.5	0.273
Beta-blockers (%)	85.7	87.0	85.1	0.304
ACE/ARB (%)	75.8	74.1	75.8	0.625
Statins (%)	61.5	64.8	60.23	0.236
LVMi (g/m <sup>2</sup> )	146.1 ± 41.23	162.9 ± 38.68	136.1 ± 40.83	<0.001
LVEF (%)	56.90 ± 6.31	52.32 ± 6.18	59.23 ± 5.96	<0.001
Hemoglobin (g/dL)	11.29 ± 1.10	11.91 ± 1.09	10.96 ± 1.02	0.108
Total cholesterol (mg/dL)	189.5 ± 38.64	187.6 ± 37.18	190.3 ± 37.10	0.312
LDL cholesterol (mg/dL)	117.8 ± 31.14	114.6 ± 30.46	118.5 ± 28.75	0.411
HDL cholesterol (mg/dL)	43.99 ± 18.03	44.23 ± 17.55	43.71 ± 15.03	0.699
Triglycerides (mg/dL)	171.1 ± 60.84	168.8 ± 58.77	172.1 ± 53.6	0.328
PTH, range (pg/mL)	380 (0.0-1212)	351 (0.0-899)	440 (0.0-1212)	0.242
Albumin (g/dL)	3.66 ± 0.37	3.68 ± 0.36	3.65 ± 0.32	0.731
CRP, range (mg/dL)	7.34 (0.19-112.1)	10.31 (0.019-112.1)	6.89 (0.28-59.8)	0.021
Troponin T, range (μg/L)	0.057 (0.00-0.773)	0.082 (0.00-0.773)	0.039 (0.029-0.742)	0.069
NT-proBNP (fmol/mL)	321.2 ± 104.5	340.7 ± 104.9	216.8 ± 109.8	0.213
Sodium (mmol/L)	137.6 ± 2.62	137.2 ± 2.61	137.8 ± 2.69	0.434
Potassium (mmol/L)	5.75 ± 0.69	5.76 ± 0.67	5.75 ± 0.63	0.796
Calcium (mmol/L)	2.45 ± 0.23	2.45 ± 0.23	2.46 ± 0.24	0.682
Phosphate (mmol/L)	2.24 ± 0.35	2.20 ± 0.21	2.25 ± 0.23	0.267
Ca x P product (mg <sup>2</sup> /dl <sup>2</sup> )	48.87 ± 9.55	47.19 ± 9.13	49.27 ± 9.51	0.245
TAC (μmol/L)	257.3 ± 31.91	249.2 ± 31.72	260.6 ± 32.84	0.018

CAD: coronary artery disease; MI: history of myocardial infarction; ACE/ARB: angiotensin-converting enzyme inhibitors/angiotensin receptor blockers; LVMi: left ventricular mass index; LVH: left ventricular hypertrophy; LVEF: left ventricle ejection fraction; PTH: parathormone; CRP: C-reactive protein; NT-proBNP: N-terminal prohormone brain natriuretic peptide; TAC: total antioxidant capacity; TOC: total oxidant capacity; oxLDL: oxidized LDL; HSP27: heat shock protein 27.

point for HSP27 was 21.2 μg/L. The ROC curves are presented in Figure 2 and in Table 3.

#### 4. Discussion

The key finding of our study is that low serum HSP27 level is an independent and strong predictor of abnormal QRS-T angle in HD patients.

Interest in the QRS-T angle dates back to 1934, when Wilson developed the concept of a “ventricular gradient.” Recently, there has been renewed interest in the QRS-T angle. Abnormalities in depolarization mirror structural abnormalities, while those in repolarization reflect changes in regional action potential duration and the direction of repolarization sequence associated with electrical instability and SCD. QRS-T angle is an established marker of global repolarization heterogeneity, possibly related to underlying

structural and functional myocardial abnormalities [3, 6–8, 11, 14–16, 18]. In our study, abnormal QRS-T angle was found in 30% of HD patients. It is in agreement with the results of de Bie et al. [19], who applied a similar methodology and the same cut-off points for normal and abnormal QRS-T values. Some other authors [7, 16] found abnormal QRS-T angle in 40% of HD patients. This difference may be due to methodological differences in QRS-T angle calculation and differences between cut-off values reported in different studies, as well as the differences in the prevalence of comorbidities in the groups of the studied patients. Good evidence exists that in HD patients, widened QRS-T angle predicts both all-cause mortality and CV mortality and is particularly helpful in predicting SCD [7, 16, 18, 19]. Although it is well known that QRS-T angle reflects heterogeneity of the myocardial action potential, the mechanisms linking abnormal repolarization with clinical outcomes

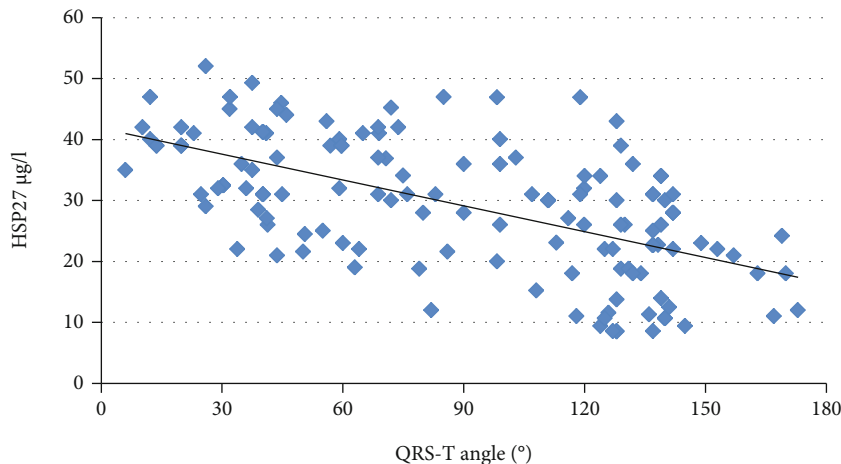


FIGURE 1: Relation between QRS-T angle and HSP27 levels ( $r = -0.612$ ). HSP27: heat shock protein 27.

TABLE 2: Factors influencing QRS-T angle estimated by multivariate stepwise regression analysis.

Dependent variable	Independent variables	B	St. error	Beta	p
QRS-T	HSP27	- 0.489	0.019	0.336	<0.001
	LVMI	10.35	5.47	0.219	0.009
Model ( $R = 0.649$ , $R^2 = 0.399$ )					

HSP27: heat shock protein 27; LVMI: left ventricular mass index.

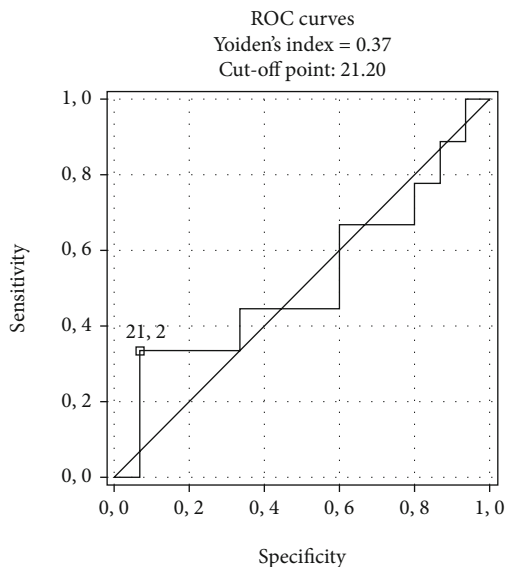


FIGURE 2: Receiver operating characteristic (ROC) curve of heat shock protein 27 (HSP27) in predicting abnormal QRS-T angle.

remain unclear. In our study, we have shown that low HSP27 and high LVMI were independent predictors of high QRS-T angle. Increased left ventricular mass (LVM) is highly prevalent in HD patients and universally associated with cardiovascular morbidity and mortality [30, 31], including SCD [32]. The relation between QRS-T and LVMI is in line with some but not all previous studies. In the study by Tereshchenko et al. [7], as in our study, the authors found a relationship between widened QRS-T angle and left ventricular hypertrophy, but not with the left ventricular ejection

fraction (LVEF). In the study by de Bie et al. [19], contrary to our study, the authors found a relationship between QRS-T angle and the LVEF but not LVMI.

To our knowledge this is the first study demonstrating a relationship between widened QRS-T angle and low HSP27. HSP27 exerts cytoprotective effects, has antioxidant properties, inhibits apoptosis, and participates in protein repair. There is also growing evidence that HSP27 exerts cardioprotective effects [23, 26, 33]. Our results may be in line with our previous study showing that low HSP27 levels are associated with increased cardiac mortality, including SCD [27]. Recent studies have revealed that cardioprotective effects may result from antiapoptotic as well as antioxidant properties. In our study, we found differences in oxidative parameters between normal and abnormal QRS-T groups. Moreover, we found differences in serum oxLDL between normal and abnormal QRS-T groups. While these differences lost their significance in multiple regression analysis, they might nonetheless play a role in myocardial pathology in HD patients. Similarly, our study revealed differences between serum oxLDL between normal and abnormal QRS-T angle groups. Recent studies have shown that HSP27 may contribute to the reduction of LDL oxidative modification, thus demonstrating that HSP27 plays a protective role in atherogenesis [27, 34, 35]. In addition, our previous study showed that inflammation may play a role in the pathogenesis of myocardial inhomogeneities in HD patients [36], and HSP27 is known to be involved in modulating inflammation. It is worth emphasizing that the results of ROC analysis revealed that the HSP27 cut-point value predicting abnormal QRS-T angle was similar to the HSP27

TABLE 3: Receiver operating characteristic (ROC) curve (Figure 2) of heat shock protein 27 (HSP27) in predicting abnormal QRS-T angle.

	Area	95% confidence interval	Sens/spec (%)	Cut-off
HSP27	0.643	0.621-0.698	0.624/0.601	21.2

value predicting the occurrence of contrast-induced nephropathy [24]. Given the above results, we can conclude that low HSP27 levels are associated with increased heterogeneity of myocardial action potential as expressed by the QRS-T angle. However, at this stage of research, we cannot determine whether the relationship is merely descriptive or whether the HSP27 protein is involved in the pathogenesis of increased myocardium repolarization heterogeneity. To determine if HSP27 is only a marker of disease severity versus a potential therapeutic target requires further studies.

Moreover, our study also had other limitations. First, we evaluated HSP27 level as well and spatial QRS-T angle values only once in each patient. However, it is likely that serial rather than single measurements of both measures might have better characterized overall results. Second, the inverse Dower transform utilized for derivation of the X, Y, and Z leads by our Cardiax device is not necessarily the scientifically most optimal transform [37].

## 5. Conclusions

Low HSP27 levels are associated with increased heterogeneity of myocardial action potential, as expressed by increased spatial QRS-T angle.

## Data Availability

All data used and/or analyzed in the present study are presented in the manuscript or available from the corresponding author on request.

## Conflicts of Interest

The authors declare that they have no conflicts of interest.

## Acknowledgments

This study was funded by the Medical University of Lublin (award number PW232, recipient—Andrzej Jaroszyński). The project is supported under the program of the Ministry of Science and Higher Education under the name “Regional Initiative of Excellence” in 2019–2022 (project number: 024/RID/2018/19, financing amount: 11,999,000.00 PLN).

## References

- [1] K. Johansen, G. Chertow, R. Foley et al., “US Renal Data System 2019 Annual Data Report: Epidemiology of Kidney Disease in the United States,” *American Journal of Kidney Diseases*, vol. 75, no. 1, pp. S1–S64, 2020.
- [2] J. Jankowski, J. Floege, D. Fliser, M. Böhm, and N. Marx, “Cardiovascular disease in chronic kidney disease: pathophysiological insights and therapeutic options,” *Pathophysiological*

*Insights and Therapeutic Options. Circulation*, vol. 143, no. 11, pp. 1157–1172, 2021.

- [3] T. T. Jaroszyński, T. Z. Schlegel, T. Zaborowski et al., “The value of ventricular gradient for predicting pulmonary hypertension and mortality in hemodialysis patients,” *Scientific Reports*, vol. 12, no. 1, p. 456, 2022.
- [4] J. Carracedo, M. Alique, C. Vida et al., “Mechanisms of cardiovascular disorders in patients with chronic kidney disease: a process related to accelerated senescence,” *Developmental Biology*, vol. 8, 2020.
- [5] I. Kardys, J. Kors, I. Van Der Meer, A. Hofman, D. A. van der Kuip, and J. C. Witteman, “Spatial QRS-T angle predicts cardiac death in a general population,” *European Heart Journal*, vol. 24, no. 14, pp. 1357–1364, 2003.
- [6] A. Oehler, T. Feldman, C. Henriksson, and L. Tereshchenko, “QRS-T angle: a review,” *Annals of Noninvasive Electrocardiology*, vol. 19, no. 6, pp. 534–542, 2014.
- [7] L. Tereshchenko, E. Kim, A. Oehler et al., “Electrophysiologic substrate and risk of mortality in incident hemodialysis,” *Journal of the American Society of Nephrology*, vol. 27, no. 11, pp. 3413–3420, 2016.
- [8] P. Poulidakos, K. Hnatkova, S. Skampardon, D. Green, P. Kalra, and M. Malik, “Sudden cardiac death in dialysis: arrhythmic mechanisms and the value of non-invasive electrophysiology,” *Frontiers in Physiology*, vol. 10, p. 144, 2019.
- [9] P. Rautaharju, C. Kooperberg, J. Larson, and A. LaCroix, “Electrocardiographic predictors of incident congestive heart failure and all-cause mortality in postmenopausal women: the Women’s Health Initiative,” *Circulation*, vol. 113, no. 4, pp. 481–489, 2006.
- [10] A. Aro, H. Huikuri, J. Tikkanen et al., “QRS-T angle as a predictor of sudden cardiac death in a middle-aged general population,” *Europace*, vol. 14, no. 6, pp. 872–876, 2012.
- [11] J. Waks, C. Sitlani, E. Soliman et al., “Global electric heterogeneity risk score for prediction of sudden cardiac death in the general population: the atherosclerosis risk in communities (ARIC) and cardiovascular health (CHS) studies,” *Circulation*, vol. 133, no. 23, pp. 2222–2234, 2016.
- [12] O. May, C. Graversen, C. Johansen, and H. Arildsen, “A large frontal QRS-T angle is a strong predictor of the long-term risk of myocardial infarction and all-cause mortality in the diabetic population,” *Journal of Diabetes and its Complications*, vol. 31, no. 3, pp. 551–555, 2017.
- [13] K. Kück, J. L. Isaksen, C. Graff et al., “Spatial QRS-T angle variants for prediction of all-cause mortality,” *Journal of Electrocardiology*, vol. 51, no. 5, pp. 768–775, 2018.
- [14] T. Yamazaki, V. Froelicher, J. Myers, S. Chun, and P. Wang, “Spatial QRS-T angle predicts cardiac death in a clinical population,” *Heart Rhythm*, vol. 2, no. 1, pp. 73–78, 2005.
- [15] A. Jaroszyński, A. Wysokinski, A. Bednarek-Skublewska et al., “The effect of a single dialysis session on spatial QRS-T angle in haemodialysis patients,” *Nephrology, Dialysis, Transplantation*, vol. 25, no. 11, pp. 3723–3729, 2010.
- [16] S. Skampardon, D. Green, K. Hnatkova, M. Malik, P. Kalra, and D. Poulidakos, “QRS-T angle predicts cardiac risk and correlates with global longitudinal strain in prevalent hemodialysis patients,” *Frontiers in Physiology*, vol. 10, p. 145, 2019.
- [17] A. Jaroszyński, J. Furmaga, T. Zapolski, T. Zaborowski, S. Rudzki, and W. Dąbrowski, “The improvement of QRS-T angle as a manifestation of reverse electrical remodeling following renal transplantation in end-stage kidney disease

- patients on haemodialysis,” *BMC Nephrology*, vol. 20, no. 1, p. 441, 2019.
- [18] D. Poulidakos, K. Hnatkova, D. Banerjee, and M. Malik, “Association of QRS-T angle and heart rate variability with major cardiac events and mortality in hemodialysis patients,” *Annals of Noninvasive Electrocardiology*, vol. 23, no. 6, article e12570, 2018.
- [19] M. de Bie, M. Koopman, A. Gaasbeek et al., “Incremental prognostic value of an abnormal baseline spatial QRS-T angle in chronic dialysis patients,” *Europace*, vol. 15, no. 2, pp. 290–296, 2013.
- [20] J. A. Inia and E. R. O’Brien, “Role of heat shock protein 27 in modulating atherosclerotic inflammation,” *Journal of Cardiovascular Translational Research*, vol. 14, no. 1, pp. 3–12, 2021.
- [21] H. Zhang, K. Jia, D. Sun, and M. Yang, “Protective effect of HSP27 in atherosclerosis and coronary heart disease by inhibiting reactive oxygen species,” *Journal of Cellular Biochemistry*, vol. 120, pp. 2859–2868, 2019.
- [22] E. Martínez-Laorden, J. Navarro-Zaragoza, M. Milanés, M. Laorden, and P. Almela, “Cardiac protective role of heat shock protein 27 in the stress induced by drugs of abuse,” *International Journal of Molecular Sciences*, vol. 21, no. 10, p. 3623, 2020.
- [23] C. Cruz Junho, C. Bueno Azevedo, R. Stafim et al., “Heat shock proteins: connectors between heart and kidney,” *Cell*, vol. 10, no. 8, p. 1939, 2021.
- [24] A. Jaroszyński, T. Zaborowski, S. Głuszek et al., “Heat shock protein 27 is an emerging predictor of contrast-induced acute kidney injury on patients subjected to percutaneous coronary interventions,” *Cell*, vol. 10, no. 3, p. 684, 2021.
- [25] X. Tian, L. Zhao, X. Song et al., “HSP27 inhibits homocysteine-induced endothelial apoptosis by modulation of ROS production and mitochondrial caspase-dependent apoptotic pathway,” *BioMed Research International*, vol. 2016, 9 pages, 2016.
- [26] R. Shan, N. Liu, Y. Yan, and B. Liu, “Apoptosis, autophagy and atherosclerosis: relationships and the role of Hsp27,” *Pharmacological Research*, vol. 166, p. 105169, 2021.
- [27] A. Jaroszyński, A. Jaroszyńska, T. Zaborowski, A. Drelich-Zbroja, T. Zapolski, and W. Dąbrowski, “Serum heat shock protein 27 levels predict cardiac mortality in hemodialysis patients,” *BMC Nephrology*, vol. 19, no. 1, p. 359, 2018.
- [28] L. Hickson, S. Negrotto, M. Onuigbo et al., “Echocardiography criteria for structural heart disease in patients with end-stage renal disease initiating hemodialysis,” *Journal of the American College of Cardiology*, vol. 67, no. 10, pp. 1173–1182, 2016.
- [29] R. Scherptong, I. Henkens, S. Man et al., “Normal limits of the spatial QRS-T angle and ventricular gradient in 12-lead electrocardiograms of young adults: dependence on sex and heart rate,” *Journal of Electrocardiology*, vol. 41, no. 6, pp. 648–655, 2008.
- [30] L. Di Lullo, A. Gorini, D. Russo, A. Santoboni, and C. Ronco, “Left ventricular hypertrophy in chronic kidney disease patients: from pathophysiology to treatment,” *Cardiorenal Medicine*, vol. 5, no. 4, pp. 254–266, 2015.
- [31] C. Zoccali, F. Benedetto, F. Mallamaci et al., “Left ventricular mass monitoring in the follow-up of dialysis patients: prognostic value of left ventricular hypertrophy progression,” *Kidney International*, vol. 65, no. 4, pp. 1492–1498, 2004.
- [32] I. Mostovaya, M. Bots, M. van den Dorpel et al., “Left ventricular mass in dialysis patients, determinants and relation with outcome. results from the COncvective TRAnsport STudy (CONTRAST),” *PlosOne*, vol. 9, no. 2, article e84587, 2014.
- [33] Z. Batulan, V. Pulakazhi, Y. Li et al., “Extracellular release and signaling by heat shock protein 27: role in modifying vascular inflammation,” *Frontiers in Immunology*, vol. 7, 285, p. 2016, 2016.
- [34] K. Rayner, Y. Chen, T. Siebert, and E. O’Brien, “Heat shock protein 27: clue to understanding estrogen-mediated atheroprotection?,” *Trends in Cardiovascular Medicine*, vol. 20, no. 2, pp. 53–57, 2010.
- [35] M. Ghayour-Mobarhan, H. Saber, and G. Ferns, “The potential role of heat shock protein 27 in cardiovascular disease,” *Clinica Chimica Acta*, vol. 413, no. 1-2, pp. 15–24, 2012.
- [36] K. Bołtuć, A. Bociek, R. Dziugięł et al., “Neutrophil-lymphocyte ratio (NLR) reflects myocardial inhomogeneities in hemodialyzed patients,” *Mediators of Inflammation*, vol. 2020, Article ID 6027405, 2020.
- [37] D. Cortez and T. Schlegel, “When deriving the spatial QRS-T angle from the 12-lead electrocardiogram, which transform is more frank: regression or inverse Dower?,” *Journal of Electrocardiology*, vol. 43, no. 4, pp. 302–309, 2010.